# THE TREATMENT OF CO-PRODUCED COAL SEAM GAS WATER USING RAW AND PRE-TREATED NATURAL ION EXCHANGERS

**Oscar Andres Santiago Urrea**

Bachelor Civil Engineering, Universidad de Los Andes (COL) 2010

Master Degree Water Resources, The University of Adelaide (AU) 2012

Submitted in fulfilment of the requirements for the degree of

Doctor of Philosophy

School of Medical & Applied Sciences

Central Queensland University

Australia

March, 2016

# Abstract

Coal seam gas (CSG) is obtained by pumping water from the saturated coal seam to reduce the pressure allowing the methane gas to desorb. The co-produced water from the gas extraction process has a geochemical signature mainly determined by the moderate levels of salinity, sodicity and dissolved trace elements. Typically, CSG co-produced water requires treatment to be suitable for beneficial re-use, since untreated co-produced water can cause soil infiltration damage and nutritional imbalance for crops and livestock. CSG water from the Bowen Basin (Queensland) was used in this study and has a typical ionic composition of $Na^+$-$Cl^-$-$HCO_3^-$.

In this study, two natural ion exchange materials, zeolite and scoria, were used for the removal of $Na^+$, $Sr^{2+}$ and $Ba^{2+}$ from CSG co-produced water. Following XRD analysis, the mineral composition of the zeolite material was found to be consistent of clinoptilolite (41%) and mordenite (29%), while the scoria material presented as diopside (35%), forsterite (33%) and anorthite (29%) characteristic. The real exchange capacity exhibited by the zeolite material was 75 meq/100 g, while the real exchange capacity determined for the scoria was 28 meq/100 g.

Adsorption capacity and kinetic rates for $Na^+$ ions were favoured by the use of small fraction sizes of natural forms of the zeolite and scoria material, which increased the accessibility of available adsorption sites on the material for cation interaction, consequently, an optimised fraction size of 0.6 – 0.3 mm was used in all studies.

Equilibrium studies used a ratio of 20:1 for solution and material (50 mL : 2.5 g) for 72 h showing that the scoria and zeolite material treated with $NH_4^+$ exhibited greater adsorption capacities for $Na^+$, $Sr^{2+}$ and $Ba^{2+}$ than the natural form. The maximum $Na^+$ adsorption observed in the scoria and zeolite materials enriched with $NH_4^+$ was 17 and 45 meq/100 g, which corresponds to 61% and 60% of the measured real exchange capacity, respectively. The scoria and zeolite materials enriched with $NH_4^+$ for $Sr^{2+}$ adsorption were 4.5 and 8 meq/100 g (44 and 80% removal of the initial $Sr^{2+}$

concentration). The maximum $Ba^{2+}$ adsorption achieved using the scoria and zeolite in $NH_4^+$ form was 5.8 and 10.6 meq/100 g (40 and 94% removal of the initial $Ba^{2+}$ concentration). Competitive uptake studies were undertaken to determine selectivity isotherms and coefficients that showed the scoria material's selectivity series was $Ba^{2+}$ $>Sr^{2+} >> Ca^{2+} > K^+ > Na^+$, while, the zeolite material exhibited selectivity for $K^+$ $>Ba^{2+}> Sr^{2+} >> Ca^{2+} > Na^+$. Other cations present in CSG water compete with $Na^+$ for adsorption sites, reducing its adsorption capacity to 10 and 38 meq/100 g for scoria and zeolite. The adsorption and desorption of $Na^+$ ions studied in batch mode showed that the ability of scoria and zeolite to adsorb cations decreased with the number of regeneration cycles.

The effect of the flow rate on the removal of $Na^+$ by the scoria and the zeolite material in a fixed bed column experiment was relatively small (5% reduction when using flow rates of up 10 BV/h). Columns packed with the scoria and the zeolite material exhibited a larger $Na^+$ dynamic adsorption capacity (breakthrough capacity) when treated with $NH_4^+$ as well as larger desorption capacities than the same materials in $K^+$ form. Nonetheless, the adsorption capacity exhibited for both materials was approximately 50% of the real exchange capacity. The maximum bed volumes obtained before the breakpoint ($C/C_0 = 0.3$, output concentration) with a flow rate of 5 BV/h for the scoria material in $NH_4^+$ form using CSG water was 1.5 BV, while zeolite in $NH_4^+$ form exhibited 4.5 BV.

These results showed that in using any natural and pre-treated ion exchange material as a CSG water treatment technology, allow the adsorption of $Na^+$ ions with evident improvement for pre-treated materials. Batch and column type experiments showed that chemical conditioning increased the zeolite and scoria ion selectivity towards cations such as $Ba^{2+}$, $Sr^{2+}$ and $Na^+$ present in high concentrations in CSG water. Ion selectivity was found to be correlated to the incoming hydrated cation size and its energy of hydration. The outcomes obtained from the experimentation indicates that natural ion exchangers are suitable for the removal of cations present in CSG water through ion exchange. Nonetheless, limitations to the use of natural and pre-treated ion exchange materials were identified. The high salinity characteristic of CSG water needs to be corrected with other treatment methods or mixed with low salinity water,

before the CSG water can be beneficially re-used. The use of natural ion exchange material for the treatment of CSG water may consist of a multi-column arrangement with several trains operating in parallel allowing continuous treatment and facilitate the regeneration of the column without the need to stop the treatment.

# Acknowledgements

This research project has been a truly life-changing experience for me and it would not have been possible without the support and advice that I have received from many people.

First and foremost, I want to thank my principal supervisor Dr. James Chapman for all the support and encouragement he has given me to pursue this PhD, especially during the tough times. It has been an honour to work with James; without his positive attitude, unconditional guidance and feedback this research work would not have been achievable. I would also like to thank Professor Kerry Walsh and Associate Professor Ted Gardner for their invaluable insights, suggestions and willingness to meet me frequently throughout the development of this project despite their busy schedules. I really appreciate their dedication and support at the various stages of my research.

I would also like to acknowledge the immense collaboration from my fellow researchers and the CQUniversity community that has made my time enjoyable, and also enriched me both personally and professionally. Special thanks to Anthony Kodel for the useful discussions and brainstorming sessions. I appreciate the massive help and guidance provided during my experimental work by the laboratory assistants across the Schools of Medical and Applied sciences, and Engineering and Technology at CQUniversity.

I gratefully acknowledge the funding sources that have made my PhD possible: The Co-Funded Industry Scholarship supported by a joint venture between CQUniversity and Arris Pty Ltd (Australia). The work is grounded by reference and access to an Arris Pty Ltd coal seam gas water treatment facility. Additionally, Arris Pty Ltd provided the media used in this research project, access to the CSG water, the CSG water data and additional analytical support. I would also like to thank Jim Kelly and Ben Kele (Arris Pty Ltd) who, since the beginning of the project have offered me their valuable help, advice, access to information and financial support. Ben's previous work (Master and Doctoral theses) provides the foundation from which this project

developed. Without Jim's and Ben's support this project would not have been possible. Thank you to both of you.

Lastly, I would like to thank my family for all their love and encouragement. Words cannot express how grateful I am to my parents who have supported me in all of my pursuits. And finally to Andrea, who has been by my side every single minute of this PhD, and without who, I would not have had the courage to embark on this journey in the first place.

*Gracias a toda mi familia. Especialmente a mi mamá, mi papá y mi hermana. Esta tesis tiene el nombre SANTIAGO-URREA. Y es el fruto del trabajo, enseñanzas y persistencia que aprendí de ustedes. A mi mamá le dedico mi trabajo de investigación, te amo mami.*

# Statement of Authorship and Originality of Thesis

The work contained in this thesis has not been previously submitted to meet requirements for an award at CQUniversity or any other tertiary institution. To the best of my knowledge and belief, the material presented in this thesis contains no material previously published or written by another person except where due reference is made.

Signature:

Date:                    March 31$^{st}$, 2016

# Copyright Statement

This thesis may be freely copied and distributed for private use and study, however, no part of this thesis or the information contained therein may be included in or referred to in publication without prior written permission of the author and/or any reference fully acknowledged.

<span style="color:red">Signature redacted</span>

Signature:

Date:            March $31^{st}$, 2016

# Table of Contents

# List of Figures

# List of Tables

# List of publications and presentations

- Santiago, O., Walsh, K., Kele, B, Gardner, E. & Chapman, J. (2016). Novel pre-treatment of zeolite materials for the removal of sodium ions: potential materials for coal seam gas co-produced wastewater. *SpringerPlus, Chemistry and Materials Science*. Acepted. Manuscript ID: *15-03119*.

- Santiago, O., Gardner, E., Walsh, K. & Chapman, J. (2015) The use of natural ion exchange technology for the treatment of co-produced water from coal seam gas industry. The International Water Association (IWA). 12th IWA Leading Edge Conference on Water and Wastewater Technologies, Hong Kong, China, June 2015.

- Santiago, O., Walsh, K., Gardner, E. & Chapman, J. (2015). The treatment of coal seam gas co-produced water unsing nautral ion exchange materials. Innovative research addressing indsutry issues. Higher Education Conference, Universities Australia. Canberra, Australia, March 2015.

# Chapter 1:  Introduction

## Background

Technology has enabled the safe extraction of gas from coal seams to provide a commercial source of natural gas aptly called Coal Seam Gas (CSG). The CSG extraction involves the management of two equally important natural resources, the evolved natural gas and co-produced CSG water (Reddy, 2010). The gas is obtained from the coal seam, whereby methane desorbs from the coal seam and flows to the surface by pumping water from the saturated seam to reduce the pressure (Abousnina *et al.*, 2015).

CSG co-produced water management has become a challenge for the CSG industry, governmental agencies, land owners and the general public due to the quantity and quality of water involved. Water production of a typical CSG well decreases exponentially over time after the well operation. In Australia, CSG co-produced water is estimated to be around 450 gigalitres per year, and it is projected that over the next 25 years CSG operations could extract 7,500 gigalitres from groundwater systems, creating major environmental concerns in relation to the water disposal procedure and overall reuse (Abousnina *et al.*, 2015; Berger, 2012). Surat and Bowen Basins in Queensland (Australia) have been epicentres of CSG operations and CSG production. In this study CSG operations located in the Bowen Basin was used as a case study along with the investigation of CSG co-produced water from this site.

CSG co-produced water quality has a geochemical signature mainly determined by the levels of salinity, sodicity and dissolved trace elements (metal cations dissolved in water) (Batley & Kookana, 2012). Typically, CSG co-produced water needs treatment to render it suitable for beneficial use due to the high salinity and high concentration of sodium. Untreated CSG water can cause soil dispersion, and thus decrease infiltration and cause nutritional toxicities or imbalance for crops and livestock (DEWS, 2013; Hamawand *et al.*, 2013). The cost of treating and handling CSG co-produced water can be determinant on the feasibility of a CSG operation (Fell Consulting Pty Ltd, 2014). Furthermore, current water treatment technologies, in some

cases, are ineffective due to the chemical composition of the water (Davies, 2013; Mannhardt, 2009). Therefore, there is a need in the CSG industry for a cost-effective alternative treatment that complies with the water quality guidelines required for beneficial water re-usage (DEHP, 2013).

The potential use of natural materials for adsorption or ion exchange processes have been a focus of research over the last decade (Can, 2004; Erdem *et al.*, 2004; Ismael *et al.*, 2012; Spiridonov *et al.*, 2015). Natural adsorption systems are often characterised as cost effective processes, demonstrating low capital and operations costs, and reduced disposal issues (Gedik & Imamoglu, 2008; Inglezakis *et al.*, 2004; Perić *et al.*, 2004). It is established that natural materials exhibit exceptional adsorption capacity and selectivity towards cations. However, adsorption or ion exchange processes of natural materials is complex and variable due to the unique mineralogical heterogeneity, particular porous structure, and adsorption capacity intrinsic of each material (Perić *et al.*, 2004). It is therefore of special interest to this project to characterise the use of the natural materials for the removal of cations present in CSG co-produced water.

The treatment of CSG co-produced water through ion exchange using natural zeolite materials has been approached by different research groups (Ganjegunte *et al.*, 2011; Taulis & Milke, 2009; Wang *et al.*, 2012; Zhao *et al.*, 2008; Zhao *et al.*, 2009). Research has focused on the removal of sodium from CSG operations in the USA, New Zealand and Australia (Surat Basin only) using natural zeolites. These studies have shown that the major and trace chemical composition of the CSG co-produced water is different from site to site. For that reason, it is an interest of this research project to determine the geochemical signature of Bowen Basin CSG water and to use natural adsorption materials sourced from the eastern coast of Australia for the removal of metal ions (cations) dissolved in CSG water.

## Motivation and objectives of the research

The importance of mitigating any environmental impact that may be caused from the CSG operations motivates this research, and especially in the context of managing co-produced water. The treatment strategies investigated, aim to provide the CSG

industry, landholders, the general public, governmental agencies and end-users with a reliable and cost-effective solution that can potentially reduce any environmental concerns over the use of treated co-produced water.

The aim of this research is to develop a low cost and effective alternative for the treatment of CSG co-produced water using locally sourced natural scoria and zeolite materials for the removal of dissolved metal ions found in CSG water including $Na^+$, $Sr^{2+}$ and $Ba^{2+}$. The objectives of this thesis were:

- To determine the chemical composition of the co-produced water from the research site located in the Bowen Basin;

- To characterise mineralogical, chemical, physical and the adsorptive properties of Australian natural scoria and zeolite;

- To evaluate the scoria and zeolite adsorption capacity for $Na^+$, $Sr^{2+}$ and $Ba^{2+}$ under varying process conditions such as initial concentration, particle size, and material treatment, among others;

- To evaluate the effect of competing cations present in CSG water on the adsorption of $Na^+$;

- To evaluate the adsorption and desorption (regeneration) of cations from the scoria and the zeolite using different regenerate solutions, and finally to;

- Identify the ability of the scoria and zeolite material for dynamic adsorption in fixed bed columns using synthetic solutions and field-collected CSG water.

## Thesis Outline

The thesis document is divided into a number of chapters, each explaining different aspects of this research project along with a brief description of the content of each chapter is given below:

**Chapter 1: Introduction**

A brief background on CSG and co-produced water operations and environmental challenges of managing water resources. The context, motivation and research objectives are described.

**Chapter 2: Literature review**

This chapter details the CSG extraction process, the coal seam co-produced water characteristics, environmental impacts and current treatment methods of CSG water. Innovative adsorption treatment techniques using natural ion exchangers are also described. A review of the characteristics of natural ion exchangers as well as previous research involving the use of natural materials is discussed.

**Chapter 3: Case study, CSG water from Bowen Basin operations**

A brief history of the development of coal seam gas production in the Bowen and Surat Basins in the central region of Queensland (QLD), Australia is presented. Identification of the characteristics of the CSG co-produced water from Bowen Basin operations is presented. Finally, CSG water from the Bowen Basin is compared with CSG water from different sites.

**Chapter 4: Materials and methods**

This chapter presents the materials and methods used in the experiments of Chapters 5-8. Experimental and analytical methods used in the characterisation of fundamental properties are given for the natural exchangers used for the treatment of co-produced CSG water are also presented.

**Chapter 5: Characterisation of natural ion exchangers**

This chapter presents physicochemical properties of natural ion exchangers used in this study such as mineral and elemental composition, determination of surface area,

and determination of the cation exchange capacity from scoria and zeolite natural materials.

## Chapter 6: Equilibrium Studies

Equilibrium studies describe the theory and models used to determine equilibrium adsorption isotherms as well as the theory of selectivity for natural ion exchangers are presented. Equilibrium experiments describe the removal of $Na^+$, $Sr^{2+}$ and $Ba^{2+}$ cations for natural and treated forms of scoria and zeolite. Experimental results are analysed using adsorption equilibrium isotherms models such as Langmuir, Freundlich among others are given. The interaction and competition on the adsorption of $Na^+$ ions over $Ca^{2+}$, $Sr^{2+}$ and $K^+$ ions is studied and discussed by selectivity experiments.

## Chapter 7: Kinetic studies

Kinetic theory and models are explained in this chapter as well as models that describe diffusion processes occurring in adsorption processes. Kinetics studies that determined the overall performance and efficiency of natural materials for the removal of cations present in CSG co-produced water are discussed. The kinetics experiments describe the effect of particle size on the adsorption of $Na^+$ ions, and adsorption rates for $Na^+$, $Sr^{2+}$, $Ba^{2+}$ using natural and treated forms of adsorbents. Additionally, adsorption and desorption cycles are presented; these were conducted for the determination of the performance and efficiency of natural and treated scoria and zeolite for the removal of $Na^+$ ions using different chemical treatments are shown in this chapter.

## Chapter 8: Column studies

The design, modelling and operation of ion exchange columns using natural and treated material are described in this chapter. The assessment on performance of adsorption and desorption of cations contained in CSG co-produced water determined experimentally and validated with fixed bed models is discussed.

**Chapter 9: Conclusions and recommendations**

The main findings and conclusions on the performance of the adsorption of cations in CSG co-produced water are summarised in this chapter. Recommendations and further studies on the use of natural ion exchange for the treatment of CSG co-produced water are discussed.

# Chapter 2:  Literature Review

## Introduction

Population and economic growth and technology advancement, drive increase for energy demand using sources such as coal, oil, natural gas, uranium, wind, solar, hydro, coal seam gas, shale gas and geothermal resources (NRC, 2010; Reddy, 2010). The most abundant fossil energy source on Earth is coal, but its use results in one of the highest emissions of carbon dioxide ($CO_2$) per gigajoule of energy produced when compared to other fossil fuels (Schraufnagel, 1993). In this new era of high demand for cleaner fossil energy alternatives, resources such as natural gas are gaining acceptance (NRC, 2010). Natural gas is considered a cleaner fuel, since natural gas emits less $CO_2$ upon combustion of the primary constituent gas methane ($CH_4$) producing 53 kg of $CO_2$ per gigajoule of energy released in comparison to coal or petroleum produces 94 kg and 74 kg, respectively for the same amount of energy (NRC, 2010). Natural gas has been traditionally produced from underground reservoirs as a by-product of petroleum extraction process (Reddy, 2010). A growing energy demand coupled with technology advances have led to the exploration and recovery of large volumes of gas from unconventional sources (Bishop, 2006; Reddy, 2010). Some of the non-traditional sources include quantities from large deposits that reside in low permeability reservoirs, coal, sandstone and shale (All-Consulting & Montana Board of Oil & Gas Conservation, 2002; Ayoub *et al.*, 1991).

Several countries are now planning and/or producing methane gas from coal deposits from un-minable coal seams that are often too deep, poor quality, thin or represent another difficult mining condition. This gas is often referred to as CSG or coalbed methane (CBM) (Benson *et al.*, 2005; Reddy, 2010; Rice & Nuccio, 2000). A major characteristic of CSG field developments is that water from the coal formation must be pumped out of the seam producing about 400 ML per gigajoule of energy (Rice *et al.*, 2000; Richard *et al.*, 2011). This water is called co-produced CSG water. Managing large volumes of CSG co-produced water represents an important challenge

for CSG operators due to the particular geochemical characteristics and the potential environmental impacts this escaping body of water may have.

## Coal seam gas and co-produced water

The geologic process of coalification involves conversion of plant material and organic debris with heat and pressure to produce coal (Reddy, 2010; Ross *et al.*, 2013; Taulis & Milke, 2007; Van Voast, 2003). Coalification generates large quantities of methane, carbon dioxide and nitrogen gas, which are mainly adsorbed and absorbed in the underground coal beds, being physically trapped by confined pressures of water and overburden (Ayoub *et al.*, 1991; Bechtel *et al.*, 2007). The coal seam matrix, cleats and void spaces are saturated with water that constantly pressurises gas molecules within the coal structure (Bishop, 2006; USEPA, 2013). Usually, coal seams are confined, both above and below, by impermeable layers of clays, mudstones or shale (NRC, 2010).

The CSG mining process is carried out by drilling a hole and pumping water from the coal seam lowering the aquifer pressure, allowing the methane gas to desorb from the coal matrix (Jamshidi & Jessen, 2012). The dewatering of the coal seam by pumping water from the well is essential because it permits methane gas to desorb from the coal and flow as free gas up the well to the surface (USEPA, 2013). CSG wells are drilled in different ways depending on the coal rank and operation type available at the site, natural fracturing and availability of coal seams (Schraufnagel, 1993). Drilling technology can help to dramatically boost methane recovery rates and also reduce the operation footprint. A horizontal drilling approach eliminates the need for hundreds of vertical single wells (Abousnina *et al.*, 2015).

For natural gas extraction, cased wells are drilled (100 – 1500 m below ground) to the coal seam, where the casing effectively isolates the coalbed and prevents well collapse (All-Consulting, 2012). As the pressure within the coalbed reduces, caused by a natural decompression of the coal seam, both methane gas and co-produced water come to the surface (Figure 2.1). The gas is then directed to a processing plant or gas pipeline. The CSG co-produced water is stored in an impoundment for its subsequent treatment or disposal (All-Consulting & Montana Board of Oil & Gas Conservation, 2006).
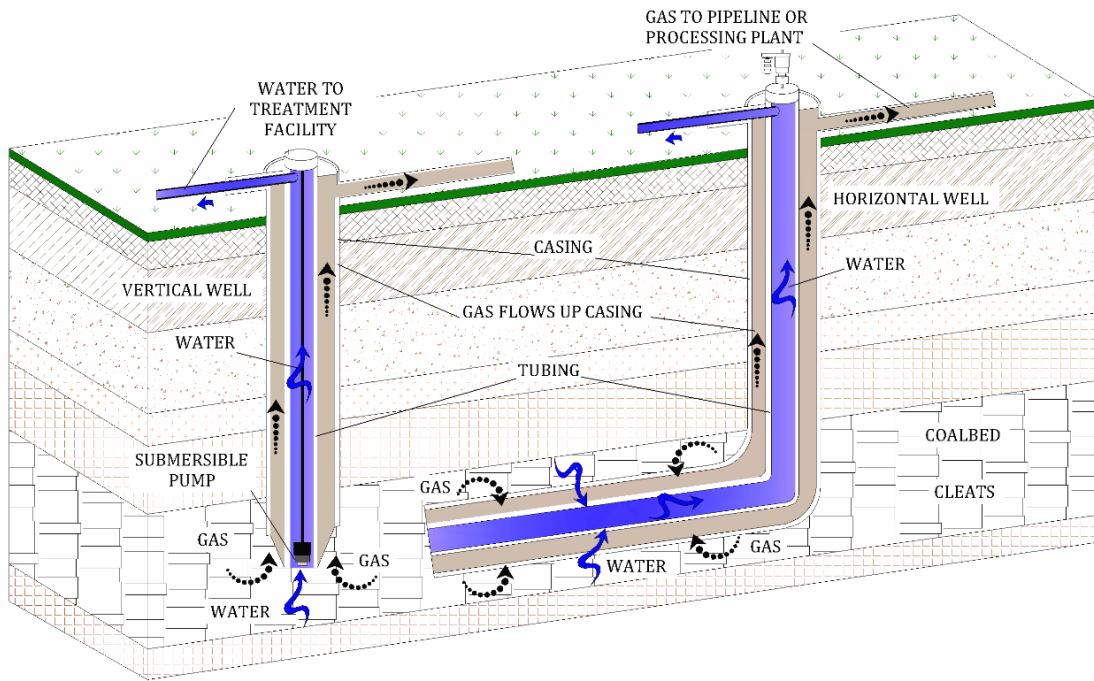
**Figure 2.1 A schematic of the profile diagram showing vertical and horizontal well drilling. CSG well diagram for the extraction of methane gas and co-produced water (USEPA, 2013; Jamshidi & Jessen, 2012).**
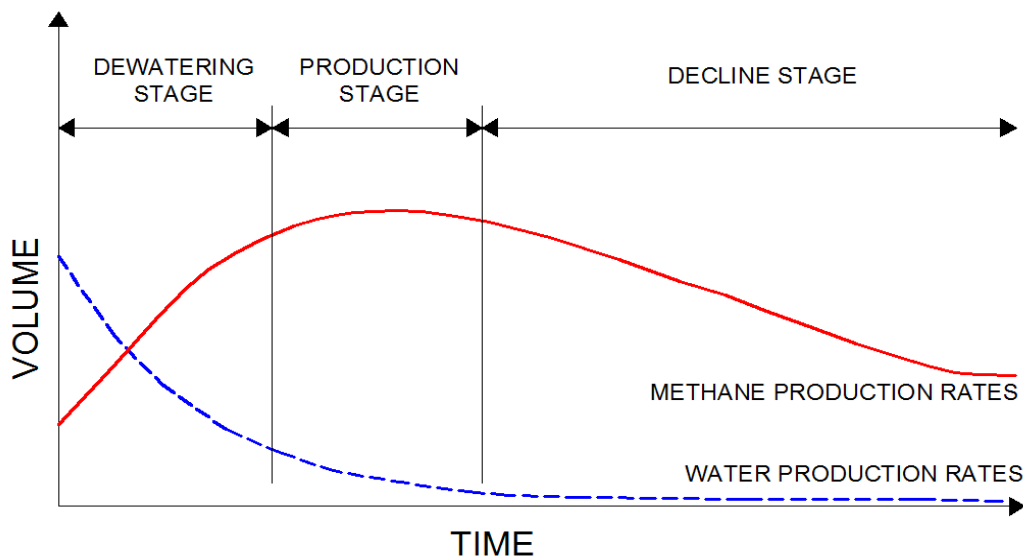


**Figure 2.2 A process chart to illustrate the typical changes in the rate of water and gas production from a CSG well (Hamawand *et al.*, 2013).**

A typical CSG well lifespan ranges from 5 - 20 years and the maximum methane extraction is reached after water is removed (Anderson, 2013; Benson *et al.*, 2005; Environmental Protection Agency, 2010; Hamawand *et al.*, 2013). CSG wells go through three main production stages (Berger, 2012; Hamawand *et al.*, 2013;

Schraufnagel, 1993). (i) An early stage that requires large volumes of groundwater to be pumped from the coalbed to reduce pressure and initiate the methane gas desorption process (dewatering stage). (ii) A stable stage (production stage) in which natural gas is produced in large volumes and groundwater pumped from the coalbed decreases. (iii) A final stage, in which gas production declines (decline stage) and the groundwater is maintained low (Figure 2.2). CSG resources worldwide are estimated to be around $256 \times 10^{12}$ m$^3$, the majority of the resources are located in North America, Asia Pacific and the former Soviet Union (Figure 2.3) (Hamawand *et al.*, 2013; Pacwest, 2012; Reddy, 2010).



**Figure 2.3 Global map of the regions rich in natural gas and the potential for coal and shale gas extraction (Pacwest, 2012).**

The total worldwide CSG co-produced water based on the total CSG operation is between 1696 – 5090 GL/year (All-Consulting, 2003; All-Consulting & Montana Board of Oil & Gas Conservation, 2002). The total CSG production and estimation of co-produced water from countries in which CSG is recovered from coalbeds is shown in Table 2.1(Bishop, 2006; Hamawand *et al.*, 2013; Richard *et al.*, 2011).

**Table 2.1 Total worldwide CSG production and an estimation of CSG co-produced water (Abousnina *et al.*, 2015).**

| Country | Gas production (x10$^9$ m$^3$/year) | Total CSG water (GL/year) | |
|---|---|---|---|
| USA | 52.0 | 1,355 | - 4,066 |
| Australia | 6.2 | 162 | - 485 |
| China | 1.4 | 36 | - 109 |
| Canada | 0.8 | 22 | - 66 |
| India | 0.06 | 1.5 | - 4.4 |
| Europe | 4.6 | 110 | - 330 |
| Total | 65.1 | 1,696 | - 5,090 |

## Australian context

Extensive exploration and notable production for CSG is occurring in Australia. Commercial production of CSG commenced in 1996 at Moura Mine (Bowen Basin) in Queensland. Since then, CSG production has increased significantly, becoming an integral resource of the upstream gas industry in eastern Australia (Hamawand *et al.*, 2013; Yusaf *et al.*, 2014). Large and rich deposits are located in the Australian states of Queensland and New South Wales; where the Queensland coal basins account for 90% of the CSG produced in Australia, especially from the Bowen and Surat Basins (Figure 2.4) (Hamawand *et al.*, 2013; Vacher *et al.*, 2014; Yusaf *et al.*, 2014). CSG production in Queensland has achieved high commercial acceptance, with a number of liquefied natural gas (LNG) processing plants in operation along the eastern coast (Nghiem *et al.*, 2011).

CSG production in Australia has increased from $0.025 \times 10^9$ m$^3$ to $6.2 \times 10^9$ m$^3$ per year over the last 15 years, and accounts for 10% of total gas production (Hamawand *et al.*, 2013). During 2010 and 2011, 98% of Queensland CSG production came from Bowen ($3 \times 10^9$ m$^3$/y) and Surat ($2.8 \times 109$ m$^3$/y) Basins (Williams *et al.*, 2012b). CSG co-produced water volume was estimated to be 300 GL per year in 2008, and is projected to increase over the next 25 years CSG operations extracting up to 7,500 GL from groundwater systems (Averina *et al.*, 2008; DEHP, 2012b).
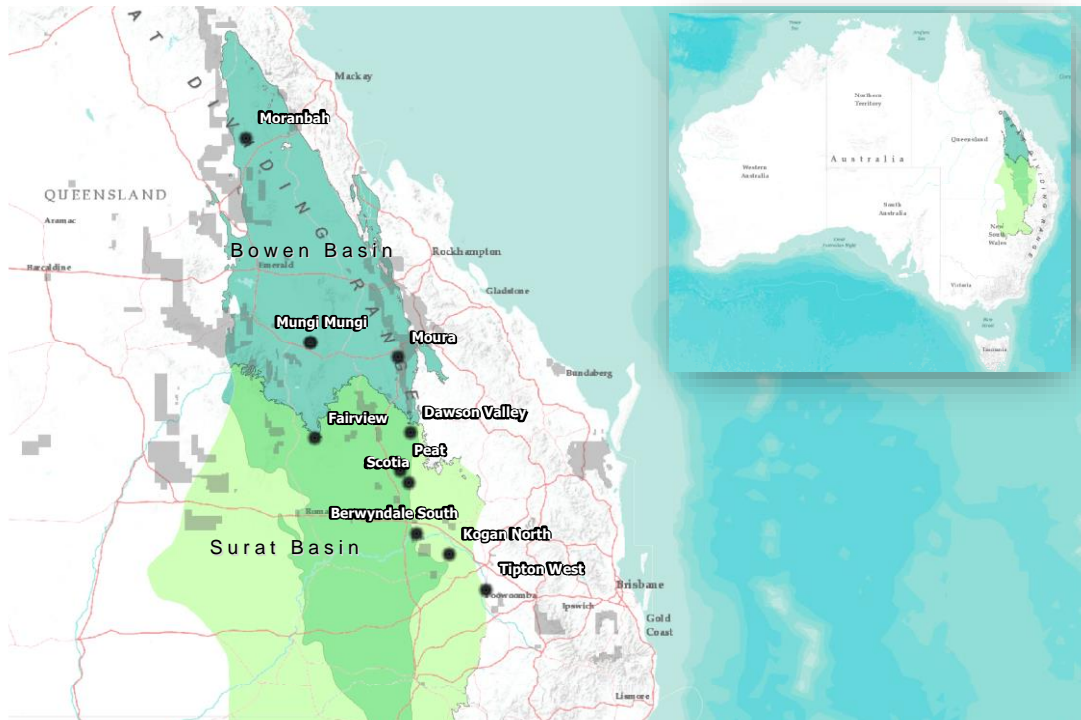
**Figure 2.4 CSG gas exploration and production in Australia and Queensland (Geoscience-Australia, 2015).**

Coalbed groundwater has a unique chemistry that relates to the geological, geochemical, physical, and biological processes during coalification (All-Consulting, 2003; All-Consulting & Montana Board of Oil & Gas Conservation, 2002; Taulis & Milke, 2007). Owing to the unique coalification process, CSG co-produced water is variable from site to site in quantity and chemical composition (NRC, 2010; Reddy, 2010). Nonetheless, CSG water is categorised as a brackish water due to the high concentration of total dissolved solids (TDS), slightly basic pH, alkaline and depleted sulphate, magnesium and calcium (Abousnina *et al.*, 2015; Hamawand *et al.*, 2013; Mannhardt, 2009; Yusaf *et al.*, 2014). The typical ionic composition of CSG water is $Na^+$-$Cl^-$-$HCO_3^-$ or $Na^+$-$HCO_3^-$ and the ionic concentrations of the CSG water reflect the processes of recharge, flow, flushing and discharge of groundwater (All-Consulting, 2003; USEPA, 2010; Rice *et al.*, 2000; Richard *et al.*, 2011; Taulis & Milke, 2007; Taulis & Milke, 2012).
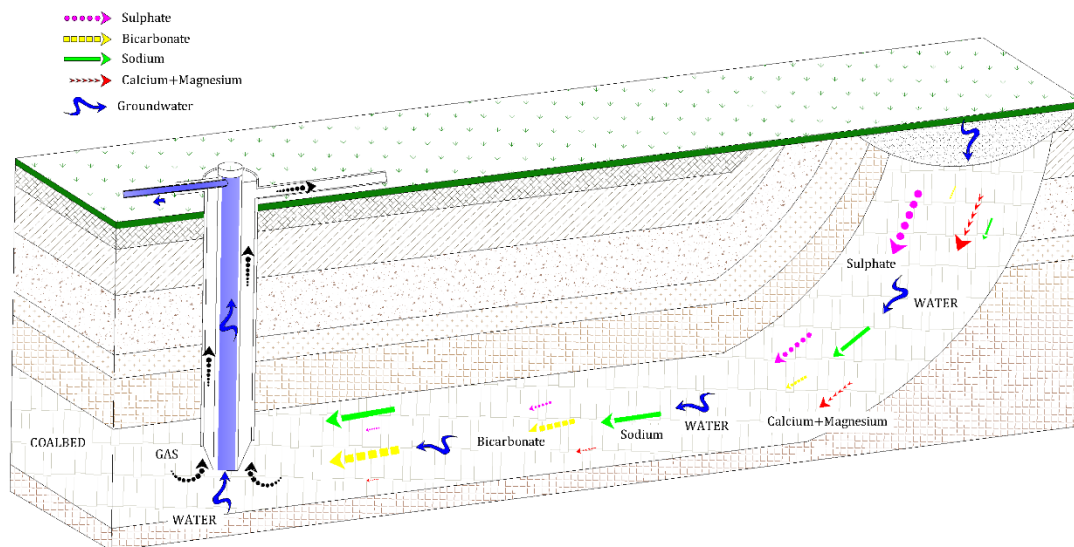
**Figure 2.5 Geochemical evolution and concentration of ions present in coalbed water. Calcium and magnesium are depleted due to precipitation or ion exchange, sulphate is reduced through coalification, resulting in concentrated sodium, chloride and bicarbonate. The arrows' size represent the concentration of the respective ion (Taulis, 2007).**

The geochemical nature of all CSG waters reflects a background of chloride and sodium, and a succession of the processes linked to coalification (Anderson, 2013; Arthur & Seekins, 2010; Averina *et al.*, 2008). Coalbeds have a stratigraphic association with marine transitional beds in which chloride and sodium are the substantial components of CSG waters (Taulis & Milke, 2012). Dissolution of sodium feldspar as water seeps through the recharge points areas and flow through the coal aquifer is another factor for the increased sodium content (Figure 2.5).

Whether the influence of $Na^+$ and $Cl^-$ are from marine sources or groundwater interactions, the geochemical process is linked to the reduction of sulphate during the formation of methane gas that produces the enrichment of dissolved carbonate that results in the depletion of calcium and magnesium during the process (Lemay, 2006). When fresh water seeps along the recharge path towards the coal aquifer, it dissolves sulphate ions contained along the flow or through the weathering and oxidation of pyrite or marcasite, which are sulphate minerals. As water containing dissolved sulphate enters deeper in the coalbed, biochemical reduction of dissolved sulphate precipitates the sulphides. The anaerobic environment in which coalification occurs reduces the sulphate concentrations that exists within the aquifer. A by-product of

sulphate reduction is the dissolved hydrogen sulphite that in some cases includes the presence of iron precipitate forming iron sulphite (Mcbeth *et al.*, 2003).

The relatively high concentration of bicarbonate in CSG water is mainly due to the production of methane gas resulting from the sulphate reduction that generates large amounts of carbon dioxide, carbonic acid and bicarbonate, which leads to an alkaline pH. Bicarbonate is the dominant dissolved specie since pH falls between 6.3 and 10 according with the carbonate chemistry (Jackson & Reddy, 2007a). Carbonate can also be found in CSG water due to dissolution of carbonate by oxygenated water that seeps down to the coalbed.

Calcium and magnesium ions are depleted from CSG water due to two main processes in the aquifer. First, the elevated bicarbonate concentrations that causes precipitation of calcium and magnesium, producing calcite and dolomite. Depletion of calcium and magnesium can also occur due to ion exchange. When groundwater encounters clays or shale deposits, calcium and magnesium ions are exchanged for other ions such as sodium, hence few calcium and magnesium ions ever reach the coal seam (Jackson & Reddy, 2007b; Lemay, 2006). As water flows into deeper aquifers, calcium and magnesium concentrations are gradually decrease while sodium ions may increase in concentration.

When discussing the properties of CSG co-produced water, water quality parameters include: the total dissolved solids (TDS), pH, electrical conductivity (EC), concentration of major ions (mg/L or meq/L) and sodium adsorption ratio (SAR, an expression of concentration of sodium, relative to the concentration of calcium and magnesium). Ion concentrations can be displayed graphically in a Scholler diagram (Figure 2.6), which shows the concentrations of CSG waters worldwide.
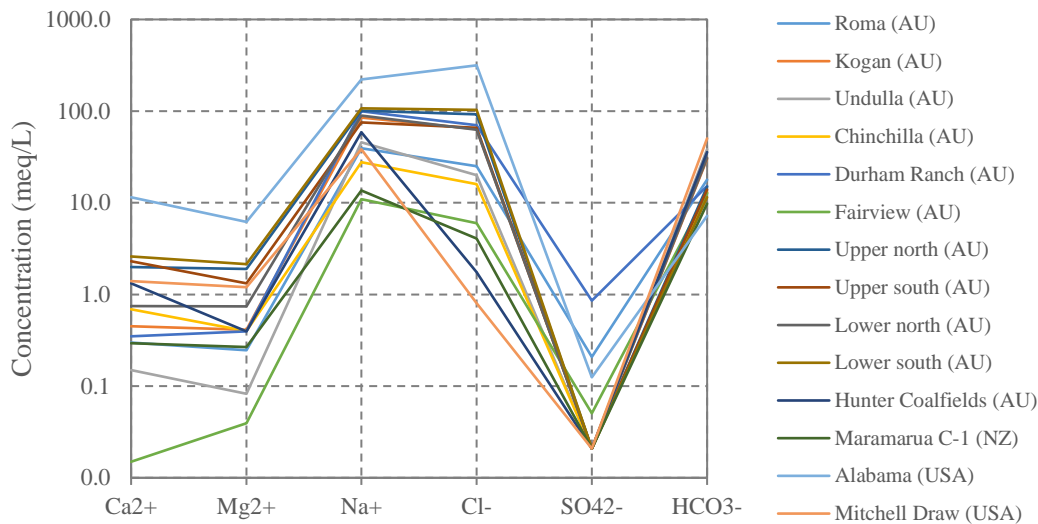
**Figure 2.6 Schoeller diagram for CSG co-produced water from coal basins in Australia, United States of America and New Zealand (Abousnina *et al.*, 2015; Averina *et al.*, 2008; Benson *et al.*, 2005; Hamawand *et al.*, 2013; Jackson & Reddy, 2007a; Manthey, 2014; Mcbeth *et al.*, 2003; Taulis & Milke, 2007).**

Water constituents from CSG operations have similar characteristics ($Na^+$-$Cl^-$-$HCO_3^-$ or $Na^+$-$HCO_3^-$ type) across the different coalbed basins around the world but concentrations can vary dramatically (Taulis & Milke, 2007). A summary of the major constituents of CSG co-produced water from two coal basins in the United States of America, three from Australia, and one in New Zealand. CSG water in general has elevated levels of salinity, ionic concentration dominated by $Na^+$-$Cl^-$-$HCO_3^-$ or $Na^+$-$HCO_3$ (Table 2.2).

The overall coalification process generates by-products other than what is contained in CSG water such as inorganic and organic chemicals, and naturally occurring radioactive materials (Jackson & Reddy, 2007a; Mcbeth *et al.*, 2003; Stearman *et al.*, 2014; Taulis & Milke, 2012). Many of the naturally occurring inorganic and organic chemicals found in the coalbed may be transferred to groundwater through the long-term contact with the coal.

**Table 2.2 Characteristics of CSG co-produced water in some different basins worldwide (Abousnina *et al.*, 2015; Averina *et al.*, 2008; Benson *et al.*, 2005; Hamawand *et al.*, 2013; Jackson & Reddy, 2007a; Manthey, 2014; Mcbeth *et al.*, 2003; Taulis & Milke, 2007).**

| Country | | Australia | | | | | | | | | | | New Zealand | USA | |
|---|---|---|---|---|---|---|---|---|---|---|---|---|---|---|---|
| Basin | | Surat Basin | | | | | | Bowen Basin | | | | Gloucester Basin | Maramarua | Black Warrior Basin | Powder River Basin |
| Location | | Roma | Kogan | Undulla | Chinchilla | Durham Ranch | Fairview | Upper north | Upper south | Lower north | Lower south | Hunter Coalfields | Maramarua C-1 | Alabama | Mitchell Draw |
| pH | mg/L | 8.1 | 8.4 | 8.4 | 7.8 | | | 7.9 | 7.9 | 8.0 | 7.8 | 8.4 | 7.7 | 7.5 | 8.2 |
| TDS | mg/L | | | | | | | 5810.0 | 4488.0 | 4838.0 | 5846.0 | | 776.0 | 16846.0 | 3460.0 |
| Conductivity | mS/cm | 3.4 | 9.0 | 5.0 | 2.8 | | | 10.5 | 7.9 | 8.6 | 11.1 | 4.4 | 1.3 | | |
| Sodium | mg/L | 904.0 | 1955.0 | 1050.0 | 636.9 | 2290.0 | 251.9 | 2324.0 | 1730.0 | 2054.0 | 2464.0 | 1351.2 | 312.8 | 5103.0 | 880.0 |
| Calcium | mg/L | 6.0 | 9.0 | 3.0 | 13.8 | 7.0 | 0.3 | 40.0 | 46.0 | 15.0 | 52.0 | 26.5 | 5.9 | 231.0 | 28.0 |
| Magnesium | mg/L | 3.0 | 5.0 | 1.0 | 4.8 | 4.8 | 0.5 | 23.0 | 16.0 | 9.0 | 26.0 | 4.8 | 3.2 | 75.0 | 14.6 |
| Potassium | mg/L | 3.0 | 9.0 | 4.0 | 3.9 | | | 17.0 | 10.0 | 8.0 | 12.0 | 29.0 | | 15.0 | 35.2 |
| SAR | | 75.0 | 129.1 | 133.7 | 37.5 | 162.6 | 66.0 | 72.2 | 55.8 | 103.1 | 69.4 | 63.2 | 25.6 | 74.4 | 33.4 |
| Chloride | mg/L | 891.0 | 2250.0 | 711.0 | 564.3 | 2481.5 | 212.7 | 3280.0 | 2330.0 | 2223.0 | 3670.0 | 62.2 | 143.9 | 11198.0 | 28.4 |
| Bicarbonate | mg/L | 861.0 | 1451.0 | 1841.0 | 624.3 | 732.0 | 610.0 | 719.0 | 667.0 | 1482.0 | 550.0 | 1717.4 | 471.6 | 347.0 | 2416.0 |
| Sulphate | mg/L | 10.0 | <1 | <1 | <1 | 41.2 | 2.4 | <1 | <1 | 1.0 | 1.0 | | <2 | 6.0 | 1.0 |

Investigations carried out in the CSG basins in USA and Australia, have identified trace elements present in the co-produced water including: iron (Fe), aluminium (Al), zinc (Zn), arsenic (As), boron (B), selenium (Se), cadmium (Cd), strontium (Sr) and barium (Ba) (Jackson & Reddy, 2007b; Mcbeth *et al.*, 2003; Tang *et al.*, 2014). These inorganic trace elements were found in a wide range of low concentrations ($< 8$ mg/L), below the maximum level for human drinking water and aquatic life (Abousnina *et al.*, 2015; Mcbeth *et al.*, 2003; Nghiem *et al.*, 2011; Stearman *et al.*, 2014).

Other naturally occurring by-products of the coalification process are the semi-volatile organic compounds (benzene, toluene, ethylbenzene and xylenes often collectively named BTEX), along with polycyclic aromatic hydrocarbons (PAH such as naphthalene, phenanthrene, among others) which may be present in some CSG waters (Fakhru'l-Razi *et al.*, 2009; Leusch & Bartkow, 2010). Recent studies carried out in Australia have shown that the presence of these organic compounds is low and does not exceed the Australian Drinking Water Guidelines or USEPA Guidelines (Stearman *et al.*, 2014; Tang *et al.*, 2014). In addition to the organic compounds, some locations also present radioisotopes of radium, thorium and uranium that are transferred to the co-produced water in low levels are considered a low risk (Kinnon *et al.*, 2010; Stearman *et al.*, 2014; Tang *et al.*, 2014).

The water management of the co-produced water depends largely on its composition or water quality. CSG water is either disposed of or reused for beneficial usage. Depending on the water quality of the CSG water, surface discharge without treatment can be done directly or after being amended/treated to meet discharge specifications (EPA Queensland, 2008). CSG water can also be used for irrigation, wetlands, to supplement water supplies, or be injected into suitable subsurface aquifer formations with and without treatment according with the water quality specifications of the existing aquifer (All-Consulting, 2003). CSG operators are in charge of managing the co-produced water from their operations and regulators require that CSG producers find beneficial uses for the extracted water while minimising and remediating the negative environmental impacts that co-produced water could cause on the environment (EPA Queensland, 2010a; DERM, 2005).

Frequently, the cost of treating and handling CSG co-produced water is, to an extent, determinant on the feasibility of CSG operations. Because current methods are focused on the utilisation of desalination methods for the water treatment, that includes ion exchange pre-treatment, reverse osmosis for removal of solutes, remineralisation of treated water and brine management (USEPA, 2010). Therefore, water treatment technologies are required to treat CSG water at low capital and operating costs.

## Environmental impacts and beneficial use of co-produced CSG water

CSG water may affect the freshwater environment such as the ephemeral or perennial rivers, increasing the bottom sedimentation, bank scouring, or channel erosion affecting the stream ecology (Biggs *et al.*, 2012; Hamawand *et al.*, 2013; Vacher *et al.*, 2014). Freshwater ecosystems can be detrimentally affected due to exposure to elevated concentrations of TDS, bicarbonate, magnesium, chloride, and/or sulphate, impacting the chemistry of the waterways and also to some freshwater organisms (Khan & Kordek, 2014). Similar adverse effects on freshwater ecosystems may be observed if desalinated water with low salinity is released to ecosystems.

The direct impact of salinity on a particular species is likely to disrupt ecosystems processes such as: nutrient cycling, recycling and energy flow through trophic webs underpinning the overall health and integrity of the ecosystem (Davies, 2013). Toxic effects would be expected for simple multicellular organisms due to their lack of cellular osmoregulatory capabilities (Taylor *et al.*, 2013). It is also suggested that some of the macroinvertebrates individuals in the ecosystems in receiving CSG waters could benefit from the change in salinity, resulting in an overall shift of species composition of the particular ecosystem.

In Queensland, disposal of CSG water to waterways is considered appropriate only where no other feasible option for beneficial use can be found, and the disposal is a contingency measure to support beneficial use during high rainfall events. Environmental values will be protected despite the discharge and assessed relevant water quality guidelines (DEWS, 2012; DEHP, 2012a; DEHP, 2012b; DEWS, 2010b).

CSG waters may be applied to terrestrial environments either as a means of disposal by infiltration and evaporation or beneficial use for irrigation or dust suppression. In either case, disposal or beneficial use, inorganic dissolved salts present in the CSG water can accumulate over time within the soil profile by ion exchange processes affecting the physical and mechanical properties of the soil, the degree of dispersion of soil particles, permeability and stability of aggregates (DEWS, 2012; DERM, 2010b; DERM, 2011; Hamawand *et al.*, 2013).

Land application using CSG co-produced water may have adverse effects on soils and plants due to the high salinity and sodium concentration (Ezlit *et al.*, 2010). Salinity is the main driver of soil dispersion, which is directly related to permeability. Since CSG waters often have high sodium concentrations, interactions with this metal and soil can cause deterioration of the physical condition of the soil, such as waterlogging, formation of crusts and reduction of soil permeability. In some extreme cases, due to the physical damage of the soil structure infiltration rates are dramatically reduced, preventing plants or crops from accessing water for their normal growth (Johnston *et al.*, 2008; Oster, 1994). In contrast, calcium and magnesium cations when applied to soils enhance soil flocculation.

Salinity is referred as the accumulation of salt at the plants root levels reducing soil porosity, hydraulic conductivity and water storage, while high sodium concentration is often referred to sodicity and the sodium accumulation on the cation exchange complex of soil (Biggs *et al.*, 2012; DERM, 2011; Van De Graaff & Patterson, 2001).

Measures to prevent infiltration issues in soils due to irrigation with saline water with high sodium content include use of threshold values for soils based on the exchangeable sodium percentage (ESP). This index represents a proportion of sodium adsorbed by the soil as the proportion of cation exchange capacity (DERM, 2009; Ezlit *et al.*, 2010; Johnston *et al.*, 2008). Another index of use is the sodium adsorption ratio (SAR), which is an expression of the sodium concentration relative to concentrations of calcium and magnesium.

ESP is determined by the ratio of sodium cations to the total soil cation exchange capacity, and it is calculated using Eq. 2.1, where $Na^+$ is the exchangeable sodium, and

CEC is the cation exchange capacity of given soil. The units for ESP and CEC are milliequivalents per mass of soil (meq/100 g) (DERM, 2009). SAR is the exchange ratio of sodium to calcium and magnesium cations, and can be calculated using Eq.2.2, where $Na^+$, $Ca^{2+}$ and $Mg^{2+}$ are concentrations expressed in milliequivalents per litre (meq/L) (Rengasamy & Marchuk, 2011).

$$ESP = \frac{100*Na^+}{CEC} \qquad\qquad \textbf{Equation 2.1}$$

$$SAR = \frac{Na^+}{\sqrt{\frac{Ca^{2+}+Mg^{2+}}{2}}} \qquad\qquad \textbf{Equation 2.2}$$
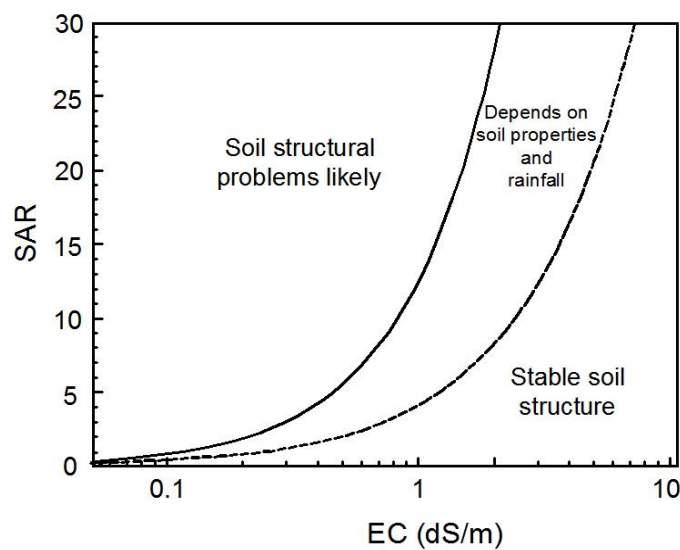


**Figure 2.7 Prediction and assessment of irrigation water in relation of its SAR and EC (DERM, 2011).**

The relationship between the SAR and the EC of irrigation water in relation to soil structure is shown in Figure 2.7. Water quality of CSG operations varies widely in the ranges of 300-180,000 mg/L for TDS and SAR greater than 50 (Arrow Energy Ltd, 2011; Mannhardt, 2009). It is expected that irrigation with this saline and high sodium concentration water causes dispersion of the soil in which it is being applied according with Figure 2.7. Infiltration rates in soils often decrease as SAR increases or as salinity increases, which in CSG waters both of these parameters is driven by the sodium concentration. Additionally, crops irrigated with high SAR waters and sodium can suffer of sodium accumulation in plant leaves causing leaf burn and limiting plant growth (Huang & Natrajan, 2006; Jackson & Reddy, 2007a; Johnston *et al.*, 2008; Oster, 1994). Although, SAR and ESP are acceptable indicators of possible soil

dispersion or flocculation, soil properties and external conditions could also influence the infiltration processes, which is the water with properties that fall in the area between the two curves in Figure 2.7.

If CSG co-produced water is likely to cause soil and vegetation problems, water quality parameters need to be adjusted before using the water for any beneficial use or disposal (Ezlit *et al.*, 2010; Hamawand *et al.*, 2013; Stearman *et al.*, 2014; Taulis, 2011). Therefore, CSG water needs to be treated in order to be suitable for a beneficial use such as irrigation, dust suppression or land disposal. State of Queensland (DEWS, 2012; DEHP, 2012a; DERM, 2010a; EPA Queensland, 2008) elaborated guidelines for beneficial use of irrigation or land disposal with CSG water based on the ANZECC minimum water quality requirements for irrigation (ANZECC, 2000). These guidelines apply the following criteria for the general approval to re-use CSG water for irrigation or land application purposes:

1. Irrigation shall not be applied to good quality agricultural land;
2. The maximum electrical conductivity (EC) shall not exceed 3,000 μS/cm;
3. The pH must be within the range of 6 - 8.5;
4. The maximum SAR shall not exceed 6 - 12;
5. The maximum bicarbonate ion concentration shall not exceed 100 mg/L;
6. The maximum fluoride concentration shall not exceed 1 mg/L;
7. Flood or related surface irrigation is specifically excluded;
8. Irrigation shall not be undertaken in circumstances where soil erosion is likely to occur;
9. Irrigation shall not be undertaken at a rate that results in water run-off to permanent water courses; and
10. The concentration of heavy metals described in ANZECC guidelines for irrigation water shall not be exceeded.

Water quality standards directed by the State of Queensland for the use of CSG co-produced water for irrigation (Table 2.3) minimise the impact of CSG water on soils by having a low SAR and reasonable EC parameters. Nonetheless, in order to ensure soil structure and avoid toxic effects, treated CSG water should be used in order to achieve a stable soil structure (Figure 2.8).

**Table 2.3 Water quality parameters for agricultural irrigation water for short term trigger values and water quality trigger values (low risk) for livestock watering using CSG co-produced water (DEHP, 2012b; DERM, 2010a; DERM, 2011; EPA Queensland, 2005; EPA Queensland, 2008).**

| Characteristic | | Short term trigger value in irrigation water (Short term use up to 20 years) (mg/L) | Trigger values for livestock drinking water (mg/L) |
|---|---|---|---|
| EC (dS/m) | | 1 to 3 | - |
| SAR | | 6 to 12 | - |
| TDS | Beef Cattle | | 5,000 |
| | Dairy Cattle | 1,500 to 5,000 | 4,000 |
| | Sheep/Horse/Pig | | 6,000 |
| Aluminium | | 20 | 5 |
| Arsenic | | 2 | 0.02 |
| Barium | | 2 | - |
| Beryllium | | - | 300 |
| Bicarbonate | | 100 | - |
| Boron | | 2 | 5 |
| Cadmium | | 0.05 | 0.01 |
| Calcium | | - | 1,000 |
| Chloride | | 700 | 2,000 |
| Chromium | | 1 | 1 |
| Cobalt | | 0.1 | 1 |
| Cooper | | 5 | 0.4 |
| Dissolved Oxygen | | - | > 3 |
| Ethylbenzene | | - | 0.3 |
| Fluoride | | 2 | 2 |
| Iron | | 10 | - |
| Lead | | 5 | 0.05 |
| Lithium | | 2.5 | - |
| Manganese | | 10 | - |
| Mercury | | 0.002 | 0.002 |
| Molybdenum | | 0.05 | 0.15 |
| Nickel | | 2 | 1 |
| Nitrate | | - | 100 |
| Nitrite | | - | 10 |
| Radionuclide | Gross alpha (excluding K-40) | - | 0.5 Bq/L |
| | Radium 226/228 | - | 5 Bq/L |
| | Uranium 238 | - | 0.2 Bq/L |
| Selenium | | - | 0.02 |
| Sodium | | 465 | - |
| Sulphate | | - | 1,000 |
| Toluene | | - | 0.8 |
| Uranium | | - | 0.2 |
| Vanadium | | - | 0.1 |
| Xylenes | | - | 0.6 |
| Zinc | | 5 | 2.5 |

The targeted parameters for SAR are 6-12 and EC are 2-5 dS/m. These parameters guarantee that the water used for irrigation or land application may have minimal impact on the soils structure because it is within the area of the on the graph where no soil or vegetation problems would be encountered (Bern *et al.*, 2013; DERM, 2009). Additionally, irrigation with water containing excess of sodium, chloride, boron, and/or zinc may significantly reduce crop yield due to toxicity for plants and potential accumulation in soils, threshold values are shown in Table 2.3 (ANZECC, 2000; DERM, 2009).

Among the beneficial uses of CSG co-produced water, livestock watering is a potential option. However, only suitable water with high quality should be used for successful livestock production. Guidelines have been developed to protect the livestock industry and reduce human health risk associated with livestock watering when CSG co-produced water is used. Trigger water quality parameters for livestock are presented in Table 2.3. Some animal species can tolerate salinity better than others and older animals are able to tolerate higher salinity levels than younger animals (Nghiem *et al.*, 2011; Oldridge & Whatman, 2009). Feed livestock with CSG co-produced water may produce residues of contaminants in animal products that can affect directly human health. Queensland Government (DEHP, 2013) and ANZECC (2000) provided the minimum guidelines for livestock watering using co-produced water from CSG operations to safeguard and provide new resources to the livestock industry (Table 2.3) (ANZECC, 2000; DERM, 2009).

Summarising, the chemical signature of CSG co-produced waters can be described as $Na^+$-$Cl^-$-$HCO_3^-$ or $Na^+$-$HCO_3^-$ type with high salinity, low concentrations of calcium, magnesium, sulphate and low content of trace elements and organic compounds. The high sodium concentrations lead to high salinity and high SAR which may have significant impact in the environment when CSG water is used for land, waterway discharge or agriculture applications without the corrective treatment and water quality standards needed for beneficial usage or disposal. CSG water in Australia usually exhibits low levels of trace elements and organic compounds. Nonetheless, the minimum water quality standards must be a guarantee for all uses and disposal methods as per the state government policies prior usage.

# Current treatment methods for CSG co-produced water

The variability of major and trace elements in CSG water challenges the selection of available technologies to accomplish the task of treatment, and adequate integration of multiple treatment processes is often required (Abousnina *et al.*, 2015; Fakhru'l-Razi *et al.*, 2009; Fell Consulting Pty Ltd, 2014). A typical treatment process (Figure 2.8) involves the removal of fine particles by disc filtration followed by ultrafiltration membranes. Then, synthetic ion exchange resins are used to remove ions that may precipitate prior to the reverse osmosis system. The final product water is chemically conditioned adjusting pH and conductivity for beneficial use. Along the treatment process, the use of chemicals to avoid scaling/fouling and periodic chemical cleaning of filtration systems is unavoidable.
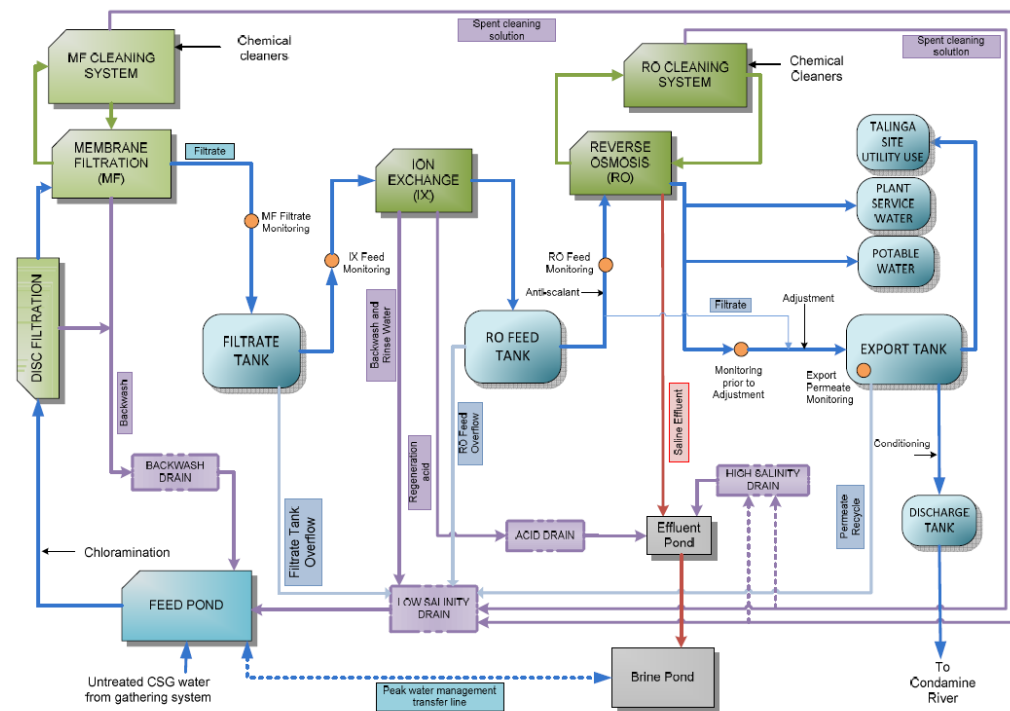


**Figure 2.8 Talinga Water treatment facility process schematic at Australia Pacific LNG (Australia Pacific Lng Pty, 2011).**

The current technologies used to treat CSG water are referred to as desalinisation processes, which are able to reduce the salinity and concentration of other ions (Arrow Energy Ltd, 2011; Hamawand *et al.*, 2013). The membrane processes, distillation, electrodialysis and ion exchange resins preferred for the treatment are costly (AUD $ 2/m$^3$) and in some cases ineffective due to the chemistry and composition of the CSG

water (Fell Consulting Pty Ltd, 2014; Mannhardt, 2009). Therefore, a combination of these technologies is usually necessary to reduce salinity and ionic concentration of some elements that compose CSG water (for example Figure 2.8). In only a few cases, CSG waters require little to no treatment to achieve water quality parameters dictated for beneficial use or discharge policies.

The overall costs of managing CSG co-produced water can constrain the gas production making it unprofitable, since the treatment cost is about 3 - 15% of the sale price of the gas (Fell Consulting Pty Ltd, 2014). To exemplify, a CSG project in which the surface discharge, irrigation, disposal and impoundments of co-produced water requires an investment of AUD $1.6 billion to accord with an environmental impact statement (Fell Consulting Pty Ltd, 2014). For instance, a CSG operator in Queensland invested AUD $1 billion by 2014 in water treatment facilities and water infrastructure for the management of the co-produced water (Q.G.C. Pty Ltd, 2013). Therefore, there is a need in the CSG industry for a cost-effective treatment alternative that complies with the water quality required for beneficial usage and disposal.

Additionally, membrane filtration generates large volumes of concentrated CSG water (10 – 15% of inflow water) as wastewater that requires additional disposal, increasing capital and operating costs for the management of co-produced water (Fell Consulting Pty Ltd, 2014; Hamawand *et al.*, 2013). Often, further costly technologies to reduce concentrated volumes such as membrane distillation, brine concentrator, may also be required.

### Chemical adjustment and granular filtration

Chemical adjustment is a simple and relatively inexpensive technique used to neutralise the pH of CSG waters (USEPA, 2010). Since CSG water presents high alkalinity, suitable acidic substances (either weak or strong acids) are added in to neutralise the pH and provide buffering. This chemical enhancement will have little to no effect on the composition of major dissolved ions found in CSG water. Although the chemical adjustment is a simple and inexpensive alternative, ongoing water monitoring is required to adapt the treatment to the influent water quality parameters. Chemical addition (such as NaOH) as well as aeration of CSG waters is often used to facilitate sedimentation and precipitation of oxidising metals such as iron, which is an

important aesthetic quality parameter. Filtration through sand or activated carbon granular media is usually used to reduce turbidity that may increase after chemical addition due to solubilisation of some suspended particles and slow precipitation of metals (Mannhardt, 2009). Media filtration removes solid particles, precipitated metals and some other contaminants found in suspension in CSG water.

### Membrane filtration

To reduce ionic concentration levels, membrane treatment and particularly reverse osmosis (RO) has been used in broad applications including desalination of seawater, brackish water and industrial applications (Li, 2012; Mccool *et al.*, 2010). An evaluation of the economic feasibility of several desalination technologies was carried out in Australia in 2004, and concluded that RO technology is the most economic technology for the treatment of CSG water (Fell Consulting Pty Ltd, 2014; Mannhardt, 2009). Contaminants such as heavy metals and organics can also be removed through membrane filtrate using ultrafiltration (UF) and reverse osmosis (RO) membranes, as seen in Figure 2.9 (Mannhardt, 2009; Mondal & Wickramasinghe, 2008; Nghiem *et al.*, 2015).
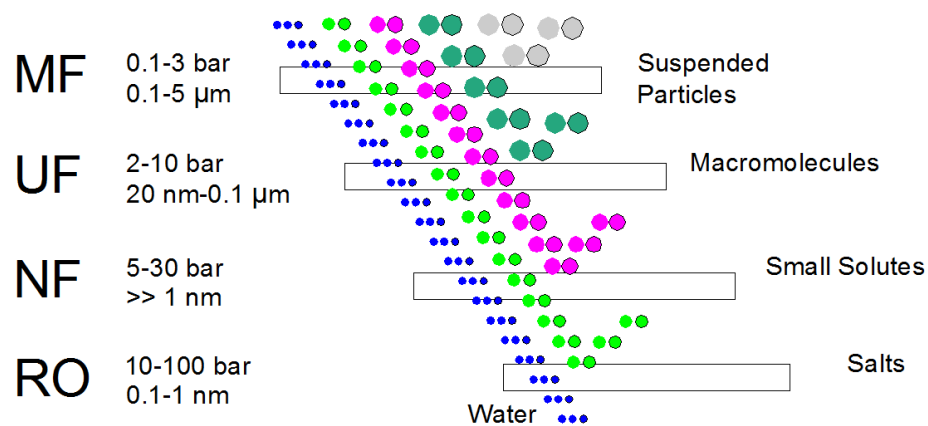


**Figure 2.9 Membrane technology for separation solutes (Howe *et al.*, 2012). Mircofiltration (MF), ultrafiltration (UF), nano filtration (NF) and reverse osmosis (RO) are comcercial membrane tehcnologies available.**

The RO membrane element is a semipermeable material that allows the water flow through but not suspended particles and dissolved solutes that may be contained in the feed water (Figure 2.9). Membrane elements are able to remove suspended particles of about 0.1 to 5 micrometres as well as in solutes of 0.1 to 1 nanometres in size.

Pressure is essential in the process to remove the particles. The smaller the particle size and the lower the desired concentration of the effluent the greater pressure is needed. The main drawbacks of using membrane technology for the treatment of CSG waters are the high energy demand of the process to operate at elevated pressures, the high capital and operational costs associated with the process, and the creation of a concentrated stream with higher concentration of dissolved inorganic salts that may pose significant impact to the environment (Abousnina *et al.*, 2015; Howe *et al.*, 2012; Nghiem *et al.*, 2011). RO membranes are typically a polyamide think film composite (TFC) membrane in a spiral wound configuration or hollow fibre with a pore size of approximately $0.0005\mu m$ (Figure 2.10) (Li, 2012).
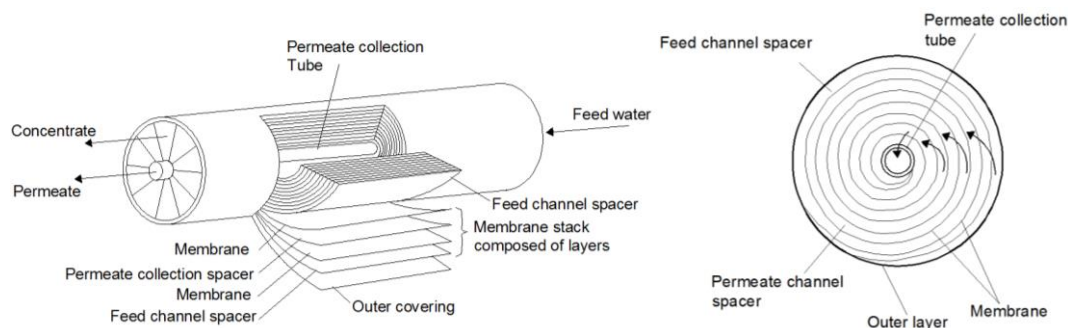


**Figure 2.10 Spiral wound membrane element (Greenlee *et al.*, 2009).**

Membranes used for desalinisation of CSG water are susceptible to fouling through different mechanisms. The primary sources of fouling and scaling are particulate matter, precipitation of salts which is known as scaling, oxidation of soluble metals and biological matter (Van De Lisdonk *et al.*, 2000). The average life span of a RO membrane element is 2-5 years depending feed conditions (Alghoul *et al.*, 2009). For CSG waters, pH needs to be corrected due to the high alkalinity attributed to bicarbonate ions that may cause precipitation, scaling and fouling of metals during the RO process, the target pH is a neutral to slightly acidic (6-7). Anti-scalant is used in RO processes and modifies the pH of the feed stream, reducing the salt and metals precipitate. Permeate water obtained from RO system is typically low in hardness and alkalinity, and acidic pH, thus post-treatment is required (Li, 2012).

### Electrodialysis

Electrodialysis (ED) and electrodialysis reversal (EDR) processes are considered as a membrane application in which ions are separated through semipermeable membrane

under the influence of an electrical potential. The electrical driven process reduces dissolved contaminants present that may be in CSG waters. Membranes are ion selective, charged negatively for cation selective membrane and positively charged for anion selective membrane, therefore rejecting ions of different charge (Figure 2.11) (Valero *et al.*, 2011). By placing multiple membranes next to each other separated by channelled spacers, water can flow across the membrane surface, and ions can flow through membranes and be removed from solution (Figure 2.11).
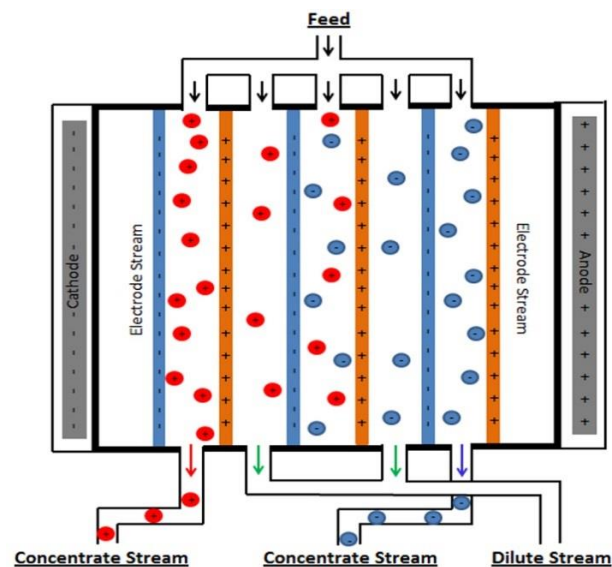


**Figure 2.11 Schematic of EC system principles (Valero *et al.*, 2011). Water flows through the channels, voltage is applied causing ions to migrate towards the opposite charge and restrain by membranes.**

ED and EDR can deal with TDS concentrations as high as 15,000 mg/L, removing up to 95% of the salt content (Mcgovern & Zubair, 2014). It is considered an attractive technology for the treatment of CSG water due to long membrane lifespan of 8-10 years and reduced cost of maintenance. This technology has not been adopted by CSG operators but research studies have highlighted the major economical and operational benefits of implementing EDR for the treatment of co-produced waters (Sajtar & Bagley, 2009).

### Ion exchange resins

Ion exchange is a process used in water treatment applications to remove specific dissolved ions that are in excess for different applications. In potable treatment applications, ion exchange technology is primarily used for water softening (removal

of $Ca^{2+}$ by exchange with $Na^+$), and demineralisation (Alchin, 2013). Ion exchange systems are a potentially attractive option for treatment CSG waters as it desalinate water by targeting nauseous ions with the potential of generating relatively small brine volume by using resins able to remove positive and negative ions (Millar *et al.*, 2015a). Additionally, ion exchange is currently used in most RO systems as water softener as for the pre-treatment of CSG water (Venkatesan & Wankat, 2011).
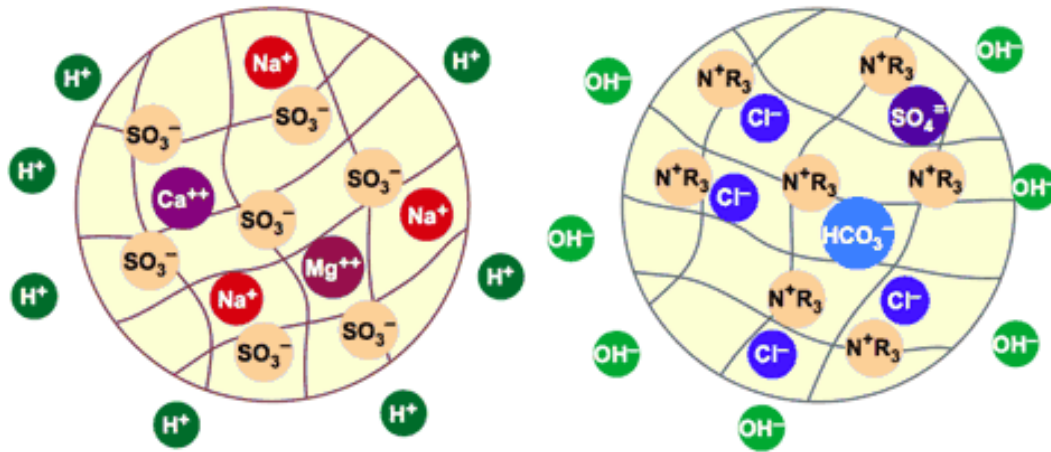


**Figure 2.12 Resins beads with cation (left) and anion (right) exchange capacities. The negative charge on the resin allows to exchange $H^+$ for cations dissolved in solution such as $Na^+$ or $Ca^{2+}$. While, positive charged resin is able to remove anions such $Cl^-$ or $HCO_3^-$ by exchanging $OH^-$. Combination of these two resins allow demineralisation of the solution (Crittenden *et al.*, 2012).**

Ion exchange materials are synthetic polymeric resins, which are specially designed to selectively remove cations and anions (Figure 2.12). Resins are strong acid exchangers and strong base exchangers that are able to exchange a wide range of cations and anions for hydrogen ions ($H^+$) or hydroxide ions ($OH^-$), respectively. Often hydrogen and hydroxide ions may be subsequently neutralised by pH adjustment (Helfferich, 1962).

A typical strong acid cation resin has a capacity between 180 to 220 meq/L, and a strong base anion exchange resin has a total capacity of 110 to 140 meq/L (Helfferich, 1962). The operating capacity of resins is about 40 to 70% of the total capacity depending on the operation conditions. Cationic resins are able to remove many cations following this selectivity order $Pb^{2+} > Ca^{2+} > Mg^{2+} > Na^+ > H^+$. Selectivity order for some of the anions that are able to be removed with anionic resins are $SO_4^- > NO_3^- > Cl^- > HCO_3^- > OH^- > F^-$ (Wachinski, 2006). From the selectivity series, it is

clear that $Na^+$ is less selective than other ions and may have low removal rates when used for treatment of CSG water. When concentration of ionic contaminants is high, as $Na^+$ in CSG water, the resins are loaded quickly, requiring increased frequencies of regeneration; this can be an uneconomical treatment method. Also, non-ionised contaminants in CSG waters will not be removed by ion exchange.

Currently different commercial processes using synthetic ion exchange resins are used in treatment of CSG water, which are Higgins Loop, Drake system and Eco-Tec RecoPur System (Richard, 2011). The Higgins Loop is a continuous counter current ion exchange contactor packed with resins and divided in four zones or loops, which are adsorption, regeneration, backwashing and pulsing. This process is able to reduce 98% of sodium concentration, lower TDS and treat about 4000 $m^3$ per day per unit (All-Consulting & Montana Board of Oil & Gas Conservation, 2002). The Drake system is a variation of Higgins Loop for treatment of CSG waters rich in sodium bicarbonate and able to minimise the amount of brine. Finally, Eco-Tec RecoPur System uses a combination of resin beads in order to remove cations and anions simultaneously producing about 4300 $m^3$ per day (Richard, 2011).

## The adsorption process

Adsorption is the process that describes the capture of solute from solution by transferring solute to the external and internal surfaces of a solid material (Thomas & Crittenden, 1998). The solute that undergoes adsorption onto the surface is the adsorbate, and the solid onto which the solute is adsorbed is called the adsorbent. Adsorption can be classified in two main categories according to the type of bond formed between the adsorbate and adsorbent:

- Physical adsorption: In physical adsorption, the adsorbate is confined to the surface by relatively weak van der Waals forces (Inglezakis & Poulopoulos, 2006). Weak bonds formed makes physical adsorption a nonspecific reversible reaction that it is driven by the adsorbate which can desorbs in response to a decrease in solution concentration or displacement by more strongly adsorbed species (Crittenden *et al.*, 2012).

- Chemical adsorption: Occurs when the adsorbate reacts with the adsorbent forming a covalent or ionic bonds. Covalent bonds are formed with shorter bond length and higher bond energy for particular functional groups on the adsorbent (Thomas & Crittenden, 1998). Consequently, covalent bonds are stronger than those formed through ionic bonding, hence it is usually an irreversible process. Ionic bonding is related to ion exchange processes in which attraction forces between ions or charged functional groups in solution are attracted to the adsorbent, displacing ions of the same charge on the surface of the adsorbent following Coulomb's law and making the process reversible (Crittenden *et al.*, 2012; Inglezakis & Poulopoulos, 2006).

### Adsorption and ion exchange

The ion exchange process is similar to adsorption, since the diffusion process occurs by mass transfer from a solution phase to a solid phase, which is common in both processes (Inglezakis & Poulopoulos, 2006). Ion exchange is a sorption process where charged ions are adsorbed, while in the case of adsorption the adsorbed species are electrically neutral. It is generally accepted that ion exchange and adsorption processes are sorption processes and are grouped together in practical applications (Inglezakis & Poulopoulos, 2006; Kumar & Jain, 2013; Wachinski, 2006).

The sorption process has been studied for decades and mathematical models and approaches have been developed originally for adsorption rather than merely for ion exchanges processes (Helfferich, 1962). However, sorption models are applicable with minor modification to ion exchange processes according to the practical application. The applicability of sorption theories on ion exchange depends more on the mode of operation than on the particular mechanism of solute uptake. Modifications in the theories are focused on the ion exclusion and ligand exchange. A significant feature of physical adsorption is the rate of the process, which is generally too high and consequently is controlled by mass or heat transfer resistance, rather than by intrinsic sorption kinetics (Clifford, 1999; Kammerer *et al.*, 2010).

### Materials used for adsorption processes

There are a number of materials that are currently used in different applications ranging natural to those that are synthetically manufactured for removal of exceptional contaminants. Some of the adsorbent materials used include: activated carbon, activated alumina, silica gels, ion exchange resins and synthetic molecular sieves (Wachinski, 2006).

### Activated carbon

Activated carbon is an adsorbent that has proven to remove organic and inorganic compounds for water treatment applications. Activated carbon is made from carbonaceous materials such as coal, hard wood, rice husks, bagasse ash, nutshells, and saw dust among others. However, these materials are not intrinsically porous and hence activation to generate fine porous is needed. Activation of the material is achieved by steam or carbon dioxide at elevated temperatures reaching 1000 °C to remove tarry carbonisation formed during pyrolysis, thereby cleaning pores in the material (Qi & Levan, 2005). Generally, the total surface area of activated carbon ranges between 300 – 1500 $m^2/g$ and the pore volume ranges between 0.7 – 1.8 $cm^3/g$ (Clifford, 1999). Activated carbon has a micro-crystalline structure, which is often organophilic hence efficient removal of organic compounds.

### Activated alumina

Bauxite is a naturally occurring hydrated alumina oxide rock that is activated by heating to 230 - 815 °C that creates a large porous surface known as activated alumina. The activation of bauxite is a complex process because the crystal structure undergoes various stages of hydration over the whole process due to changes in temperature (Inglezakis & Poulopoulos, 2006). The activated surface exhibits acidic and basic characteristics that reflect the amphoteric nature of the aluminium metal and high affinity for water (able to neutralise acid and base). Activated alumina has a large surface area between 200 – 400 $m^2/g$ and pore diameters in the range of 2 – 5 nm (Thomas & Crittenden, 1998). Activated alumina is usually used for adsorption processes that occur at elevated temperatures such as percolation treatment of petroleum products and drying air.

**Silica gels**

Silica gel is probably the most widely used desiccant due to its hydrophilic nature, large capacity to adsorb water and regeneration capability. Silica gel is partially dehydrated from polymeric colloidal silicic acid. It is formed when sodium silicate is acidified producing agglomerate of microparticles followed by heating expelling water leaving a hard, glassy porous structure. Surface area of silica gel typically ranges between $300 - 850$ m$^2$/g and pore diameter in the range of $22 - 150$ Å (Thomas & Crittenden, 1998). Silica gels are used for dehydration of air and gases.

**Molecular sieves**

Molecular sieves are used for their effective separation by their intrinsic shape and selectivity towards contaminants. The most common molecular sieves are zeolites which are a porous crystalline aluminosilicate structure of $SiO_4$ and $AlO_4$ tetrahedral joined by oxygen atoms (Inglezakis & Poulopoulos, 2006). Molecular sieves such as zeolite occur naturally and can be synthetically produced. Over 40 natural occurring zeolites are known and have important commercial use. More than 150 types of zeolite have been synthesised for a wide range of applications being type A and X the most commercially used (Thomas & Crittenden, 1998). Both A and X zeolites are synthetised by using different aluminium, silica and sodium ratios resulting in a hydrogel which is dried at 100 °C (El-Kamash, 2008). The theoretical cation exchange capacity for these synthetic molecular sieves is about 545 meq/100 g, but often in water treatment applications exhibit 82 meq/100 g (El-Kamash *et al.*, 2005).

Cavities contained within the framework of a molecular sieve are connected by channels, which are of molecular dimensions and into which adsorbate molecules can penetrate. The process of adsorption and desorption of molecules in molecular sieves are based on differences in molecular size, shape and other properties such as polarity. Molecular sieves have a surface area ranging between $600$ -$700$ m$^2$/g and pore sizes between $3.9 - 8$ Å (Thomas & Crittenden, 1998).

Synthetic molecular sieves can be manufactured with different Si/Al ratios. Consequently, different cationic structures and thus different adsorptive properties may be tailored for the appropriate choice of framework structure, achieving higher selectivity during the separation process. Synthetic molecular sieves are extremely

polar and therefore separations may occur using both molecular sieving and polar surface effects. Commercial molecular sieves are produced by the crystallisation of gels under hydrothermal conditions in closed systems at a set temperature ($25 - 200$ °C) over hours or longer (Thomas & Crittenden, 1998). Crystals are then mixed with clay binder to form pellets (spheres or extrudes) before being dried and fired to produce calcination, providing the final product. Synthetic molecular sieves with high ionic affinity are used in water treatment application for removal of contaminants, such as $Cs^+$, $Sr^{2+}$, $Zn^{2+}$ and $Cd^{2+}$ (El-Kamash et al., 2005).

**Polymeric resin adsorbents**

Resins are porous polymers with 0.6 mm of diameter onto which functional groups are attached containing a fixed ion that cannot be removed or displaced. To preserve the electrical neutrality of the resin, each fixed ion is neutralised with a counter ion. This counter ion is mobile and can migrate into and out of the resin bead. The cation resin beads have sulphonate ($SO_3^-$) groups attached to the resin structure, attracting positive charge ions such as sodium. The anion resin beads have similar structure, but the functional group comprises of quaternary ammonium cations ($N(CH_3)_3^+$). Each ion going into the bead is replaced by an ion getting out of the bead, preserving electrical neutrality and this process is known as ion exchange (Harland, 1994; Wachinski, 2006). Ion exchange resins are used as adsorbents for a broad range of applications, including water softening and demineralisation.

## The ion exchange theory

Ion exchange process is defined as the reversible exchange between ions in solution phase (adsorbate) and ions in a solid phase (adsorbent) (Helfferich, 1962). Ion exchange occurs in a two-way transfer between solution and solid phase. Ions transferred to the solid phase must be exchanged by an equal amount of ions shifted from the solid phase to the solution phase to maintain electrical neutrality and stoichiometry in both phases (Harland, 1994; Helfferich, 1962; Inglezakis & Poulopoulos, 2006).

The ion exchange process is described by the following equation:
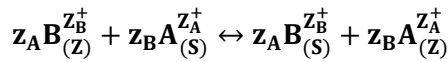
$$z_A B_{(Z)}^{Z_B^+} + z_B A_{(S)}^{Z_A^+} \leftrightarrow z_A B_{(S)}^{Z_B^+} + z_B A_{(Z)}^{Z_A^+} \qquad \text{Equation 2.3}$$

where, $z_A$ and $z_B$ are the charges of the exchanging cations A and B, and subscripts S and Z correspond to the solution and solid phase correspondingly. When the exchanger is loaded with ions A comes in contact with a solution containing counter ions B, ions A will be exchanged for ions B in equivalent amounts and will change phase from solution to solid. This exchange will lead to changes in solution content of A and B ions until equilibrium is reached. The concentration ratio of A and B ions may not necessary be the same in both phases after equilibrium (Townsend, 1986; Townsend & Coker, 2001). The metric unit used to measure ion exchange or ion interaction is millimol [mmol] which can be calculated as the concentration of the element or functional group divided by its equivalent molecular weight in milliequivalents [meq] (equivalent molecular weight is the element or functional group molecular weight divided by its valency).

An ion exchanger consists of a framework of negative or positive electric surplus charge with associated mobile counter ions (Helfferich, 1962). The features that characterise an ideal exchanger are controlled by effective ion exchange capacity, rate of exchange, ion selectivity, mechanical strength, consistency of particle size and effective surface area (Harland, 1994). Ion exchange between a solid exchanger and water containing electrolytes occurs without structural changes to the solid exchanger. The ions in the solution rapidly diffuse into the molecular framework of the exchanger. The exchanged ions diffuse out of the exchanger and into the bulk solution.

Ion exchange is an intrinsic property of both natural and synthetic zeolite materials. Natural zeolites exhibit ion exchange, adsorption and molecular sieving properties as well as a widespread abundance worldwide generating a particular interest for its use in practical applications in water treatment (Inglezakis & Poulopoulos, 2006). Other commonly available natural materials such as basaltic material also exhibit comparable adsorption capacities as zeolite materials. Basaltic material such scoria has been used in a number of applications from construction to water filtration featuring promising results in the adsorption of heavy metals such as $Cd^{2+}$, $Cu^{2+}$, $Pb^{2+}$, $Zn^{2+}$ and $As^{3+}$ from aqueous solutions (El-Shafai & Zahid, 2013; Kwon et al., 2005).

The ion exchange properties of a material can be studied in batch and fixed bed column mode. The batch mode is conducted to determine the performance of the material under comparable conditions with measurement of the effective cation exchange capacity, adsorption kinetics, adsorption behaviour at different concentrations, cation selectivity and performance of treated material. Use of fixed bed columns allow study of dynamic behaviour, which is the most common adsorption arrangement used in water treatment applications.

## Natural zeolites

Natural zeolite minerals are ion exchangers with a crystalline, porous three dimensional aluminosilicate structure capable of exchanging alkali ($Na^+$ or $K^+$) and alkaline ($Ca^{2+}$) cations. The zeolite structure is based on a tetrahedral $(SiAl)O_4$ three dimensional framework with four oxygen atoms shared by an adjacent tetrahedral (Figure 2.13) (Townsend & Coker, 2001; Zaidi, 2012). This crystal framework has a channel structure of molecular dimensions ranging from 3-10 Angstroms (Å). The negative surplus charge of the zeolite comes from the $Si^{4+}$ which is substituted by $Al^{3+}$ and balanced with cations such as $Na^+$, potassium $K^+$, $Ca^{2+}$ or $Mg^{2+}$ (Pabalan & Bertetti, 2001). The exchangeable cations in a zeolite structure are loosely held in the anionic framework. Therefore, cations can be removed easily by washing the zeolite with demineralised water or a concentrated solution of another cation. Ion exchange behaviour in zeolites depends on the framework topology, ion size and shape, ionic charge and concentration of external electrolyte solution (Pabalan & Bertetti, 2001).

Natural zeolites are the main mineral components in altered volcaniclastic and sedimentary rocks ranging in age and composition (Clifford, 1999). They form by alteration mainly of volcanic glass in various geological environments, under variable geochemical and temperature conditions. Temperature is a determinative factor in zeolitic alteration, controlling the type of zeolite species, which may form, as well as the reaction rate. The Greek name for zeolite is to boil "$\zeta\acute{\varepsilon}\iota\nu$", and stone "$\lambda\acute{\iota}\theta o\varsigma$" which describes the behaviour under fast heating conditions, when zeolites seem to boil due to the rapid loss of water (Inglezakis & Zorpas, 2012b). The most common zeolites worldwide are chabazite, clinoptilolite, erionite, mordenite and phillipsite (Inglezakis & Poulopoulos, 2006). These zeolites differ in molecular structure and thus ion

exchange capacity, and channel dimensions. Zeolites are commercially utilised due to a number of important characteristics:

- Defined framework structure and uniformity of molecular sized channels and cavities in which cations diffuse in order to be exchange sites within the crystal structure;

- The molecular zeolite framework permits the sieving of molecules in fluids such as gas or water (Clifford, 1999). Molecular sieving properties have great potential for industrial applications for separation process;

- High rate of exchangeable cations determined by the number of negative sites created by the aluminium content in the framework. The higher the aluminium concentration the greater the negative charges for cations (Worch, 2012). However, dealumination can occur in natural zeolites under given circumstances.
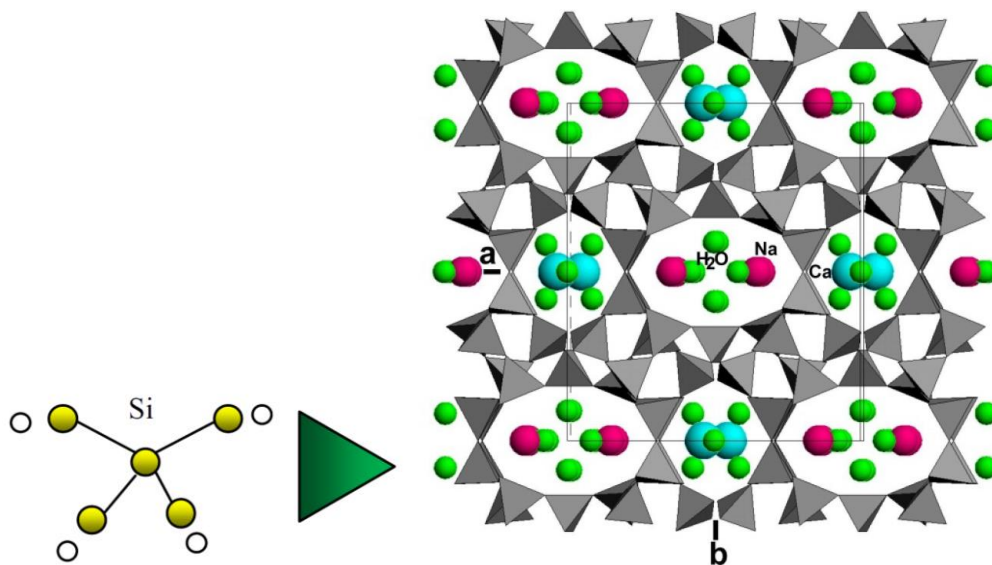


**Figure 2.13 Tetrahedral (SiO₄) structure and composition of the framework structure of a clinoptilolite structure with water molecules and cations on the exchangeable sites for a,b phase (Inglezakis & Zorpas, 2012b).**

Natural zeolites have benefits over other exchange materials in that they are relatively cheap, with a range of zeolites available with selectivity towards some ions. However, the efficiency of zeolites in water treatment applications depends on the particle size, cation exchange capacity, initial concentration of contaminants, pH of the feeding

solution, ion strength of the solution, temperature, contact time, anions and organic compounds (Margeta *et al.*, 2013).

**Table 2.4 Natural zeolites typical composition and properties (Pabalan & Bertetti, 2001).**

| Zeolite | Typical Unit-Cell Formula | Specific gravity | Channel dimension (Å) | Ion exchange capacity (meq/100 g) |
|---|---|---|---|---|
| Analcime | $Na_{16}(Al_{16}Si_{32}O_{96}).16H_2O$ | 2.24-2.29 | 2.6 | 454 |
| Chabazite | $(Na_2Ca)6(Al_{12}Si_{24}O_{72}).40H_2O$ | 2.05-2.10 | 3.7x4.2 | 381 |
| Clinoptilolite | $(Na_4K_4)(Al_8Si_{40}O_{96}).24H_2O$ | 2.16 | 3.9x5.4 | 254 |
| Erionite | $(Na_2Ca_6K)9(Al_9Si_{27}O_{27}).27H_2O$ | 2.02-2.08 | 3.6x5.2 | 312 |
| Ferrierite | $(Na_2Mg_2)(Al_6Si_{30}O_{70}).18H_2O$ | 2.14-2.21 | 4.3x5.5 3.4x4.8 | 223 |
| Heulandite | $Ca_4(Al_8Si_{28}O_{72}).24H_2O$ | 2.10-2.20 | 4.0x5.5 4.1x4.7 | 291 |
| Laumontite | $Ca4(Al_8Si_{16}O_{48}).16H_2O$ | 2.20-2.30 | 4.6x6.3 | 425 |
| Mordenite | $Na_8(Al_8Si_{40}O_{96}).24H_2O$ | 2.12-2.15 | 2.9x5.7 | 229 |
| Phillipsite | $(Na_2K)10(Al_{10}Si_{22}O_{62}).20H_2O$ | 2.15-2.20 | 4.2x4.4 2.8x4.8 | 387 |

Regardless of the formation mechanism and mineral composition, zeolite deposits are characterised as sedimentary deposits. The most common parent material for zeolite materials is volcanic glass of silicic, alkali or mafic composition. Feldspar and silica may also act as precursors in the formation of zeolite minerals (Inglezakis & Poulopoulos, 2006). Natural zeolites are presently limited to authigenic (precipitation or crystallisation), and alteration settings in finely crystalline sedimentary rocks including: analcime, chabazite, clinoptilolite, erionite, ferrierite, heulandties, laumonite, mordenite and phillipsite (Mumpton, 1999). Table 2.5 lists the typical formulae based on their chemical composition and properties for some natural zeolites. The cation exchange capacity (CEC) is a function of the degree of substitution of aluminium with silicon, and frequently the relationship is described by the silicon – aluminium ratio (Si/Al). The closer Si/Al is to unity, the higher the CEC would be greater because aluminium was included within the framework, providing additional exchangeable sites (Auerbach *et al.*, 2003).

### Vesicular basaltic volcanic rock - Scoria

Vesicular volcanic rocks have proved to be an efficient low-cost sorbent material for the treatment of complex industrial wastewaters containing heavy metals and arsenic (Kitsopoulos, 1999; Kwon *et al.*, 2005; Kwon *et al.*, 2010; Morgan-Sagastume &

Noyola, 2008). Scoria material is formed of vesicular fine to coarse fragments, the characteristic colours are reddish or black, and the material is light weight. Glass and phenocrysts basaltic materials such as scoria consist of plagioclase, olivine, hornblende and pyroxene minerals, with fine iron oxides and small amounts of clay minerals (Alemayehu & Lennartz, 2009).

Volcanic rocks have received considerable interest for heavy metals removal mainly due to their valuable characteristics as a natural adsorbent material such as: high surface area, low cost, large available quantities, and cation capacity (Table 2.5). Volcanic rocks are formed from volcanic magma and the most abundant rocks are pumice and scoria. These materials are often found in areas of young volcanic activity in places such as Italy, Turkey, Greece, Central America and East Africa (Alemayehu & Lennartz, 2009; Hay, 1986; Silva *et al.*, 1993).

**Table 2.5 Physical and chemical characteristic of scoria material (Alemayehu *et al.*, 2011; Kwon *et al.*, 2005).**

| Chemical Composition | Scoria - Ethiopia | Scoria-Korea |
|---|---|---|
| $SiO_2$ | 47.4 | 48.02 |
| $Al_2O_3$ | 21.6 | 15.18 |
| $Fe_2O_3$ | 8.9 | 12.24 |
| CaO | 12.4 | 8.66 |
| $K_2O$ | 0.5 | 1.36 |
| $Na_2O$ | 3.0 | 2.67 |
| MgO | 3.3 | 7.84 |
| $TiO_2$ | 1.7 | 2.41 |
| Others | 1.2 | 1.66 |
| **Physical properties** | | |
| Particle size (mm) | 0.075-0.425 | 0.1-0.2 |
| Porosity (%) | 36.0 | |
| Particle density (g/cm$^3$) | 2.96 | |
| Specific surface area (BET) (m$^2$/g) | 2.5 | 4.77 |
| Cation exchange capacity (meq/100 g) | 0.09 | 16.1 |

The chemical composition of basaltic scoria (Table 2.5) includes $40 - 60\%$ $SiO_2$ and $10 - 25\%$ $Al_2O_3$. Other elements in oxide form that are characteristic of scoria are $Fe_2O_3$ and CaO with about 15% each. This composition might be analogous to ion exchange materials such as zeolite but it has different mineral structures that are different compared to zeolite. Plagioclase minerals such as anorthite that are often present in scoria have a silicon tetrahedral framework substituted by aluminium, which

creates a negative charge that is balanced by cations, similar to those properties described for zeolite materials. Kwon *et al.* (2010) and Alemayehu and Lennartz (2009) used scoria for the removal of divalent heavy metals and arsenic from aqueous solutions, showing that this material effectively reduced concentrations of cations in solutions.

## Cation exchange capacity (CEC)

The cation exchange capacity (CEC) of an ion exchanger can be described as the number of moles of adsorbed cation charges that can be displaced by an index ion per unit mass of exchanger (Rhoades, 1982). In general terms, the CEC of an exchanger sample is the maximum negative surface charge indicating the potential cation exchange capacity of a soil sample (Zaidi, 2012).

The method commonly used to estimate CEC of a cation exchanger involves equilibration of a batch of sample solution of the exchanger with a solution of a known cation and calculating the uptake of the cation (Cerri *et al.*, 2002; Rhoades, 1982). However, it is important to recognise that CEC is only the amount uptake by unit of mass of exchanger under the specific conditions of the test (Lehto & Harjula, 1995).
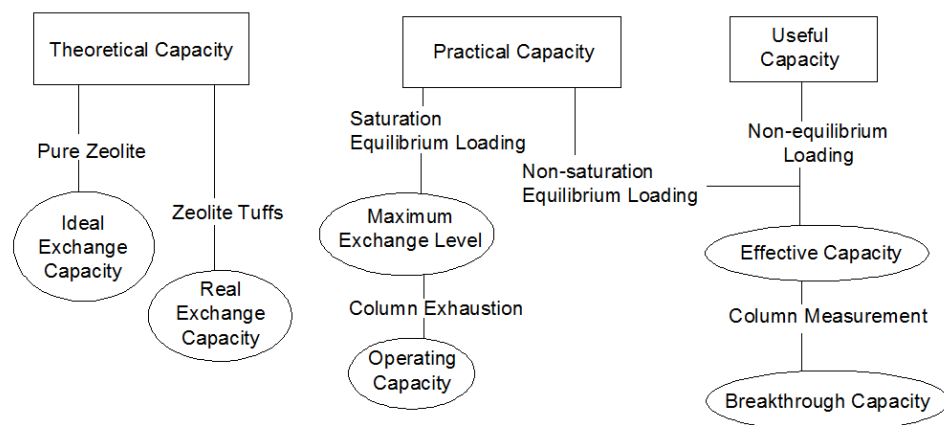


**Figure 2.14 Ion exchange definitions for natural exchangers (Inglezakis, 2005).**

IUPAC (1971) defines and standardises ion exchange terminology in the context of synthetic ion exchangers. Inglezakis (2005) introduced new terminology for natural exchangers. It was proposed to divide the capacity of natural exchange system in seven different types including ideal, theoretical, real, maximum, operating, breakthrough

and effective exchange capacity. Inglezakis (2005) split the capacity in three different categories, theoretical, practical and useful capacity. Each of these categories are further sub-divided depending on the exchanger's purity and methodology used to determine the capacity (Figure 2.14).

The theoretical or ideal exchange capacity in natural cation exchangers can be deduced from their aluminium content. The exchanger is rarely present in a pure state, and thus the elevation of real exchange capacity is commonly used. The maximum real exchange level is obtained from equilibrium behaviour at a specific temperature and concentration of the solution. Operating capacity is influenced by the dynamics of the column experiment and hence the operational conditions will impact the capacity.

An accurate CEC determination is crucial for the assessment of any ion exchange material, since the effectiveness of the exchanger for a determined application is based on this value. The REC is the one that measures the actual amount of cations that can be desorbed by ion exchange means, therefore it is the capacity of the material. The effective capacity can be evaluated under ion exchange process for a particular system in batch mode.

The dynamic adsorption capacity determined in fixed bed columns corresponds to breakthrough capacity. Often breakthrough and effective exchange capacities are a fraction of the theoretical exchange capacity, since the ion exchange process depends on the type of cation in solution, concentration, and other factors that interfere with the exchange process (Inglezakis, 2005; Kitsopoulos, 1999).

## Adsorption kinetics

Kinetics in ion exchange systems are influenced by the combined effects of concentration gradients, electrical charge gradients, ionic interactions and chemical interactions in either phase (Harland, 1994). Reaction kinetics are considered a mass transfer process from the solution to the adsorbent in a determined time lapse until equilibrium is reached. The rate of adsorption is often limited by diffusion processes on the external surface of the adsorbent and within the porous sites available on the adsorbent. The ion exchange and adsorption processes can be characterised in four steps (Worch, 2012):

1. Transport of the adsorbate from the solution to the hydrodynamic layer around the adsorbent particle;

2. Transport over boundary layer to the external surface of the adsorbent particle known as film diffusion or external diffusion;

3. Transport through the internal framework of the adsorbent (intraparticle diffusion) by the diffusion in the pore liquid (pore diffusion); and

4. Energetic interaction between the adsorbate molecules and final adsorption sites.

Overall, the first and the fourth characteristic of adsorption kinetics occur very fast. Hence, the majority of the total rate of adsorption process is mainly determined by film and intraparticle diffusion. These two adsorption processes occur in series and then the slower process is the one that determines the total adsorption rate (Islam *et al.*, 2004; Kumar & Jain, 2013).
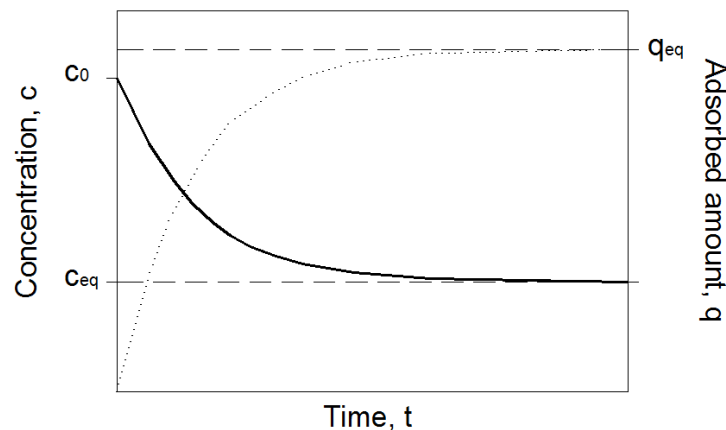


**Figure 2.15 Typical adsorption kinetic curve expressed in adsorbed amounts (q) until equilibrium (dotted curve), and the reduction in concentration (C) of the solute in solution at equilibrium in time (Worch, 2012).**

Experimentally, kinetic curves (Figure 2.15) can be obtained by mixing adsorbent with the solution containing sorbate in a batch mode experiment, measuring the concentration in the solution and loading on the adsorbent with time. During the adsorption process, initial concentration ($C_0$) of the adsorbate decreases from its initial value to an equilibrium concentration ($C_q$) as seen in Figure 2.15 solid line. Every time step represents an equilibrium concentration ($q_t$) in the adsorption system and

equilibrium is given by the amount of adsorbate balanced on the adsorbent during the adsorption process until total equilibrium ($q_{eq}$) of the system is reached (dotted line). Experimental adsorption kinetic curves for the adsorption of the solute shows a characteristic uptake behaviour of the adsorbent and the factors that influence the adsorption rates and diffusion over the transport of solute from solution phase to solid phase (El-Kamash *et al.*, 2005). To describe and quantify the changes in the adsorption process of ions over time, kinetic models can be applied. Kinetic adsorption models such as pseudo-first order, pseudo-second order and Elovich models that allow the determination of adsorption capacity and the adsorption rate are widely used for adsorption applications. For the determination of the transport mechanisms in the adsorption process, the film and the pore diffusion models can be applied to the experimental data (Argun, 2008). The used models are described in Chapter 7.

**Equilibrium isotherm and selectivity**

The adsorption equilibria depend on the interactions of the adsorbed and adsorbent as well considering the properties of the solutions that are in contact with the adsorbent material, often described by adsorption equilibrium isotherms. Furthermore, if the solution contains more than one element, they will inevitably compete for sorption sites located in the adsorbent (Qi & Levan, 2005). Therefore, equilibrium in this scenario for individual element in complex mixtures depends on these natural interactions, described by selectivity isotherms.

The equilibrium in an ion exchange process as described in Eq. 2.3 depends on the amount of adsorbed on the adsorbate concentration and also temperature (Worch, 2012). To simplify the ion exchange equilibrium, it is assumed that the reactions occur at a constant temperature. The ion exchange equilibrium isotherm shows the ionic behaviour of the exchanger as a function of the experimental initial conditions (Figure 2.16). The adsorption at equilibrium ($q_e$) is determined by the difference between the initial concentration and the equilibrium concentration of the solute in solution by a determined mass and volume of adsorbent. To create an adsorption isotherm curve for different initial concentrations, the resulting concentration at equilibrium ($C_e$) is plotted against the adsorption at equilibrium (Figure 2.16). The curve reaches a plateau when no further adsorption is achieved despite an increment initial concentration, reaching the adsorption capacity for the material ($q_{eq}$).
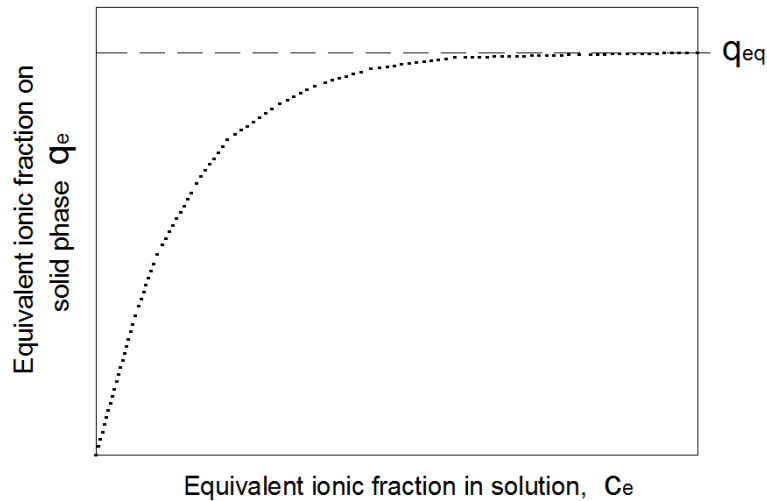
**Figure 2.16 Typical adsorption isotherm curve, where $C_e$ is the concentration at equilibrium and $q_e$ is the adsorption achieved at equilibrium (Worch, 2012).**

Experimental adsorption isotherms show the capacity of the material for a range of initial concentrations and maximum practical capacity. Models that relate the adsorption capacity can be fitted to the experimental data in order to determine adsorption parameters that describe capacity and affinity for the sorbent. The most widely used models for adsorption equilibrium of adsorbent materials are: Langmuir, Freundlich, Sips and Toth, discussed in Chapter 6 (Günay *et al.*, 2007; Rajic *et al.*, 2010).

The ion exchange selectivity isotherm is analysed using a constant total normality of two different ions at different ratios and a known mass of adsorbed. The equilibrium is then plotted in terms of equivalent fractions of the liquid phase ($X$) and solid phase ($Y$) of one of the ions in solution. The phases' equivalent fractions are expressed by the following relationships:

for liquid,

$$X_A = \frac{C_{A(s)} z_A}{C_{A(s)} z_A + C_{B(s)} z_B} \quad ; \quad X_B = 1 - X_A \qquad \qquad \textbf{Equation 2.4}$$

where $C_A$ is the concentration of ion A in solution [meq/L] and $C_B$ is the concentration of ion B in solution [meq/L], and $Z_a$ and $Z_b$ are the valency of the ions as per Eq. 2.3;

for solid,

$$Y_A = \frac{\text{Equivalents of exchanging ion A}}{\text{Total cations of exchanger}} \; ; \; Y_B = 1 - Y_A \qquad \qquad \textbf{Equation 2.5}$$
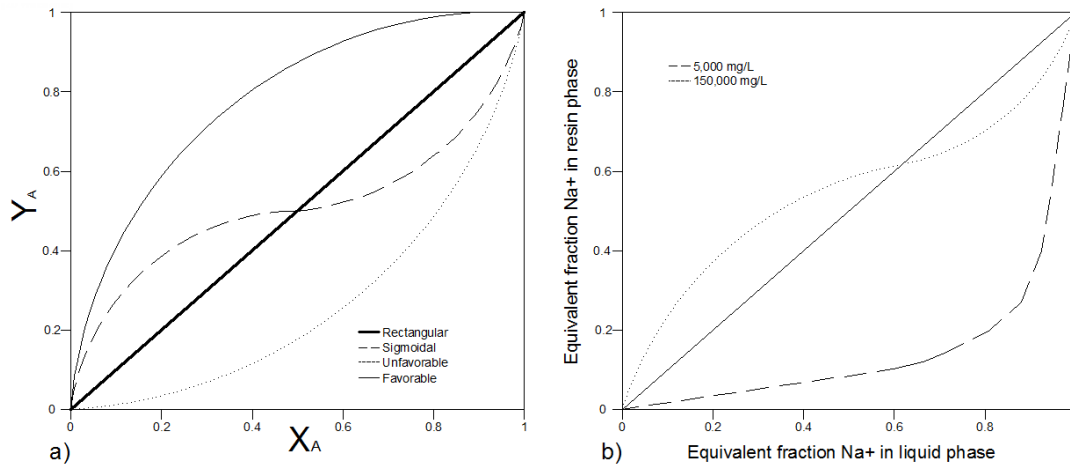


**Figure 2.17 a) Typical ion exchange isotherms b) Ion exchange isotherms for a Na$^+$/Ca$^{2+}$ on synthetic exchanger (Colella, 1996; Harland, 1994).**

Ion exchange isotherms can be classified in four different types (Figure 2.17(a)). When the solution and the solid phase contain the same equivalent fraction following equilibrium, the linear isotherm is found in which both species are preferred equally (rectangular isotherm). In a favourable isotherm, the curve indicates that the exchanger phase loading is always greater than the liquid phase concentration, indicating a preference for that particular ion (that is ion A). An unfavourable isotherm is when the exchanger phase is always lower than the liquid phase, demonstrating no preference for ion A (Townsend & Coker, 2001). The sigmoidal scenario represents regions when loading in solid phase for ion A occurs, but others with no preference towards that ion.

Figure 2.17(b) shows the ion exchange isotherms for a system containing sodium and calcium in a solution phase for a high and low saline solution. The high salinity isotherms show that Na$^+$ is less preferred than Ca$^{2+}$. The low salinity isotherm shows that at low Ca$^{2+}$ is preferred over the Na$^+$ but turns unselective at high concentrations of Ca$^{2+}$.

Natural zeolites usually exhibit strong preference behaviour towards ions with low energy density, small hydrated radii (hydration of an ion depends on electrostatic

attraction of water molecules around it), and low hydrated energy (energy released when one mole of ions experience hydration) (Pabalan & Bertetti, 2001). Thus zeolites are less selective for $Na^+$ than other cations (Table 2.7).

**Table 2.6 Cation exchange selectivity in clinoptilolite (Zeolite) (Margeta *et al.*, 2013).**

| Selectivity Series | Reference / Element of interest |
|---|---|
| $Cs^+ > Rb^+ > K^+ > Na^+ > Li^+$ ; $Ba^{2+} > Sr^{2+} > Ca^{2+} > Mg^{2+}$ | Ames (1960, 1961) - $Cs^+$ |
| $Pb^{2+} \approx Ba^{2+} \gg Cu^{2+}, Zn^{2+}, Cd^{2+} > \mathbf{Na^+}$ | Semmens et al. (1978) – Heavy metals |
| $Pb^{2+} > NH_4^+, Ba^{2+} > Cu^{2+}, Zn^{2+} > Cd^{2+} > Co^{2+}$ | Blanchard et al. (1984) - $NH_4^+$ |
| $Pb^{2+} > Cd^{2+} > Cs^+ > Cu^{2+} > Co^{2+} > Cr^{3+} > Zn^{2+} > Ni^{2+} > Hg^{2+}$ | Zamzow et al. (1990) – Heavy metals |
| $Cs^+ > NH_4^+ \gg \mathbf{Na^+}$ | Howery et al. (1965) - $Cs^+$ |
| $Cs^+ > Rb^+ > K^+ > NH_4^+ > Ba^{2+} > Sr^{2+} > \mathbf{Na^+} > Ca^{2+} > Fe^{2+} > Al^{3+}$ $> Mg^{2+} > Li^+$ | Mumpton (1999) |
| $Pb^{2+} > Cr^{3+} > Fe^{2+} > Cu^{2+}$ | Inglezakis et al. (2004) |

## Treatment and regeneration on natural ion exchangers

Pre-treatment or regeneration of natural exchange materials is crucial for their real and practical applicability (Semmens *et al.*, 1981). If a natural exchanger can be pre-treated or regenerated multiple times, then it can be used and reused for a water treatment application reducing volume of waste material reducing operational costs (Katsou *et al.*, 2011).

Natural ion exchangers can be regenerated by single or combined treatment involving chemical or thermal modification using acids, bases and inorganic salts (Akdeniz, 1999; Hedstrom, 2001; Jha & Hayashi, 2009; Katsou *et al.*, 2011; Wang & Peng, 2010; Wu *et al.*, 2008). These modifications result in migration of cations from the crystal framework and their replacement by the introduced cation. Modification with inorganic salts is a recognised effective regeneration technique. Treatment with high concentrations of inorganic salts, such as $NaCl$, $CaCl_2$ and $NH_4Cl$ are often used and needed to displace ions on the exchanger framework.

Treatment with acids or bases is one of the most common used and simple methods used in regeneration of natural exchangers. Use of inorganic bases such as $NaOH$ or $Ca(OH)_2$ and acid solutions like $HCl$ or $HNO_3$ can result in a substantial increase in adsorption properties over the natural form due to removal of competing cations from the matrix (Margeta *et al.*, 2013). However, treatment with acid or base solutions may

lead towards pore blockage of the exchanger framework. This can be explained as due to dissolution of natural crystal framework by the acid or base solutions (Ates & Hardacre, 2012; Wang & Nguyen, 2016; Wang *et al.*, 2012; Watanabe *et al.*, 2003). The removal of aluminium from the framework reduces the CEC (Inglezakis *et al.*, 1999; Inglezakis *et al.*, 2001c; Semmens & Martin, 1988; Wang & Peng, 2010).

## Fixed bed and column dynamics

Fixed bed columns are used for water treatment since their operation allows water to percolate through granular media such as ion exchange or adsorbents. Adsorption and ion exchange in fixed bed columns depend on the initial concentration of the feed water, flow rate, height of the adsorbent/ion exchange bed and the particle sizes of the bed (Inglezakis, 2010a; Inglezakis & Grigoropoulou, 2004; Stylianou *et al.*, 2007). Often in column studies the unit of Bed Volume (BV) is used and refers to a volume of liquid equal to the volume of material packed in the bed (Inglezakis *et al.*, 2001a).

During the adsorption process, adsorbate ($C_0$, influent concentration) is percolated through the bed of particles accumulating adsorbate until equilibrium is reached (C, effluent concentration). Equilibrium is reached by successive layers from the inlet to outlet of the column ($V_B$). Once the last layer of the column reaches equilibrium ($V_E$), then it is considered that the fixed bed reached exhaustion (Figure 2.18). Since natural exchangers have a slow kinetics there is not a sharp boundary between loading boundaries within the column profile (Medvidović *et al.*, 2006).

$V_B$ is the number of bed volume (BV) treated, $V_I$ represents the breakthrough point at number of BV in which the maximum effluent concentration of ions before regeneration. $V_E$ represents the number of BV when the fixed bed column reached exhaustion (Figure 2.18). The parameters used to characterise a fixed bed are usually bulk density ($\rho_B$), bed porosity ($\varepsilon_B$), adsorbent mass ($m_A$), adsorbent volume ($V_A$), and adsorbed volume ($V_R$). From the fixed bed characteristics, it is possible to estimate, linear flow velocity ($v_F$), residence time ($t_r$), effective flow velocity ($u_F$), and throughput as bed volumes (BV). All of these parameters and characteristics combined with adsorption kinetics are components of the breakthrough model for fixed bed column adsorption (Worch, 2008; Worch, 2012).
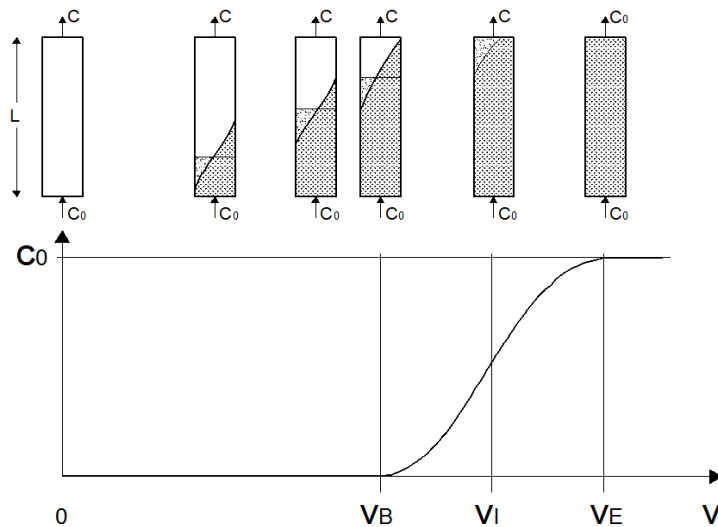
**Figure 2.18 Solution of initial (C₀) concentration flowing through the column and exiting with a reduced concentration (C). The breakpoint occurs in $V_I$ (C/C₀), and the material is exhausted after $V_E$ (C/C₀ = 1). Column profile is the typical breakthrough curve for a fixed bed column (Harland, 1994; Worch, 2012).**

The breakthrough models used for fixed bed column adsorption are Thomas, Bohart-Adams, and Yoon-Nelson (Xu *et al.*, 2013). These models describe the breakthrough curve by fitting empirical mathematical relationships to the experimental data, providing with an estimate adsorption capacity and number of BVs before breakpoint. The used models are described in Chapter 8.

## Using natural zeolite and scoria for the treatment CSG co-produced water

The primary concerns for using CSG co-produced water for irrigation include: high concentration of dissolved salts  and an excessive $Na^+$ ion concentration that can cause soil dispersion (Biggs *et al.*, 2012; DERM, 2009; DERM, 2011; Rengasamy & Marchuk, 2011; Van De Graaff & Patterson, 2001). Different authors (Belbase *et al.*, 2013; Huang & Natrajan, 2006; Taulis & Milke, 2009; Vance *et al.*, 2007; Wang & Nguyen, 2016; Wang *et al.*, 2012; Zhao *et al.*, 2008) have proposed the use of natural zeolite to provide the CSG industry with a cost-effective treatment, alternative to their operations. Huang and Natrajan (2006) used zeolite in $Ca^{2+}$ form sourced from New Mexico (USA) to reduce the concentration of $Na^+$ (500 mg/L) from CSG water finding that the natural zeolite had a very low usable $Na^+$ exchange capacity of about 10 meq/100 g. Taulis and Milke (2009) used Ngakuru zeolites for the removal of $Na^+$

(304 mg/L) from New Zealand CSG waters removing about 11-20 meq/100 g natural ion exchange material and a maximum removal of 40.9 meq/100 g when zeolite was pre-treated with 1 M KCl. Wang *et al.* (2012) carried out $Na^+$ adsorption tests using CSG water (563 mg/L) with Escott Australian zeolite in natural and acid treated material. The authors found that acid treated zeolite form enhanced the adsorption $Na^+$ by 30%, when compared with the natural form. These studies have determined that the zeolites have large cation exchange capacity with a low $Na^+$ adsorption reached. Additionally, natural materials have been used in water treatment applications to remove contaminants from industrial wastewaters that are also presented in CSG produced water (Erdem *et al.*, 2004; Inglezakis *et al.*, 2007; Oren & Kaya, 2006; Wingenfelder *et al.*, 2005).

Natural adsorption materials, such as zeolite and scoria, in theory, have the physical and chemical properties to remove pollutants and cations found in excess in CSG waters. These materials have high adsorption capacity, cation exchange properties, stability of the crystal framework, molecular sieving properties and distinctive porosity, appropriate from the removal of cations from solution. Therefore, in this study natural and treated adsorption materials, such as zeolite and scoria, will be used to remove cations from CSG water. The use of these materials could become a suitable technology for the treatment of CSG co-produced waters in the reduction of contaminants that could have negative impacts on soils, vegetation, livestock watering and environment.

Batch and column type studies are carried out to determine the effectiveness of both materials in their natural and treated form on the removal of cations present in CSG water. With a reduction in $Na^+$ concentration, the sodicity of the CSG water will be reduced together with the values for SAR, increasing the likelihood of the treated water being used for beneficial usage such as irrigation and livestock.

## Conclusions

CSG co-produced water represents an important challenge for CSG operators due to the large volumes produced, geochemical characteristics and the potential

environmental impacts of this escaping body of water. The total volume of CSG water produced worldwide is estimated to be between 1696 – 5090 GL/year.

CSG water is categorised as a brackish water due to the high concentration of total dissolved solids (TDS), high conductivity, with a chemical signature that follows $Na^+$-$Cl^-$-$HCO_3^-$ or $Na^+$-$HCO_3^-$ type, low concentrations of calcium, magnesium, sulphate and low content of trace elements. This composition may have significant impact in the environment when CSG water is used for land, waterway discharge or agriculture applications without the corrective treatment and the water quality standards need for beneficial usage or disposal.

The current technologies used to treat CSG water are referred to as desalinisation processes, which are able to reduce the salinity and concentration of other ions using a combination of filtration, membrane processes, and ion exchange resins. The combination of these technologies is often necessary to meet the regulatory parameters for beneficial usage due to the geochemical signature of the co-produced water, increasing the associated cost of the treatment of CSG water.

Alternative methodologies for the treatment of CSG water can be implemented using natural ion exchange materials, such as natural scoria and zeolite, which provide adsorption for metal ions of concern present in the CSG water. In this study, both scoria and zeolite materials were used to determine the adsorption equilibrium and kinetic properties for metal ions present in CSG water, and study the selective adsorption behaviour of metal ions that compete during the uptake process. Fixed bed columns packed with scoria and zeolite were used to determine the dynamic adsorption of metals ions, along with the recovery of adsorptive properties of the adsorbent material through regeneration process.

# Chapter 3:  Case study, CSG water from Bowen Basin operations

## Brief history of site

Over the last decade, the Surat and Bowen Basins in Australia have been epicentres of CSG operations and gas production. Since the Surat Basin has been more extensively mined (coal), studies are in abundance on this particular sedimentary basin. Expanding CSG operations have moved into the southern part of the Bowen Basin, in an effort to search for new gas resources (Figure 3.1).
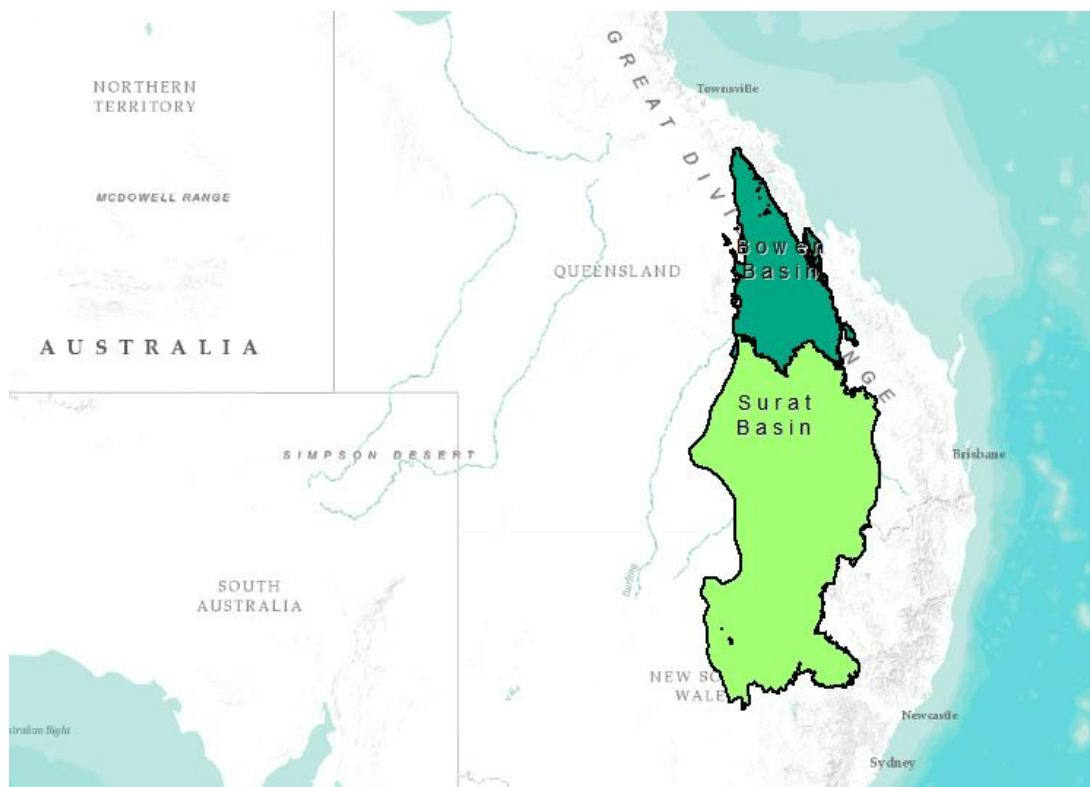


**Figure 3.1 Map showing the sedimentary Surat and Bowen Basins in the state of Queensland (Geoscience-Australia, 2015).**

Exploratory efforts for CSG detection in the Bowen Basin started in the late 1970's. These efforts were without major success, principally due to a misunderstanding of the regional geology of the targeted coal measures, lack of knowledge of the stress regimes

and finally, a lack of understanding on the influence of coal permeability and inappropriate well completion techniques (Averina *et al.*, 2008; Baker & Slater, 2008; Cook, 2013).

The early CSG operations had the aim of pre-draining the methane from the coal seam prior to coal mining. It was not until the mid-1990s that CSG production started to become a viable operation separate to coal mining, as a result of: (i) the identification of coal targets, (ii) application of low cost drilling techniques, (iii) development of practical means of stimulating gas recovery, and (iv) the implementation of effective well completions (Baker & Slater, 2008; Berger, 2012).

New technologies and processes now allow safe and profitable gas extraction. In just under a decade, CSG operations have moved from an exploratory phase to a major component of the production of the eastern Australian gas production industry. This development has been driven by good exploration and recovery techniques, putting Australia as a world leader in the CSG industry (Hamawand *et al.*, 2013; Oldridge & Whatman, 2009; Williams *et al.*, 2012a).
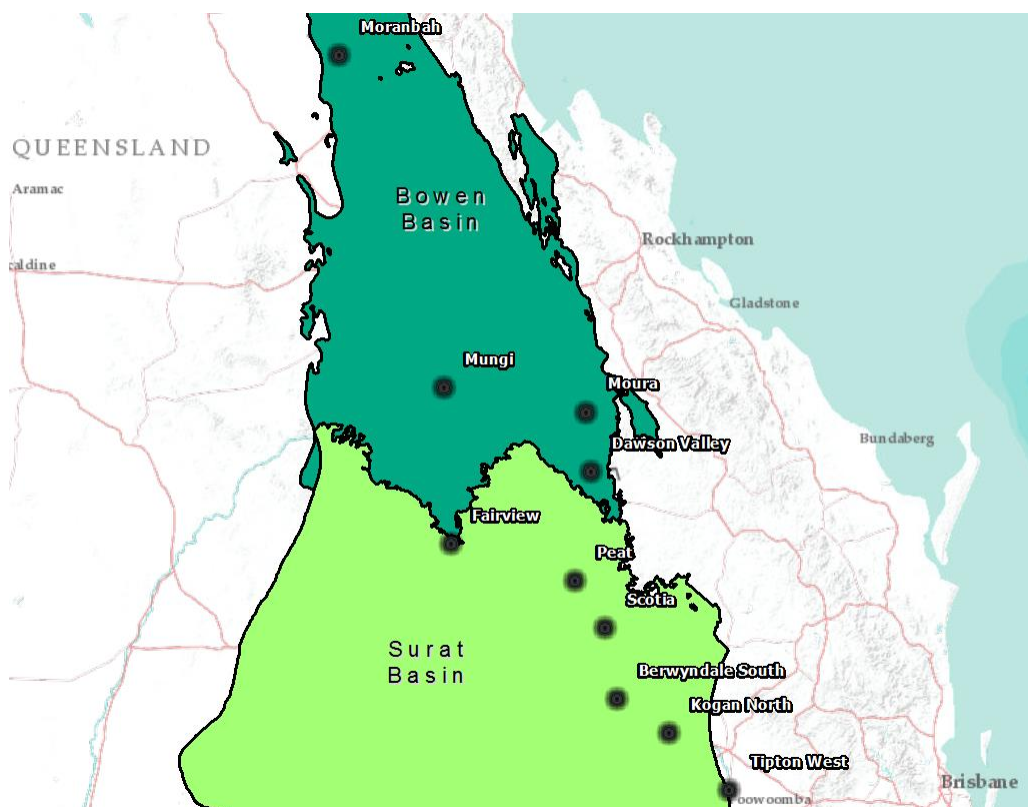


**Figure 3.2 Major CSG operations in the State of Queensland across the Bowen and Surat Basins.**

Other major CSG projects occurring in the Bowen and Surat Basins are taking place at Fairview, Moranbah, Peat, Scotia and Spring Gully. Additionally, a large number of pilot operations are being developed and proposed in the northern and central parts of the Bowen Basin (Figure 3.2). Operations in the Bowen Basin in 2008 were extracting an approximate $1.5 \times 10^9$ m$^3$ (58 PJ/y) of methane gas, while operations in the Surat Basin produced approximately $3.22 \times 10^9$ m$^3$ (120 PJ/y) of gas (Baker & Slater, 2008). Nonetheless, operation and production in these basins are on the rise and further operation is expected to develop across these basins.

The Bowen Basin operation comprises of developments at Moranbah, Moura, Mungi and Nipan areas. These operations are based on the recovery of CSG from the thick gassy coals of the Baralaba Coal Measures of the Late Permian age. Coal measures in this area are made of up to 10 seams with an aggregate coal thickness of up to 30 m, found at depths ranging from 300 to 1,000 m (Baker & Slater, 2008). Some of the gas produced in the Bowen Basin region is used at the ammonia and ammonium nitrate (explosives) plant at Moura. The majority of the excess production of gas is fed to the Queensland Gas Pipeline to supply markets in Gladstone. The gas is then liquefied and exported. It was estimated that $1.9 \times 10^8$ m$^3$ of methane gas was extracted per year in 2008 (7.3 PJ/y) (Baker & Slater, 2008).

The Bowen Basin region has a rich mixture of industries including coal, coal seam gas, cattle, cotton, crops and explosives manufacturers (Ammonium Nitrate plant). Recently in Queensland, the productive agriculture capacity is being impacted by many factors including climate change, scarcity of water and loss of farmland. Public concerns have been raised due to the impacts that CSG activities could have on surface and groundwater resources, further impacting agricultural productivity (Berger, 2012; Kinnon *et al.*, 2010). Inappropriate disposal of saline groundwater produced by the CSG activity could have adverse impacts on agricultural soils.

Given the significant generation of water impacted and used by a typical CSG operation field and the fast development of the CSG industry across the state of Queensland, innovative treatment strategies are required. These water clean-up strategies for beneficial re-use of water are required to meet strict legislative and regulatory frameworks, according to the Coal Seam Gas Water Management Policy

2012 (DEHP, 2012a). Currently, CSG operators must seek approval of the government requirements and minimum standards agency for environmental impact assessment and CSG water management plans for beneficial re-use (DEHP, 2013). Current guidelines enforce standards that provide protection to the environment when used for beneficial use including irrigation, livestock watering, coal washing, industrial use, and augmentation of public water supply (DEHP, 2013).

As part of the CSG co-produced water management strategies at Bowen Basin CSG operations, Arris Pty Ltd constructed a pilot water treatment plant for the treatment of the CSG water. The Arris Pilot Plant was designed to test the concept of shandying water from an ion exchange process using zeolite and scoria media with low salinity RO treated water with the aim of reducing the SAR and producing water fit for purpose (Kele, 2005a, 2016-Unpublished Doctoral Dissertation). Trials commenced before the start of this research project and continued to run. The zeolite and scoria used in this study had been identified for its suitability in CSG water treatment by another research project being conducted at CQU (Kele, 2016-Unpublished Doctoral Dissertation). The sodium exchange properties of natural zeolites at a recycled water test site in 2003 were described by Kele (2005b); Kele *et al.* (2007); Kele *et al.* (2005). The zeolite and scoria used in this study had been identified for its suitability in CSG water treatment by another research project, with the sodium exchange properties of scoria first established in a series of trials conducted on effluent from the Springsure and Sunrise at 1770 sewage treatment plants during 2006 and 2007 (Kele, 2016-Unpublished Doctoral Dissertation). A variety of scoria and zeolite media were tested for sodium exchange properties with CSG water from wells in the Bowen and Surat basins. A variety of scoria and zeolite media were tested for sodium exchange properties with CSG water from wells in the Bowen and Surat basins (Kele, 2016-Unpublished Doctoral Dissertation). The zeolite and scoria media in this research exhibited the best results for sodium reduction in the Bowen basin CSG water (Kele, 2016-Unpublished Doctoral Dissertation). Data from this site was provided by Arris to help frame the issues involved in CSG water quality (Table 3.1). For convenience, this site is referred to as the research site.

## Composition of CSG water from Bowen Basin operations

On-site water quality monitoring program was conducted by Arris Pty Ltd in their pilot plant providing valuable information about raw co-produced water at Bowen Basin CSG operation. In order to characterise the co-produced water from this site, composite samples were collected from the receiving inlet tank at the pilot treatment water facility. This tank was fed by 18 nearby active CSG production wells. Samples were taken in a monthly basis for 14 months during 2013-2014 with the aim to identify the major elements and compounds in CSG co-produced waters. Methods, procedures and materials for water quality sampling were specified by a NATA accredited laboratory. The summary of the water quality parameters from CSG co-produced water is shown in Table 3.1.

The characterised CSG water from this site had a high alkalinity with an average pH of 8.3. Electrical conductivity was found to be 6.0 dS/m, representing a brackish water value. The total dissolved solids (TDS) averaged at 4,092 mg/L. These composite water samples showed a typical geochemical signature for CSG waters with elevated pH and TDS values overall (Berger, 2012; Davies, 2013; Health, 2013; Kinnon *et al.*, 2010; Nghiem *et al.*, 2015; Nghiem *et al.*, 2011; Taulis & Milke, 2007). The ionic composition was dominated by sodium ions with an average concentration of 1,156 mg/L, and low average concentrations of calcium, magnesium and potassium. Consequently, the Sodium Adsorption Ratio (SAR) averaged 67, which is similar to reported SAR values for CSG waters at a number of gas fields operating in the Bowen Basin and CSG operations around the world (All-Consulting & Montana Board of Oil & Gas Conservation, 2002; Averina *et al.*, 2008; Benson *et al.*, 2005; Davies, 2013; Hamawand *et al.*, 2013; Huang & Natrajan, 2006; Jackson & Reddy, 2007a; Taulis & Milke, 2007; Van Voast, 2003; Zhao *et al.*, 2008; Zhao *et al.*, 2009).

On average, chloride and bicarbonate ions were present in high concentrations of 1,993 mg/L and 618 mg/L respectively, while sulphate concentrations were low (10 mg/L). The major ionic distribution and concentrations found for CSG water at the Bowen Basin operation are shown graphically in Figures 3.3 and 3.4.

**Table 3.1 Water quality data over a 14-month period from the Bowen Basin CSG operation, supplied by Arris Pty Ltd.**

| | Date | 4-Feb-13 | 25-Feb-13 | 25-Mar-13 | 22-Apr-13 | 20-May-13 | 17-Jun-13 | 15-Jul-13 | 12-Aug-13 | 9-Sep-13 | 7-Oct-13 | 4-Nov-13 | 2-Dec-13 | 9-Jan-14 | 7-Feb-14 | Average |
|---|---|---|---|---|---|---|---|---|---|---|---|---|---|---|---|---|
| pH | | 8.55 | 8.16 | 8.33 | 8.33 | 8.08 | 8.76 | 8.60 | 8.65 | 7.08 | 9.03 | 7.25 | 8.85 | 8.94 | 8.09 | 8.34 |
| EC | dS/m | 5.60 | 3.04 | 5.63 | 5.95 | 5.50 | 7.85 | 8.05 | 7.60 | 6.26 | 6.18 | 6.50 | 7.59 | 4.55 | 3.96 | 6.02 |
| TDS | mg/L | 3,808.00 | 2,067.20 | 3,828.00 | 4,046.00 | 3,740.00 | 5,338.00 | 5,474.00 | 5,168.00 | 4,257.00 | 4,202.00 | 4,420.00 | 5,160.00 | 3,094.00 | 2,692.80 | 4,092.50 |
| Na | mg/L | 1,167.00 | 1,152.00 | 1,040.00 | 1,121.00 | 1,073.00 | 1,533.00 | 1,524.00 | 1,419.00 | 1,016.00 | 1,111.00 | 1,034.00 | 1,421.00 | 875.10 | 703.30 | 1,156.39 |
| K | mg/L | 31.59 | 35.03 | 35.38 | 43.59 | 9.17 | 79.26 | 77.62 | 67.94 | 144.00 | 105.50 | 148.60 | 110.40 | 33.80 | 22.52 | 67.46 |
| Mg | mg/L | 4.18 | 6.39 | 5.49 | 5.60 | 1.51 | 6.27 | 6.07 | 5.27 | 12.31 | 5.42 | 9.80 | 4.65 | 2.49 | 3.10 | 5.61 |
| Ca | mg/L | 13.44 | 29.78 | 24.88 | 24.54 | 7.95 | 10.48 | 10.14 | 8.29 | 138.30 | 7.19 | 90.68 | 8.68 | 3.20 | 19.33 | 28.35 |
| SAR | | 71.30 | 50.00 | 49.20 | 53.10 | 91.40 | 92.50 | 93.50 | 94.90 | 22.22 | 76.22 | 27.50 | 96.80 | 89.24 | 39.20 | 67.65 |
| Hardness | mg/L | 51.00 | 37.00 | 85.00 | 84.00 | 26.00 | 52.00 | 50.00 | 42.00 | 396.03 | 40.25 | 267.00 | 41.00 | 18.21 | 61.00 | 89.32 |
| Alkalinity | mg/L | 740.00 | 644.00 | 620.00 | 570.00 | 570.00 | 850.00 | 810.00 | 760.00 | 620.00 | 680.00 | 450.00 | 390.00 | 500.00 | 450.00 | 618.14 |
| Cl | mg/L | 1,792.00 | 749.00 | 1,843.00 | 1,860.00 | 1,774.00 | 3,317.00 | 3,310.00 | 2,298.00 | 2,330.00 | 2,283.00 | 1,993.00 | 2,075.00 | 1,071.00 | 1,207.00 | 1,993.00 |
| SO4 | mg/L | 11.50 | 10.20 | 11.50 | 10.20 | 11.50 | 10.20 | 11.50 | 10.20 | 11.50 | 10.20 | 11.50 | 10.20 | 11.50 | 10.20 | 10.85 |
| F | mg/L | 0.63 | 0.52 | 0.85 | 1.18 | 1.46 | 2.36 | 2.27 | 2.35 | 0.82 | 0.64 | 1.19 | 1.03 | 0.52 | 0.80 | 1.19 |
| Br | mg/L | 5.57 | 2.60 | 4.01 | 2.23 | 1.50 | 3.91 | 4.10 | 3.85 | - | - | - | 2.70 | 0.95 | - | 2.24 |
| S | mg/L | 27.85 | 2.86 | 1.70 | 3.61 | 13.50 | 14.32 | 13.43 | 9.61 | 24.02 | 11.65 | 11.93 | 16.42 | 2.16 | 1.16 | 11.02 |
| Fe | mg/L | <0.02 | <0.02 | <0.02 | 0.01 | 0.03 | 0.03 | <0.02 | 0.01 | 33.99 | 0.50 | 45.42 | 0.98 | 0.15 | 2.08 | 8.32 |
| B | mg/L | 1.40 | 0.68 | 1.34 | 1.89 | 1.16 | 1.86 | 1.88 | 1.65 | 0.90 | 1.05 | 1.53 | 1.25 | 0.83 | 0.68 | 1.29 |
| Mn | mg/L | <0.02 | 0.05 | 0.01 | 0.01 | 0.01 | <0.02 | <0.02 | 0.00 | 1.66 | 0.01 | 0.89 | 0.03 | <0.02 | 0.09 | 0.28 |
| Al | mg/L | 0.01 | 0.13 | 0.08 | 0.30 | 0.18 | 0.16 | 0.06 | 0.34 | 0.16 | 0.67 | 0.04 | 8.08 | 3.50 | 7.96 | 1.55 |
| Zn | mg/L | 0.02 | <0.005 | <0.005 | <0.005 | <0.005 | <0.005 | <0.005 | <0.005 | <0.005 | <0.005 | <0.005 | - | <0.005 | <0.005 | 0.01 |
| Sr | mg/L | 3.69 | 1.53 | 5.12 | 5.64 | 2.29 | 3.03 | 2.88 | 2.67 | 9.01 | 1.69 | 8.06 | 2.77 | 1.61 | 2.94 | 3.78 |
| Ba | mg/L | 11.14 | 3.70 | 17.78 | 20.86 | 6.86 | 9.92 | 9.59 | 8.89 | 24.40 | 2.80 | 23.36 | 9.06 | 3.58 | 27.05 | 12.78 |
| As | mg/L | - | - | 0.01 | 0.01 | 0.03 | 0.01 | 0.01 | 0.01 | <0.005 | <0.005 | <0.007 | - | - | - | 0.01 |
| TSS | mg/L | - | - | 10.00 | 40.00 | 360.00 | 20.00 | 20.00 | 40.00 | 100.00 | 15.00 | 113.00 | - | - | - | 51.29 |
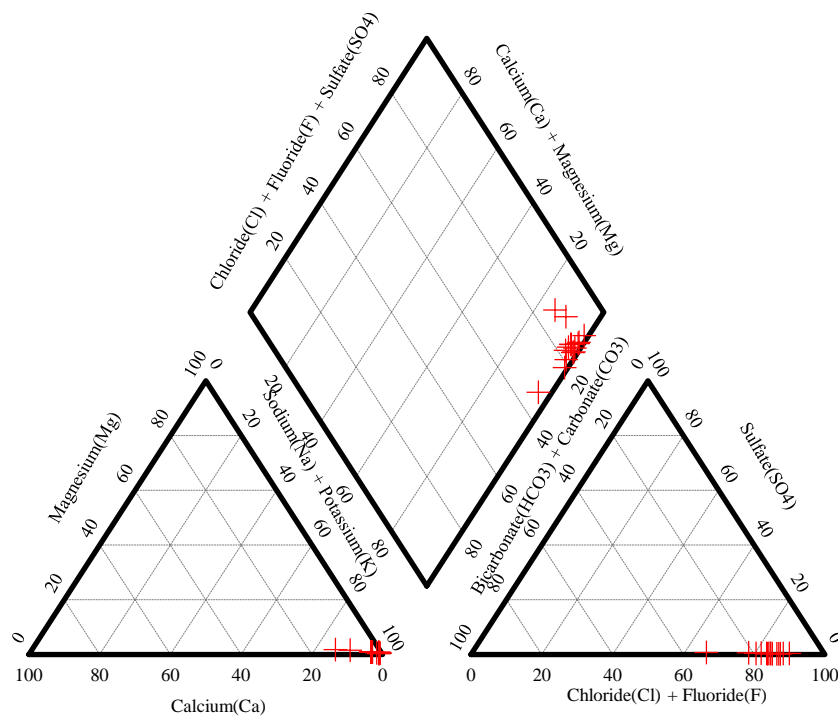
**Figure 3.3 Piper diagram of CSG water from research site operations for 14 monthly samples over 2013 -2014. The relative concentration of ions (cations in the left-bottom triangle, anions in the right-bottom triangle), and ion combinations (diamond chart).**
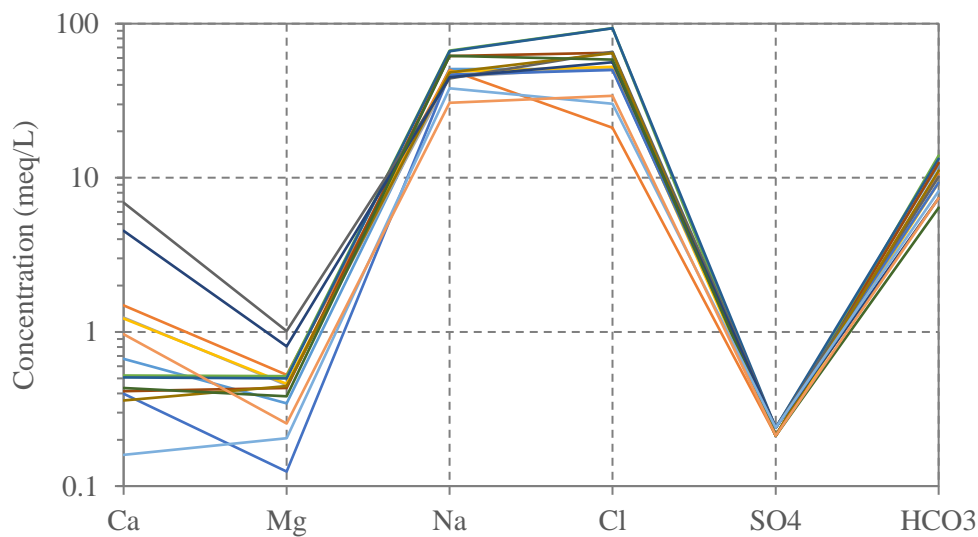


**Figure 3.4 Schoeller diagram showing the major ionic composition of CSG water from the research site. Each coloured line represents the ionic concentrations of a single water sample.**

Figure 3.3 highlights an excess of sodium ions compared to other ions such as calcium or magnesium, thus, data points are clustered near to the upper limit on the sodium-potassium axis. For the anions, the CSG water has a prevalence of bicarbonate and

chloride ions and limited occurrence of sulphate ions, hence data points are grouped near to the maximum values on the chloride-fluoride and bicarbonate-carbonate axis. These analyses are consistent with the general characterisation for CSG water reported for CSG water in the Surat Basin, where low calcium, magnesium and negligible sulphate concentrations were detected and CSG groundwater presented an alkaline pH $(8-9)$, salinity $(2160-4040\ \mu S/cm)$ and an ionic composition $Na^+$-$Cl^-$-$HCO_3^-$ (Tang *et al.*, 2014).

The variation in ionic composition between monthly samples was considered in Figure 3.4. The diagram shows the concentration of major ions in meq/L, plotted on a logarithm scale. The monthly samples were consistent in composition of sodium, chloride and bicarbonate ions, with no seasonal pattern evident. Calcium ions were the most variable. In general, the CSG water from the Bowen Basin operations can be described in ionic terms as a $Na^+$-$Cl^-$-$HCO_3^-$ type of CSG water.

The CSG water exhibited an average total dissolved solid value of (TDS) of 4092 mg/L, which corresponds to 12% of the TDS concentration present in seawater (35,000 mg/L), and four-fold the maximum TDS value for drinking water (500 mg/L). Most of the salinity or TDS was a product of the high concentration of $Na^+$, and together with low concentrations of $Ca^{2+}$ and $Mg^{2+}$, the sodicity of the water was high (SAR values averaged 67). Both parameters, TDS/salinity and SAR, are over the recommended values for beneficial use (EC = 3,000 $\mu S/cm$; SAR= 6-12).

Although the major composition can be described by $Na^+$-$Cl^-$-$HCO_3^-$, there are other important elements present in trace amounts such as $Fe^{2+}$, $Ba^{2+}$, $Sr^{2+}$, $B^{3+}$ (>2 mg/L). Trace elements of concern that were identified in the CSG water are $Sr^{2+}$ (3.7 mg/L) and $Ba^{2+}$ (12.7 mg/L). The concentration of $Ba^{2+}$ is over the maximum levels for beneficial use (2 mg/L). Other contaminants such as organic compounds and radioactive elements were typically below guideline thresholds and in most of the cases below detection limits (Appendix A).

This ionic characterisation was consistent with international reports for CSG co-produced water as well as those at other Surat and Bowen Basin sites (All-Consulting & Montana Board of Oil & Gas Conservation, 2002; Averina *et al.*, 2008; Benson *et*

*al.*, 2005; Davies, 2013; Hamawand *et al.*, 2013; Huang & Natrajan, 2006; Jackson & Reddy, 2007a; Taulis & Milke, 2007; Van Voast, 2003; Zhao *et al.*, 2008; Zhao *et al.*, 2009). Figure 3.5 compares the average concentrations of major ions in the research site with those reported for different CSG operation sites across the Bowen and Surat Basins.
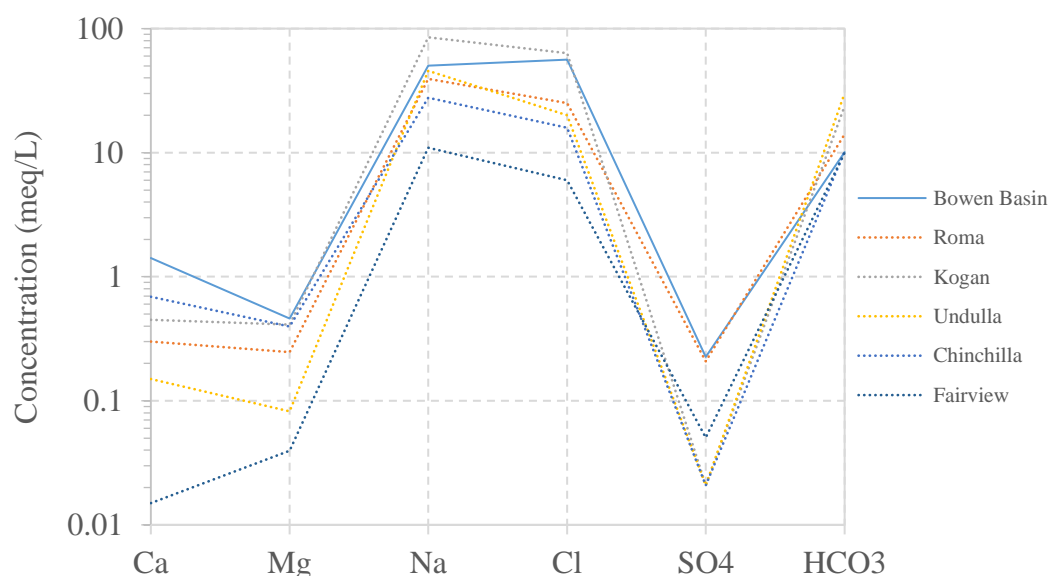


**Figure 3.5 Schoeller diagram for major ions found in research site (labelled 'Bowen Basin') compared with other CSG water across Surat and Bowen Basins (Abousnina *et al.*, 2015; Averina *et al.*, 2008; Benson *et al.*, 2005; Hamawand *et al.*, 2013).**

$Na^+$ and $Cl^-$ concentrations for the Bowen Basin water was the second highest after the Kogan CSG site in the Surat Basin. Sites such as Chinchilla and Fairview located at the northern part of the Surat Basin, presented larger values for $HCO_3^-$ than for $Cl^-$, giving a chemical signature $Na^+$-$HCO_3^-$-$Cl^-$ different to the Bowen Basin research site. This site-to-site variation, requires a number of considerations in the design and operation of water treatment facilities for CSG co-produced water treatment.

## Adequate management of CSG water from Bowen Basin

Adequate management of co-produced water from CSG extraction is necessary to reduce any environmental risks associated with this type of water. The chemical compositions of CSG water from the Bowen Basin research site may have environmental impacts on surface water, land and livestock watering due to the high salinity (TDS = 4092 mg/L and EC = 6.0 dS/cm), high sodium concentration (1156

mg/L), and high SAR (67). Additionally, trace elements were identified in this water body, such as $Sr^{2+}$ and $Ba^{2+}$, with concentrations over the limit for beneficial use of CSG water ($Sr^{2+}$ =3.7 mg/L and $Ba^{2+}$ =12.7 mg/L).

In response to the CSG water characterisation the following recommendations can be made:

1. Reduction of sodium ions and hence SAR is required.
2. $Sr^{2+}$ and $Ba^{2+}$ are atypically high and require reduction.
3. Overall salinity needs to be treated.

## Conclusions

The research site CSG co-produced water has a unique signature and is atypical for the Bowen Basin. The ionic composition follows $Na^+$-$Cl^-$-$HCO_3^-$ type, with high concentration of trace elements. Therefore, the project focussed on the removal of $Na^+$, $Sr^{2+}$ and $Ba^{2+}$ using a series of natural and enhanced zeolite and scoria materials. Both materials have been characterised in terms of their capabilities for the removal of cations present in CSG water. A series of adsorption studies have been performed to determine the effectiveness of both materials on the adsorption of cations considering the capacity, rate of adsorption, cation selective behaviour, and reconditioning of adsorptive properties of the material for re-use.

# Chapter 4:  Materials and methods

## Introduction

This chapter details the materials and methods used throughout the thesis. Natural sorbent materials were firstly characterised to understand their physical and chemical nature. Fundamental chemical experiments provided insight into the performance of the materials for adsorption kinetics, equilibrium, ion exchange and then the ability of these materials to exchange synthetic and site sampled CSG co-produced water.

## Materials selection and preparation

Natural sorbent materials; zeolite and scoria, were chosen for the treatment of CSG co-produced water, based on the recommendations of Kele (2005a, 2016-Unpublished Doctoral Dissertation). This media was selected as the best performers in regards to sodium exchange from the trial that examined 12 different zeolite and scoria media with CSG water from the research site (Kele, 2007, 2008). Zeolite (1 m$^3$) and Scoria (1 m$^3$) was sourced by Arris Pty Ltd from mines on the Australian Eastern Seaboard. The media used in this research project is the same as that used in the Arris Pilot Plant for continuity. The sorbent material samples were received in their natural form with no modification or treatment. Particle size of the supplied material was variable ranging from 0.075 mm to 5 mm.

Both materials were size sorted, particles that were larger than 2 mm were ground with a stationary Jaw Crusher (Essa, JC3000) for 5 minutes to reduce the particle size. The sorbent materials were mechanically sieved (Essa, test sieves) into different fraction sizes using a sieve shaker for 10 min (Essa, 3D Digital Sieve Shaker). The particle size fractions were 1.8 - 0.6 mm (Fraction I), 0.6 – 0.35 mm (Fraction II) and < 0.355 mm (Fraction III).

Each size fraction was washed thoroughly with ultrapure water (typical resistivity of 18.2 MΩ·cm at 25 °C, Milli-Q Millipore) until debris and impurities were no longer visible in the wash (Gedik & Imamoglu, 2008). Materials were oven dried over 48 h

at 110 °C until weight remained constant (Kocaoba *et al.*, 2007; Yazdani *et al.*, 2012). The dried material was then stored in sealed containers before use or treatment for batch and column type experiments to eliminate the introduction of moisture or water sources.

## Material characterisation of natural adsorbents

### Scanning Electron Microscopy (SEM)

The surface morphology of the natural materials was characterised using a scanning electron microscope (SEM), JOEL/EO JSM-6360, fitted with an energy dispersive x-ray spectroscope (EDS). SEM produces high-energy electrons from a focused beam that generate a variety of signals at the surface of the sample. Signals originated from the electron-sample interface reveal texture, chemical composition, crystalline structure and orientation of the sample.

Zeolite and scoria material in a dried natural form (0.6 – 0.35 mm) were gold coated in a vacuum gold sputter coating chamber in order to eliminate the charge effect due to low conductivity of the material that generates image distortion or drift (Agar Sputter Coater - Automatic). Once coated, the samples were mounted on aluminium stubs (JOEL Aluminium specimen mount) using double-sided conductive carbon tape (PELCO Tabs$^{TM}$) and placed into the microscope vacuum chamber where micrographs were captured. For EDS analysis, dried natural samples were loaded into the microscope chamber for quantitative chemical composition analysis. Typical instrument settings for the micrographs were: working distance (WD) of 5-10 mm, accelerating voltages between 5 – 15 kV, spot size ranges of 5 – 27, secondary electron image signal (SEI), and various magnifications (x230 – x8,000).

### X-ray fluorescence (XRF)

X-ray fluorescence (XRF) spectrometer is an X-ray instrument used for non-destructive chemical analyses of rocks, minerals and fluids for elemental composition. A Shimadzu EDX-Ray fluorescence unit was used to assess Fe, Si, Al, Ca, K, Mn, Na, Mg, P, S, Ti, Ba, Zn, Cu, Cr, and Ni content.

Zeolite and scoria materials were ground to a pressed pellet, and placed into a melting crucible. Heat was applied (XRF Scientific, muffle furnace at 1000°C for 30 min) until sample melted and a glass bead formed. XRF analysis was conducted on the prepared samples and processed using PANalytical's XRF software.

## X-ray diffraction (XRD)

X-ray powder diffraction (XRD) was used for the identification of crystalline structures (phases) and atomic spacing in each of the sorbent materials.

The assessment of the crystalline structure of the samples was achieved using an XRD generator, PANalytical X'Pert Pro PW3040 diffractometer at 40 kW and 40 mA. The scanning angular range was 5° to 80° with a step of 2θ angles, allowing the scanning to obtain all possible diffraction directions of the matrix due to the random orientation of the powdered sample. The radiation used in the analysis was CoKα at λ= 1.789 Å at angular speed of 0.04426° (2θ/second) and step size of 0.0167°. Transformation of detected diffracted peak rays identified the crystalline structure of each sample since each had a unique d-spacing.

Sample preparation was carried out by powdering the sample using a tungsten carbide ring mill with ethanol as the grinding until a fraction size of around 20 microns was obtained. The powdered sample was then pressed into a back-packed sample holder and loaded for analysis. The qualitative mineral identification was undertaken using the X'Pert HighScore Plus software, which were matched to the mineralogy of the sample with the database (SIROQUANT$^{TM}$ V3).

## Surface Area Analysis

The surface areas of the zeolite and scoria materials, were determined by the physical adsorption of nitrogen gas on the surface of each sample at liquid nitrogen temperatures, using Brunauer, Emmett and Teller (BET) analysis method. The amount of adsorbed gas is correlated to the total surface area of particles including pores on the surface in unit of area per mass of sample ($m^2/g$). The volume of gas adsorbed to the surface of the particles was measured at the boiling point of nitrogen (-196 °C).

Multipoint and single BET analysis was undertaken using a Micromeritics Gemini VII 2390. Each sample (1-2 g) was introduced in a sample tube and placed on the degasser where the sample was treated with a cold flow of nitrogen for 18 h. The samples were degassed before analysis testing where nitrogen continued to flow to reduce reabsorption of any gases. After a zero calibration of the equipment, the sample were removed from the degasser for analysis.

## Cation Exchange Capacity

The cation exchange capacity (CEC) was characterised using a classification criteria given by Inglezakis (2005). With capacity divided into theoretical, real, maximum level.

### Theoretical exchange capacity

The theoretical exchange capacity (TEC) was determined from the chemical composition using the XRF characterisation data for each of the materials. The equivalent concentration of all the exchangeable ions per 100 grams of material were added together, determining the TEC and expressing the TEC in units of meq/100 g.

### Real exchange capacity

Following a method described by Holmes *et al.* (1987), dried samples for the following size ranges: coarse (0.6 – 0.35 mm) and fine (< 0.35 mm) were assessed.

Real exchange capacity (REC) was determined using $NH_4^+$, which displaces cations such as $Na^+$, $K^+$, $Mg^{2+}$ and $Ca^{2+}$. A sample of material (1.0 g) was mixed with 25 mL aliquots of 1.0 M ammonium acetate (Analytical reagent Chem-Supply) ($NH_4C_2H_3O_2$) at pH 7 in a centrifuge tube, placed on an orbital shaker (Bioline 8500) at 25 °C and 300 rpm for 72 h. Samples were centrifuged and the supernatant analysed for alkaline and alkali earth elements by inductively coupled plasma optical emission spectrometry (Agilent 720 ICP-OES). The equivalent concentration of exchangeable ions in the supernatant were totalised and expressed in meq/100 g of material to obtain the REC.

### Maximum exchange level

The maximum exchange level (MEL) was measured by equilibrating 30 g of zeolite or scoria material with 600 mL monoionic solutions containing $Na^+$, $Sr^{2+}$ and $Ba^{2+}$ of varied concentrations at constant temperature for 72 h on an orbital shaker at 25 °C

and 300 rpm (Bioline 8500). The supernatant of the system in equilibrium was analysed by ICP-OES and the total equivalent concentration of exchangeable ions per unit of mass expressed in meq/100 g corresponded to the MEL.

## Solution preparation and analytical analysis

### Chemicals and reagents

Sodium chloride, sodium bicarbonate, sodium fluoride, potassium chloride, magnesium chloride, strontium chloride, barium chloride were purchased from Chem-Supply, Australia and were used without further modification. Solutions were made with ultrapure water typical resistivity of 18.2 M$\Omega$·cm at 25 °C, Milli-Q Millipore.

### Synthetic solutions

The water chemistry of a surrogate CSG co-produced water was based on the initial characterisation performed for the CSG water from Bowen Basin research site (Chapter 3). The synthetic CSG water was prepared using appropriate amounts of analytical grade inorganic chemicals dissolved in ultra-pure water. The concentration of major and trace elements found in the site sample water was used to inform the synthetic water sample composition. Sodium salt was used in three forms: chloride, bicarbonate and fluoride. Other components, such as potassium, calcium, magnesium, strontium and barium found in the CSG water were used in their chloride salt form. The concentration of inorganic salts used to create the synthetic CSG co-produced water from research site in the Bowen Basin are shown in Table 4.1.

Synthetic single cation solutions were prepared using Chem-Supply analytical grade inorganic and acid chemicals. All the synthetic solutions made for adsorption studies were in chloride form containing $Na^+$, $Ca^{2+}$, $K^+$ $Ba^{2+}$ and $Sr^{2+}$ ions at concentrations ranging from $2x10^{-5}$ M up to 0.1 M; except for $Na^+$ in bicarbonate and fluoride forms which were made also at 0.1 M.

### Research site (Bowen Basin CSG co-produced water)

To obtain information on the raw co-produced water from research site, a series of composite samples were collected from the receiving inlet tank at the pilot treatment water facility that is fed by 18 nearby active CSG production wells (Figure 3.1).

Samples were taken on a monthly basis for 14 months during 2013-2014 with the aim of identifying the major elements and compounds in CSG co-produced waters. Methods, procedures and materials for water quality sampling were specified by a NATA accredited laboratory and an example report shown in Appendix section.

CSG water for adsorption studies was collected in pre-cleaned HDPE sample containers that were pre-washed with CSG water prior to filling. Field CSG water from research site in the Bowen Basin was transported in 25 L HDPE plastic containers, and were filtered using 0.45 µm membrane filters (Advantec®, mixed cellulose ester) and analysed by ICP-OES, prior experimentation.

**Table 4.1 Composition of synthetic CSG co-produced water used for batch and column studies.**

| Cation | Typical field CSG water concentration | | Compound | Mass inorganic salt required | Cation concentration surrogate CSG water | |
|---|---|---|---|---|---|---|
| | mg/L | meq/L | | g/L | (mg/L) | meq/L |
| $Na^+$ | 1156.38 | 50.30 | $Na^+$- $Cl^-$ | 2.346 | 1423.25 | 40.14 |
| | | | $Na^+$- $HCO_3^-$ | 0.847 | 615.74 | 10.09 |
| | | | $Na^+$- $F^-$ | 0.002 | 1.23 | 0.06 |
| $K^+$ | 67.45 | 1.73 | $K^+$- $Cl^-$ | 0.128 | 61.16 | 1.72 |
| $Mg^{2+}$ | 5.61 | 0.12 | $Mg^{2+}$- $Cl_2^-$ - $6H_2O$ | 0.046 | 16.36 | 0.46 |
| $Ca^{2+}$ | 28.34 | 0.35 | $Ca^{2+}$- $Cl_2^-$ - $2H_2O$ | 0.103 | 50.15 | 1.41 |
| $Sr^{2+}$ | 3.78 | 0.02 | $Sr^{2+}$- $Cl_2^-$ - $6H_2O$ | 0.011 | 3.05 | 0.08 |
| $Ba^{2+}$ | 12.78 | 0.05 | $Ba^{2+}$- $Cl_2^-$ - $2H_2O$ | 0.021 | 6.61 | 0.18 |

## Analytical analysis of water samples

Measurements of the basic water quality parameters such as electrical conductivity, pH, temperature, salinity and TDS were performed using a portable multi-parameter meter sympHony (VWR) (ThermoFisher). Calibration of each probe was performed in the laboratory daily using Chem-Supply pH (4.01, 7.00 and 12.45) and conductivity (100 µS/cm, 2764 µS/cm and 12.88 mS/cm) standard solutions.

The analysis of all liquid samples was undertaken using an Agilent 720 ICP-OES using the US EPA Method 6010b for Inductively Coupled Plasma Atomic Emission Spectrometry. An ICP multi-element standard solution Merck was used for calibration purposes.

Each sample was filtered using a 0.45 μm membrane filter (Advantec®, mixed cellulose ester) and diluted with ultrapure water and 2% $HNO_3$ reducing the pH to less than 2, due to a high concentration of dissolved metals. Prior to sample analysis, a calibration series was run in order to determine instrument detection limits (IDLs), method of detection limits (MDLs) and the linear dynamic range of the instrument. A calibration blank and calibration standard for a three-point calibration curve was performed. A calibration check, using standard solutions as well as calibration verification from stock solutions independent from calibration standard solution was performed.

Samples were analysed in batches of 50. At the beginning and at the end of every run, initial calibration, blank solution and a verification solution was analysed after every 10 samples in order to provide internal quality control of the results. If the measurements on the verification solutions was greater than 10% of the expected value, corrections on the calibration were made. During analysis, every element was analysed in triplicate for every sample and used by the instrument to estimate relative standard deviation (RSD) automatically. If the RDS result was above 5%, the analysis was stopped and corrected before continuing with a further run.

## Experimental procedure

### Batch adsorption studies

### Natural material batch treatment

Treatment of scoria and zeolite sorbent materials in their natural state consisted of an elution stage with inorganic salts and acid solutions until a near homoionic state was reached. The single cation treatment solutions made were at 1.0 M using ultrapure water and analytical grade reagents (Chem-Supply): calcium chloride ($CaCl_2$); potassium chloride (KCl); ammonium acetate ($NH_4C_2H_3O_2$); and hydrochloric acid (HCl).

For batch studies the material treatment was performed in a batch mode using a ratio of 30 g of material (0.6 – 0.35 mm) in 1,000 mL of single cation solution, over a period of 24 h in an incubator orbital shaker (Bioline 8500) at constant temperature and speed

of 25 °C and 300 rpm. The material was then washed with ultrapure water, while monitoring the conductivity and presence of chloride ions (Cl⁻) using silver nitrate (AgNO₃ Chem-Supply). Washing ceased when the washing solution stopped forming silver chloride precipitation with the addition of silver nitrate (Gedik & Imamoglu, 2008). For a typical acid treatment, pH was monitored during the washing stage and ceased when neutral pH values were achieved. Finally, the treated materials were oven dried for 24 h at 110°C to remove excess water and stored in sealed containers for further use in batch and column experiments.

**Effect of particle size in adsorption and ion exchange processes**

In the study of adsorption rate, natural forms of zeolite and scoria in fraction sizes were used including 1.8 - 0.6 mm, 0.6 – 0.35 mm, and < 0.35 mm.
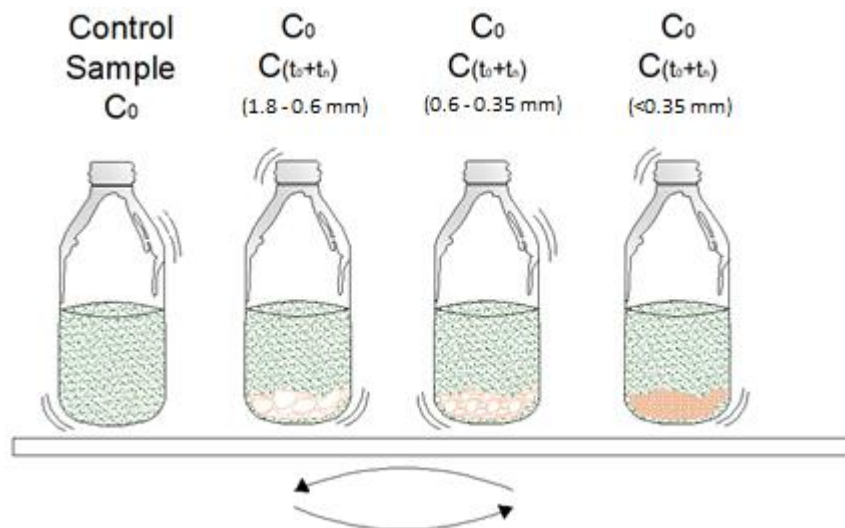


**Figure 4.1 Batch mode experiment figure used to study the effect of particle size on the adsorption capacity of the material. The control sample is the reference concentration; three different fraction sizes were contacted with solutions until equilibrium was achieved to determine the adsorption properties.**

The kinetic adsorption test was performed in a batch type experiment using a 1 L HDPE container with 30 g of material and 600 mL of a solution containing sodium chloride (NaCl) at 0.1 M on an orbital shaker at 300 rpm and 25 °C for fraction sizes 1.8 - 0.6 mm, 0.6 – 0.35 mm, and < 0.35 mm (Figure 4.1). Aliquots of 1 mL were withdrawn from the container at several intervals, where the total volume withdrawn was less than 2% of the total volume used (Inglezakis *et al.*, 2004). Samples were taken with high frequency during the first 720 min, then for the following 72 h samples were

taken in 12 h intervals. Aliquots were diluted with ultrapure water with 2% $HNO_3$ for analysis using ICP-OES to determine total metal ion concentration. The experiments were carried out in duplicate in order to observe reproducibility of the results, and the mean value was reported.

**Adsorption kinetics studies**

To study the kinetic adsorption behaviour, the materials were placed in a solution of known concentrations of single or a mixture of cations in a batch experiment. The interaction between the solution and the adsorbent was continuously monitored taking 1 mL aliquot at different times until the system reached equilibrium. A schematic of the adsorption experiment is shown in Figure 4.2.
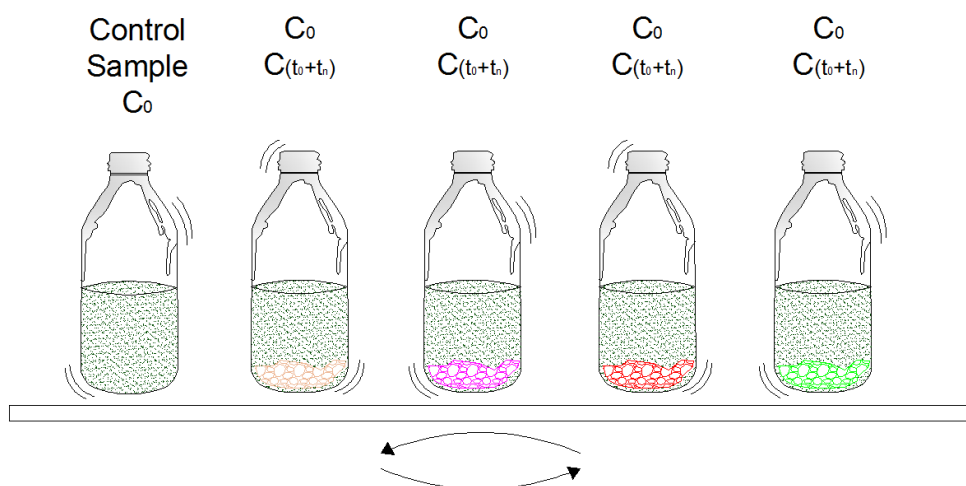


**Figure 4.2 Experimental set-up for the adsorption kinetics of cations in solution using natural and treated scoria and zeolite, colours represent material in treated form. From each system, a 1 mL aliquot is withdrawn every at different times determining the adsorption kinetic uptake.**

Kinetic batch type experiments were conducted using 30 g of natural and treated material (0.6 – 0.35 mm) in contact with 600 mL of solution, performed in a 1 L HDPE container. Each container was placed on an orbital shaker at 300 rpm at a constant temperature of 25 °C for 720 min. The solutions used were: (i) sodium chloride (NaCl) at 0.1 M, (ii) strontium chloride ($SrCl_2$) at $4.5 \times 10^{-4}$ M, (iii) barium chloride ($BaCl_2$) at $4.5 \times 10^{-4}$ M, (iv) synthetic CSG water, and (v) field-collected CSG water from research site. Sample aliquots of 1 mL were withdrawn from the container at intervals, where the total sample volume was less than 2% of the total volume of the solution. Samples were taken with high frequency during the first 720 min, then every 12 h samples were

taken up to 72 h. Samples were diluted with ultrapure water and 2% $HNO_3$ for analysis by ICP-OES. Mean concentration values of the duplicates were used to determine adsorption.

### Behaviour of Na$^+$ adsorption in presence of different anions

In order to investigate the effect of sodium adsorption under the presence of different anions found in CSG water a kinetic trial experiment was developed. Zeolite and scoria material were in contact with sodium in Cl$^-$, HCO$_3$$^-$, and F$^-$ forms made up at 0.1 M, respectively. The methodology for determination of adsorption kinetics was followed.

### Treatment and regeneration of natural materials

The treatment and regeneration of both materials was performed with 30 g of material (0.6 – 0.35 mm) in contact with 1 L solutions of calcium chloride ($CaCl_2$), potassium chloride (KCl), ammonium acetate ($NH_4C_2H_3O_2$), hydrochloric acid (HCl), all made at 1.0 M (Figure 4.3).



**Figure 4.3 Method for the treatment, regeneration, and adsorption/desorption of zeolite and scoria material.**

The solution and adsorbent material were in contact with the retrospective solutions over a period of 24 h on an orbital shaker at constant 25 °C and 300 rpm. The adsorbent

materials were then, rinsed with ultra-pure water and dried at 105 °C for 24 h prior to adsorption kinetic tests with solutions containing cations of interest (Figure 4.3).

Once the material had reached exhaustion, the material was rinsed with ultra-pure water to remove excess of the adsorption solution, and then the regeneration process was performed. The regeneration process followed the methodology for the treatment of scoria and zeolite previously discussed.

After the regeneration stage, the material was separated from the solution using a membrane filter of 0.45 µm pore size (Advantec®, mixed cellulose ester). A 1 mL aliquot was taken from the supernatant and diluted with ultra-pure water with $HNO_3$ at 2% for ICP-OES analysis to determine the concentration of desorbed cations during the treatment or regeneration stages. The adsorption and regeneration cycles were repeated five times, where the reversibility of the adsorption process and potential reusability of both materials was determined.

### Equilibrium adsorption studies

Batch equilibrium isotherm studies were carried out to determine the maximum adsorption of cations using natural and treated zeolite and scoria. In a batch mode, 2.5 g of material (0.6 – 0.35 mm) was placed in a plastic (HDPE) container with 50 mL solutions at different initial concentrations composed of single cations. The material was introduced into the known concentration solution at a constant temperature of 25 °C and placed on an orbital shaker at 300 rpm for 72 h, where the system reached equilibrium. The solutions that were used for equilibrium isotherms were sodium chloride (NaCl), strontium chloride ($SrCl_2$) and barium chloride ($BaCl_2$), at different concentrations ranging from 0.1 M to $2x10^{-5}$ M. The material was separated from the solution and the supernatant was used to determine the concentration of metals. The experiments were carried out in duplicate in order to observe the overall reproducibility of the results, where the mean value was reported.

### Selectivity isotherms for major metals

A selectivity experiment was carried out with two cations in the solution at different ratios at a constant total ion concentration in contact with the zeolite and scoria materials (Townsend & Coker, 2001). The experiment used 30 g of natural material in

a 1 L HDPE container with 600 mL of a binary ion solution agitated on an orbital shaker at 300 rpm for 72 h and constant temperature of 25 °C. The binary solution had a constant ion concentration containing two major metals ions found in the CSG co-produced water. The selectivity isotherms were developed for sodium interactions with calcium, potassium and strontium, which are cations that could compete with sodium for the adsorption or exchange sites on zeolite and scoria material. Mean concentration values of the duplicates were used to determine adsorption.

One of the binary solutions trailed was sodium and calcium where the total concentration of the solution was made at 0.01 M, where sodium and calcium were present in different ratios. Single solutions at the same concentration were trailed in order to determine the boundary conditions of the selectivity isotherm using a solution made up of 100% sodium or 100% calcium. The mechanics of the selectivity experiment as well as a selectivity curve with the possible scenarios for the adsorption behaviour of cation present in a binary solution is shown in Figure 4.4. Equilibrium was achieved after 72 h where the supernatant was separated from the absorber. Samples were diluted with ultrapure water and 2% $HNO_3$ for analysis using ICP-OES.



**Figure 4.4 Typical ion exchange isotherm curves determined experimentally using binary ion solutions.**

## Column adsorption studies

### Column design

Column studies were performed to evaluate and compare the natural adsorbent materials in terms of their capacity, regeneration and treatment in a dynamic flow through mode experiment.



**Figure 4.5 Schematic diagram of the column set-up and experimental procedure for adsorption evaluation in flow through conditions.**

Adsorption studies were conducted in a fixed bed column arrangement packed with the zeolite and scoria materials (Figure 4.5). The column had to maintain geometrical equivalences for the fixed bed arrangement to avoid flow misdistribution and low liquid hold up usually found in adsorption configurations (Inglezakis, 2010b; Inglezakis *et al.*, 2001a; Inglezakis *et al.*, 2001b). The geometrical considerations for the column were:

$$\frac{Z}{D} \geq 5 \quad ; \quad \frac{D}{d_p} \geq 12 \quad ; \frac{Z}{d_p} \geq 50 \qquad\qquad \textbf{Equation 4.1}$$

where $Z$ is the bed height, $D$ is the bed diameter, $d_p$ is the particle size of the granular material.

The column used in the trials was made of Plexiglas with an internal diameter of 22 mm and height of 400 mm. The column had a glass bead mesh at the bottom (inlet) and at the top a paper filter (Whatman, qualitative 3) with a rubber stopper placed in order to prevent any loss of material. The column bed was composed of zeolite/scoria material in a fraction size of 0.6 – 0.35 mm, the column was packed with a bed height of 380 mm, and the total volume of material used was 144.45 mL (144.45 mL = 1 BV). Column, bed and geometrical considerations are shown in Table 4.2.

**Table 4.2 Fixed bed column dimensions and geometrical considerations.**

| Parameter | Dimensions | |
|---|---|---|
| Z | 380 | mm |
| $d_p$ | 0.50 | mm |
| D | 22 | mm |
| BV | 144.45 | mL |
| Flow | Up | up/down |
| Z/D | 17.27 | OK |
| Z/$d_p$ | 760 | OK |
| D/$d_p$ | 44 | OK |

Solutions were fed at flow rates into the column in an up flow mode using a peristaltic pump (LongerPump BT100-2J with YZ-1515X pump head). An up flow mode was preferred since this mechanism prevents channel or flow misdistribution during the column's operation. The solution that exited the column from the top was collected in 10 mL sample polypropylene vials at different intervals until the adsorption capacity of the material was exhausted. Samples were diluted with ultrapure water and 2% $HNO_3$ for analysis by ICP-OES to determine the cations present following the column filtration experiment.

### Experimental validation of column up flow mode

Validation of the column arrangement used in this study was performed primarily to evaluate possible hydraulic issues during the normal operation of the fixed bed and column under up flow mode (Appendix D). The packed columns were rinsed with ultrapure water for 5 BV (723 mL) until the water exiting the column had a constant pH and electrical conductivity similar to the feeding solution prior to the validation test.

The hydraulic behaviour of the packed column was investigated using a trace high salinity (EC = 10,000 mS/cm) solution. The solution was pumped in up flow mode at 1, 5, 10 BV/h. The existing solution was continuously monitored for pH and electrical conductivity. Results obtained from the solution that passed through the column at different flow rates were used to create breakthrough curves (profile of the effluent solution) of the packed column in order to determine the hydraulic behaviour of the column, identifying possible flow misdistribution, low liquid hold up, fingering and other hydraulic related issues that could affect the column performance.

### Adsorption column studies

The column study assesses the zeolite and scoria in natural and treated form under flow through conditions in terms of their operational capacity to adsorb cations present in CSG water from research site in the Bowen Basin. Each of the column trials produced a breakthrough curve showing the adsorption performance of each material using a synthetic solution and field CSG water.

In short, the column was packed with 145 mL of dried natural or treated material. The operation of the column during the adsorption process was in an up flow mode using solutions of sodium chloride (NaCl) at 0.1 M, synthetic CSG water and field CSG water from research site. The effect of flow rate on the adsorption process of sodium ions was studied using three volumetric flow rates, 1, 5 and 10 BV/h by controlling the speed on the peristaltic pump for a total of 20 BV. The exiting solution was sampled continuously and analysed by ICP-OES to generate a breakthrough curve profile for each flow rate, material state and also the solution used.

Field CSG water from research site was used as the inflow solution for the fixed bed columns at 5 BV/h for a total of 20 BV in up-flow mode. The average equivalent composition of the CSG water consisted of 49 meq/L of $Na^+$; 1 meq/L of $Ca^{2+}$; 0.6 meq/L of $K^+$; 0.4 meq/L of $Mg^{2+}$; 0.07 meq/L of $Sr^{2+}$; and 0.02 meq/L of $Ba^{2+}$.

### Material treatment, regeneration and desorption of cations in column mode

Treatment, regeneration and following desorption processes were assessed using scoria and zeolite materials to determine behaviour and performance. The adsorption process exhausted the material reaching the practical adsorption capacity after a large

number of BV of operation. The regeneration cycle was then performed using 5 BV of ultrapure water pumped up-flow rinsing and removing the excess solution (mainly NaCl solutions) used for the adsorption process. Rinsing with 5 BV guarantees the removal of all the solution excess.

Initial treatment of natural materials and regeneration of exhausted material were performed in an up-flow mode over a period of 24 h using 5 BV of potassium chloride (KCl) and ammonium acetate ($NH_4C_2H_3O_2$) solutions made at 1.0 M. The regeneration procedure was developed based on the batch regeneration tests and validated for 5 BV to assure that complete regeneration was achieved. Once the regeneration process was finished, excess of regenerate solution was rinsed using 5 BV of ultrapure water and checking the electrical conductivity of the rinsing solution, before the following adsorption trial was started.

A maximum of 5 regeneration cycles was performed. A sample from the regeneration supernatant was collected for elemental composition determining the performance of the cation desorption in each regeneration cycle, and the potential reuse of zeolite and scoria material in fixed bed columns.

## Data analysis and modelling

The experiments were carried out in duplicates in order to observe reproducibility of the results, and the mean value of the replicates, which did not vary by more than 5% were reported, or otherwise stated.

The equilibrium and kinetic models implemented for the adsorption studies have two or more than two adjustable parameters that require to be fitted to the experimental data by a non-linear least square analysis (Millar *et al.*, 2015b). The non-linear model equations were implemented in Matlab R2012b (MathWorks®) and fitted to the experimental using the sum of the squared error (SSE).

$$SSE = \sum_{i=1}^{p}(q_{e,calc} - q_{e,means})^2{}_i \qquad \textbf{Equation 4.2}$$

The diffusion and breakthrough empirical models were fitted to the experimental data, using the mathematical linear expression fitting the model parameters using SSE

implemented in Microsoft Excel and the Solver function (Chu, 2010; Millar *et al.*, 2015a; Motsi, 2010; Negrea *et al.*, 2011; Nguyen *et al.*, 2015).

# Chapter 5: Characterisation of natural ion exchangers

## Introduction

The characterisation of the zeolite and scoria materials determines their physical, mineralogical and chemical nature. The material characterisation included surface morphology and composition by the use of SEM combined with EDS; the qualitative and quantitative composition determined by XRD and XRF elemental features; surface area of adsorbents by BET analysis; and finally the real cation exchange capacity.

## Scanning Electron Microscopy (SEM) and EDS

### Zeolite material

The surface of the zeolite material in its natural state exhibited a drusy texture (Figure 5.1) with a secondary porous characteristic. The secondary porous features are probably made of volcanic shards that have been pseudo morphed by the crystals of the zeolite material. Crystalline inorganic salts were observed on the surface formed through processes of evaporation during the oven drying stages. The secondary pore sizes ranged from 1 to 5 µm. The zeolite material is considered to be a microporous structure with pores to be in the range of 4 Å in diameter (Pabalan & Bertetti, 2001).
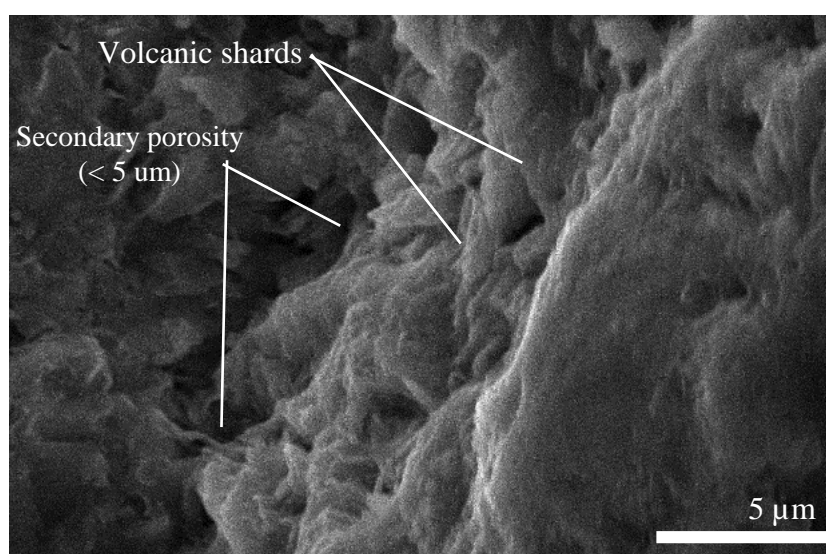


**Figure 5.1 SEM micrograph of natural zeolite at x5,000 magnification. Surface and morphological structures are detailed.**

The natural zeolite presented a high concentration of silicon and aluminium oxides, which are expected due to the aluminosilicate nature, accompanied by both alkali and alkaline metals often deemed exchangeable (Table 5.1). The natural zeolite contained a large amount of potassium (3.98±0.39 %w/w) and calcium (3.74±1.05 %w/w) and elevated amounts of iron (6.55±0.39 %w/w), almost 50% of the amount of calcium in the form of an oxide. Sodium and magnesium were also present but in lower concentrations. The natural zeolite may be characterised as a calcium/potassium rich material in its natural form (Shoumkova, 2011).

**Table 5.1 EDS oxide elemental composition (%w/w) of natural and treated zeolite material (n=3; Mean Value ± SD).**

| Zeolite | $Na_2O$ | MgO | $Al_2O_3$ | $SiO_2$ | $K_2O$ | CaO | $Fe_2O_3$ | N | Total |
|---|---|---|---|---|---|---|---|---|---|
| Natural | 2.55±0.39 | 2.02±0.13 | 12.99±0.81 | 68.39±1.97 | 3.98±0.39 | 3.74±1.05 | 6.55±0.39 | - | 100.22 |
| Potassium | 0.90±0.57 | - | 14.47±0.25 | 63.29±0.52 | 16.30±0.2 | 0.60±0.13 | 4.04±0.81 | - | 99.60 |
| Acid | 2.59±0.39 | 3.74±0.78 | 14.40±2.3 | 70.65±1.07 | 1.55±0.21 | 4.41±0.32 | 3.06±0.64 | - | 100.40 |
| Ammonium | 1.64±0.36 | - | 17.36±1.09 | 63.88±1.40 | 1.63±0.26 | 0.14±0.02 | 5.22±0.44 | 11.07±0.44 | 100.95 |

Zeolite, when treated with $K^+$, exhibited a similar morphology and topography as the one observed for the natural zeolite. The potassium has displaced exchangeable cations contained on the zeolite material modifying the elemental composition of the surface of the material and making potassium more available than other cations (16.30 ± 0.2 %w/w), a four-fold the concentration increase for $K^+$ when compared to the natural zeolite (Table 5.1). The concentration of alkali and alkaline ions such as sodium (0.90±0.57 %w/w) and calcium (0.60 ± 0.13 %w/w) were smaller following the $K^+$ treatment. Magnesium has also been removed from the surface of the zeolite. The silicon oxide (63.29 ± 0.52 %w/w) was also lower in the concentration on the zeolite structure, and it is believed to correspond to impurities contained in the natural zeolite.

Surface morphology of the zeolite treated with hydrochloric acid at 1.0 M was consistent with those surfaces observed for natural and inorganic salt treatments. The EDS results for acid treated zeolite showed that the aluminosilicate composition of the zeolite material was unchanged, despite the acid treatment, and probable loss of aluminium content. The aluminium (14.40 ± 2.3 %w/w) content exhibited on the surface of the zeolite is analogous to the natural zeolite form (Table 5.1). The cations of potassium (1.55 ± 0.21 %w/w) and iron (3.06 ± 0.64 %w/w) were reduced to half

their original concentrations after acid treatment when comparing to the natural state of the zeolite. Other cations present on the zeolite surface remained unchanged, indicating the reduced efficiency of the treatment to remove exchangeable cations.
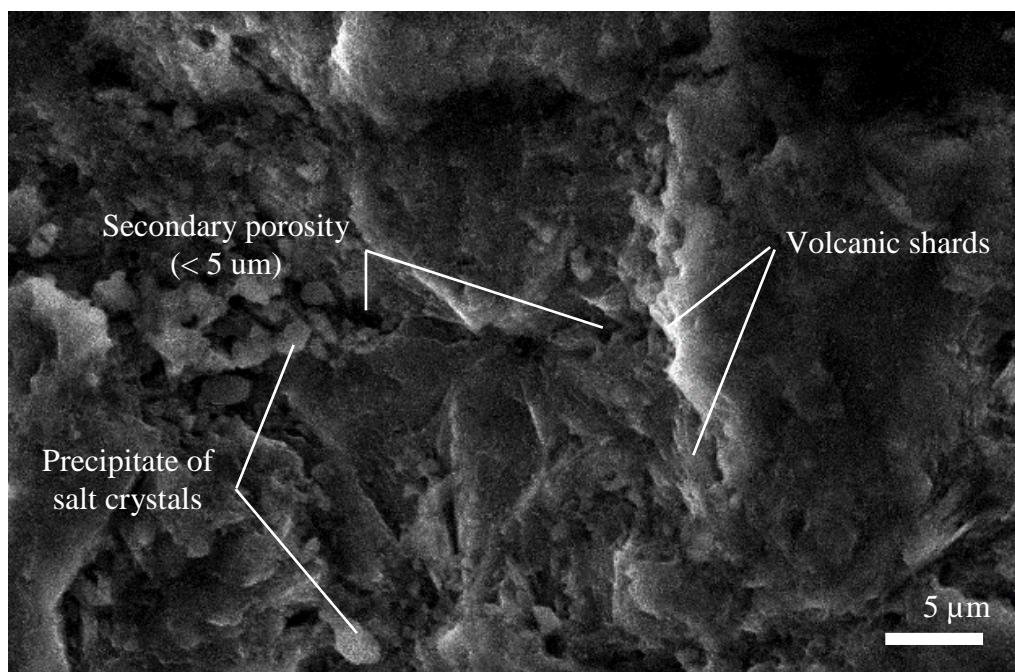


**Figure 5.2 SEM micrograph of ammonium treated zeolite at x2,700.**

The zeolite material when treated with ammonium cations presented similar surface morphology to that observed in the natural material state, with inner shards formed by crystals with a druse morphology as depicted in Figure 5.2. The elemental composition of the ammonium treated zeolite (Table 5.1) exhibited the aluminosilicate with a reduction of silicon oxide ($63.88 \pm 1.4$ %w/w) believed to be impurities, while additional aluminium ($17.36 \pm 1.09$ %w/w) was detected on the surface when compared to the natural form. The concentration of metals was lower after treatment. Nitrogen ($11.07 \pm 0.44$ %w/w) on the surface of the material showed that ammonium treatment was able to remove alkali and alkaline elements that were present on the natural zeolite, since large reduction of the exchangeable cations was observed.

**Scoria material**

The scoria material (Figure 5.3) exhibited a vesicular surface texture, which can be attributed to the product of trapped gas during the original formation of the material. Vesicles and voids on the surface of the material had on average a diameter of 70 µm and contained small crystal deposits (Figure 5.3).

A

Vesicles

Precipitate of
salt crystals

100 µm

B

Precipitate of
salt crystals

Void pores
(< 1um)

5 µm
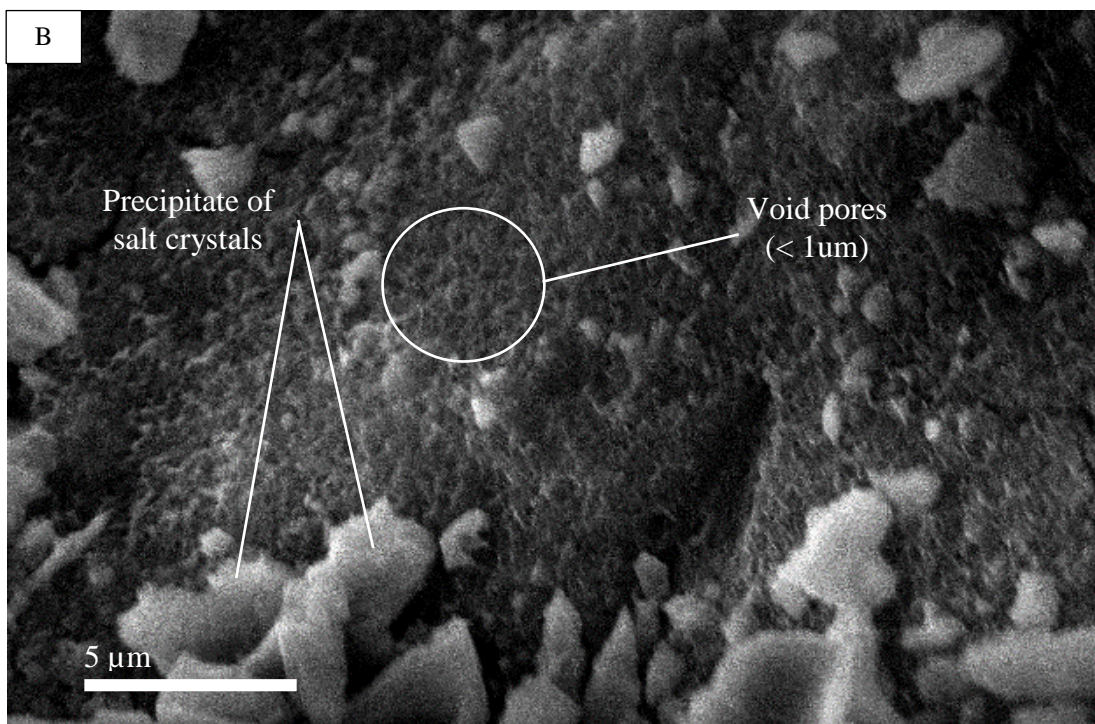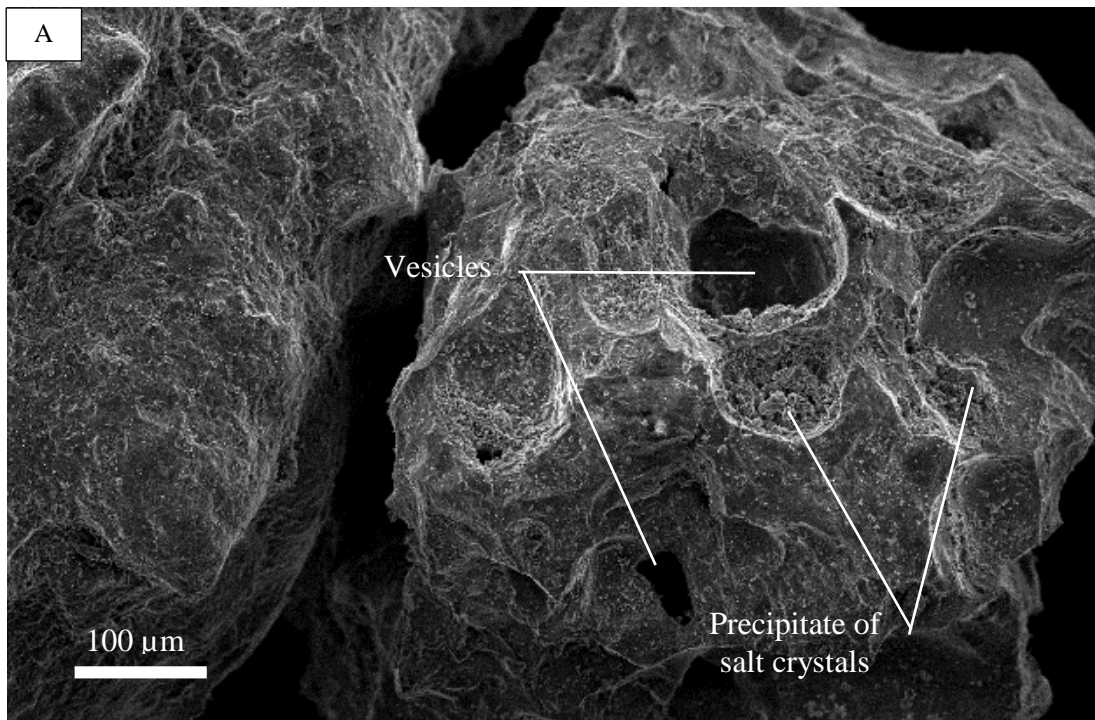
**Figure 5.3 SEM micrographs of natural scoria material at different magnifications x160 and x5,000.**

An elemental analysis of the surface of the natural scoria material showed that the material followed the geochemical characteristics often observed of a basalt type formation demonstrated by the abundant silicon oxide, aluminium and iron oxides

concentrations (Table 5.2). The total mean alkali composition (10.31 %w/w) was found to be greater than the total mean alkaline (7.52 %w/w), making this material an alkali basalt related to a feldspar formation (Benjamin *et al.*, 2007).

**Table 5.2 EDS oxide elemental composition (%w/w) of natural and treated scoria material (n=3; Mean Value ± SD).**

| Zeolite | $Na_2O$ | MgO | $Al_2O_3$ | $SiO_2$ | $K_2O$ | CaO | $Fe_2O_3$ | N | Total |
|---|---|---|---|---|---|---|---|---|---|
| Natural | 7.72±0.31 | 3.45±0.05 | 12.60±0.1 | 48.77±1.1 | 2.59±0.24 | 4.33±0.35 | 20.62±1.13 | | 100.08 |
| Potassium | 4.42±0.22 | 3.88±0.35 | 10.60±0.6 | 54.13±1.95 | 8.02±0.43 | 7.7±0.558 | 11.31±2.21 | | 100.15 |
| Acid | 9.53±0.22 | 4.85±0.26 | 11.55±0.05 | 57.73±0.36 | 2.41±0.66 | 6.71±0.46 | 7.36±0.81 | | 100.14 |
| Ammonium | 2.12±0.07 | 3.71±0.35 | 11.42±0.26 | 54.47±0.53 | 0.88±0.05 | 5.38±0.25 | 11.31±0.83 | 10.81±0.32 | 100.09 |

When the scoria is treated with potassium chloride at 1.0 M, the surface texture is similar to its natural form showing vesicles ranging from 50 − 100 µm distributed across the surface. EDS elemental analysis (Table 5.2) showed that the major components of the basaltic structures were preserved following the $K^+$ treatment. Treatment increased the concentration the potassium (8.02 ± 0.43 %w/w) on the surface by reducing sodium and iron oxide.



Structural damage

100 µm
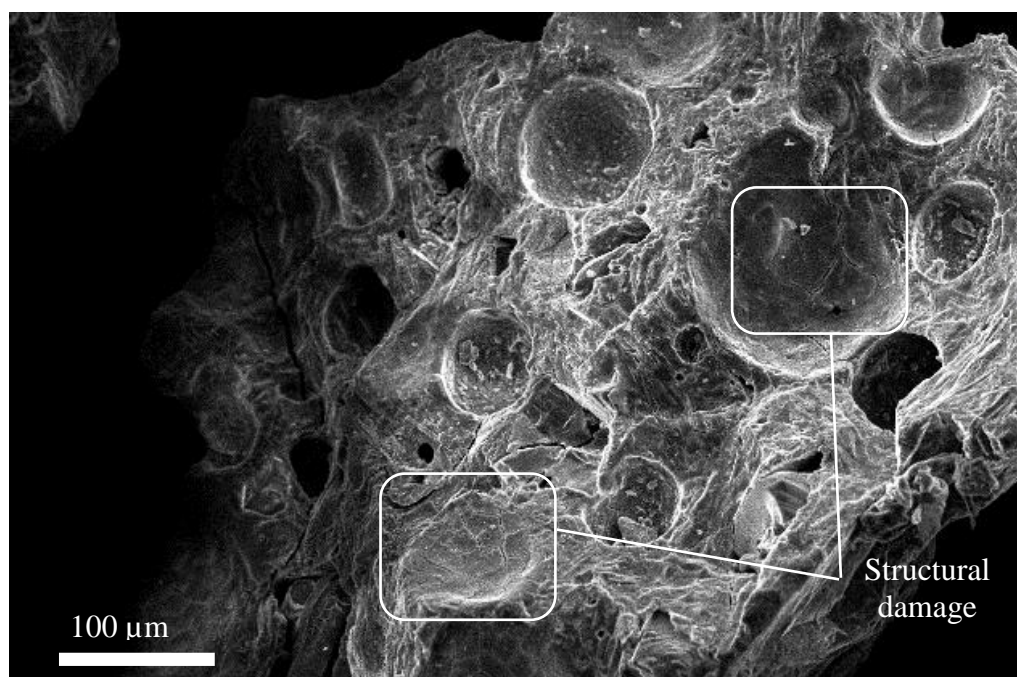
**Figure 5.4 SEM micrographs of acid treated scoria at different magnifications x100.**

The surface of acid treated scoria showed that a salt crystal layer had no formed and caused evident structural surface damage (Figure 5.4). As a result of the acid treatment,

the material became soluble, producing fissures across the scoria that may also compromise the stability and adsorption properties of the material. The elemental composition of the surface of this acid treated scoria material showed a significant reduction in the iron oxide composition when compared to its natural form of about 65%. Alkali and alkaline cations were present at similar concentrations to that observed for the natural scoria form (Table 5.2).

Following an ammonium treatment of the scoria surface (Table 5.2) the geochemical characteristics of the determined basalt type rock were maintained after treatment. Total mean alkali composition (3.0 %w/w) was decreased together with the iron oxide composition, while the total mean alkaline (9.09 %w/w) composition remained relatively constant when compared to natural scoria form. The nitrogen composition determined by EDS was approximately 10.81 %w/w, which indicates that ammonium cations were adsorbed onto the surface of the material.

Material treatment with acid, ammonium and potassium solutions have resulted in surface modifications reflected on the cation content, which has been noticeable. A marked difference between natural and treated forms are considerable and statistically show how much the concentration of magnesium, calcium and sodium have been changed as a result of treatment.

## X-ray fluorescence (XRF)

XRF analysis (Table 5.3) revealed silicon-aluminium levels, characteristic of aluminosilicate material structure. Calcium was the major balancing ion followed by sodium, iron, potassium and magnesium for the zeolite, while iron was the largest chemical signature for the scoria. XRF results agree corroborated using SEM-ED spectroscopy. Similarly, high aluminium and silicon compositions with alkaline and alkali cations in other zeolites using XRF analysis have also been observed (Baker *et al.*, 2009; Castaldi *et al.*, 2008; Du *et al.*, 2005; Hlavay *et al.*, 1982; Ho & Ho, 2012; Jha & Hayashi, 2009; Korkuna *et al.*, 2006; Taulis & Milke, 2009; Wang *et al.*, 2012).

An important characteristic of zeolite materials is the silicon aluminium ratio (Si/Al), this ratio denotes the type of zeolite and the capacity of the said zeolite to exchange

ions. The amount of aluminium present within the framework can vary over a wide range. Nonetheless, most zeolites found in nature, have lower Si/Al ratios, with some of the $Si^{4+}$ in the framework substituted by $Al^{3+}$ giving the zeolite a net negative charge balanced with positive ions. The Si/Al ratio calculated for the zeolite material using XRF was found to be 5.50 (mol/mol). The ratio of Si/Al for a clinoptilolite and mordenite zeolite are reported to be between 2.92 to 5.04 and 4.19 to 5.79, respectively (Alberti *et al.*, 1997; Colella, 1996; Du *et al.*, 2005; Wang *et al.*, 2012).

**Table 5.3 Chemical composition of zeolite and scoria in natural form performed by XRF. LOI = loss on ignition determined gravimetrically; Detection limit 0.01%.**

| Chemical composition | Natural zeolite used in this study (% w/w) | Escott Zeolite (Wang *et al.*, 2012) | Natural scoria used in this study (% w/w) | Scoria – Korea (Kwon *et al.*, 2005) |
|---|---|---|---|---|
| $Fe_2O_3$ | 1.34 | 1.37 | 11.62 | 12.24 |
| $SiO_2$ | 72.84 | 68.26 | 46.23 | 48.02 |
| $Al_2O_3$ | 11.69 | 12.99 | 13.30 | 15.18 |
| CaO | 2.85 | 2.09 | 8.74 | 8.66 |
| $K_2O$ | 1.04 | 4.11 | 0.98 | 1.36 |
| MnO | 0.02 | 0.06 | 0.18 | |
| $Na_2O$ | 1.83 | 0.64 | 2.13 | 2.67 |
| MgO | 0.87 | 0.83 | 13.39 | 7.84 |
| $P_2O_5$ | 0.03 | 0.06 | 0.51 | |
| $SO_3$ | <0.01 | 0.49 | 0.01 | |
| $TiO_2$ | 0.18 | 0.23 | 1.63 | 2.41 |
| BaO | 0.13 | | 0.04 | |
| $Cr_2O_3$ | <0.01 | | 0.08 | |
| NiO | <0.01 | | 0.05 | |
| LOI | 7.140 | 8.87 | 1.01 | 1.66 |
| Total | 100.06 | | 99.95 | |

The sum of $Na^+$, $K^+$, $Ca^{2+}$ and $Mg^{2+}$ cations represents the theoretical exchange capacity (TEC), 154 meq/100 g (Table 5.3). Typical theoretical cation exchange capacities for pure clinoptilolite and mordenite zeolites are 222 meq/100 g and 229 meq/100 g, respectively (Colella, 1996; Pabalan & Bertetti, 2001). However, a significant part of the cations identified as 'exchangeable' within the zeolite framework may have limited possibilities to be exchanged because these cations may be located in inaccessible sites upon the structure and furthermore, some of these cations exist as impurities of the material that do not participate in the overall ion exchange process (Inglezakis *et al.*, 2002).

Scoria contained a high concentrations of magnesium oxide, which is consistent with an olivine mineral structure often contained in a scoria material. Silicon and aluminium content observed in the scoria correspond to a feldspar and pyroxene type mineral. The major chemical composition agrees with other scoria materials described by Kwon *et al.* (2005) for silicon and aluminium content (Table 5.3). The substitution of silicon by aluminium that occurs in a plagioclase feldspar mineral structure generates an imbalance on the charge counteracted by exchangeable cations, giving the scoria material ion exchange properties (Kwon *et al.*, 2010). The Si/Al ratio calculated form the XRF values in Table 5.3 was 3.07 (mol/mol), which is comparable to chabazite (1.43-4.18) or erinonite (3.05-3.99) zeolites (Colella, 1996).

The determination of the theoretical exchange capacity (TEC) was calculated taking into account the mineralogical and elemental composition. The structure that was identified to have ion exchange properties was the plagioclase feldspar and typically calcium is only exchangeable. Thus the cation capacity of the material was estimated to be approximately 46 meq/100 g. This result was greater than other studies reported for scoria, where cation exchange capacity was seen to be 16.1 meq/100 g (Kwon *et al.*, 2005) and 0.09 meq/100 g (Alemayehu & Lennartz, 2009) using XRF.

## X-ray diffraction (XRD)

### Natural zeolite material

The zeolite sample presented major diffraction peaks at 11.5°, 25.5° and 31° which are indicative peaks for the type and quantity of a particular crystalline structure present in the sample (Figure 5.5). These peaks were then compared with the XRD SIROQUANT database using the Rietveld process, simulating the XRD patterns from known crystalline structures of the minerals with variation in parameters, such as, mineral abundance and crystal type until the pattern fits the measured XRD. The XRD method had an accuracy of around ± 3 %w/w with a 95% confidence accurately indicating the mineral composition of the natural zeolite sample.
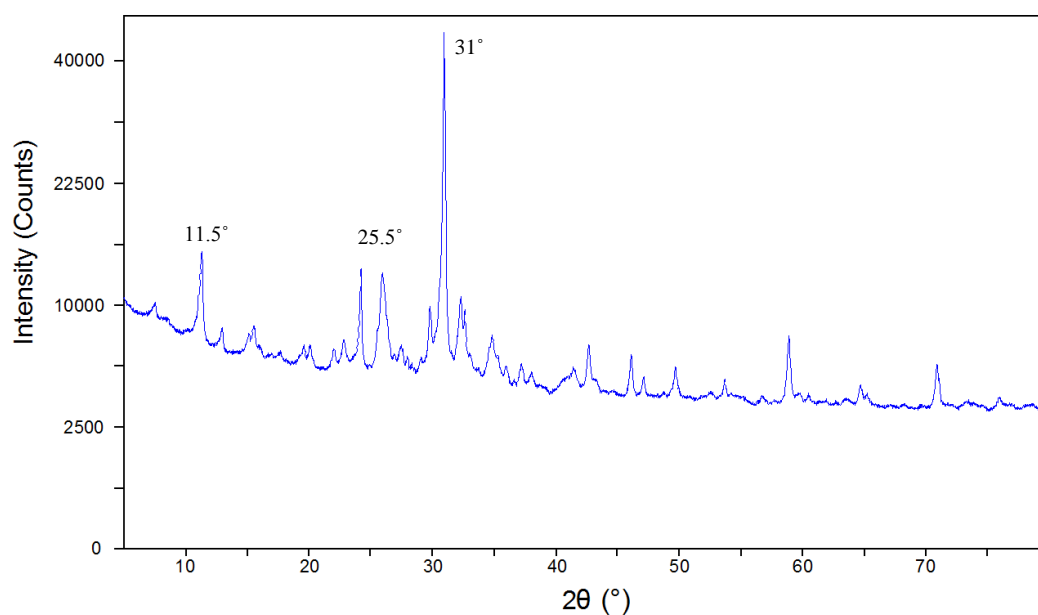
**Figure 5.5 X-ray diffractogram of the natural zeolite sample used in this study. The picks in the figure depicts minerals found in the sample, being the major Quartz (11.5°), mordenite (25.5°) and clinoptilolite (31°).**

**Table 5.4 Quantitative XRD results for zeolite material.**

| Mineral | Typical unit cell formula | (%w/w) |
|---|---|---|
| Quartz | $SiO_2$ | 30 |
| Mordenite | $(Ca, Na_2, K_2)Al_2Si_{10}O_{24} \cdot 7H_2O$ | 29 |
| Clinoptilolite | $(Ca,Na)_2\text{-}3Al_3(Al,Si)_2Si_{13}O_{36} \cdot 12H_2O$ | 41 |
| Total | | 100 |

The major minerals present were clinoptilolite (41 %w/w), mordenite (29 %w/w) and quartz (30 %w/w) (Table 5.4). These data agree with other Australian zeolites as clinoptilolite (Ho & Ho, 2012; Wang & Nguyen, 2016). Quartz ($SiO_2$) comprises a significant amount of the total zeolite sample and due to the known intrinsic low adsorption or ion exchange properties of this mineral, the material can be considered as an impurity within the zeolite composition. The other two minerals found in the zeolite sample correspond to known natural zeolite minerals and constitute the 70 %w/w of the material used in this study.

### Zeolite mineralogical analysis

Mordenite and clinoptilolite are zeolite type materials that occur in a variety of geological settings. These materials are the product of the alteration of sedimentary

minerals, as temperature and pressure modify finely the crystalline rock composition (Inglezakis & Zorpas, 2012b).

Although zeolites have similar chemical compositions to each other – from different regions, a common sub-unit crystal structure with a specific array of aluminosilicate $(AlSi)O_4$ tetrahedral is always present. The natural spaces and channel interconnection in dehydrated zeolites determines the physicochemical features for the adsorption or the ion exchange processes (Alberti *et al.*, 1997). The size of these channels is limited by the aperture between the tetrahedron bounded oxygen atoms. There are three crystal structure variations in zeolite materials, which are: (1) chains, (2) sheet and (3) framework. The chain structure forms an acicular needle shape like a prismatic crystal. The sheet structure occurs when crystals are flattened or tabular with good basal cleavage. The framework structure exhibits crystals that are equivalent in all directions and dimension (Alberti *et al.*, 1997).
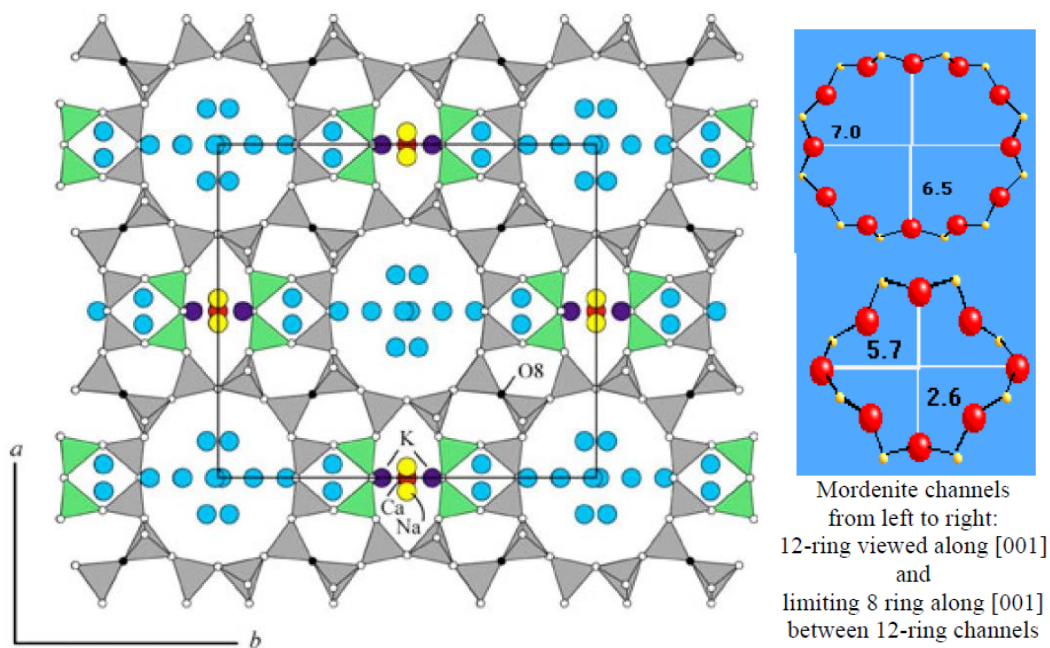


**Figure 5.6 Diagram to show the crystal structure and channel composition of mordenite. Water molecules are shown in blue, potassium, calcium and sodium ions are shown in purple, red and yellow respectively (Inglezakis & Zorpas, 2012b; Mineralogy, 2015).**

Mordenite's morphology corresponds to an orthorhombic single crystal arrangement, like thin fibres, depicted by the features shown in Table 5.5. Mordenite pores consist of 12 and 8-12 ring channels system (Figure 5.6), which form tube-like structures interconnected with oxygen atoms. The channel structure and dimensions are shown

in Table 5.5 and Figure 5.6. Mordenite has a particular topology in its system of channels and cavities, which are denominated as intracrystalline, where channels are parallel and are not interconnected allowing migration of guest molecules to diffuse unidirectionally.

**Table 5.5 Zeolite crystal characteristics (Barthelmy, 2014; Shoumkova, 2011).**

| Mineral | Channels Dimension (Å) | Crystal system | | Crystal cell dimensions (Å) |
|---|---|---|---|---|
| Mordenite | 6.5 x 7.0<br>2.6 x 5.7 | Orthorhombic pyramidal |  | a = 18.11<br>b = 20.51<br>c = 7.52 |
| Clinoptilolite | 3.6 x 4.6<br>3.1 x 7.5<br>2.8 x 4.7 | Monoclinic prismatic |  | a = 17.66<br>b = 17.96<br>c = 7.40 |
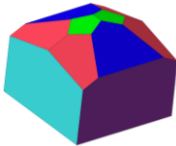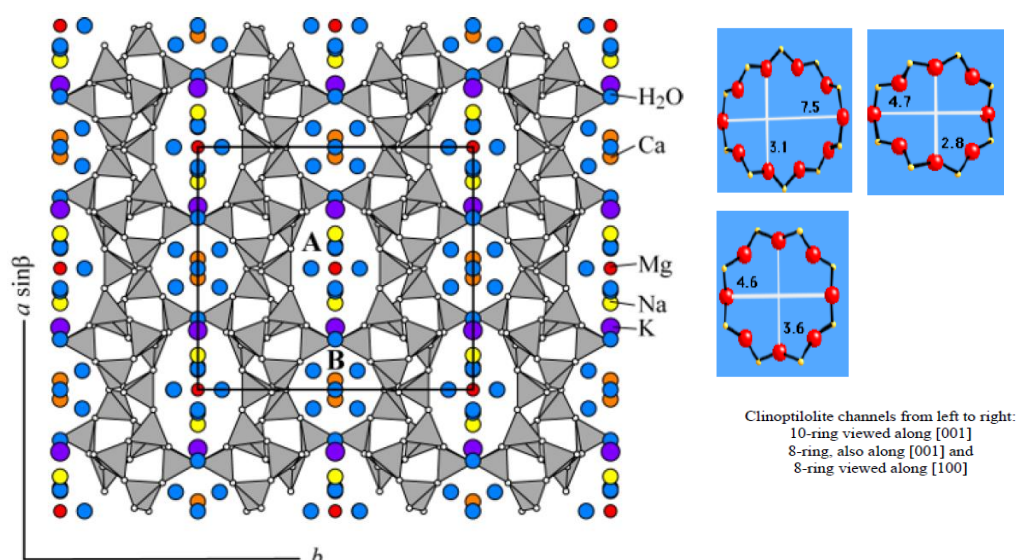


**Figure 5.7 Diagram to show crystal structure and channel composition of clinoptilolite. Water molecules are coloured blue, potassium, calcium, magnesium and sodium ions are shown in purple, orange, red and yellow respectively (Inglezakis & Zorpas, 2012b; Mineralogy, 2015).**

The crystal morphology of clinoptilolite is a monoclinic prismatic in nature (Table 5.5). The clinoptilolite structure has an interconnected system of channels that permits a diffusion or migration of molecules in two dimensions, like a sheet structure. Every oxygen ion within the structure is connected to either silicon or aluminium ion. Clinoptilolite zeolite is composed of three-ring channel system that conforms to sheets,

alternating eight and ten sides as shown in Figure 5.7 with a range of pore sizes (Table 5.5). These rings stacked together form channels through the crystal structure.

## Natural scoria material

An XRD diffractogram of the natural scoria material (Figure 5.8) demonstrated major diffraction peaks at 42°, 32°, 34°, 37° and 61°. These peaks were then matched to the XRD SIROQUANT database, using known crystal structures and mineral abundance until a match was found within a 95% confidence for qualitative and quantitative mineral distribution.
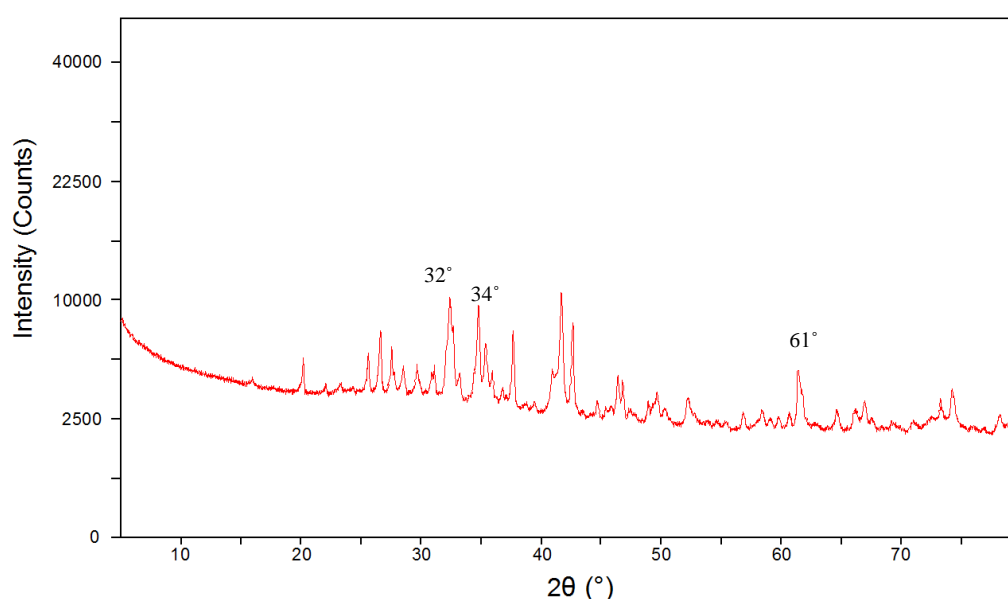


**Figure 5.8 X-ray diffractogram of the natural scoria sample used in this study. The picks in the figure depicts minerals found in the sample, being the major Forsterite (32˚), anorthite (30˚) and diopside (34˚).**

**Table 5.6 Quantitative XRD results for scoria material.**

| Mineral | Typical unit cell formula | (%w/w) |
|---|---|---|
| Quartz | $SiO_2$ | 1 |
| Forsterite | $Mg_2SiO_4$ | 33 |
| Anorthite | $CaAl_2Si_2O_8$ | 30 |
| Ankerite | $Ca(Fe,Mg,Mn)(CO_3)_2$ | 1 |
| Diopside | $Ca(Mg,Fe)(Si,Al)_2O_6$ | 34 |
| Hematite | $Fe_2O_3$ | 1 |
| Total | | 100 |

The diffraction analysis indicated that the major minerals were diopside (35 %w/w), forsterite (33 %w/w) and anorthite (29 %w/w) (Table 5.6). The remaining 3 %w/w (Quartz, Ankerite and Hematite) represent impurities during the formation of the material (Lima *et al.*, 1999; Silva *et al.*, 1993). This composition is consistent with that reported by Alemayehu and Lennartz (2009) and Kwon *et al.* (2005); Kwon *et al.* (2010), who also found that scoria was a mixture of olivine (forsterite), pyroxene (diopside) and hematite minerals.

**Scoria mineralogical analysis**

Diopside is a calcium and magnesium silicate, the typical chemical composition is given in Table 5.6. This mineral is a common silicate mineral in the pyroxene family that occurs in metamorphous siliceous limestone and dolomite (Barthelmy, 2014). Diopside may form chemical replacements with ferrous iron replacing the magnesium in the molecular structure. The crystal system of diopside is monoclinic prismatic with restricted channels that may interfere with the molecular sieving, adsorption or ion exchange properties (Table 5.7, Figure 5.9).

Table 5.7 Crystal characteristics for major minerals found in natural scoria (Barthelmy, 2014).

| Mineral | Crystal system | | Crystal cell dimensions (Å) |
|---------|----------------|---|-----------------------------|
| Diopside | Monoclinic prismatic |  | a = 9.76<br>b = 8.92<br>c = 5.25 |
| Forsterite | Orthorhombic di-pyramidal |  | a = 4.75<br>b = 10.19<br>c = 5.98 |
| Anorthite | Triclinic Pinacoidal |  | a = 8.17<br>b = 12.87<br>c = 14.16 |
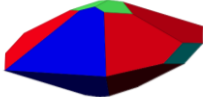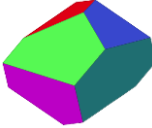
Forsterite, the second most abundant mineral found in the scoria material is also known as olivine. Forsterite is often found in ultramafic igneous rocks or in dolomitic limestones and has a high melting point above 1,500 °C which is considered practically infusible (Mineralogy, 2015). Forsterite has an orthorhombic di-pyramidal crystal that contains $SiO_4^{4-}$ and $Mg^{2+}$ molecular composition, single covalent bond with oxygen

atoms with a silicon atom in the centre. This arrangement makes the forsterite structure dense and hence may interfere with the adsorption or ion exchange processes.
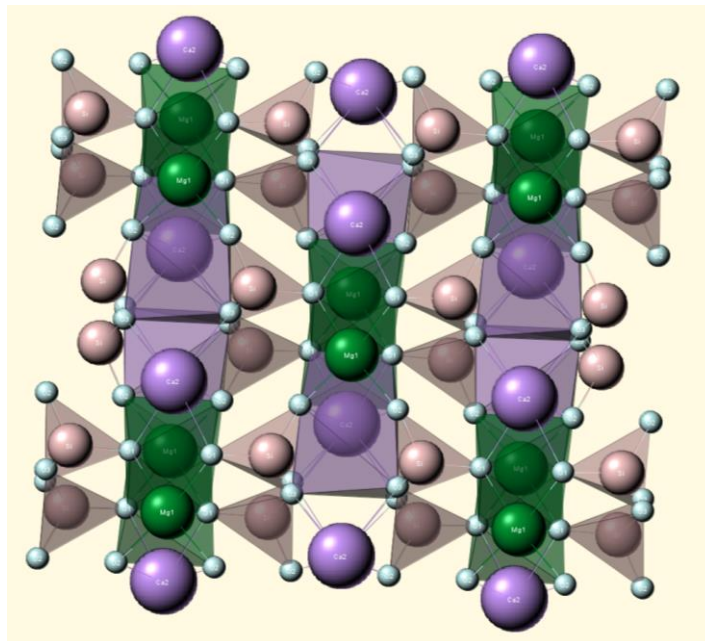


**Figure 5.9 Diopside crystal structure (a,b phase). Calcium, magnesium, silica and oxygen ions are coloured in purple, green, brown and silver respectively (Barthelmy, 2014).**
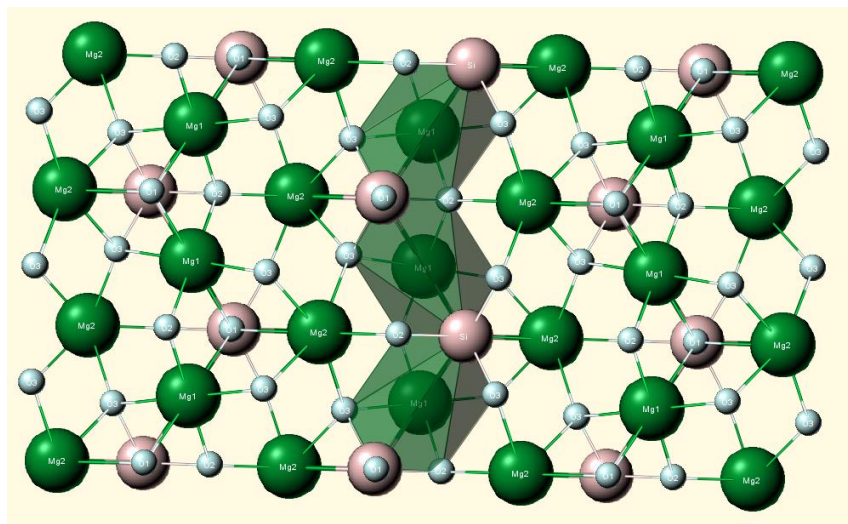


**Figure 5.10 Forsterite crystal structure (b,c phase). Magnesium, silica and oxygen ions are shown in green, brown and silver respectively (Barthelmy, 2014).**

Anorthite is the third most abundant mineral present in the characterised scoria material (Table 5.6) and is classified as a plagioclase feldspar tectosilicate containing $45 - 50\%$ of the $Si^{4+}$ in the tetrahedral framework substituted by $Al^{3+}$ (Hay, 1986). As observed for zeolites, the crystal structure framework presents a deficit balance with

cations that in the case of anorthite, is balanced mainly by calcium. It is also known that about 10% of the calcium in the crystal structure may be replaced by sodium in proportion of the total charge of the structure. Alberti *et al.* (1997) suggested that framework structures such as feldspar minerals have reduced channels that restrict adsorption or ion exchange interactions. The crystal system is triclinic pinacoidal with a dimension of the crystal cell (Table 5.7, Figure 5.11).
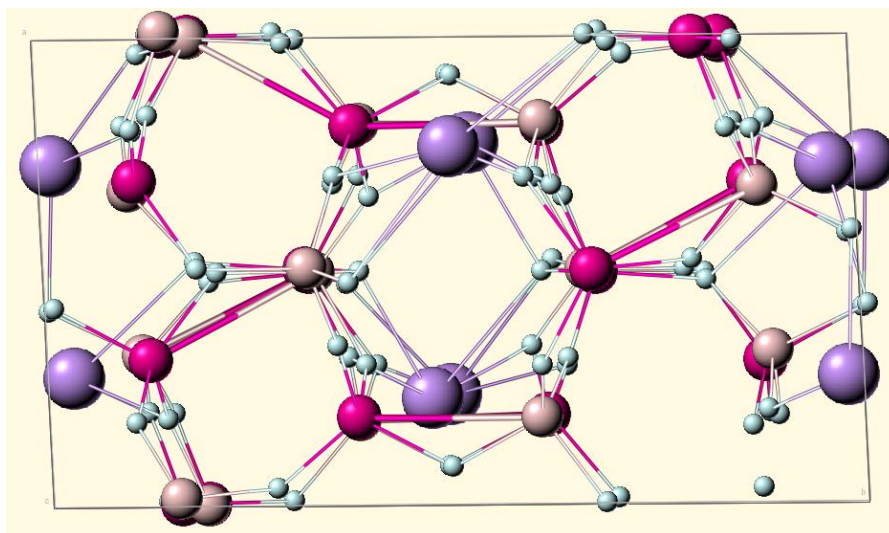


**Figure 5.11 Anorthite crystal structure (a,b phase). Calcium, silica, aluminium and oxygen ions are shown in purple, brown, magenta and silver, respectively (Barthelmy, 2014).**

## Real exchange capacity (REC)

The real exchange capacity (REC) measures the amount of ions that are exchangeable by equilibration using $NH_4^+$ ions that displace the natural ions on the material (Chapman, 1965; Thomas, 1982). Two replicate dried samples were used to determine the REC for coarse (0.6 – 0.35 mm) and fine (< 0.35 mm) particle grades of each material.

### REC of natural zeolite

The most abundant cations desorbed by the ammonium ion were calcium, sodium and magnesium, with small amounts of potassium and iron (Figure 5.12). The mean concentrations of desorbed cations in the coarse zeolite particle were approximately 50% lower than the observed desorbed cations in the fine particle sizes. This reduction could be explained by the surface area of the particle and the availability of cations to reach exchange sites within a zeolite particle. On average coarse particles have a

surface area of 0.79 mm$^2$ and volume of 0.065 mm$^3$, while fine particles exhibit 0.41 mm$^2$ and 0.024 mm$^3$, the surface area and volume ratio for the coarse is 12, while for fine particles is about 17. The fine material has a higher surface area to volume when compared to the coarse particles. This surface area to volume increase translates into additional exchange sites being available that in turn, increase the capacity and availability of the material to exchange cations.
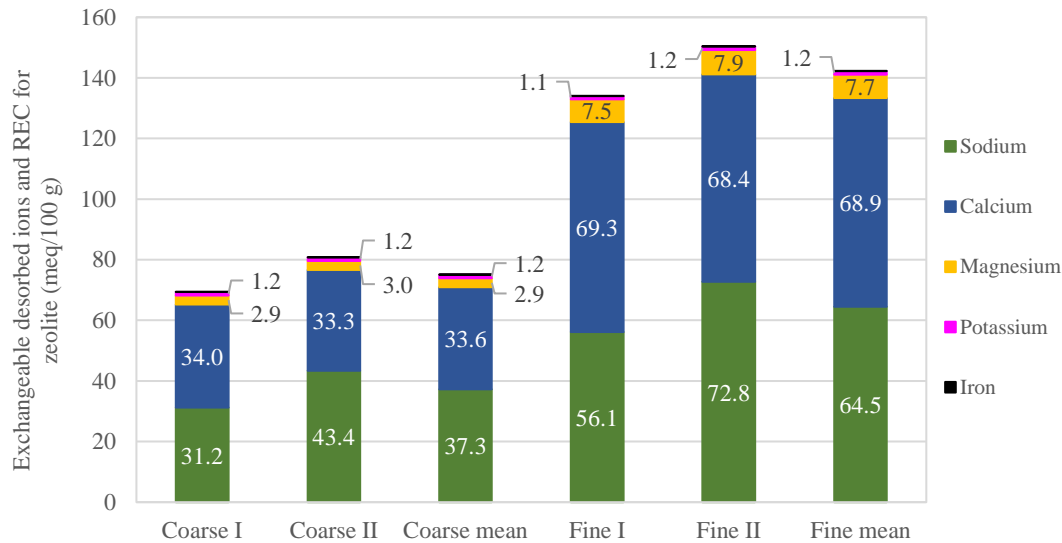


**Figure 5.12 Exchangeable cations and real exchange capacity of natural zeolite material.**

The REC for the coarse and fine zeolite material was 75.14 meq/100 g and 142.28 meq/100 g, respectively. The REC of the fine zeolite material was smaller than the theoretical exchange capacity of 154 meq/100 g. Therefore, not all the cations that were identified in the XRF can be considered as exchangeable because they could be impurities existing in the zeolite particle such as; quartz, and thus cannot take part in the ion exchange process.

## REC of natural scoria

Similarly, scoria displayed calcium and sodium as major desorbed cations followed by lower concentrations of magnesium and potassium (Figure 5.13). The REC for the coarse material was calculated to be 28.41 meq/100 g, while the fine scoria material exhibited a capacity of 34.29 meq/100 g. The calculated REC for the fine scoria particles is smaller than the TEC of 46 meq/100 g found by XRF analysis, hence 26% of the cations found on the material are not exchangeable.
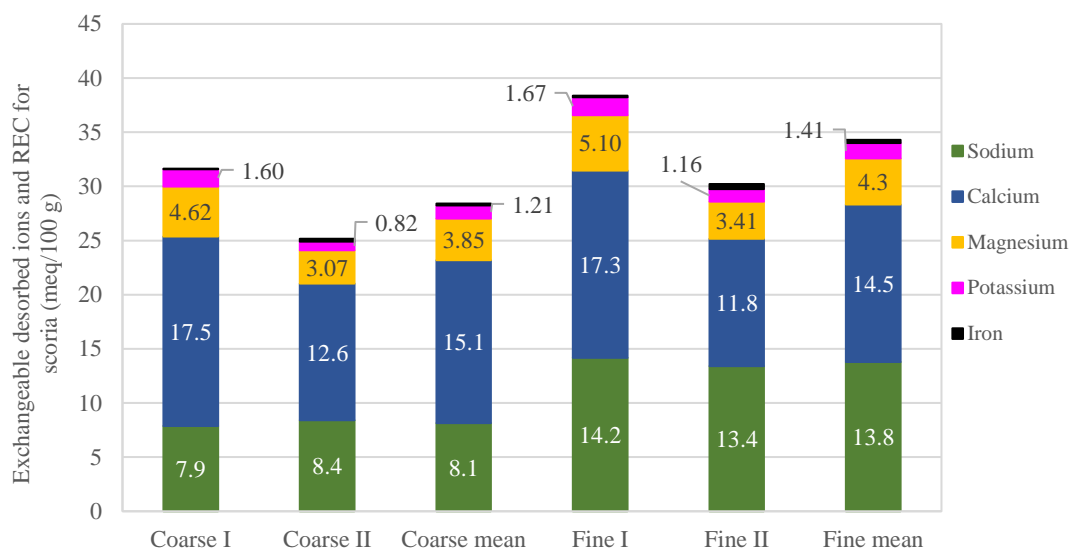
**Figure 5.13 Exchangeable cations and real exchange capacity of natural scoria material.**

The coarse and fine particle sizes exhibited similar amounts of desorbed cations, although the finer particles had a larger surface area to volume ratio than the coarse particles. Therefore, exchangeable cations were totally removed in both cases.

## Surface area and porosity analysis

The BET method determined the total surface and mesoporous area which correspond to void spaces in the material between 2 – 50 nm. From those results micropore volume of each material under analysis was calculated (Table 5.8).

**Table 5.8 Surface and porosity of natural materials.**

| Parameter | Zeolite | Scoria |
|---|---|---|
| Surface area (m²/g) | 9.8 | 4.5 |
| Pore volume (cm³/g) | 0.0019 | 0.0009 |

Surface area measurements for the zeolite material in its natural state used in this study (Table 5.8) were found to be in agreement with other studies that used Australian natural zeolite sourced from a different location by Wang *et al.* (2012). In the case of the scoria material, the surface area agrees with studies performed by Kwon *et al.* (2010) using natural scoria from Korea with a surface area of 4.77 m²/g, characterised using BET analysis. The value for pore volume in the scoria material reflected the lack of microporous structure which is characteristic of this type of material.

Other studies have shown higher surface area results for natural zeolites ranging from 15-20 m²/g (Ates & Hardacre, 2012; Kowalczyk *et al.*, 2006). Since the pore volume of the material was estimated from its surface area, the pore volume of the zeolite used in this study is a fraction of pore volume described by Kowalczyk *et al.* (2006) and Ates and Hardacre (2012) that ranged between 0.016 to 0.052 cm³/g.

## Conclusions

EDS analysis showed that the surface of both materials can be modified by the treatment of inorganic salts and acid. The surface elemental composition indicates that naturally contained cations can be effectively removed by those cations introduced during a treatment. For instance, zeolite and scoria treated with $K^+$ resulted in an increment on the $K^+$ ions that fourfold the concentration from their natural state. SE-microscopy examining the acid treated scoria, presented significant structural damage, which can be attributed to the solubilisation of iron from the framework confirmed with EDS analysis, this may compromise the adsorption or ion exchange capacity of the material.

The zeolite material characterised in this study was a natural blend of two known minerals, clinoptilolite (41 %w/w) and mordenite (29 %w/w). The scoria exhibited a natural combination of diopside (35 %w/w), forsterite (33 %w/w) and anorthite (29 %w/w). Both materials have an aluminosilicate framework where $Si^{4+}$ is substituted by $Al^{3+}$ in the tetrahedral crystal, creating a charge imbalance that is often neutralised with cations.

The zeolite has demonstrated a larger CEC than scoria. The zeolite TEC calculated from XRF analysis was 154 meq/100 g, and REC of 75.1 meq/100 g (coarse fraction) and 142.2 meq/100 g (fine fraction). The TEC calculated for scoria was 46 meq/100 g, considering the XRD and XRF results. The REC measured for fine and coarse material was 28.4 and 34.2 meq/100 g respectively. The REC of the scoria is only 38% of the REC exhibited by the zeolite for coarse particles. Additionally, a smaller fraction size provided a larger adsorption capacity for both materials, since larger amounts of exchangeable cations were desorbed for the fine particles. It is then suggested that reduced particle sizes will exhibit greater adsorption rates.

# Chapter 6: Equilibrium studies

## Equilibrium isotherms models

The adsorptive behaviour of an ion exchange system can be described using isotherm curves. Isotherm curves are based on equilibrium concentration data for total initial concentration of the solution that is in contact with the exchanger material at a constant temperature. The adsorption amount ($q_e$) and efficiency (E) for each total initial solution are typically calculated using Equation 6.1 and 6.2, where $C_0$ and $C_e$ are initial and the equilibrium concentration, $V$ is the volume of aqueous solutions and $m$ is the mass of adsorbent.

$$q_e = (C_0 - C_e)\frac{V}{m}$$                                     **Equation 6.1**

$$E = (C_0 - C_e)\frac{100}{C_0}$$                                   **Equation 6.2**

The relationship between the adsorbent and the surrounding aqueous solution at equilibrium can be described by numerous expressions that commonly use two or more unknown parameters. Notably, adsorption and ion exchange use common approach despite the inherent differences, thus, theoretical approach for equilibrium processes including empirical, mass-action or surface complexation models can be used. The latter approaches present a series of advantages and disadvantages, while empirical models are conductive to provide clear illustrations of the key aspects of the ion exchange interaction (Millar *et al.*, 2015b). The isotherm models used in this study were: Langmuir, Freundlich, Sips and Toth (Table 6.1).

The Langmuir adsorption model is frequently applied to isotherms that describe physisorption of ions by the sorbent surface and assumes that adsorption takes place at specific homogeneous sites on the sorbent. $K_L$ (meq/100 g) and $a_L$ (L/meq) are parameters related to the adsorption capacity and energy of adsorption, respectively. $q_m$ (meq/100 g) is given by $K_L/a_L$, which is the theoretical maximum monolayer adsorption. In contrast to the Langmuir model, the Freundlich adsorption model

assumes a heterogeneous surface with non-uniform distribution of the adsorption. $K_f$ (L/100 g) and $n$ (dimensionless) Freundlich parameters describe the adsorption capacity and measure the adsorption affinity, respectively.

**Table 6.1 Adsorption equilibrium models used in this study for the adsorption of cations.**

| Model | Non-linear equation | Linear equation | Model parameters |
|---|---|---|---|
| Langmuir | $q_e = \dfrac{K_L a_L C_e}{1 + a_L C_e}$ | $\dfrac{C_e}{q_e} = \dfrac{1}{(q_m K_L)} + \dfrac{C_e}{q_m}$ | $K_L$ , $a_L$ |
| Freundlich | $q_e = K_f C_e^{1/n}$ | $\ln q_e = \ln K_f + \dfrac{1}{n_f} \ln C_e$ | $K_f$ , $n$ |
| Sips | $q_e = \dfrac{q_m a_s C_e^{1/n}}{1 + a_s C_e^{1/n}}$ | | $q_m$ , $a_s$ , $n$ |
| Toth | $q_e = \dfrac{q_m C_e}{(K_{To} + C_e^n)^{1/n}}$ | $\ln\left(\dfrac{q_e}{q_m}\right) = \ln C_e - \left(\dfrac{1}{n}\right)\ln(K_{To} + C_e^n)$ | $q_m$ , $K_{To}$ , $n$ |

That is $q_e$, adsorption (meq/100 g); $C_e$, concentration at equilibrium (meq/L); $K_L$, Langmuir capacity (meq/100 g); $a_L$, energy of adsorption (L/meq); $K_f$, Freundlich capacity (L/100 g); n, Freundlich constant; $a_s$, Sips monolayer capacity (L/meq); $K_{To}$, Toth constant.

The Sips model combines Langmuir and Freundlich models together, and takes into account the energetic heterogeneity of sorbent surfaces. At low concentrations, the Sips model is approximated by the Freundlich model, whereas at high concentrations the Sips model predicts the monolayer adsorption capacity characteristics of the Langmuir model. $q_m$ (meq/100 g), $a_s$ (L/meq) and $n$ parameters are the monolayer adsorption capacity. Sips constants relate to the energy of adsorption and the heterogeneity parameter. The Toth model is based on Langmuir equilibrium model considering continuous distribution of site affinities.

Equilibrium models presented in non-linear forms were used to describe the experimental data by implementing a non-linear least square fitting process in Matlab® R2012b (MathWorks®). The error function utilised was the sum of error squared (SSE).

## Selectivity coefficients

The selectivity or unselectively property of the exchanger can be measured by the separation factor ($\alpha$), which, can be obtained from an isotherm curve for a given point of the curve under consideration and calculated using Eq. 6.3. If the separation factor is equal to one, the exchanger does not exhibit clear adsorption preference over a

particular ion. If $\alpha$ is greater than one ($>1$), it means that the exchanger is selective towards that ion, but if it is lower than one ($<1$), selectivity is observed for the competing ion. Where $E_{A(z)}$ and $E_{A(s)}$ are the rational equivalent fractions on the exchanger and the solution, respectively (Harland, 1994).

$$\alpha = \frac{E_{A(z)}(1-E_{A(s)})}{E_{A(s)}(1-E_{A(z)})}$$
$\qquad\qquad$ **Equation 6.3**

The separation factor varies as a function of the composition of both the solid and liquid phases at equilibrium. The selectivity of the system can be described by the selectivity coefficient ($K$), which is the mass actions relationship and defined in Eq. 6.4.

$$K = \frac{E_{A(z)}{}^{z_A^+}(1-E_{A(s)})^{z_B^+}}{E_{A(s)}{}^{z_A^+}(1-E_{A(z)})^{z_B^+}}$$
$\qquad\qquad$ **Equation 6.4**

Where, $Z_A^+$ and $Z_B^+$ are the valency of the ions that compete for the sites of adsorption (Harland, 1994). For the exchange of ions with equal valency, the separation factor and selectivity coefficient becomes the same expression. However, for heterovalent ion exchange, the selectivity is determined with Eq. 6.4.

The objective of this chapter was to investigate the adsorptive equilibrium properties of scoria and zeolite for the removal of cations present in CSG water using equilibrium models. Additionally, cation selectivity was studied to determine the materials adsorption preferences and behaviour for cations of interest.

## Results and Discussion

In this chapter the adsorption equilibrium and the selectivity preferences of scoria and zeolite are shown. A series of equilibrium studies determined the maximum capacity of natural and treated materials for the adsorption of $Na^+$, $Sr^{2+}$ and $Ba^{2+}$ using single cation solutions. Adsorption equilibrium models were fitted to the experimental equilibrium data in order to quantify the adsorption performance of the materials using a two parameter adsorption isotherm model, Langmuir and Freundlich, and three-parameter isotherm models, Sips and Toth.

Selectivity and affinity were studied in batch type experiments with natural materials in order to identify and classify the adsorption affinity towards $Na^+$ over other ions such as $Ca^{2+}$, $K^+$ and $Sr^{2+}$ present in the CSG water from the Bowen Basin research site. Field CSG water is a mixture of cations, which may compete with each other for adsorption sites, reducing the adsorption of cations of interest. This study aimed to describe the competitive adsorption behaviour of cations for scoria and zeolite material through cation selectivity.

## Removal of $Na^+$ ions using natural and treated natural exchangers

The adsorption behaviour of natural and treated forms of scoria and zeolite for the removal of $Na^+$ ions from aqueous solutions at different initial concentrations showed that as the initial concentration of $Na^+$ was increased, the amount of cations adsorbed increased per unit of mass of the exchanger material (Figure 6.1 and 6.2). The adsorption of cations reached a maximum equilibrium or saturation point, where no further $Na^+$ removal was observed. This is because the material reached the maximum practical adsorption capacity and the $Na^+$ adsorption process is the product of the driving force of cations displacing exchangeable ions from the exchanger framework, incorporating the incoming $Na^+$ cations that are higher in concentration in the solute, where the adsorption process is driven by the concentration gradient.
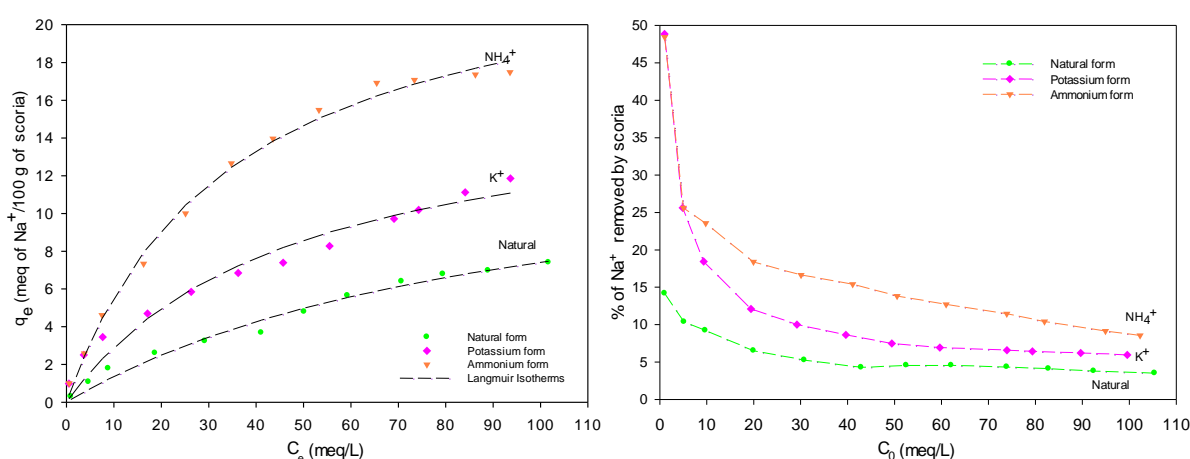


**Figure 6.1 The adsorption equilibrium isotherms and removal performance for $Na^+$ ion using natural and treated scoria. REC = 28.4 meq/100 g. Langmuir equilibrium isotherm curves fitted to the data (Left). Removal performance at different initial concentrations (Right). $NH_4^+$ enhanced scoria showed larger $Na^+$ adsorption and removal compared to other forms of the material. At high $Na^+$ concentrations, it was removed by 10% of the initial concentration with a maximum adsorption of 17.4 meq/100 g. Each data point is a mean of two replicates, which did not vary by more than 5%.**
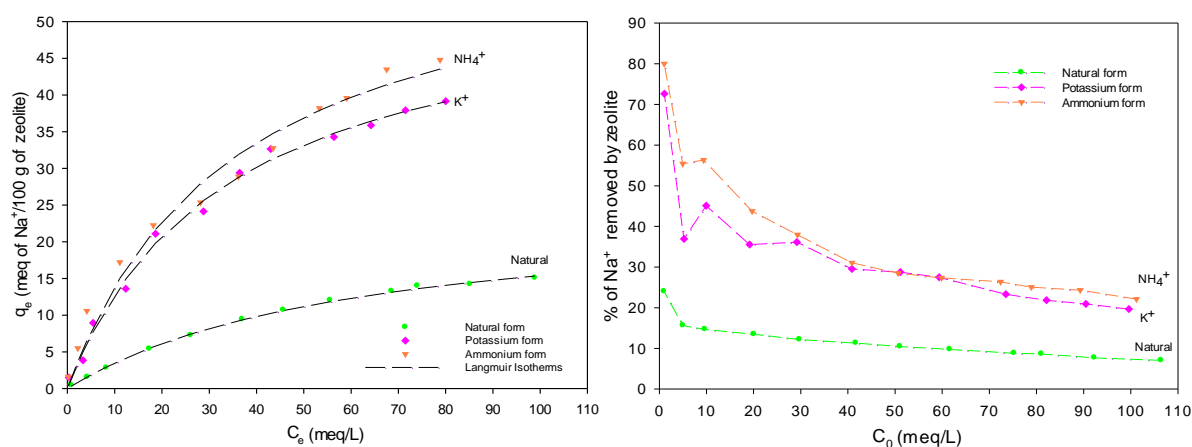
**Figure 6.2 The adsorption equilibrium isotherms and removal performance for Na$^+$ ion using natural and treated zeolite. REC = 75.1 meq/100 g. Langmuir equilibrium isotherm curves fitted to the data (Left). Removal at different initial concentrations (Right). Zeolite enhanced with NH$_4^+$ and K$^+$ presented similar behaviour in adsorption of Na$^+$, while natural form exhibited reduced adsorption. NH$_4^+$ form achieved 45 meq/ 100 g with a 22% removal of the initial concentration. Each data point is a mean of two replicates, which did not vary by more than 5%.**

The materials in their natural form exhibited lower adsorption of Na$^+$ ions for all the initial concentrations when compared with the same material treated with K$^+$ or NH$_4^+$ ions (Figures 6.1 and 6.2). The scoria material enriched with NH$_4^+$ achieved an adsorption approximately 2.3 times greater than the natural material form, and 47% higher than the K$^+$ enriched scoria. When the zeolite material was enriched with NH$_4^+$ a three-fold adsorption for Na$^+$ was observed, while zeolite treated with K$^+$, exhibited a capacity that was twofold the capacity of zeolite in its natural form. The maximum Na$^+$ adsorption observed for the scoria and zeolite materials in NH$_4^+$ form were 17.38 and 45.34 meq per 100 g, respectively. Both natural materials exhibited a reduced adsorption of Na$^+$ at high initial concentrations, the NH$_4^+$ treatment has significantly increased the Na$^+$ adsorption and removal. The treated materials exhibited approximately 60% of the REC.

**Table 6.2 Calculated equilibrium adsorption isotherm constants for the uptake of Na⁺ in solution by scoria and zeolite in natural and treated form. Model fit is characterised by the sum of squares error term (SSE).**

| Model | Scoria | | | Zeolite | | |
|---|---|---|---|---|---|---|
| | Natural | K⁺ form | NH₄⁺ form | Natural | K⁺ form | NH₄⁺ form |
| Langmuir | | | | | | |
| $K_L$ | 14.63 | 16.67 | 24.75 | 24.71 | 55.51 | 63.14 |
| $a_L$ | 0.010 | 0.021 | 0.029 | 0.016 | 0.029 | 0.028 |
| $q_m$ | 1434.80 | 786.41 | 849.48 | 1490.90 | 1862.03 | 2236.53 |
| SSE | 1.095 | 2.431 | 1.513 | 0.662 | 7.241 | 3.520 |
| | | | | | | |
| Freundlich | | | | | | |
| $K_f$ | 0.375 | 1.076 | 1.972 | 1.007 | 3.989 | 4.573 |
| $n$ | 1.531 | 7.155 | 2.001 | 1.657 | 1.877 | 1.896 |
| $1/n$ | 0.653 | 0.139 | 0.499 | 0.603 | 0.532 | 0.527 |
| SSE | 0.861 | 0.301 | 3.206 | 2.048 | 6.480 | 3.625 |
| | | | | | | |
| Sips | | | | | | |
| $q_m$ | 52.79 | 89.77 | 24.12 | 22.50 | 54.44 | 255.39 |
| $a_s$ | 0.0008 | 0.0003 | 0.0308 | 0.0201 | 0.0311 | 0.0001 |
| $1/n$ | 0.715 | 0.568 | 1.031 | 1.082 | 1.020 | 0.588 |
| SSE | 0.873 | 1.170 | 1.5 | 0.593 | 3.514 | 3.752 |
| | | | | | | |
| Toth | | | | | | |
| $q_m$ | 129.58 | 319.12 | 21.64 | 19.86 | 52.93 | 620.88 |
| $K_{TO}$ | 0.003 | 0.020 | 0.027 | 0.017 | 0.029 | 0.024 |
| $n$ | 0.310 | 0.189 | 1.319 | 1.397 | 1.081 | 0.232 |
| SSE | 0.917 | 1.374 | 1.435 | 0.523 | 3.507 | 4.054 |

The adsorption equilibrium experimental data was fitted with the Langmuir, Freundlich, Sips and Toth adsorption isotherms. The calculated equilibrium adsorption parameters are shown in Table 6.2 and the calculated Langmuir adsorption isotherm curves were plotted (Figure 6.1 and 6.2). The two-parameter model, Langmuir and Freundlich, presented a higher sum of square error (SSE) than the three-parameter models, Sips and Toth. This fitting behaviour was expected, since a larger number of parameters for the model improves the fitting of the experimental data. Nonetheless, all of these models gave good fitting responses to the experimental results in terms of describing the equilibrium behaviour denoted by SSE (Table 6.2).

The Langmuir's capacity constant ($K_L$) reflects the effect that the treatment had over the uptake of $Na^+$ ions. Materials treated with $NH_4^+$ exhibited the largest capacity of 63 and 24 meq/100 g for zeolite and scoria respectively, while natural and $K^+$ forms reached a fraction of that adsorption capacity observed for materials enhanced with $NH_4^+$ (Table 6.2). For instance, the scoria in a natural and $K^+$ enriched state, exhibited 59.8% and 67.3% of the adsorption capacity achieved by the material treated with $NH_4^+$. Similarly, the zeolite reached 39.1% and 87.9% of the $NH_4^+$ capacity for natural and $K^+$ enriched forms for this material.

The fraction of $Na^+$ removed from varied starting concentrations in solutions was explored (Figures 6.1 and 6.2). The adsorption equilibrium curves show that the adsorption of $Na^+$ increased when initial concentration of the solute increased. The performance of $Na^+$ ions removed by the materials demonstrated that, at lower concentrations, both materials in their various treated forms, presented larger $Na^+$ removal from the solution, than for the same exchangers at higher initial concentrations. These results indicate that cations introduced through the treatment, facilitate the adsorption of $Na^+$. The $Na^+$ removed by the scoria material in different forms at low concentrations ($< 5$ meq/L) reached up to 48% of the initial concentration. The removal rate rapidly drops as initial $Na^+$ concentration is increased, (below 10% removed of the initial concentration) of 100 meq/L. Analogously, the zeolite material exhibited a large $Na^+$ concentration removal at low concentrations ($< 10$ meq/L) using the $NH_4^+$ (79%) and $K^+$ (71%) treated material. This result was followed by a rapid decay on the removal of $Na^+$ achieving approximately 20% of the initial concentration at high $Na^+$ concentrations (100 meq/L).

The $Na^+$ adsorption behaviour indicates that higher removal rates occurred at low concentration only, while at high concentrations of $Na^+$ (typical of CSG waters) the removal will achieve a maximum of 10% and 25% of the initial $Na^+$ concentration using scoria and zeolite treated with $NH_4^+$. The adsorption equilibrium and overall sodium removal performance was enhanced by the chemical treatment of the zeolite and scoria material when compared to their natural states.

Previous studies (Alemayehu & Lennartz, 2009; Alemayehu *et al.*, 2011; Kwon *et al.*, 2005; Kwon *et al.*, 2010) that have used natural, untreated scoria for the adsorption of heavy metals in low concentrations, have shown similar equilibrium behaviour and

adsorption performance for the removal of $Na^+$. The experimental data for this study corroborates the findings of these authors, highlighting the use of scoria to effectively remove sodium but furthermore, heavy metal ions. Other research used Langmuir and Freundlich models to describe ion uptake by a zeolite. Ganjegunte *et al.* (2011) and also Zhao *et al.* (2008) studied the equilibrium behaviour of a natural zeolite for the removal of $Na^+$, and their experimental data was fitted with Freundlich and Langmuir models, respectively. Günay *et al.* (2007) used both Sips and Toth models to describe the adsorption equilibrium of clinoptilolite in natural and treated form for the removal of lead, and found that these models presented a lower SSE than Freundlich and Langmuir. The SSE from all the models obtained for $Na^+$ adsorption using zeolite and scoria was lower than those reported by Günay *et al.* (2007), accurately representing the experimental data.

Natural scoria and zeolite adsorbed $Na^+$, but the maximum adsorption was only 25.7% and 19.7% of the measured REC. $NH_4^+$ treated scoria and zeolite materials adsorbed $Na^+$ up to 61.1% and 60.3% of the measured REC, respectively. The exchange interaction observed for the natural and treated materials could be related to the cation hydration size, initial composition of pre-existing ions, availability and also the accessibility of the exchange sites (Zhao *et al.*, 2008). For instance, the hydration energy of $K^+$ (-322 kJ/mol) and $NH_4^+$ (-307 kJ/mol) ions is much lower than $Ca^{2+}$ (-1577 kJ/mol), which was the major ion, found within the framework of the natural states of the zeolite and scoria determined in the EDS and XRF analysis performed, *vide supra*, Chapter 5. Therefore, materials treated with $K^+$ and $NH_4^+$ ions have increased the exchange interaction with $Na^+$ due to the lower energy of hydration (Oueslati *et al.*, 2009).

## Removal of $Sr^{2+}$ ions using natural and treated natural exchangers

The adsorption equilibrium behaviour of $Sr^{2+}$ for the scoria and zeolite was investigated due to high concentration found from the characterisation of CSG water for the Bowen Basin research site. Typical concentrations of $Sr^{2+}$ range between 0.1 and 5 meq/L.

The $Sr^{2+}$ concentration range employed (0.1 - 5 meq/L) was not sufficient to define a plateau for the adsorption isotherms (Figure 6.3 and 6.4). Alemayehu and Lennartz

(2009) and Günay *et al.* (2007) observed analogous behaviour when studying the adsorption of divalent ions in which the concentrations were not sufficient for the equilibrium isotherms curves to exhibit a maximum adsorption or saturation point. Nonetheless, experimental data was sufficient to determine the adsorption equilibrium parameters used in the modelling. The experimental adsorption equilibrium data was fitted with two and three parameter adsorption isotherm models. Freundlich isotherms were plotted in Figures 6.3 and 6.4, equilibrium parameters are shown in Table 6.3.
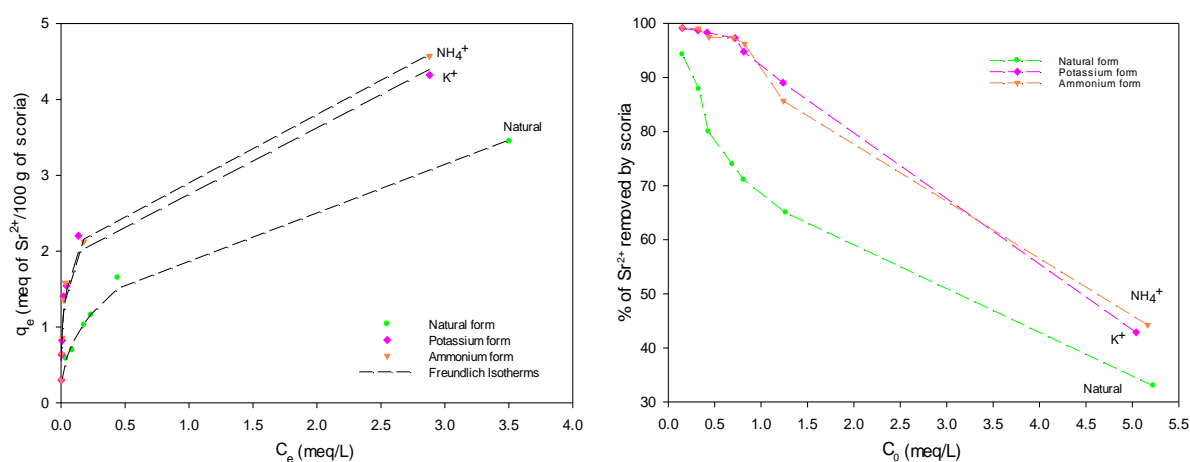


**Figure 6.3 The adsorption equilibrium isotherms and removal performance for $Sr^{2+}$ ion using natural and treated scoria. Freundlich equilibrium isotherm curves fitted to the data (Left). Removal of $Sr^{2+}$ at different initial concentrations (Right). The material was able to remove $Sr^{2+}$ at high concentrations up to 30% of its initial. At low concentrations treated scoria exhibited an additional 25% removal. Each data point is a mean of two replicates, which did not vary by more than 5%.**

The scoria treated with $NH_4^+$ exhibited the largest adsorption of $Sr^{2+}$, slightly higher than $K^+$ and also the natural state. These materials reached an adsorption of 4.5, 4.3 and 3.4 meq/100 g respectively, after equilibrium with an initial $Sr^{2+}$ concentration of 5 meq/L (Figure 6.3). The removal of $Sr^{2+}$ exhibited by the scoria when treated with $NH_4^+$ and $K^+$ for an initial 5 meq/L concentration was 44.2% and 42.8% (Figure 6.3). Although $NH_4^+$ showed a higher adsorption capacity towards $Sr^{2+}$, scoria in the natural form achieved 3.4 meq/100 g, which was a 24% lower than the adsorption values $Sr^{2+}$. The effective removal calculated for scoria in natural form was 32.9%, which is only 11.3% lower than the maximum attained by the material in $NH_4^+$ form. For initial concentrations less than 2 meq/L, the material effectively removed > 85% and > 60% of the $Sr^{2+}$ available in solution for the treated and natural forms, respectively.

**Table 6.3 Calculated equilibrium adsorption isotherm constants for the uptake of $Sr^{2+}$ in solution by scoria and zeolite in natural and treated form.**

| Model | Scoria | | | Zeolite | | |
|---|---|---|---|---|---|---|
| | Natural | $K^+$ form | $NH_4^+$ form | Natural | $K^+$ form | $NH_4^+$ form |
| Langmuir | | | | | | |
| $K_L$ | 3.911 | 4.154 | 4.174 | 8.377 | 8.325 | 9.848 |
| $a_L$ | 1.91 | 15.11 | 15.84 | 24.276 | 33.336 | 4.345 |
| $q_m$ | 2.044 | 0.274 | 0.263 | 0.345 | 0.249 | 2.266 |
| SSE | 0.433 | 1.005 | 1.294 | 0.956 | 0.897 | 0.442 |
| | | | | | | |
| Freundlich | | | | | | |
| $K_f$ | 2.095 | 3.345 | 3.451 | 8.260 | 2.938 | 7.843 |
| $n$ | 2.48 | 3.34 | 3.45 | 2.644 | 0.074 | 1.916 |
| $1/n$ | 0.401 | 0.258 | 0.270 | 0.378 | 0.353 | 0.521 |
| SSE | 0.170 | 0.471 | 0.437 | 1.218 | 3.414 | 0.521 |
| | | | | | | |
| Sips | | | | | | |
| $q_m$ | 9.376 | 6.233 | 11.497 | 8.379 | 8.234 | 12.241 |
| $a_s$ | 0.099 | 2.115 | 2.871 | 24.22 | 38.27 | 2.15 |
| $1/n$ | 0.511 | 0.447 | 0.348 | 0.998 | 0.94 | 0.807 |
| SSE | 0.130 | 0.242 | 0.400 | 0.956 | 0.889 | 0.386 |
| | | | | | | |
| Toth | | | | | | |
| $q_m$ | 34.632 | 9.687 | 34.402 | 8.188 | 8.093 | 18.156 |
| $K_{TO}$ | 14.124 | 727.408 | 24243.64 | 22.689 | 26.983 | 4.246 |
| $n$ | 0.017 | 0.216 | 0.117 | 1.206 | 0.879 | 0.485 |
| SSE | 0.147 | 0.211 | 0.381 | 0.954 | 0.879 | 0.395 |

The Freundlich model gave the best description for the behaviour of the scoria material for the adsorption of $Sr^{2+}$ in terms of a low SSE (Table 6.3). Nonetheless, Sips and Toth models provided similar fitting for the experimental data. The Langmuir model showed that the parameter related with the energy of adsorption ($a_L$) for treated forms was 7 times larger than the material in natural scoria. This behaviour is consistent with the adsorption behaviour of the material towards $Na^+$ for the treated forms.

In contrast to the behaviour of the scoria, the adsorption equilibrium behaviour of zeolite exhibited that in all cases, similar adsorption was achieved (Figure 6.4). Natural and $K^+$ enriched zeolites were able to reduce the concentration of $Sr^{2+}$ in solution after equilibrium to below 0.1 meq/L, 99 - 97% of the initial solute content was removed

(Figure 6.4). However, at initial concentration of the $Sr^{2+}$ higher than 2 meq/L, the zeolite material in $K^+$ form showed less adsorption for $Sr^{2+}$ than the natural form, behaving similar to the $NH_4^+$ zeolite enriched material.
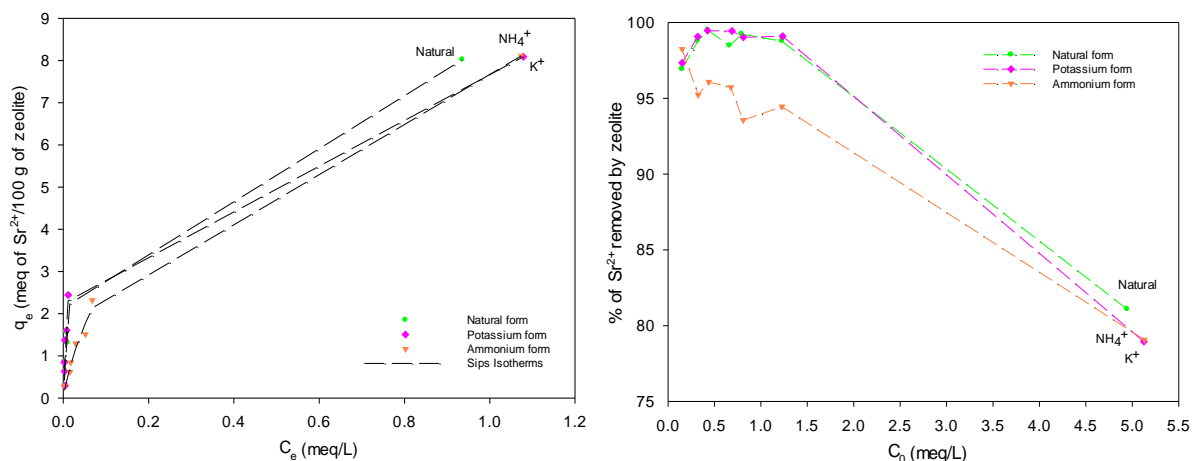


**Figure 6.4 The adsorption equilibrium isotherms and removal performance for $Sr^{2+}$ ion using natural and treated zeolite. Freundlich equilibrium isotherm curves fitted to the data (Left). Removal of $Sr^{2+}$ at different initial concentrations (Right). The $Sr^{2+}$ adsorption behaviour was similar for the zeolite in natural and enriched forms, reducing approximately 80% of the initial concentration. Each data point is a mean of two replicates, which did not vary by more than 5%.**

Although the $NH_4^+$ enriched zeolite exhibited a slightly reduced adsorption value of $Sr^{2+}$, when compared with natural zeolite, the difference was found to be 5% lower. The $NH_4^+$ form achieved a removal performance in the range of 98 – 94% of the initial $Sr^{2+}$ concentration for concentrations below 2 meq/L. At the initial concentration of 5 meq/L, the $Sr^{2+}$ adsorption achieved for the zeolite in all the cases of 8.0 meq/100 g, with an effective removal rate of 80% of the initial $Sr^{2+}$ concentration (Figure 6.4).

The model that best described the adsorption of $Sr^{2+}$ using zeolite was the three-parameter model of Sips, demonstrating the lowest SSE (Figure 6.4). The maximum adsorption described by the model was 12.2 meq of $Sr^{2+}$ per 100 g for zeolite enriched with $NH_4^+$.

Alemayehu and Lennartz (2009) and Kwon *et al.* (2005), who studied the adsorption performance of scoria towards divalent ions, found that the material showed a positive adsorption towards $Cd^{2+}$ and $Zn^{2+}$. These findings agree with the results found for the scoria material, in which $Sr^{2+}$ was removed more effectively by the material than $Na^+$

ions that presented a lower adsorption performance. Similar work on zeolites performed by Bektaş and Kara (2004) and El-Kamash (2008) for the adsorption of $Pb^{2+}$, $Cs^+$ and $Sr^{2+}$, determined that zeolites were able to remove up to 47 meq/100 g exhibiting larger capacities towards divalent cations. The results presented agree with the reported literature, since $Sr^{2+}$ was adsorbed in larger rates than $Na^+$ for the zeolite material.

In summary, the zeolite material demonstrated higher adsorption performance for $Sr^{2+}$ when compared to the adsorption for the cations using the scoria material. Treated material presented relatively small effects on the overall adsorption performance for the $Sr^{2+}$ concentrations ranges analysed.

## Removal of $Ba^{2+}$ ions using natural and treated natural exchangers

Similar for the investigation of $Sr^{2+}$, $Ba^{2+}$ was also used as a target investigatory metal ion found to be in excess in the CSG water from Bowen Basin site. The aim of this study was to comprehensively investigate the ability of the materials to remove the presented ions found at the site. The scoria and zeolite materials were subjected to $Ba^{2+}$ ions at different concentrations (0.1 and 5 meq/L) to determine the optimum adsorption equilibrium capacity and removal performance for each (Figures 6.5 and 6.6).
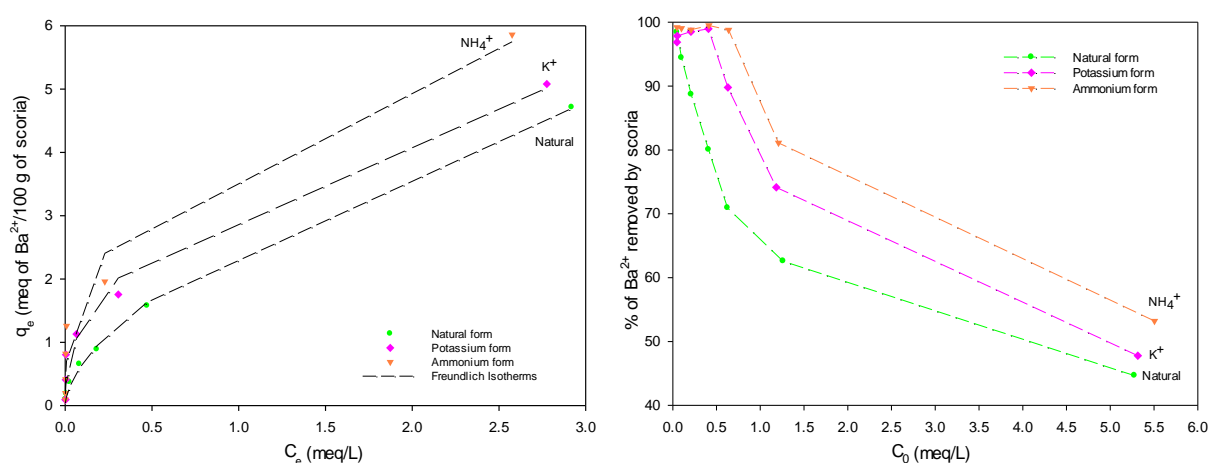


**Figure 6.5 The adsorption equilibrium isotherms and removal performance for $Ba^{2+}$ ion using natural and treated scoria. Freundlich equilibrium isotherm curves fitted to the data (Left). Removal of $Ba^{2+}$ at different initial concentrations (Right). $Ba^{2+}$ at low initial concentrations (less than 2 meq/L) removed by the scoria by about 80% and in all cases $NH_4^+$ enhanced scoria presented the largest removal. Each data point is a mean of two replicates, which did not vary by more than 5%.**

The maximum $Ba^{2+}$ adsorption was achieved by the scoria and zeolite in their $NH_4^+$ enriched forms. Enrichment increased the adsorption observed for the natural material by 20% (scoria) and 5% (zeolite). The $NH_4^+$ zeolite reached a $Ba^{2+}$ adsorption capacity of 10.61 meq/100 g (Figure 6.6), while the scoria in the same form exhibited 5.8 meq/100 g (Figure 6.5). Although, $NH_4^+$ treated materials exhibit larger adsorption for $Ba^{2+}$ ions than $K^+$ enriched and natural forms, the scoria and zeolite in their natural form exhibited a $Ba^{2+}$ adsorption value of 4.7 and 10.13 meq/100 g (Figure 6.5 and 6.6), respectively.

The $Ba^{2+}$ removal behaviour showed that scoria in all forms was able to reduce the $Ba^{2+}$ concentration by 90% of the initial concentration for an original concentration less than 0.2 meq/L (Figure 6.5). Nonetheless, the scoria removal at the high range of $Ba^{2+}$ (5 meq/L) exhibited a removal greater than 40% of the initial concentration in all cases. The zeolite material treated with either $NH_4^+$ or $K^+$ achieved a removal of $Ba^{2+}$ ions greater than 98% for all the range (0.1 and 5 meq/L) of concentrations (Figure 6.6). The natural form was able to reduce $Ba^{2+}$ by 98% for concentrations less than 0.3 meq/L, while the removal for the upper ranges of concentrations showed greater removal, 94% (Figure 6.6).
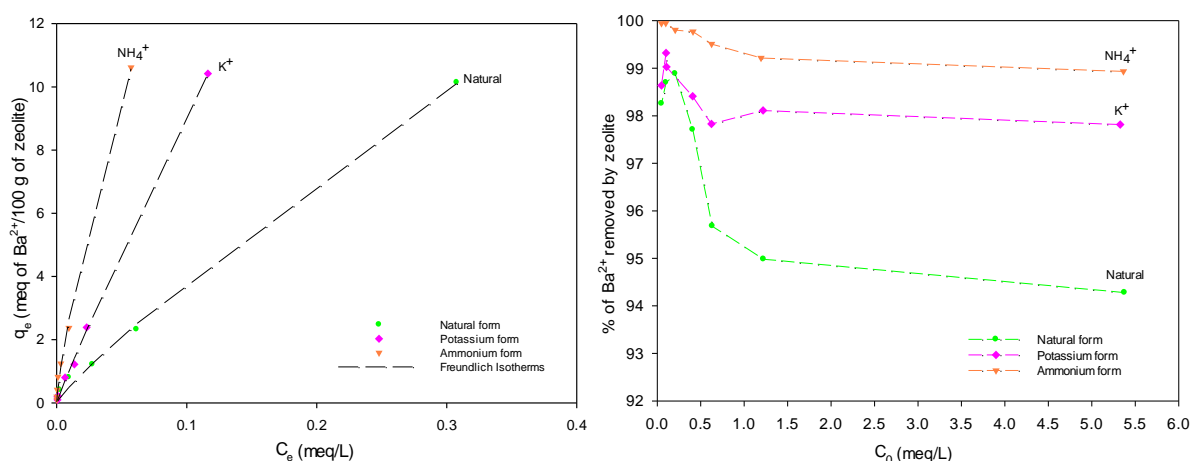


**Figure 6.6 The adsorption equilibrium isotherms and removal performance for $Ba^{2+}$ ion using natural and treated zeolite. Freundlich equilibrium isotherm curves fitted to the data (Left). Removal of $Ba^{2+}$ at different initial concentrations (Right). Zeolite in all the cases presented high adsorption for $Ba^{2+}$, saturation of the material was not evident. Removal of $Ba^{2+}$ reached 92% efficiency using zeolite. Each data point is a mean of two replicates, which did not vary by more than 5%.**

**Table 6.4 Calculated equilibrium adsorption isotherm constants for the uptake of $Ba^{2+}$ in solution by scoria and zeolite in natural and treated form.**

| Model | Scoria | | | Zeolite | | |
|---|---|---|---|---|---|---|
| | Natural | $K^+$ form | $NH_4^+$ form | Natural | $K^+$ form | $NH_4^+$ form |
| **Langmuir** | | | | | | |
| $K_L$ | 6.941 | 6.186 | 7.109 | 44.74 | 71.34 | 26.51 |
| $a_L$ | 0.715 | 1.592 | 1.798 | 0.951 | 1.470 | 11.653 |
| $q_m$ | 9.704 | 3.883 | 3.953 | 47.041 | 48.530 | 2.275 |
| SSE | 0.461 | 1.062 | 1.481 | 0.557 | 0.278 | 0.757 |
| | | | | | | |
| **Freundlich** | | | | | | |
| $K_f$ | 2.527 | 3.292 | 4.094 | 28.11 | 76.83 | 94.34 |
| $n$ | 1.728 | 2.420 | 2.785 | 1.152 | 1.076 | 1.307 |
| $1/n$ | 0.578 | 0.413 | 0.359 | 0.867 | 0.928 | 0.764 |
| SSE | 0.156 | 0.574 | 0.842 | 0.459 | 0.265 | 0.531 |
| | | | | | | |
| **Sips** | | | | | | |
| $q_m$ | | 49.544 | 63.041 | 123.861 | 58.698 | |
| $a_s$ | | 0.002 | 0.0001 | 0.224 | 1.891 | |
| $1/n$ | | 0.436 | 0.373 | 0.907 | 1.013 | |
| SSE | | 0.599 | 0.969 | 0.49 | 0.28 | |
| | | | | | | |
| **Toth** | | | | | | |
| $q_m$ | | 183.208 | 155.185 | 107.11 | 14.93 | 63.17 |
| $K_{TO}$ | | 55.48 | 762.79 | 0.425 | 6.833 | 5.972 |
| $n$ | | 0.120 | 0.109 | 0.682 | 3.074 | 0.592 |
| SSE | | 0.691 | 0.999 | 0.543 | 0.277 | 0.713 |

Adsorption isotherm models were fitted to the experimental data, model parameters are presented in Table 6.4, and the Freundlich isotherm curves shown in Figures 6.5 and 6.6. The experimental data showed that for the range of $Ba^{2+}$ concentrations employed for the equilibrium experiment, the concentration was not sufficient to define a saturation point and plateau of the adsorption curve. Indeed, the isotherm equilibrium curve presented a linear behaviour that affected the convergence of the three-parameter models, Sips and Toth. This is due to the large number of independent parameters of the model over-parameterised the fitting, causing the non-convergence. This behaviour occurred during the fitting process, as one or more parameter values were similar to each other thus producing infinite solutions. Langmuir and Freundlich models with two-parameter allowed convergence during the fitting process.

The Langmuir model showed that for the natural scoria and zeolite materials both achieved 40% and 9% of the energy of adsorption that was determined for the same material enriched with $NH_4^+$ (Table 6.4). This result indicates that the treated material has increased the $Ba^{2+}$ adsorption interactions. Freundlich constants showed that materials enriched with $NH_4^+$ had a positive adsorption for $Ba^{2+}$ ions and a much larger adsorption capacity. In fact, treated scoria and zeolite material have both exhibited a modelled capacity of 4.09 and 94.3 meq/100 g, respectively. This indicates, that the zeolite material has shown a larger affinity for $Ba^{2+}$ ions than scoria, which may be related to the higher real exchange capacity value of the zeolite than the scoria materials.

In summary, both materials, scoria and zeolite, were able to effectively reduce the concentration of $Ba^{2+}$ from solution, 40% (scoria) and 94% (zeolite) of the initial $Ba^{2+}$ concentrations. Treated zeolite exhibited a high adsorption for $Ba^{2+}$ ions that may lead towards the REC. The scoria material in all states has exhibited high affinity for $Ba^{2+}$ and an acceptable removal from solution; the lower REC of this material limited the removal of this cation at high concentrations.

### Selectivity isotherms for the removal of $Na^+$ ions and the competing $K^+$, $Ca^{2+}$ and $Sr^{2+}$ ions

CSG water has a mixture of cations that may compete with each other for the adsorption sites available on the scoria or zeolite materials. In this study, the selectivity behaviour was studied using $Na^+/K^+$, $Na^+/Ca^{2+}$ and $Na^+/Sr^{2+}$ mixtures of solutions in a chloride background at a total concentration of 0.01 M for natural scoria and zeolite (Figures 6.13 and 6.14). The isotherm graphs illustrate the selectivity of the exchanger material towards a cation relative to another cation in equivalent fractions of the solution phase ($E_{(s)}$) against the same cation in the solid phase ($E_{(z)}$) (Caputo & Pepe, 2007). There are four possible cation preference profiles that can be observed in this type of plot: the equal preference (45 ° straight line); the selective preference (concave down curve); the unselective (exponential curve); and the sigmoid that crosses preferences at one point (Colella, 1996).

The scoria material has shown a preference for $Sr^{2+}$ ions, followed by $Ca^{2+}$ and $K^+$ ions over $Na^+$ (Figure 6.7). The material showed a low and unselective behaviour for $Na^+$

ions when competing ions such as $Sr^{2+}$ and $Ca^{2+}$ were in solution, limiting the adsorption capacity of the material for the monovalent ion that is sodium. Nonetheless, this behaviour was less significant when $Na^+$ was competing with $K^+$.
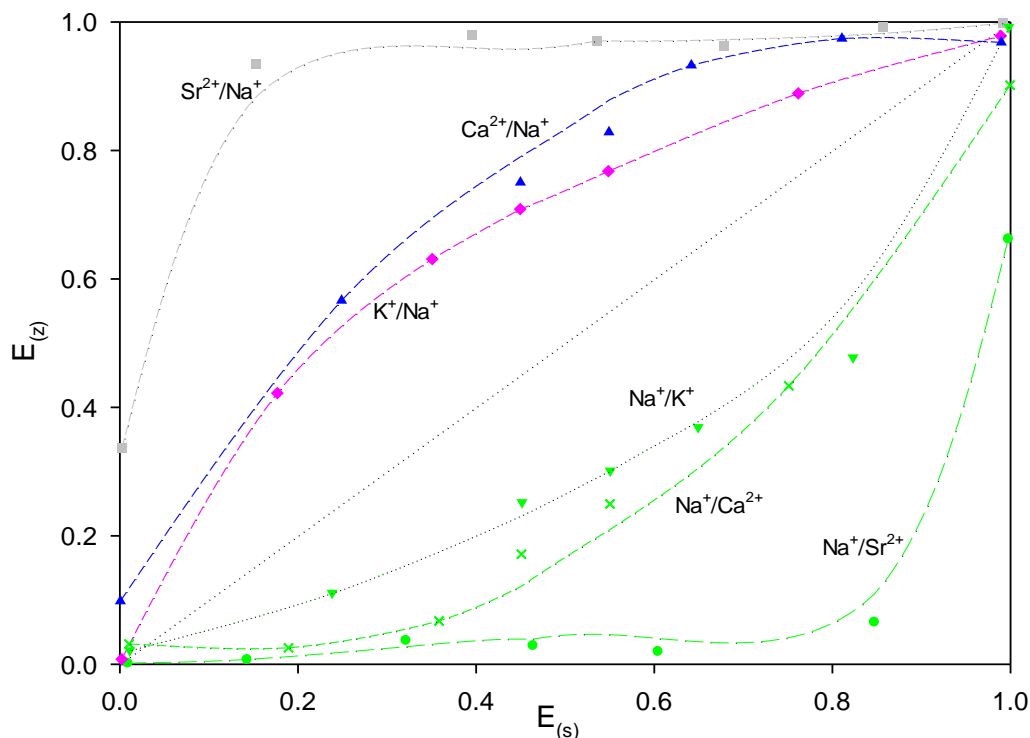


**Figure 6.7 Isotherm data for natural scoria at 25 °C using $Na^+/K^+$, $Na^+/Ca^{2+}$ and $Na^+/Sr^{2+}$ solutions at 0.01 M and $Cl^-$ anion. Each data point is a mean of two replicates, which did not vary by more than 5%. Selectivity curves showed that $Sr^{2+}$ was the ion preferred the most when competing with $Na^+$. The $K^+$ and $Na^+$ selectivity curves showed that $K^+$ was preferred but its preference was the closest to the line of equal selectivity.**

Selectivity curves for $Na^+/Sr^{2+}$ and $Na^+/Ca^{2+}$ did not proceed to completion. This is because the $Na^+$ ion in each phase did not reach unity ($E_{(z)}=1$; $E_{(s)}=1$). This can be attributed to the fact that only a fraction of the REC of the material demonstrated incomplete adsorption of the cation (Caputo & Pepe, 2007). The selectivity coefficients (Table 6.5) for the scoria material has shown the selectivity series to be $Sr^{2+} > Ca^{2+} > K^+ > Na^+$.

**Table 6.5 Values of selectivity coefficients at 25 °C for ion exchange equilibrium for natural scoria and zeolite.**

| Cation interaction | Selectivity coefficient ($K$) | |
|:---:|:---:|:---:|
| | Scoria | Zeolite |
| $K^+/Na^+$ | 1.34 | 8.34 |
| $Ca^{2+}/Na^+$ | 1.99 | 0.65 |
| $Sr^{2+}/Na^+$ | 4.88 | 1.26 |
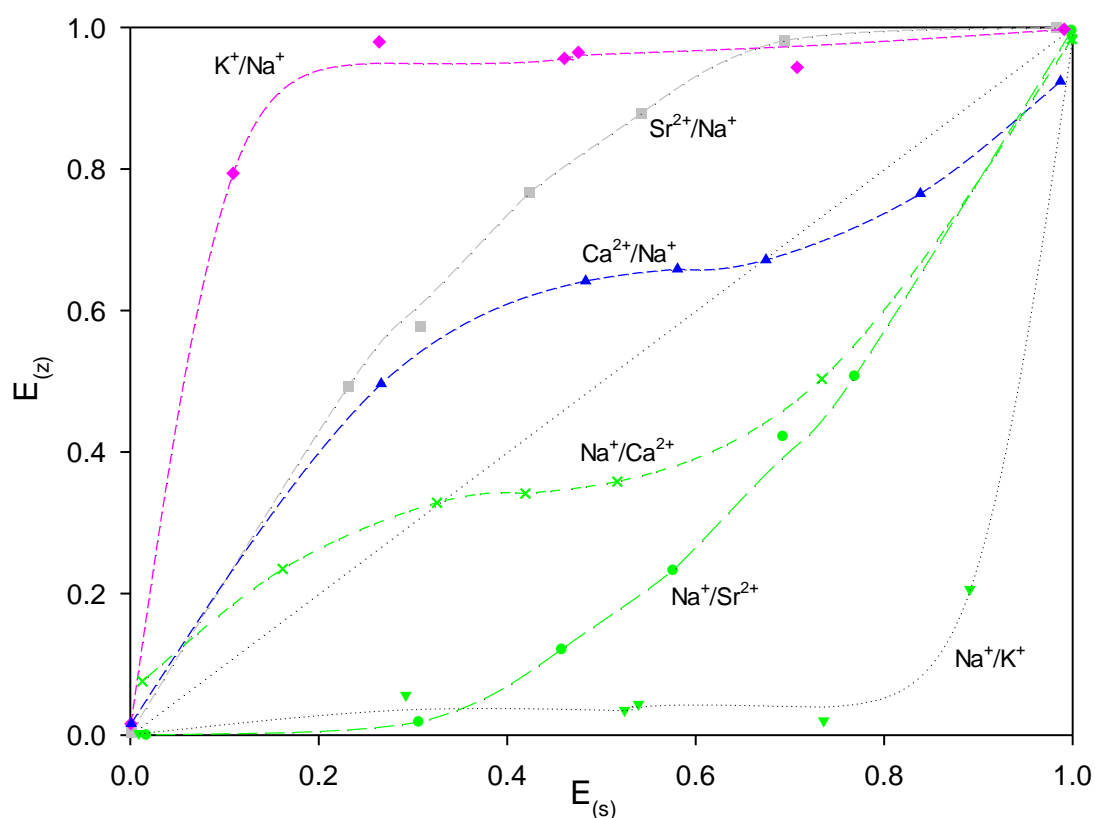


**Figure 6.8 Isotherm data for natural zeolite at 25 °C using $Na^+/K^+$, $Na^+/Ca^{2+}$ and $Na^+/Sr^2$ solutions at 0.01 M and Cl⁻ anion. Each data point is a mean of two replicates, which did not vary by more than 5%. Scoria selectivity behaviour showed that $K^+$ was preferred when competing with $Na^+$, with $Na^+$ the least preferred by the zeolite material of the cation trialled. $Na^+$ was preferred over $Ca^{2+}$ when the ratio of $Na^+$ was larger than the $Ca^{2+}$, and less preferred when $Na^+$ was in a larger ratio.**

The zeolite material has shown a greater selectivity for $K^+$ and $Sr^{2+}$ over $Na^+$, since the isotherm selectivity curves were above the equal preference line (Figure 6.8). $Ca^{2+}/Na^+$ and $Na^+/Ca^{2+}$ isotherm curves show a sigmoidal profile with preference for $Ca^{2+}$ and $Na^+$ when $E_{(s)} < 0.6$ and $E_{(s)} < 0.3$. After the inflection point on the selectivity curve, both ions, $Ca^{2+}$ and $Na^+$, were unselective or less preferential by the zeolite. The adsorption

of $Ca^{2+}$ was reduced when the competing $Na^+$ ion was in abundance, with the exchanger preference driven by the competing cation. Additionally, $Ca^{2+}$ was not able to reach unity ($E_{(z)}=1$; $E_{(s)}=1$), which may be explained by only a fraction of the REC was reached for this exchange system (REC: 75 meq/100 g). The selectivity coefficients calculated for the zeolite interaction with the competing cations showed that $K^+$ and $Ca^{2+}$ were the most and the least preferred cations for the zeolite material. The following selectivity series has been obtained $K^+ > Sr^{2+} > Ca^{2+} > Na^+$ (Table 6.5). Sposito *et al.* (1983) studied cation selectivity using $Na^+/Ca^{2+}$ for bentonite and found that the system presented no reference for $Na^+$, which agrees with the preference for $Ca^{2+}$ at low ratios and low selectivity for high ratios. Pabalan and Bertetti (2001) reviewed a number of isotherm curves for clinoptilolite material that describe the $K^+/Na^+$, $Ca^{2+}/Na^+$, $Sr^{2+}/Na^+$ competing ion interaction and showed the preference for $K^+$ and $Sr^{2+}$, and sigmoid profile exhibited by the $Ca^{2+}/Na^+$ system.

Based on the selectivity isotherms and related coefficients, the selectivity series observed for scoria in this study was $Sr^{2+} >> Ca^{2+} > K^+ > Na^+$, while for zeolite was $K^+ > Sr^{2+} >> Ca^{2+} > Na^+$. Scoria had a higher affinity for divalent cations over monovalent cations. A higher charge density of divalent cations explains the plausibility of this result, and the low charge density of monovalent ions (Langella *et al.*, 2000). The higher affinity in the selective series for $Sr^{2+}$ can be explained by the lower hydrated ionic radius (4.1 Å) and hydration energy (-1480 kJ/mol) than the divalent $Ca^{2+}$ ion (4.2 Å; -1577 kJ/mol) (Railsback, 2006). A similar pattern was observed for monovalent ions in scoria, where $K^+$ (3.1 Å; -307 kJ/mol) was preferred over $Na^+$ (3.58 Å; -406 kJ/mol) due to the lower hydrated radius and hydration energy (Kapanji, 2009).

The selectivity series for the zeolite can be explained through the Eisenman-Sherry theorem that relates the affinity of competing ions and the exchanger to characteristics such as ion size, charge density, and the framework charge density of the zeolite material (Caputo & Pepe, 2007). When monovalent ions compete against each other for exchange sites, $K^+/Na^+$, the selectivity towards the ion with low charge density is expected, in this case $K^+$, with ionic radius of 1.3 Å, while $Na^+$ has a smaller radius of 0.95 Å and also a higher charge density. This selectivity pattern is often observed for zeolites with relatively low field strength (Caputo & Pepe, 2007; Colella, 1996). For

$Sr^{2+}/Na^+$ and $Ca^{2+}/Na^+$, the zeolite was more selective for divalent cations, and the preference was related to the energy of hydration, where the cation with the lower hydration energy was preferred.

## Conclusions

Scoria and zeolite were demonstrated to adsorb sodium, strontium and barium ions. The equilibrium studies showed that materials treated with $NH_4^+$ exhibited a greater adsorption capacity for each of the said cations. When using scoria and zeolite for $Na^+$ adsorption, the system reached a maximum capacity that was lower than the REC measured for each material, consistent with a low preference for $Na^+$ ions. Nonetheless, both materials will significantly reduce the high concentration of cations often present in the CSG water such as strontium and barium.

In addition, equilibrium studies, selectivity isotherms and coefficients showed that the scoria material was more selective for higher charged cations with low hydration energy, and showed to have less affinity for monovalent cations with a larger energy of hydration and hydrated radius. The results for the scoria material has produced the following selectivity series: $Ba^{2+} > Sr^{2+} >> Ca^{2+} > K^+ > Na^+$. While, the zeolite material exhibited a higher selectivity towards cations with low charge density, small hydrated radius and low hydration energy. The selectivity series obtained for the zeolite was: $K^+ > Ba^{2+} > Sr^{2+} >> Ca^{2+} > Na^+$. Results showed that cationic properties, such as ionic/hydrated radii and hydration energy, have a fundamental role in the adsorption process and interaction between cations when using natural exchangers.

In the adsorption of cations present in the site CSG water, the scoria and zeolite will follow the selectivity series found for each material, removing cations such as $Ba^{2+}$ and $Sr^{2+}$ effectively, and achieving lower adsorption and rapid equilibrium for $Na^+$ ions. Thus, the overall treatment can be limited by the efficiency on the removal of $Na^+$ rather than the removal of other cations present in the solution.

# Chapter 7: Kinetic studies[1]

*Material from this chapter was incorporated into an accepted manuscript in the Journal Chemistry and Material Science SpringerPlus "Novel pre-treatment of zeolite materials for the removal of sodium ions: potential materials for coal seam gas co-produced wastewater".*

## DECLARATION OF CO-AUTHORSHIP AND CONTRIBUTION

| | |
|---|---|
| Title of Paper | Novel pre-treatment of zeolite materials for the removal of sodium ions: potential materials for coal seam gas co-produced wastewater |
| Full bibliographic reference for Journal/Book in which the Paper appears | SpringerPlus 2016 5:571<br>DOI: 10.1186/s40064-016-2174-9<br>Authors: Oscar Santiago (OS), Kerry Walsh (KW), Ben Kele (BK), Edward Gardner (EG) and James Chapman (JC). |
| Status | Received: 30 November 2015<br>Accepted: 15 April 2016<br>Published: 10 May 2016 |

Nature of Candidate's Contribution

Substantial contributions to experimental design, analysis and writing, and was primarily responsible for experimental execution.

Nature of Co-Authors' Contributions

BK, EG, KW and JC made substantial contributions to experimental design and to data interpretation and writing. BK provided the premise of the project, supporting data and material.

Candidate's Declaration
*I declare that the publication above meets the requirements to be included in the thesis as outlined in the Publication of Research Higher Degree Work for Inclusion in the Thesis Procedures*
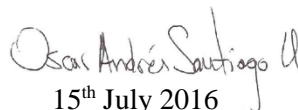
*Signature*
*Date*          15<sup>th</sup> July 2016

---

[1] Material from this chapter is incorporated into a manuscript entitled *"Novel pre-treatment of zeolite materials for the removal of sodium ions: potential materials for coal seam gas co-produced wastewater"* and accepted in the SpringerPlus Journal Chemistry and Materials Science; Manuscript ID: 15-03119

## Kinetic adsorption models

Kinetic behaviour is typically described in terms of the time that the reaction takes to reach equilibrium and the rate of the reaction. The progress of the adsorption kinetic process can be characterised by four process steps: (i) transport of the adsorbate from the bulk liquid phase to the hydrodynamic boundary layer around the adsorbent particle; (ii) transport through the boundary layer to the external surface of the adsorbent named film diffusion or external diffusion; (iii) transport into the interior of the adsorbent particle or intra-particle diffusion by diffusion in the pore liquid and; (iv) energetic interaction between the adsorbate molecules and the final adsorption sites.

A kinetic curve of an adsorbent is typically determined in a batch mode with a solution of known initial concentration ($C_0$) and volume ($V$) in contact with the adsorbent of known mass ($m$), which result in a change in the concentration in solution measured in time. During the adsorption process, the concentration decreases from the initial value (C$_0$) to equilibrium (C$_t$) and the adsorption measured at a given time interval can be determined with the following equations:

$$q_t = (C_0 - C_t) * \frac{V}{m}$$   **Equation 7.1**

$$E = \frac{C_0 - C_t}{C_0} * 100$$   **Equation 7.2**

The concentration of positive ions transferred to the solid phase of the material is $q$ expressed in meq/100 g. Where, $C_0$ and $C_t$ are the initial and balance concentration of ions in the solution at a given time $t$ expressed in equivalent form (meq/L). $V$ is the solution volume in L and $m$ is the weight of adsorbent in grams (Argun, 2008; Kocaoba *et al.*, 2007; Kumar & Jain, 2013). The ion adsorption efficiency is measured as a percentage of ions adsorbed from the initial concentration in solution at different intervals and calculated using Equation 7.2.

A curve fitting procedure is used with experimentally determined data to produce a kinetic model, where the respective mass transfer coefficients are the fitting

parameters. The kinetic models that were used consisted of pseudo-first order, pseudo-second order and Elovich's model (Table 7.1). These models are widely used for the examination of the adsorption kinetics of adsorbent materials (Malamis & Katsou, 2013).

**Table 7.1 Reaction kinetic models.**

| Model | Non-linear equation | Linear equation | Model Parameters |
|---|---|---|---|
| Pseudo-first order | $q_t = q_e(1 - e^{-k_1 t})$ | $\log(q_e - q_t) = \log(q_e) - k_1 t$ | $q_e, k_1$ |
| Pseudo-second order | $q_t = \dfrac{q_e^2 k_2 t}{(1 + q_e k_2 t)}$ | $\dfrac{t}{q_t} = \dfrac{1}{k_2 q_e^2} + \left(\dfrac{1}{q_e}\right) t$ | $q_e, k_2$ |
| Elovich | $q_t = \left(\dfrac{1}{b}\right) \ln(abt + 1)$ | $q_t = \dfrac{\ln(ab)}{b} + \dfrac{\ln(t)}{b}$ | $a, b$ |

That is $q_t$ (meq/100 g) is the adsorption at time $t$ (min); $q_e$ (meq/100 g) is equilibrium solid phase concentration; $k_1$ is first order rate constant for adsorption (min$^{-1}$); $k_2$ is second order rate constant for adsorption (min$^{-1}$); $a$ is the initial adsorption rate (meq/100 g*min); $b$ is the Elovich constant (meq/100 g).

The pseudo-first order reaction kinetic model assumes a reversible reaction with an equilibrium state being reached on both liquid and solid phases (Argun, 2008; Babak *et al.*, 2013). The pseudo-second order kinetic and Elovich equation are widely used in adsorption kinetic studies to describe the chemical adsorption of cations (Bektaş & Kara, 2004; Cincotti *et al.*, 2001; Du *et al.*, 2005; Kumar & Jain, 2013). All of these models are based on a number of assumptions including: constant temperature during the adsorption process, complete mixing of the solution, mass transfer into and within the adsorbent particle as a diffusion process and a regular shape of the adsorbent particles. These adsorption kinetic models were used in their non-linear form and fitted with non-linear least square analysis (SSE).

## Diffusion modelling

Diffusion processes occur through the bulk liquid and the liquid film layer surrounding the adsorbent particle (a process termed external diffusion or film diffusion), and also within the particle (termed intra-particle or pore diffusion) (Babak *et al.*, 2013; Karthikeyan *et al.*, 2010). Kinetic reaction models describe the adsorption equilibrium, however, they cannot identify the diffusion mechanism of the adsorption processes that have taken place. To develop an understanding of these processes, kinetic results

can be used to develop models, which separate the contribution of intra-particle or pore diffusion.

**Table 7.2 Diffusion models.**

| Model | Non-linear equation | Model Parameters |
|---|---|---|
| Intra-particle diffusion | $q_t = k_i t^{1/2} + C$ | $k_i, C$ |
| Film diffusion | $D_f = 0.23 \dfrac{r_0 \delta q_e}{t_{1/2}}$ | $D_f$ |
| Pore diffusion | $D_p = 0.03 \dfrac{r_0^2}{t_{1/2}}$ | $D_p$ |

That is where $k_i$ the intra-particle diffusion rate constant (meq/100 g*min), $C$ is the constant related to the boundary layer (Karthikeyan *et al.*, 2010), $D_f$ is the film diffusion coefficient (cm$^2$/s), $r_0$ is the radius of the particle (cm), $\delta$ is the film thickness (cm), $t_{1/2}$ is the half time for the ion exchange process (min) and $D_p$ is the pore diffusion coefficient (cm$^2$/s) (Argun, 2008; Karthikeyan *et al.*, 2010).

The rate of adsorption is often limited by the diffusion process on the external surface of the adsorbent particle (film diffusion) and within the porous sites available in the adsorbent (pore diffusion) (Argun, 2008). The examination kinetics revealed the adsorption mechanism underlining the sorption processes, which can be the product of film diffusion, pore diffusion or both. Equations in Table 7.2 were used for determination of the intra-particle, film and pore diffusion coefficients of the system.

## Results and Discussion

The adsorption of cations ($Na^+$, $Sr^{2+}$ and $Ba^{2+}$) from aqueous solutions onto the natural and treated form of zeolite and scoria materials was considered as a function of time. Adsorption kinetic and diffusion models were used to identify the adsorption rate, capacity and diffusion of $Na^+$ ions for both, natural and enhanced materials.

The effects of material fraction size, competing cations and anions on the $Na^+$ adsorption kinetics and capacity were also investigated. Regeneration studies were conducted revealing the adsorption/desorption capacity of both materials for a number of cycles.

## Effect of particle size on the adsorption process of Na⁺ ions using materials in natural form

The capacity of an adsorbent material to adsorb ions almost remains constant at different fraction sizes, since adsorption sites are intrinsic to the material and adsorption sites are unchanged by size of the adsorbent. However, accessibility of ions to interact with those available adsorption sites is facilitated when adsorbent particles are smaller because the paths for diffusion processes are shorter (Baker *et al.*, 2009; Huang *et al.*, 2010; Inglezakis *et al.*, 2007).Surface area of an adsorbent is related to the particle size, pore size and surface roughness of the material. Particles with smaller average diameter possess a larger specific surface area per volume, which enhances the adsorption process and decreases the time required to reach equilibrium (Malamis & Katsou, 2013).

Zeolite and scoria of three size fractions were used (1.8 - 0.6, 0.6 - 0.35 and < 0.355 mm) with an initial sodium chloride concentration of 0.1 M. The assessment of Na⁺ adsorbed by the material over time, and the percentage of concentration of sodium removed from the initial concentration was measured. The pseudo-second kinetic order was used to describe the Na⁺ adsorption kinetics of both materials at different fraction sizes. (Figures 7.1 – 7.4).

The Na⁺ adsorption rate and total adsorptive capacity increased with the reduction of the particle size of zeolite material (Figure 7.1). The fraction size of 1.8 - 0.6 mm showed the slowest kinetics and lowest adsorption of Na⁺ ions, while the smallest fraction size < 0.355 mm had an improvement in the total capacity and adsorption rate according with the results obtained from the modelling (Table 7.3). The largest fraction size reached a Na⁺ adsorption of 15.6 meq/100 g, while the smallest particle size achieved 27.5 meq/100 g. After 4320 min, the concentration of Na⁺ ions in solutions was decreased by 8 and 14% of the initial concentration Na⁺ when using the largest and the smallest particle sizes, respectively. Na⁺ adsorption was increased by 74% using the small fraction compared to the larger particle size (Figure 7.1).
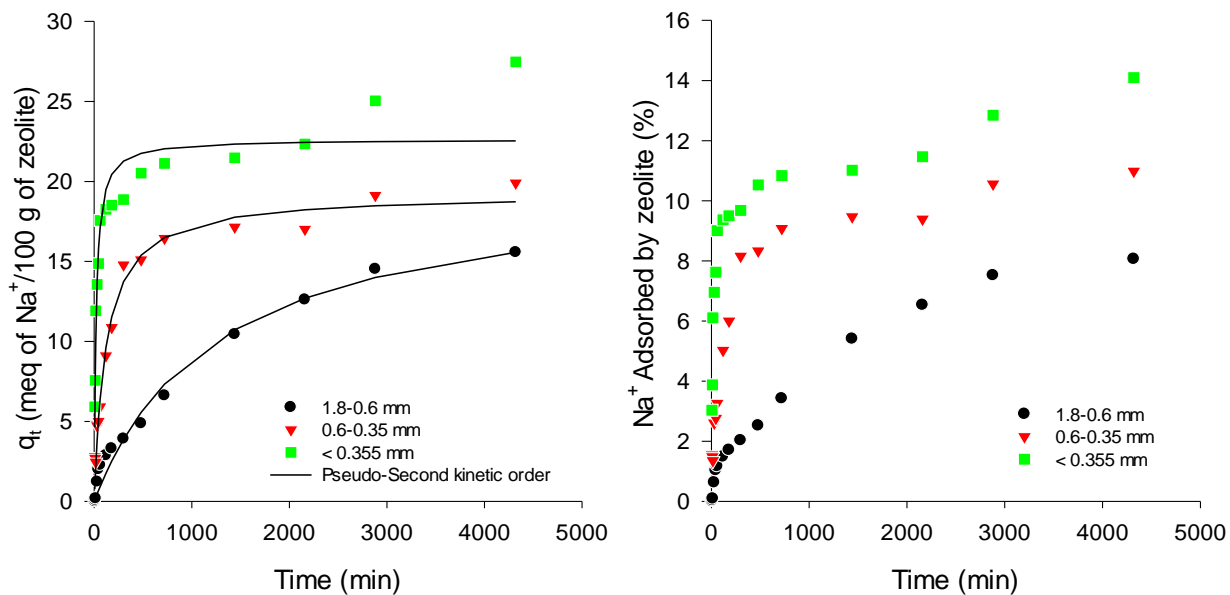
**Figure 7.1 Adsorption kinetics and Na+ removal from solution using three fraction sizes of natural zeolite. Initial Na+ concentration 0.1 M, shaking speed of 300 rpm, 25 °C and solid-liquid ratio 50 mg/L Pseudo-second kinetic order curves describing the Na+ adsorption (Left). Removal of Na+ for different size fractions (Right). The smaller particle (<0.355 mm) size of zeolite showed faster adsorption and higher capacity after 4300 min. Each data point is a mean of two replicates, which did not vary by more than 5%.**

**Table 7.3 Comparison adsorption kinetic constants for different fraction size of zeolite**

| Zeolite particle size (mm) | Exp. | Pseudo-first order | | | Pseudo-second order | | | Elovich Equation | | |
|---|---|---|---|---|---|---|---|---|---|---|
| | $q_e$ (meq/100g) | $q_e$ (meq/100g) | $k_1$ (min$^{-1}$) | SSE | $q_e$ (meq/100g) | $k_2$ (meq/100g*min) | SSE | $a$ (meq/100g*min) | $b$ (meq/100g) | SSE |
| 1.8 – 0.6 | 15.56 | 15.63 | 0.0008 | 3.04 | 14.98 | 0.0001 | 2.70 | 0.79 | 1.77 | 0.64 |
| 0.6 – 0.3 | 19.89 | 17.65 | 0.0062 | 4.99 | 19.24 | 0.0004 | 3.51 | 0.66 | 0.33 | 5.09 |
| < 0.355 | 27.47 | 21.36 | 0.0366 | 9.89 | 22.63 | 0.0022 | 7.20 | 10.66 | 0.37 | 5.72 |

The intermediate size exhibited a Na+ adsorption capacity by the end of the trial of 19.8 meq/100 g, with a Na+ removal of 11% of the initial concentration. The adsorption rate exhibited by the intermediate size was similar to the behaviour observed for the smallest fraction size during the first 300 min. The adsorption rate of zeolite using the smallest particle size was improved almost 5 times (Table 7.3). After 300 min the intermediate size particles had achieved a Na+ adsorption of 15 meq/100 g, increasing the adsorption rate by 4 times that of the largest fraction size.

The Na+ adsorption results for the different particle sizes were expected for two reasons − (i) with reduction on the diameter of a zeolite particle, the surface area for the same mass of the material is increased. For instance, a spherical particle with a

diameter of 1.2 mm has a surface area of 4.5 mm$^2$, while particles of the same mass but diameter 0.35 mm have a surface area of 15 mm$^2$. Thus, the increase on the surface area leads to make available adsorption sites that are not accessible for larger particles. (ii) a smaller particle diameter results in larger film diffusion and shorter intra-particle diffusion path, which increases the adsorption rates. The rapid adsorption rate may be related to the film diffusion and the increment in the surface area (Huang *et al.*, 2010).

Experimental data for all particle sizes was better fit (minimum SSE) using the pseudo-second order than Elovich or pseudo-first order kinetic models (Figure 7.1 and Table 7.3). The pseudo-second order model estimates a lower capacity than that found experimentally for all the particle sizes with large differences for the smallest fraction size. As expected, the adsorption rates ($k_2$) were highest for the smallest particles and lower for larger fraction sizes, where large and intermediate particle sizes exhibited 5% and 19% of the adsorption rate calculated for small fraction size. These results agree with the findings reported by Wen *et al.* (2006), who used zeolite of varied sizes for the removal of $NH_4^+$ ions, finding that smaller particle size exhibited higher adsorption capacities increasing from 68 to 72 meq/100 g, when the diameter was reduced by a fifth of the largest fraction size (from 11 to 2 mm), and the adsorption rate was improved by about 4 times (0.0028 to 0.0105 meq/100 g*min). Microporous materials, such as zeolites, exhibit a larger internal surface area due to the intrinsic crystal framework, making the inner surface as relevant as the external surface area of the material which is more accessible for smaller particles (Bektaş & Kara, 2004; Huang *et al.*, 2010; Inglezakis *et al.*, 1999; Malliou *et al.*, 1994).

$Na^+$ adsorption rates by scoria increased with the reduction of particle size (Figure 7.2). After 720 min of contact time, the smallest fraction size (< 0.355 mm) attained equilibrium at 12 meq/100 g. The intermediate fraction size reached adsorption equilibrium after 2160 min at 10 meq/100 g, while the largest fraction size (1.8 − 0.6 mm) exhibited an adsorption capacity of 10.5 meq/100 g after 4320 min but no clear equilibrium was observed (Figure 7.2). After 4320 min, the smallest size particle achieved 6.6% $Na^+$ removal of initial concentration, while 5.3% was achieved for the intermediate and larger fractions, respectively (Figure 7.2).
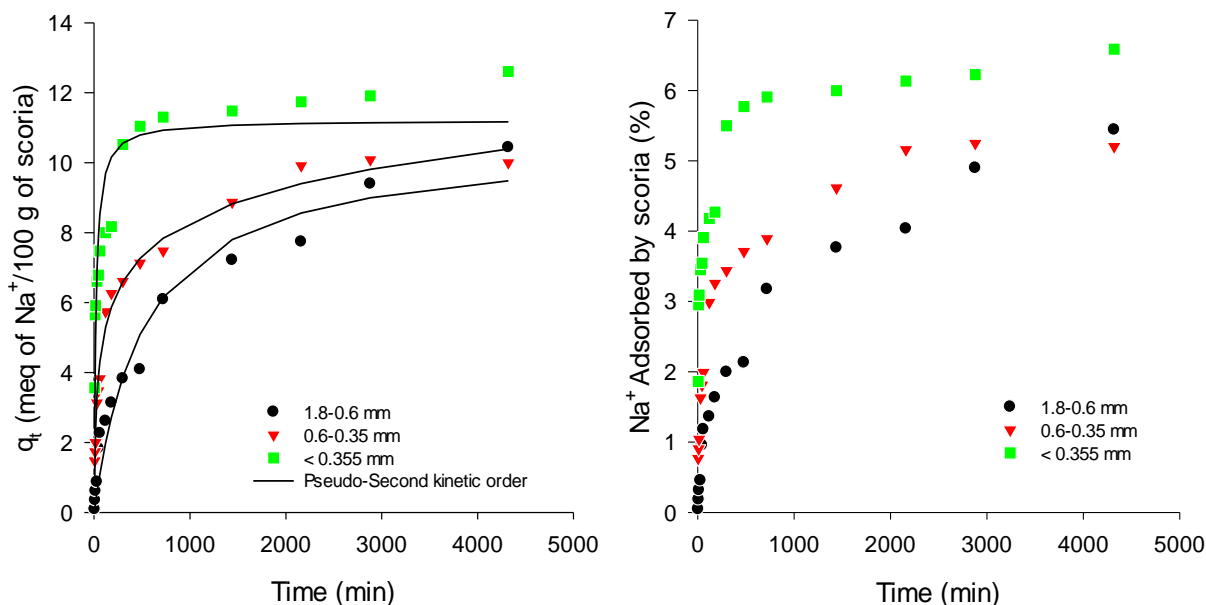
**Figure 7.2 Adsorption kinetics and Na⁺ removal from solution using three fraction sizes of natural scoria. Initial Na⁺ concentration 0.1 M, shaking speed of 300 rpm, 25 °C and solid-liquid ratio 50 mg/L Pseudo-second kinetic order curves describing the Na⁺ adsorption (Left). Removal of Na⁺ for different fractions sizes (Right). Large and intermediate particle sizes exhibited similar adsorption rates and capacities, while smallest particle slightly improved the Na⁺ adsorption. Each data point is a mean of two replicates, which did not vary by more than 5%.**

The calculated kinetic parameters using three different models are shown in Table 7.4 and kinetic curves modelled with pseudo-second order model are shown in Figure 7.2. The models reflect the effect of particle size on surface area and parameters such as, adsorption capacities at equilibrium and the rates of adsorption. The pseudo-first order model gave an estimate of the adsorption capacity at equilibrium ($q_e$) of the largest and intermediate fraction sizes as 9 meq/100 g, while that for the smallest particle size was 10.5 meq/100 g. The adsorption rate ($k_2$) calculated for the pseudo-second kinetic order model indicated a higher adsorption rate for the intermediate than the fine or large particles. This result is attributed to rapid adsorption within the first minutes, and the rapid equilibrium in the adsorption capacity as predicted by the model (Table 7.4). The smallest fraction size of scoria exhibited an adsorption rate some 50% smaller than the intermediate size (0.6 – 0.35 mm), while the calculated rate for the largest size was 1.4% of the intermediate size.

**Table 7.4 Comparison adsorption kinetic constants for different fraction size of scoria.**

| Scoria particle size (mm) | Exp. $q_e$ (meq/100g) | Pseudo-first order | | | Pseudo-second order | | | Elovich Equation | | |
|---|---|---|---|---|---|---|---|---|---|---|
| | | $q_e$ (meq/100g) | $k_1$ (min$^{-1}$) | SSE | $q_e$ (meq/100g) | $k_2$ (meq/100g*min) | SSE | $a$ (meq/100g*min) | $b$ (meq/100g) | SSE |
| 1.8 – 0.6 | 10.43 | 9.07 | 0.0016 | 3.22 | 10.62 | 0.0001 | 2.48 | 0.12 | 0.66 | 3.36 |
| 0.6 – 0.3 | 10.00 | 8.69 | 0.0092 | 3.99 | 9.11 | 0.0073 | 7.86 | 0.49 | 0.70 | 1.42 |
| < 0.355 | 12.60 | 10.57 | 0.0366 | 6.21 | 11.21 | 0.0047 | 4.26 | 7.22 | 0.78 | 2.05 |

The effect of particle size on the $Na^+$ adsorption capacity was less marked for scoria than zeolite, since the smallest fraction size increased the adsorption capacity by only 20% with a surface area four times higher than the largest particle. Therefore, a reduced number of adsorption sites were exposed with small fraction sizes. Alemayehu and Lennartz (2009) and Alemayehu *et al.* (2011) studied the effect of scoria particle size on the adsorption on $Cd^{2+}$ and $Cr^{6+}$ and determined that reduced effect on adsorption of small size particles on the adsorption of contaminants was product of the scoria dead end pores and that the adsorption of ions occurred into the macropore structure of the material. The pseudo-second model for the adsorption of $Cd^{2+}$, showed that capacity ($q_e$) was improved 15% when fine material was used, while the adsorption of $Cr^{6+}$ increased 5% in silt compared to fine sizes. These studies also demonstrated that the adsorption rates ($k_2$) for smaller particles were larger than for large particles by five times for $Cd^{2+}$, and 30 times for $Cr^{6+}$. These results are consistent with this study.

The adsorption rates and capacities of both scoria and zeolite were similar for intermediate and small particle sizes. The use of fine particles in full scale adsorption systems (packed fixed bed) may present operational issues due to the resistance to flow, requiring a high pressure system and the possible loss of material. Therefore, the particle size of 0.6-0.35 mm was used for column trials.

### Adsorption kinetics of $Na^+$, $Sr^{2+}$ and $Ba^{2+}$ ions using materials in natural form

The adsorption kinetic and removal efficiency behaviour of major ($Na^+$) and trace elements ($Sr^{2+}$ and $Ba^{2+}$) from CSG water were studied for natural forms of zeolite and scoria (Figure 7.3 – 7.4).

The natural materials exhibited low $Na^+$ adsorption capacity and rate when compared with the adsorption of the same material over $Sr^{2+}$ and $Ba^{2+}$ (Figures 7.3 and 7.4). Zeolite showed a reduction of $Na^+$ of 7.66% of the initial concentration after 720 min that allowed the removal of 16.1 meq/100 g, while the adsorption of $Sr^{2+}$ and $Ba^{2+}$ removed 28.4 and 29.7 meq/100 g that correspond to a 99% removal of the initial concentration for both cations. The $Sr^{2+}$ and $Ba^{2+}$ adsorption achieved large removal rates within the first 30 min achieving a rapid adsorption rate while $Na^+$ adsorption was progressive until equilibrium was attained. The adsorption of $Sr^{2+}$ and $Ba^{2+}$ exhibited 40% of the REC, nonetheless initial concentrations were not sufficient to exhibit values close to the real capacity (75.1 meq/100 g). The adsorption of $Na^+$ achieved 22% of the REC for zeolite.
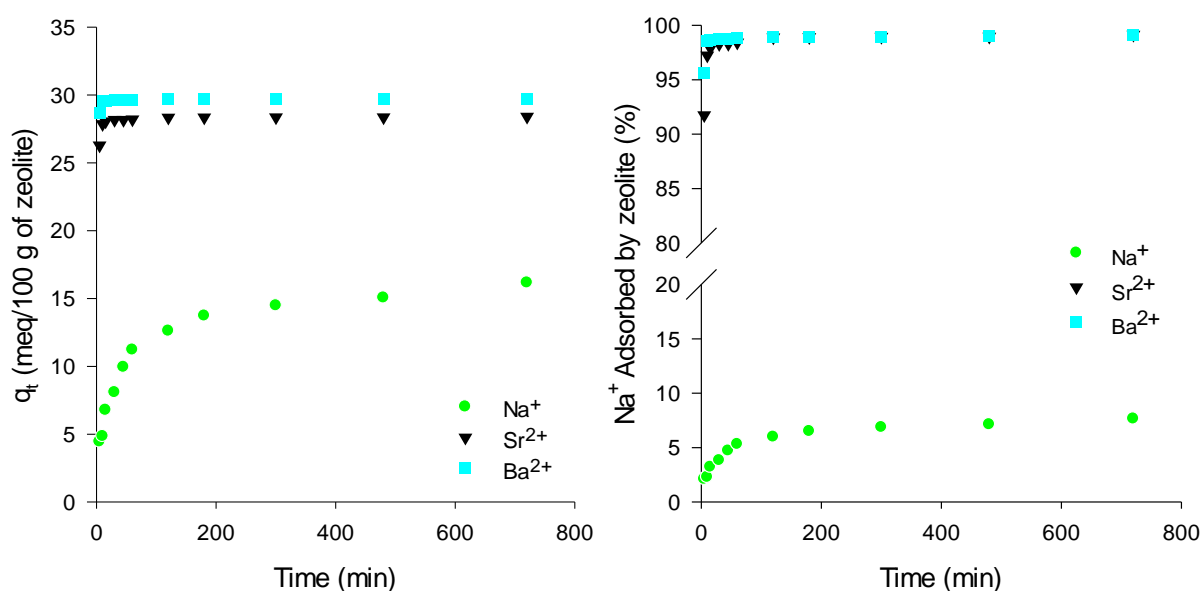


**Figure 7.3 Adsorption kinetics (left) and removal from solution (right) of $Na^+$, $Sr^{2+}$ and $Ba^{2+}$ using natural zeolite. Initial concentration ($C_o$) $Na^+$= 0.1 M, $Sr^{2+}$= 7.5 mM and $Ba^{2+}$= 7.5 mM, speed of 300 rpm and 25 °C. Larger rates and capacities were observed for $Sr^{2+}$ and $Ba^{2+}$, when compared with $Na^+$. Each data point is a mean of two replicates, which did not vary by more than 5%.**
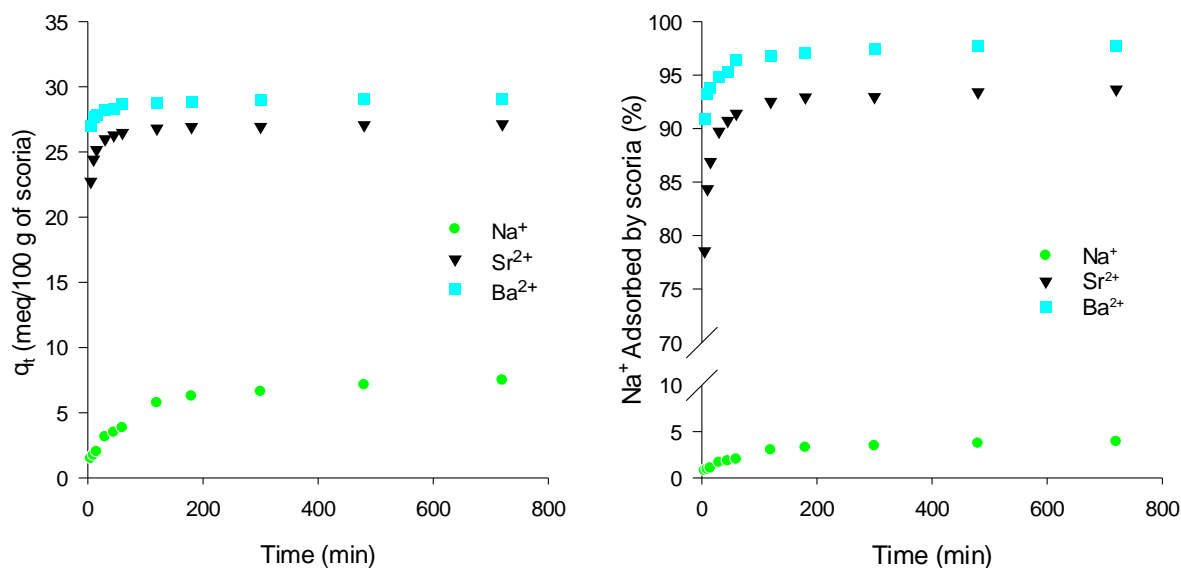
**Figure 7.4 Adsorption kinetics (left) and removal from solution (right) of Na$^+$, Sr$^{2+}$ and Ba$^{2+}$ using natural scoria. Initial concentration (C$_o$) Na$^+$= 0.1 M, Sr$^{2+}$= 7.5 mM and Ba$^{2+}$= 7.5 mM, speed of 300 rpm and 25 °C. Larger rates and capacities observed for Ba$^{2+}$ followed by Sr$^{2+}$ and Na$^+$. Each datum is an average of two replicates, which did not vary by more than 5%.**

The adsorption behaviour of Na$^+$, Sr$^{2+}$ and Ba$^{2+}$ can be explained by the cation selective behaviour of the material (Chapter 6), with higher affinity of the material for Sr$^{2+}$ and Ba$^{2+}$. The low adsorption capacity of Na$^+$ exhibited by the zeolite has also been described by Mumpton (1999), who used a zeolite in natural form with a theoretical exchange capacity of 142 meq/100 g but in practice Na$^+$ ions were adsorbed to only 11% of that capacity after 720 min. Comparable results were obtained by Zhao *et al.* (2008); Zhao *et al.* (2009) and Huang and Natrajan (2006) who used natural zeolite for the reduction of Na$^+$ present in CSG water from Wyoming and New Mexico in USA, achieving low adsorption of this cations due to the low selectivity.

Similarly, Na$^+$ adsorption for the scoria material showed low capacity when compared with adsorption capacity for cations such as Sr$^{2+}$ and Ba$^{2+}$ (Figures 7.4). The Ba$^{2+}$ adsorption reached a capacity of 29 meq/100 g that corresponds to a total removal of 97.7% of the initial concentration of this ion. The removal of Sr$^{2+}$ reached an effective removal of 93.6% from the initial concentration with an adsorption capacity of 27.1 meq/100 g. The Na$^+$ adsorption capacity of the scoria material observed after 720 min was 7.4 meq/100 g, which corresponds to a removal of 4% of the initial concentration of Na$^+$ ions. The adsorption capacities exhibited for the scoria material for Sr$^{2+}$ and Ba$^{2+}$ cations reached 80% and 85% of the REC for the material estimated as 34.2

meq/100 g. On the other hand, the adsorption of the $Na^+$ was only a fraction (21.8%) of the estimated REC, indicating low selectivity towards $Na^+$ ions.

Natural untreated scoria material demonstrated an effective adsorption and removal preference for $Sr^{2+}$ and $Ba^{2+}$ at typical concentrations in CSG water ($Sr^{2+}$ = 0.02 meq/L; $Ba^{2+}$ = 0.05 meq/L), while it showed a reduced adsorption selectivity and removal towards $Na^+$ ions. Different studies have explored the adsorption properties of scoria material for the removal of heavy metals with different valencies and found that the adsorption kinetics among the studied cations was driven by a combination of effects of valence, electrostatic attraction and hydrated radii of the cations in solution (Alemayehu & Lennartz, 2009; Alemayehu *et al.*, 2011; Kwon *et al.*, 2005; Kwon *et al.*, 2010). This is equivalent to the results presented for scoria, where $Sr^{2+}$ and $Ba^{2+}$ with higher valence and electrostatic attraction were preferred.

### Effect of treated material on the adsorption kinetics of $Na^+$

Typically, natural exchangers, especially zeolites, are chemically conditioned to improve their ion exchange performance when compared with their natural form (Gedik & Imamoglu, 2008; Inglezakis *et al.*, 2001a; Inglezakis *et al.*, 2001c; Semmens & Martin, 1988). The chemical conditioning removes certain ions from the exchanger framework that hinder ion exchange while introducing ions that enhance exchangeability for incoming ions. In this study, natural zeolite and scoria were chemically treated with single solutions of calcium chloride, hydrochloric acid, potassium chloride and ammonium acetate to investigate the performance of both materials for the removal of $Na^+$ ions present in CSG water and kinetic adsorption behaviour (Figure 7.5 and 7.7).

The treated zeolite material presented different adsorption rates and capacities. $Ca^{2+}$ and $NH_4^+$ treated zeolite displayed the least and the greatest $Na^+$ adsorption capacity, respectively. The adsorption equilibrium was attained within the first 500 min. Natural zeolite showed to be the second least performing adsorbent when in contact with $Na^+$ solution, while the other three treated zeolite materials showed favourable adsorption for $Na^+$ ions. Natural zeolite form removed 7.7% (16 meq/100 g) of the initial solution, while the zeolite enriched with $NH_4^+$ removed 21.1% (36 meq/100 g) of the initial $Na^+$.

The treatment of zeolite material with $NH_4^+$ solution incremented the capacity by 18.5 meq/100 g when compared with the natural form (Table 7.5).
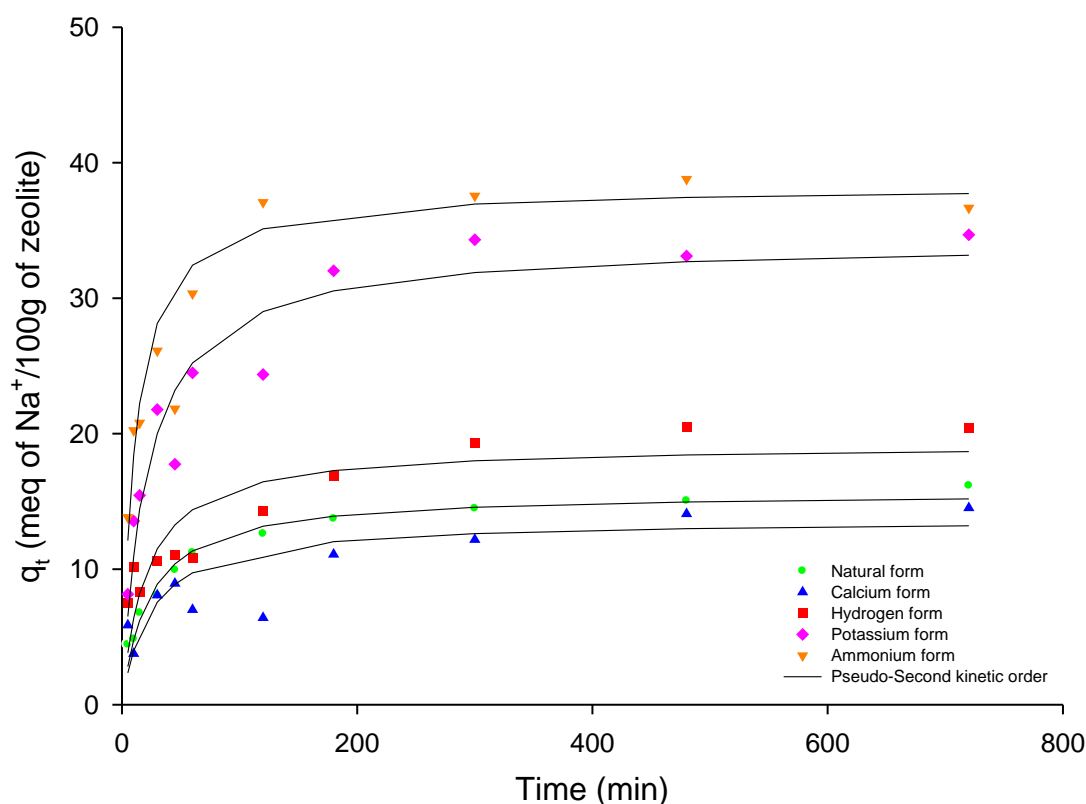


**Figure 7.5 Adsorption kinetic of $Na^+$ and pseudo-second kinetic order for enhanced and natural zeolite material. Initial $Na^+$ concentration 0.1 M, shaking speed of 300 rpm, 25 °C and solid-liquid ratio 50 mg/L. Larger $Na^+$ adsorption was achieved for zeolite enhanced with $NH_4^+$ and $K^+$, while $Ca^{2+}$ and natural material presented similar behaviour. Each data point is an average of two replicates, which did not vary by more than 5%.**

**Table 7.5 Comparison adsorption kinetic constants for different zeolite forms.**

| Zeolite Form | Exp. | Pseudo-first order | | | Pseudo-second order | | | Elovich Equation | | |
|---|---|---|---|---|---|---|---|---|---|---|
| | $q_e$ (meq/100g) | $q_e$ (meq/100g) | $k_1$ (min$^{-1}$) | SSE | $q_e$ (meq/100g) | $k_2$ (meq/100g*min) | SSE | $a$ (meq/100g*min) | $b$ (meq/100g) | SSE |
| Natural | 16.16 | 14.34 | 0.031 | 4.08 | 15.67 | 0.0020 | 2.27 | 2.54 | 0.39 | 1.83 |
| $Ca^{2+}$ | 15.52 | 12.71 | 0.026 | 6.13 | 13.63 | 0.0030 | 4.91 | 2.87 | 0.48 | 3.41 |
| $H^+$ | 20.40 | 17.90 | 0.030 | 10.29 | 19.20 | 0.0020 | 7.72 | 27.43 | 0.20 | 7.43 |
| $K^+$ | 34.68 | 31.29 | 0.033 | 12.70 | 34.14 | 0.0010 | 8.76 | 26.03 | 0.18 | 7.10 |
| $NH_4^+$ | 36.67 | 35.92 | 0.063 | 9.21 | 38.28 | 0.0020 | 4.91 | 27.43 | 0.20 | 7.73 |

The pseudo-second kinetic order exhibited the best fitting in terms of SSE and the adsorption kinetic curves are shown in Figure 7.5 (Table 7.5). Adsorption capacity ($q_e$) calculated with pseudo-second order model resembles experimental adsorption, and adsorption rate ($k_2$) for all zeolite forms exhibited similar values in the range of 0.001

– 0.003 meq/100 g. This indicates that an improvement on the adsorption capacity by using treated zeolite is not proportional to adsorption rate of the material, instead the adsorption rate of Na$^+$ ions was constant for zeolite in different forms.
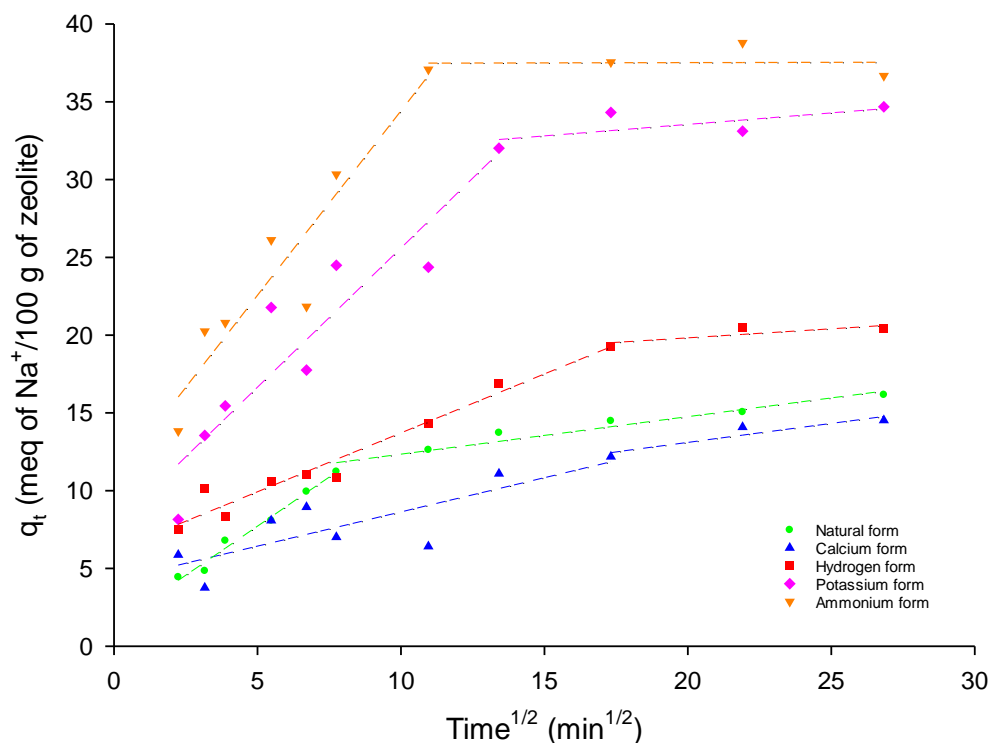


**Figure 7.6 Intra-particle diffusion model for the adsorption of Na$^+$ ions using natural and treated zeolite.**

**Table 7.6 Intra-particle diffusion model, film and pore diffusion values for the adsorption of Na$^+$ using natural and treated zeolite material.**

| Zeolite Form | Intra-particle diffusion | | | Film diffusion | Pore diffusion |
|---|---|---|---|---|---|
| | $k_i$ meq/100g*min$^{1/2}$ | $C$ meq/100g | $R^2$ | $D_f$ (cm$^2$/s) | $D_p$ (cm$^2$/s) |
| Natural | 1.26 | 1.40 | 0.99 | 2.96 x 10$^{-5}$ | 5.70 x 10$^{-5}$ |
| Ca$^{2+}$ | 0.43 | 4.23 | 0.82 | 2.66 x 10$^{-5}$ | 5.70 x 10$^{-5}$ |
| H$^+$ | 0.75 | 6.14 | 0.98 | 3.73 x 10$^{-5}$ | 5.70 x 10$^{-5}$ |
| K$^+$ | 1.79 | 7.69 | 0.93 | 4.23 x 10$^{-5}$ | 3.80 x 10$^{-5}$ |
| NH$_4$$^+$ | 2.37 | 10.71 | 0.94 | 2.01 x 10$^{-4}$ | 1.71 x 10$^{-4}$ |

Diffusion mechanisms were determined for the natural and enhanced zeolite forms for the adsorption of Na$^+$ using the intra-particle model. Film and pore diffusion equations were applied to the experimental data (Figure 7.6 and Table 7.6). In adsorption processes film diffusion occurs quickly where ions migrate from the bulk solution to the surface of the zeolite particle creating a liquid film and attaining equilibrium with

the available sites on the surface. Film diffusion is followed by the pore diffusion, which is a slower adsorption process. Intra-particle diffusion was explored in order to determine the intra-particle diffusion rate and the effect of the thickness of the boundary layer on the adsorption of $Na^+$ ions for zeolite materials Experimental kinetic data were plotted with the square root of time against the $Na^+$ adsorption exhibited by each material. If the adsorption process is controlled by intra-particle diffusion a single straight line should be observed. However, the experimental data exhibited two line segments, indicating that more than one diffusion mechanisms were involved during adsorption (Figure 7.6). The first segment for each zeolite form corresponds to the surface diffusion, which occurred on the macropores and mesopores. The second segment represents the intra-particle diffusion that took place within the micropore structure of the material.

The first segment for each zeolite form is ascribed to surface diffusion, which occurred on the macropores and mesopores. The second segment is ascribed to intra-particle diffusion that took place within the micropore structure of the material. Thus in the early stages of $Na^+$ adsorption, diffusion was highly influenced by film diffusion and most of the adsorption occurred on the material outer structure. Pore diffusion was slower, controlled by the diffusion of $Na^+$ into the inner framework. $NH_4^+$ and $K^+$ treated zeolite showed that most of the $Na^+$ adsorption took place on the surface of the material, while natural and $Ca^{2+}$ treated zeolite forms exhibited larger adsorption that took place within the material. Nguyen *et al.* (2015) used Australian iron coated zeolite for adsorption of cadmium, chromium, copper, zinc and lead; they found that the intra-particle diffusion plot exhibited two linear segments. A first adsorption, attributed to the external diffusion was followed by a second adsorption attributed to the intra-particle diffusion, which agrees with the results obtained for the adsorption of $Na^+$ using zeolite in different forms.

Film and pore diffusion coefficients for particles of natural zeolite under experimental conditions were calculated as 2.96x10$^{-5}$ $cm^2/s$ and 5.70x10$^{-5}$ $cm^2/s$, respectively. Often, when film diffusion has a larger value and internal diffusion has a lower value, the adsorption process is believed to be governed by particle diffusion. If pore diffusion coefficient results to be greater than film diffusion, the process is governed by film diffusion (Karthikeyan *et al.*, 2010). Diffusion coefficients calculated for the

natural zeolite suggested that the diffusion process was to some extent rate-limited by the film diffusion indicating the influence of the film diffusion process (Table 7.6). Additionally, when zeolite is treated with $Ca^{2+}$ and $H^+$, the material exhibited similar values as the natural form, indicating that film diffusion has influenced the adsorption of $Na^+$. Film and pore diffusion coefficients calculated for treated zeolite with $K^+$ and $NH_4^+$ indicate that film diffusion was not the rate-limiting factor (Table 7.6). Film diffusion coefficients for $K^+$ and $NH_4^+$ treated zeolite were smaller than those coefficients found for pore diffusion, which reinforced the validity of the intra-particle diffusion model.

The zeolite material exhibited particular $Na^+$ adsorption capacities when it was treated with cations such as $NH_4^+$ or $Ca^{2+}$. The adsorption interaction was greater for zeolite enhanced with $NH_4^+$ or $K^+$, while the $Na^+$ adsorption was reduced for the same material treated with $Ca^{2+}$, thus the adsorption capacity can be related to the characteristics of the cations used for the material treatment. $Na^+$ adsorption was favourable for zeolite treated with cations with low ionic field strength, small hydrated radii, and reduced energy of hydration, such as $NH_4^+$ or $K^+$ (Table 7.7).

**Table 7.7 Properties of ions used in trials and adsorption process (Kapanji, 2009; Railsback, 2006).**

| Ion | Ionic radius (Å) | Hydrated radius (Å) | Hydration energy (kJ/mol) |
|---|---|---|---|
| $Ca^{2+}$ | 1.0 | 4.2 | -1577 |
| $Sr^{2+}$ | 1.12 | 4.1 | -1480 |
| $Ba^{2+}$ | 1.34 | 4.05 | -1360 |
| $H^+$ | <0.5 | - | -1130 |
| $Na^+$ | 0.95 | 3.58 | -406 |
| $K^+$ | 1.3 | 3.1 | -322 |
| $NH_4^+$ | 1.5 | 3.3 | -307 |

In general terms, small cations have a high charge density increasing its radius when dissolved in water, since it is able to attract a large number of water molecules, such as $Ca^{2+}$, $Sr^{2+}$, $Ba^{2+}$ (Table 7.7). It is also known that the affinity and selectivity of cations in zeolites are strongly related with the hydration radius of the cations, since some large hydrated cations may be rejected during the diffusion process due to the

large size in comparison with the small pore size on the zeolite framework (Inglezakis *et al.*, 2001c; Kapanji, 2009). Hydration energy also explains the selectivity behaviour for cation exchangers, where high selectivity is observed for ions with smaller hydration energy and a lower selectivity is observed for those ions with high hydration energy such as $Ca^{2+}$, $Sr^{2+}$, $Na^+$, which require more energy (Inglezakis *et al.*, 2004).

The $Na^+$ adsorption performance of natural and treated zeolite may be explained by the same factors that influence the affinity and selectivity of cations. The natural and $Ca^{2+}$ treated zeolites had similar effect on the $Na^+$ adsorption capacity, which can be attributed to three reasons: (i) The natural zeolite presented large $Ca^{2+}$ composition when determined by XRF and EDS, therefore the $Ca^{2+}$ treated zeolite behaves similarly. (ii) $Ca^{2+}$ on the zeolite presented a high energy of hydration, which in theory requires high energy to be in a dissolved state. For instance, $Ca^{2+}$ ions required five times the energy to dissolve than $NH_4^+$ ions. (iii) the hydrated size of $Ca^{2+}$ ions may limit the intra-particle diffusion and exchange of ions because the zeolite channels are narrow and large cations can inhibit the two-way process such as $Ca^{2+}$. The adsorption of $Na^+$ and zeolite treated with $NH_4^+$ form presented the opposite scenario, since $NH_4^+$ ions required much less energy for hydration, increasing the interactions between cations that resulted in higher $Na^+$ adsorption. Furthermore, cations such as $NH_4^+$ and $K^+$ have a low hydrated radius, allowing the two-way process within the narrow zeolite channels.

$Na^+$ adsorption for scoria (natural and treated form) was investigated over 720 min (Figure 7.7). Similar to zeolite, scoria in $NH_4^+$ and $K^+$ forms exhibited larger adsorption of $Na^+$ ions, reaching 17.2 and 12.3 meq/100 g, while natural form and acid form presented an adsorption of 7.4 and 6.4 meq/100 g respectively (Table 7.8). The initial concentration of $Na^+$ was decreased by 3.9% after 720 min for natural scoria, while the same material in $NH_4^+$ form exhibited a removal of 8.6% of $Na^+$ initially in solution. The low adsorption capacity exhibited for the scoria treated with acid is ascribed to an effect of the acid treatment that partially dissolved and disintegrated the scoria framework, removing cations that are contained in the material, corroborated with the SEM and EDs results. Significant changes on the morphology of the surface after treatment caused structural changes that affected the adsorptive properties of the scoria.
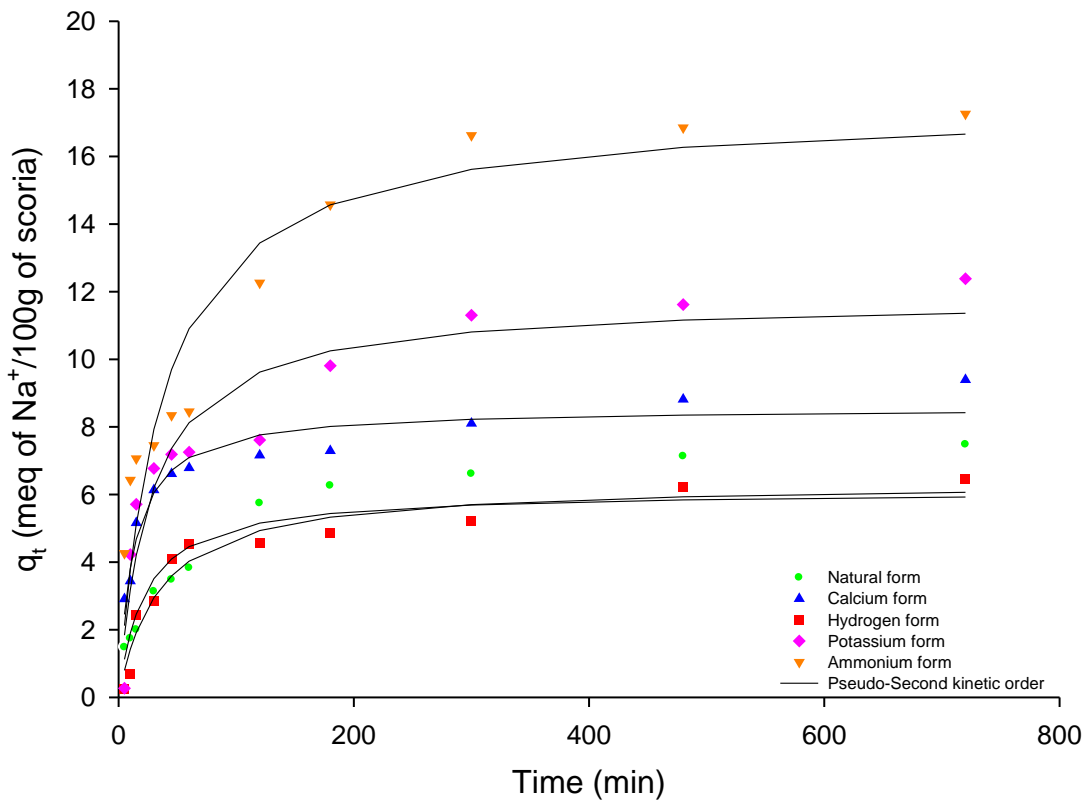
**Figure 7.7 Adsorption kinetic of Na$^+$ and pseudo-second kinetic order for natural and enhanced scoria. Initial Na$^+$ concentration 0.1 M, shaking speed of 300 rpm, 25 °C and solid-liquid ratio 50 mg/L. Larger Na$^+$ adsorption was achieved for material enhanced with NH$_4^+$, while H$^+$ showed lower adsorption than natural scoria. Each data point is a mean of two replicates, which did not vary by more than 5%.**

**Table 7.8 Comparison adsorption kinetic constants for different scoria forms.**

| Scoria Form | Exp. | Pseudo-first order | | | Pseudo-second order | | | Elovich Equation | | |
|---|---|---|---|---|---|---|---|---|---|---|
| | $q_e$ (meq/100g) | $q_e$ (meq/100g) | $k_1$ (min$^{-1}$) | SSE | $q_e$ (meq/100g) | $k_2$ (meq/100g*min) | SSE | $a$ (meq/100g*min) | $b$ (meq/100g) | SSE |
| Natural | 7.47 | 8.69 | 0.009 | 3.99 | 6.11 | 0.0073 | 7.86 | 0.49 | 0.70 | 1.42 |
| Ca$^{2+}$ | 9.39 | 7.87 | 0.059 | 2.56 | 8.56 | 0.0093 | 1.65 | 3.78 | 0.81 | 1.45 |
| H$^+$ | 6.46 | 5.60 | 0.025 | 1.83 | 6.35 | 0.0045 | 1.56 | 0.41 | 0.81 | 1.60 |
| K$^+$ | 12.38 | 10.54 | 0.029 | 4.77 | 11.78 | 0.0031 | 3.55 | 1.15 | 0.47 | 2.87 |
| NH$_4^+$ | 17.25 | 16.03 | 0.018 | 6.76 | 17.50 | 0.0015 | 5.15 | 1.91 | 0.35 | 3.57 |

The adsorption kinetic model parameters for natural and treated forms of scoria are shown in Table 7.8 and calculated pseudo-second order kinetic curves that fit the data in terms of the SSE are shown in Figure 7.7. The kinetic rates (k$_2$) found with the pseudo-second order model showed that Na$^+$ was adsorbed at a higher rate for Ca$^{2+}$ and natural scoria forms, while K$^+$ and NH$_4^+$ exhibited the lowest adsorption rates. Similar results for scoria were reported by Kwon *et al.* (2010), who studied the adsorption kinetics of divalent cation (Pb$^{2+}$) and trivalent cation (As$^{3+}$) using natural

scoria. After applying the pseudo-second order model, the authors found that the adsorption rate for the trivalent cation was three-fold the adsorption observed for divalent cation. Kwon *et al.* (2005) finding come to an agreement with the results obtained for the adsorption rates of $Na^+$, since enhanced material with divalent ions exhibited higher rates than scoria treated with monovalent cations. Nonetheless, the pseudo-second order model estimated a higher adsorption capacity for scoria treated with monovalent cations ($K^+$) than material treated with divalent cations ($Ca^{2+}$) for the removal of $Na^+$.

The experimental data allowed to determine that more than one mechanism influenced the adsorption process, where the first line segment of the uptake time course for each material can be associated with the surface diffusion that occurred on the macropores during the first minutes of adsorption (Figure 7.8). The second segment represented the intra-particle diffusion that took place within the mesopores on structure of the material. The bulk adsorption occurred as results of the surface diffusion and adsorption sites located on the macropore structure of the material.
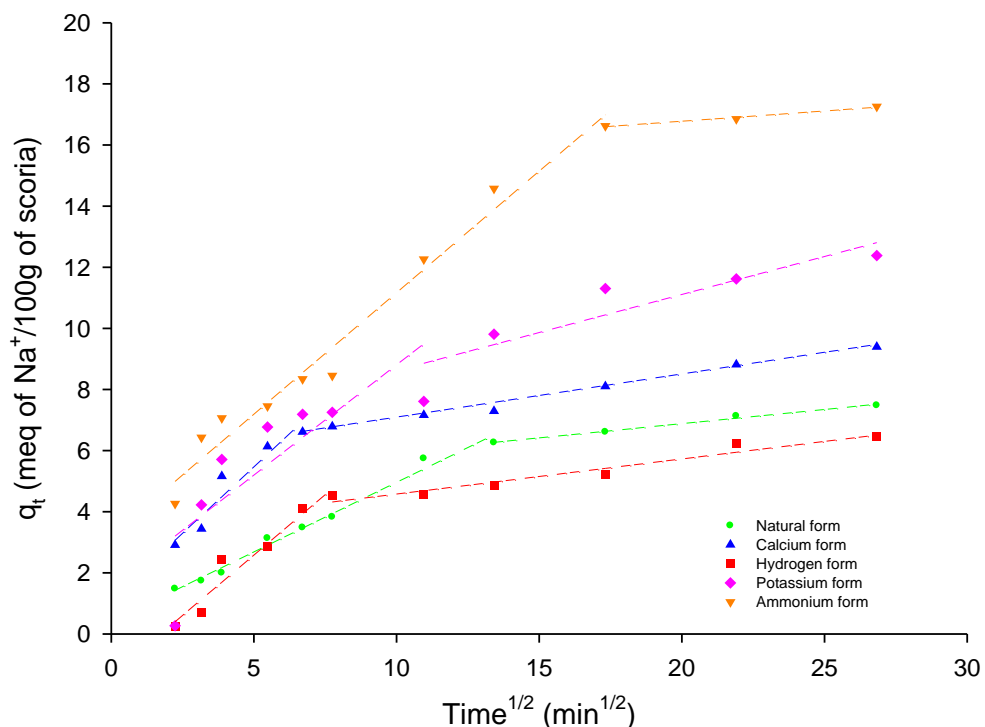


**Figure 7.8 Intra-particle diffusion model for the adsorption of $Na^+$ ions using natural and treated scoria.**

**Table 7.9 Intra-particle diffusion model, film and pore diffusion values for the adsorption of Na⁺ using natural and treated scoria material.**

| Scoria Form | Intra-particle diffusion | | | Film diffusion | Pore diffusion |
|---|---|---|---|---|---|
| | $k_i$ meq/100g*min$^{1/2}$ | $C$ meq/100g | $R^2$ | $D_f$ (cm²/s) | $D_p$ (cm²/s) |
| Natural | 0.455 | 0.40 | 0.98 | $2.28 \times 10^{-6}$ | $9.50 \times 10^{-6}$ |
| Ca²⁺ | 0.868 | 1.12 | 0.92 | $2.87 \times 10^{-6}$ | $9.50 \times 10^{-6}$ |
| H⁺ | 0.789 | 1.36 | 0.94 | $1.97 \times 10^{-6}$ | $9.50 \times 10^{-6}$ |
| K⁺ | 0.721 | 1.58 | 0.64 | $3.78 \times 10^{-6}$ | $9.50 \times 10^{-6}$ |
| NH₄⁺ | 0.795 | 3.21 | 0.97 | $3.16 \times 10^{-6}$ | $5.70 \times 10^{-6}$ |

Values for film diffusion were found to be in the range of 1.97 - 3.78x10⁻⁶ $cm^2/s$, while the values calculated for pore diffusion coefficient were in the range of 5.7 - 9.50x10⁻⁶ $cm^2/s$. These results indicated the diffusion process for all the types of scoria was governed by the film diffusion supporting the results obtained from the intra-particle diffusion model. Diffusion coefficients calculated for natural scoria suggested that diffusion process was rate-limited by the film diffusion indicating the influence of this type of diffusion on the adsorption of Na⁺.

The Na⁺ removal and adsorption performance of natural and treated scoria can be explained through the selectivity of ions and their features (Table 7.7). Scoria treated with NH₄⁺ and K⁺ had a significant improvement on the Na⁺ adsorption capacity because the cations on the scoria had smaller hydrated radii and reduced hydration energy, while scoria treated with a large cation and high energy of hydration, such as Ca²⁺, presented a lower adsorption capacity to transfer cations from the solid phase to the aqueous solution.

### Effect of co-ion on the adsorption process for the removal of Na⁺ ions

CSG water from the Bowen Basin research site showed a geochemical signature of Na⁺-Cl⁻-HCO₃⁻ but often CSG waters contain different anions at varied concentrations that may be different from the CSG water characterised in this study. Some of the typical anions in CSG waters are Cl⁻, HCO₃⁻ and F⁻ but often Cl⁻ and HCO₃⁻ are found in higher concentrations than F⁻ (Taulis & Milke, 2007; Van Voast, 2003). Additionally, it has been reported that the adsorption of cations may be affected by the presence of certain anions and studies keep focused on the adsorption behaviour of

heavy metals with different anions (Darton *et al.*, 2004; Doula & Ioannou, 2003; Fernandez *et al.*, 1994; Inglezakis *et al.*, 2003; Inglezakis *et al.*, 2005; Rendueles *et al.*, 1997). The adsorption kinetics of $Na^+$ for zeolite and scoria material in a natural form were studied using single solutions containing $Cl^-$, $HCO_3^-$ and $F^-$ ions all made at 0.1 M.

The zeolite $Na^+$ adsorption curve (Figure 7.9) demonstrated that higher adsorption was achieved for solutions made with $HCO_3^-$ and $F^-$, while adsorption of $Na^+$ was lower when the anion $Cl^-$ was present. The capacity to remove $Na^+$ ions when Cl- was present after 4320 min was 19.9 meq/100 g, while the capacity exhibited for the same cation with $HCO_3^-$ as anion was 27.4 meq/100 g that represents a 30% increment from the solution containing $Cl^-$. The adsorption capacity of $Na^+$ in presence of co-ions followed the order $HCO_3^- > F^- > Cl^-$ (Figure 7.9).
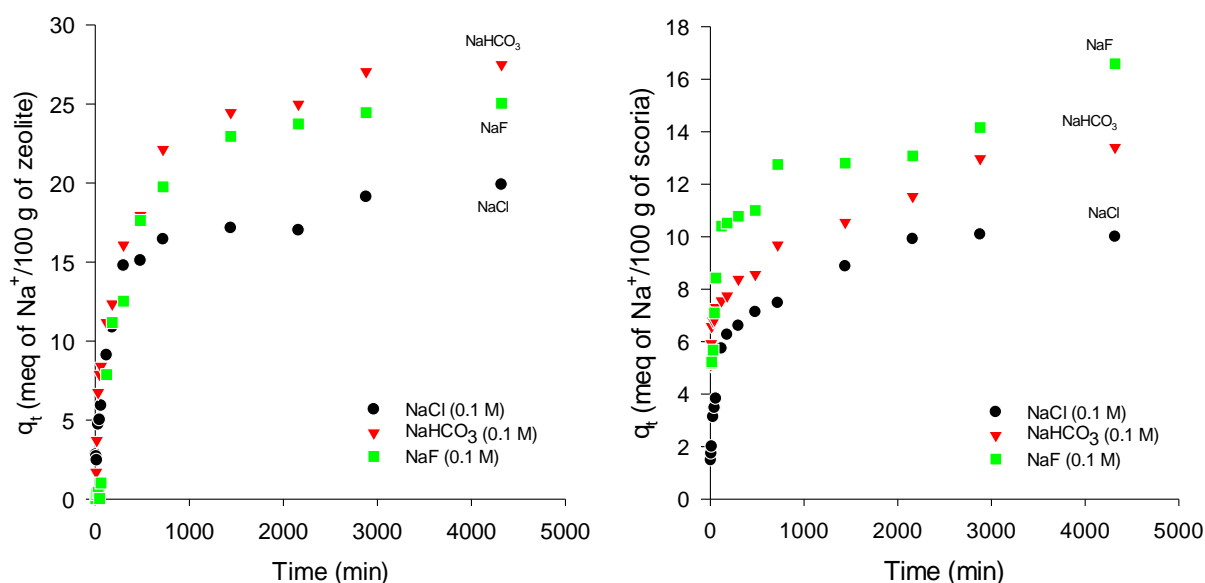


**Figure 7.9 The adsorption kinetic behaviour of $Na^+$ in presence of different anions using natural zeolite and scoria. Initial solution concentration 0.1 M, shaking speed of 300 rpm, 25 °C and solid-liquid ratio 50 mg/L. Zeolite exhibited preference for $Na^+$ in presence of $HCO_3^-$, while scoria presented higher $Na^+$ adsorption when $F^-$ was in the solution. Each data point is a mean of two replicates, which did not vary by more than 5%.**

The $Na^+$ ion solutions had the same initial concentration of 100 meq/L, similar ionic strength ranging from 0.094 to 0.097 but varied in pH. The pH for the solution made with NaCl was neutral with values about 7.0, while solutions made with $NaHCO_3$ and

NaF presented an alkaline pH above 8.0. The solution pH is expected to effect on the adsorption behaviour of metals onto zeolite materials (Ates & Hardacre, 2012; Babcock & Schulz, 1963; Inglezakis *et al.*, 2001c; Kithome *et al.*, 1999). These studies have shown that adsorption of metals decreased for low pH solutions because $H^+$ ions compete with the metals that also adsorbed. Additionally, electrostatic repulsion happens when the surface of the material is protonated, decreasing selectivity towards metal cations. Therefore, the results obtained for the $Na^+$ adsorption capacity can be explained through the difference in the pH variability of the solution, where the $Na^+$-$Cl^-$ solutions had a lower pH and presented lower selectivity than the other solutions investigated.

The adsorption rates for $Na^+$ using the natural scoria material were lowest when $Cl^-$ ions were present (with removal of 10 meq/100 g), while higher adsorption rates were observed for the solution containing $F^-$ ions (removal of 16.5 meq/100 g after 4320 min) (Figure 7.9). The presence of a different anion increased the removal of $Na^+$ ions by 60% over that observed with the anion $Cl^-$. The greater adsorption of $Na^+$ ions in the presence of $F^-$ and $HCO_3^-$ can be attributed to the alkaline composition of the solution, limiting the associated competing ion process of adsorption of $H^+$ ions over $Na^+$. Comparable behaviour was observed by Alemayehu and Lennartz (2009); Kwon *et al.* (2005); Kwon *et al.* (2010) when scoria material in its natural form was used to remove heavy metals and higher pH solutions presented higher adsorption and removal rates than those solution with lower pH. The optimal performance for the adsorption of heavy metals occurred when pH solutions were greater than 8.0, which is in agreement with the results presented for scoria in natural form (Figure 7.9).

## Adsorption kinetics of $Na^+$ ions from synthetic and field CSG water using natural and treated materials

The treatments $K^+$ and $NH_4^+$ were selected due to their high performance observed on removal of $Na^+$ using single ion solutions. The average concentration of $Na^+$ measured for the synthetic CSG was about 50 meq/L, while the average concentration of $Na^+$ in the field CSG water was 130 meq/L, which is 2.6 times higher than the average of the same CSG field.

The Na$^+$ adsorption behaviour and performance of zeolite and scoria, both natural and treated modes, using synthetic CSG water exhibited analogous trend as single Na$^+$ solutions, where materials treated with NH$_4^+$ exhibited the largest Na$^+$ capacities, while natural forms achieved the lowest capacities (Figure 7.10). The maximum capacity achieved for zeolite and scoria enhanced with NH$_4^+$ was 38.5 and 11.8 meq/100 g, respectively (Table 7.10). The Na$^+$ adsorption capacities found for both materials in all forms using synthetic CSG water were significant lower to those found for single Na$^+$ solutions. For instance, natural forms of zeolite and scoria achieved a maximum Na$^+$ adsorption of about 16.1 and 7.4 meq/100 g for single Na$^+$ cation solution, while the same materials using synthetic CSG adsorbed 5.8 and 3.9 meq/100 g of Na$^+$, correspondingly (Table 7.10). A 50% reduction in the Na$^+$ adsorption from synthetic CSG water was noted, caused by the competing effect of other cations present in solution that occupied the adsorption sites on the material reducing the Na$^+$ adsorption efficiency.
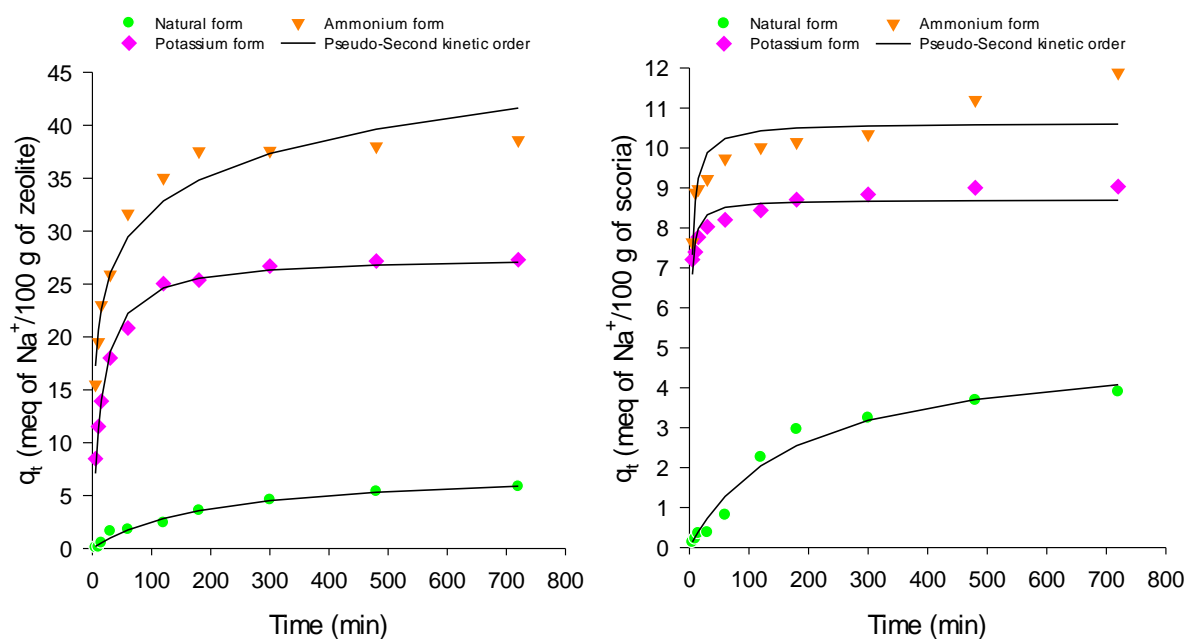


**Figure 7.10 The Na$^+$ adsorption kinetics and pseudo-second kinetic order curves for natural and enhanced zeolite and scoria using synthetic CSG water. Batch mode agitated at 300 rpm, 25 °C and a solid-liquid ratio 50 mg/L. Each data point is a mean of two replicates, which did not vary by more than 5%.**

The reduction of Na$^+$ from synthetic CSG water using different forms of zeolite and scoria were favourable when the adsorption is compared to the natural forms. The Na$^+$

reduction reached 36.4% and 11.9% of the initial $Na^+$ concentration for $NH_4^+$ enhanced zeolite and scoria, while natural zeolite and scoria removed 5.9% and 4.1% of the initial concentration, respectively. The model that best fits the experimental data was the pseudo-second order (calculated kinetic curves in Figure 7.10). $Na^+$ adsorption rates from synthetic CSG using treated forms of material were larger than adsorption rates exhibited for natural scoria and zeolite (Table 7.10). The adsorption capacity calculated using the pseudo-second order model showed an improvement in on $Na^+$ adsorption when treated materials were used.

**Table 7.10 Comparison adsorption kinetic constants for zeolite and scoria materials using synthetic CSG water.**

| Material | Exp. | Pseudo-first order | | | Pseudo-second order | | | Elovich Equation | | |
|---|---|---|---|---|---|---|---|---|---|---|
| | $q_e$ (meq/100g) | $q_e$ (meq/100g) | $k_1$ (min$^{-1}$) | SSE | $q_e$ (meq/100g) | $k_2$ (meq/100g*min) | SSE | $a$ (meq/100g*min) | $b$ (meq/100g) | SSE |
| Zeolite Natural | 5.84 | 5.87 | 0.005 | 0.88 | 7.49 | 0.0006 | 0.80 | 0.81 | 0.14 | 1.43 |
| Zeolite $K^+$ | 27.30 | 25.66 | 0.049 | 5.71 | 27.60 | 0.0025 | 2.19 | 9.08 | 0.24 | 4.44 |
| Zeolite $NH_4^+$ | 38.59 | 36.06 | 0.068 | 9.43 | 30.17 | 0.0080 | 7.79 | 33.15 | 0.20 | 5.80 |
| Scoria Natural | 3.90 | 3.95 | 0.006 | 0.62 | 5.09 | 0.0010 | 0.76 | 1.14 | 0.09 | 1.34 |
| Scoria $K^+$ | 9.03 | 8.45 | 0.332 | 1.47 | 8.70 | 0.0838 | 0.84 | - | - | - |
| Scoria $NH_4^+$ | 11.89 | 10.23 | 0.237 | 2.54 | 10.62 | 0.0417 | 1.81 | - | - | - |

Similarly, scoria and zeolite, in natural and treated forms, were used for the adsorption of $Na^+$ from field CSG water (Figure 7.11). The average concentration of $Na^+$ in the field CSG water was larger than the synthetic CSG water, which may lead towards an apparent higher adsorption capacity of the material at equilibrium. This effect can be related to the equilibrium behaviour of both materials in which a larger concentration led to higher adsorption of cations.

Treated $NH_4^+$ scoria and zeolite exhibited a larger $Na^+$ adsorption than materials in natural form for field CSG water. The adsorption achieved for $NH_4^+$ treated materials was 71.5 and 16.4 meq/100 g for zeolite and scoria, while the same materials in natural form reached a maximum $Na^+$ adsorption of 17.5 and 13.6 meq/100 g, respectively (Figure 7.11). The adsorption of $Na^+$ from field CSG water using zeolite and scoria in $NH_4^+$ achieved an increment of 54 meq/100 g (four times higher than natural zeolite material) and 2.8 meq/100 g (20% increase of the adsorption for natural scoria),

respectively. The Na$^+$ adsorption capacities when using CSG water were consistently higher than those observed for synthetic CSG water.
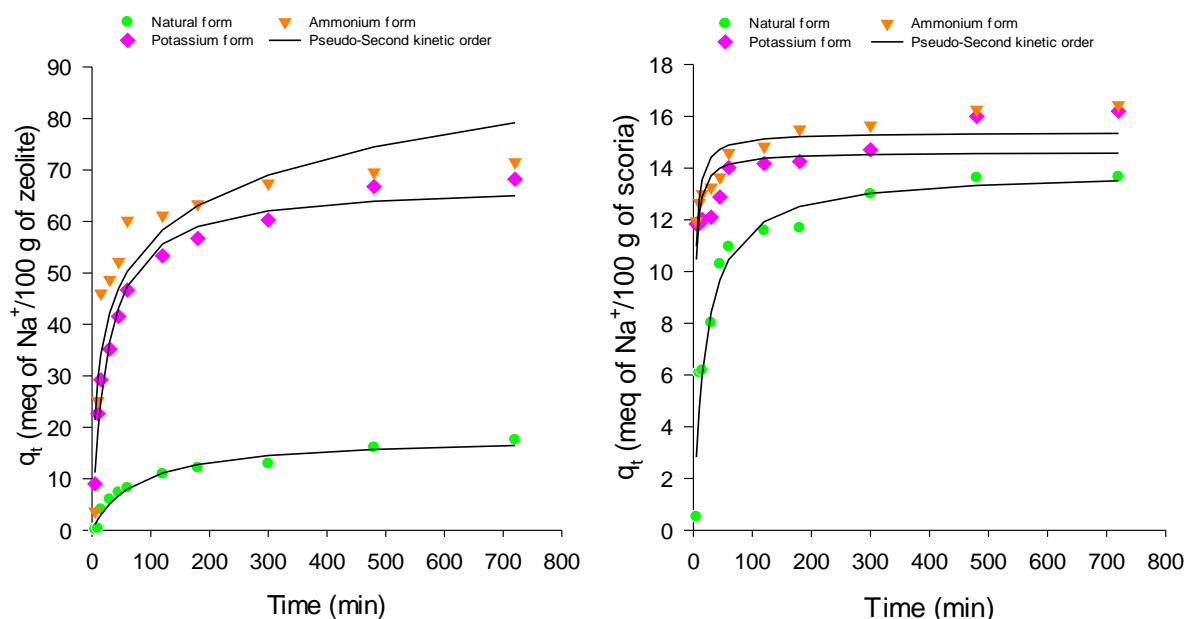


**Figure 7.11 The Na$^+$ adsorption kinetics and pseudo-second kinetic order curves for natural and enhanced zeolite and scoria using field CSG water. Batch mode agitated at 300 rpm, 25 °C and a solid-liquid ratio 50 mg/L. Each data point is a mean of two replicates, which did not vary by more than 5%.**

**Table 7.11 Comparison adsorption kinetic constants for zeolite and scoria materials using field CSG water.**

| Material | Exp. | Pseudo-first order | | | Pseudo-second order | | | Elovich Equation | | |
|---|---|---|---|---|---|---|---|---|---|---|
| | $q_e$ (meq/100g) | $q_e$ (meq/100g) | $k_1$ (min$^{-1}$) | SSE | $q_e$ (meq/100g) | $k_2$ (meq/100g*min) | SSE | $a$ (meq/100g*min) | $b$ (meq/100g) | SSE |
| Zeolite Natural | 17.57 | 15.43 | 0.0118 | 4.46 | 18.69 | 0.0007 | 3.27 | 0.60 | 0.28 | 2.22 |
| Zeolite K$^+$ | 68.23 | 60.99 | 0.0306 | 16.37 | 67.27 | 0.0005 | 8.42 | 8.052 | 0.08 | 8.37 |
| Zeolite NH$_4^+$ | 71.53 | 65.83 | 0.0030 | 19.37 | 51.80 | 0.0030 | 5.91 | 14.70 | 0.08 | 27.11 |
| Scoria Natural | 13.66 | 12.66 | 0.0387 | 3.45 | 13.87 | 0.0036 | 2.99 | 2.07 | 0.42 | 4.27 |
| Scoria K$^+$ | 16.20 | 13.98 | 0.3045 | 4.54 | 14.62 | 0.0344 | 3.39 | 42.18 | 0.42 | 4.27 |
| Scoria NH$_4^+$ | 16.44 | 14.77 | 0.2750 | 3.79 | 15.38 | 0.0324 | 2.50 | - | - | |

The adsorption kinetic model that better described the Na$^+$ adsorption using field CSG in terms of the SSE was the pseudo-second order kinetic (Table 7.11, Figure 7.11). The adsorption rate ($k_2$) for treated materials was improved when compared with adsorption rates for natural forms. Furthermore, it was noticed that Na$^+$ adsorption

capacity using scoria and zeolite and field CSG water were consistently higher than those observed for synthetic CSG water due to the large $Na^+$ ions in solution.

### Adsorption of $Na^+$ ions from single solution and desorption of ions by regeneration using chemical treatments

Once equilibrium is reached after the adsorption process, the regeneration of the material is necessary to enable the recovery of the initial sorbent properties of the material for further use. The regeneration process of natural materials is a key step in order to make the ion exchange an economical process. Regeneration employs the adsorption and desorption mechanisms by often using a single solution that displaces the ion loaded onto the material. The performance of the regeneration is determined by the cyclical ability of desorption and adsorption of ions, which indicate the reversibility of the adsorption process and reusability of the material.

The adsorption process consisted of the $Na^+$ uptake by treated zeolite and scoria until equilibrium is reached, approximately after 720 min. The adsorption of $Na^+$ ions was conducted over five regeneration cycles (Figure 7.12). The adsorption column labelled as "Cycle 0" corresponds to the adsorption achieved by the material in pre-treated form, and the subsequent adsorption columns correspond to the $Na^+$ removed after a regeneration cycle of the material.

The regeneration process consisted in placing the exhausted material with the regenerate solution for 24 h, allowing the desorption of $Na^+$ ions and adsorption of cations introduced by the regenerate solution. The treatment and regenerate solutions were made at 1.0 M containing $CaCl_2$, $KCl$ and $NH_4C_2H_3O_2$. The desorbed cations obtained after 24 h of regeneration were totalised and values are shown in the desorbed column, next to the $Na^+$ adsorption column. The performance of the regeneration process was measured by the ability to remove adsorbed cations and the ability to uptake $Na^+$ for subsequent loading cycles.
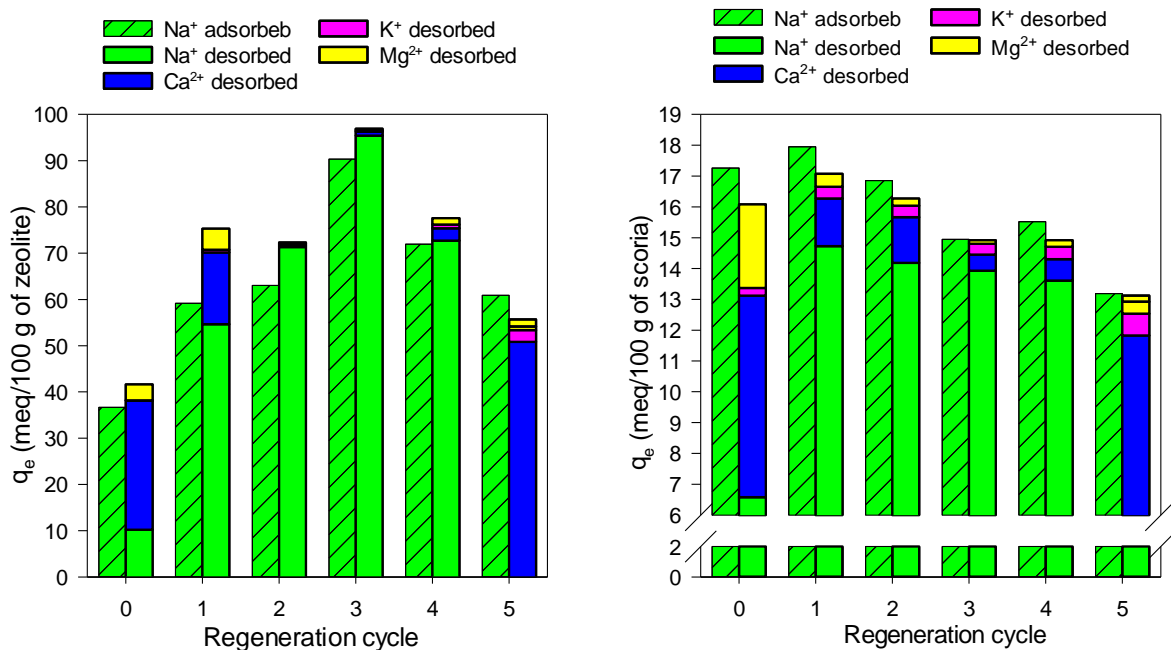
**Figure 7.12 Adsorption and desorption capacity of $Na^+$ for successive regeneration cycles for zeolite and scoria using $NH_4^+$ regenerate. Each data point is a mean of two replicates, which did not vary by more than 5%.**

The regenerate solution with the highest adsorption and desorption capacity of $Na^+$ ions for both, zeolite and scoria material, was $NH_4^+$ followed by the $K^+$ as shown in Figures 7.12 – 7.13. The $Na^+$ adsorption capacity achieved for zeolite after each regeneration cycle increased form 36.6 meq/100 g for the Cycle 0, up to 90.3 meq/100 g on the 3rd cycle (Figure 7.12). However, the capacity of the zeolite started to decrease after the peak on the $Na^+$ adsorption capacity. The increment on the adsorption capacity after the regeneration Cycle 2 can be explained by the ability of the regenerate solution to further displace exchangeable cations from the material, while the reduction on the $Na^+$ adsorption for cycles 4 and 5 can be attributed to pore clogging that leads to an irreversible desorption of cations. With the continued and steady reduction of the adsorption and desorption capacity of the material, the lifespan of the material could be calculated. The decline in the $Na^+$ adsorption will deplete the adsorption capacity of the material within the first 25 regeneration cycles, which is a longer lifespan than estimated by Katsou *et al.* (2011), who determined that clinoptilolite had an acceptable adsorption efficiency for $Pb^{2+}$ and $Zn^{2+}$ until the 12th regeneration cycle when regenerated with KCl.

Similar behaviour was observed for the desorbed cations from the zeolite regenerated with $NH_4^+$, where similar amounts of $Na^+$ were desorbed as well as significant amounts of $Ca^{2+}$ and $Mg^{2+}$ for the Cycle 0 and 1. The large amount of the desorbed cations, in Cycle 0, for zeolite and scoria (Figure 7.12) was not expected, since all materials were treated until near homoionic form was achieved. However, conversion process into homoionic form with $NH_4^+$ did not remove all the exchangeable cations during pre-treatment, with cations removed in subsequent regeneration cycles allowing the materials to increase the $Na^+$ adsorption in Cycle 1 (Figure 7.12).

The adsorption and desorption of $Na^+$ ions observed for scoria regenerated with $NH_4^+$ solutions decreased consistently as the number of cycles incremented (Figure 7.12). The maximum adsorption occurred after the first regeneration reaching 17.9 meq/100 g and slowly decreased to 13.1 meq/100 g in the fifth cycle, which corresponds to a 25% reduction in the adsorption capacity. The reduction on the $Na^+$ adsorption after each regeneration cycle can be associated to an irreversible exchange process, where cations from the regenerate solution cannot access the adsorption sites of the scoria, so reducing the effectiveness of the desorption process. Considering the decline on $Na^+$ adsorption of 25% every five regeneration cycles, it will take 20 cycles to deplete the adsorption capacity of the scoria material when using $NH_4^+$ as regenerate solution.
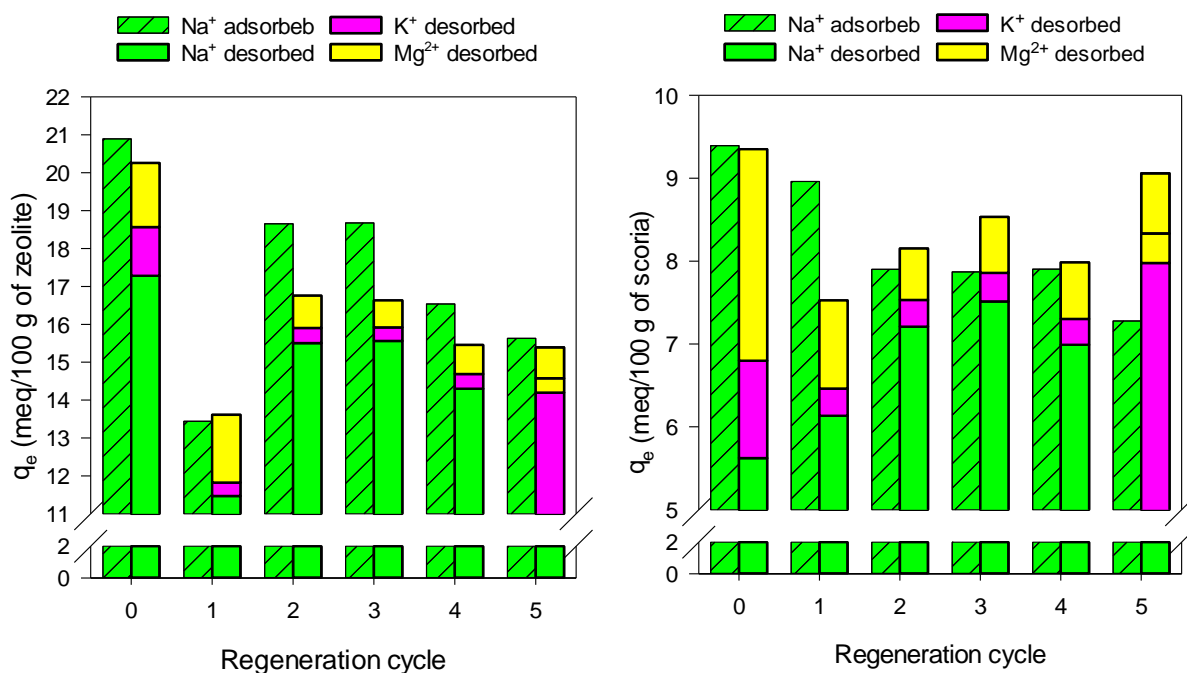


Chapter 7: Kinetic studies

The Ca$^{2+}$ treated/regenerated zeolite and scoria showed the lowest adsorption/desorption capacity for Na$^+$ ions (Figure 7.13). Despite the low adsorption ability for Na$^+$, regeneration with Ca$^{2+}$ was able to partially recover the adsorption capacity. Nonetheless, the adsorption capacity declined after each cycle by 24% and 22% after the fifth cycle regeneration for zeolite and scoria respectively. Thus the lifespan of both materials was 20 regeneration cycles when using Ca$^{2+}$ as a regenerate solution.
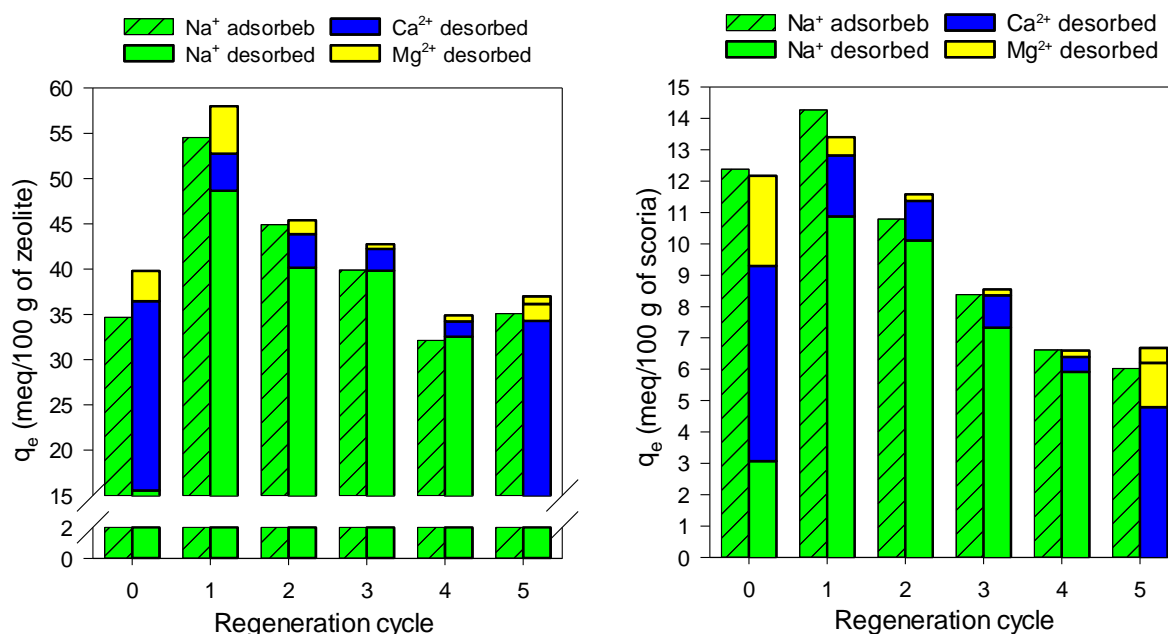


**Figure 7.14 Adsorption and desorption capacity of Na$^+$ for successive regeneration cycles for zeolite and scoria using K$^+$ regenerate. Each data point is a mean of two replicates, which did not vary by more than 5%.**

Materials regenerated with K$^+$ exhibited an initial improvement on the Na$^+$ adsorption for Cycle 1, which is then followed by rapid decline on the adsorption capacity (Figure 7.14). After the fifth regeneration cycle the zeolite and scoria diminished the Na$^+$ adsorption properties by 35% and 57%. The consistent declining trend on the Na$^+$ adsorption indicates that the K$^+$ regenerate solution was not able to remove cations, making the adsorption process to some extent irreversible. The K$^+$ regeneration

behaviour was expected to perform similar to the $NH_4^+$ regeneration, since both cations have similar hydrate radii and energy of hydration. Nonetheless, $K^+$ energy of hydration of $K^+$ is slightly larger than $NH_4^+$. The $Na^+$ adsorption capacity for scoria regenerated with $K^+$ will be depleted within the first 10 regeneration cycles, while the adsorption in zeolite will last for about 15 regeneration cycles. The $K^+$ regeneration increases the adsorption in early cycles comparable to $NH_4^+$ regeneration but depletion of the adsorptive properties of both materials will be reached faster than $Ca^{2+}$ regeneration.

The initial increment of the capacity, regeneration efficiency and adsorption capacity reduced with increased number of regeneration cycles agree with the results obtained by Argun (2008) and Katsou *et al.* (2011), where adsorption and desorption performance decreased considerably after each regeneration cycle. These authors also found that sorption properties decreased 50% from the initial regeneration after the third cycle for $Ni^{2+}$-$Na^+$ sorption, ninth cycle for $Pb^{2+}$-$K^+$ system, and fifth cycle of $Zn^{2+}$-$K^+$ sorption process.

### Adsorption of $Na^+$ ions from synthetic and field CSG water, and desorption of ions by regeneration using $NH_4^+$ solution

$Na^+$ adsorption and desorption using synthetic CSG water were studied using $NH_4^+$ regenerate solution to recover adsorptive properties of zeolite and scoria (Figure 7.15). The synthetic CSG water contained a mixture of ions that could diminish the total $Na^+$ adsorbed. Cations present in CSG water are in low concentrations but they are more selective than $Na^+$ ions.

The zeolite material regenerated with $NH_4^+$ presented a consistent adsorption capacity to $Na^+$ ions after each regeneration cycle with an average of 38 meq/100 g (Figure 7.15). The adsorption capacity towards $Na^+$ was constant even after a $5^{th}$ regeneration. Desorption of $Na^+$ ions after regeneration with NH4$^+$ solutions happened to be larger than the measured adsorption of $Na^+$ ions, demonstrating the additional desorption of exchangeable $Na^+$ ions present in the zeolite framework removed after several regeneration cycles. Desorption of $Ca^{2+}$, $K^+$, $Sr^{2+}$ and $Ba^{2+}$ was found to be relatively

equal after each regeneration cycle, providing evidence that these cations were effectively desorbed after regeneration (Figure 7.15).
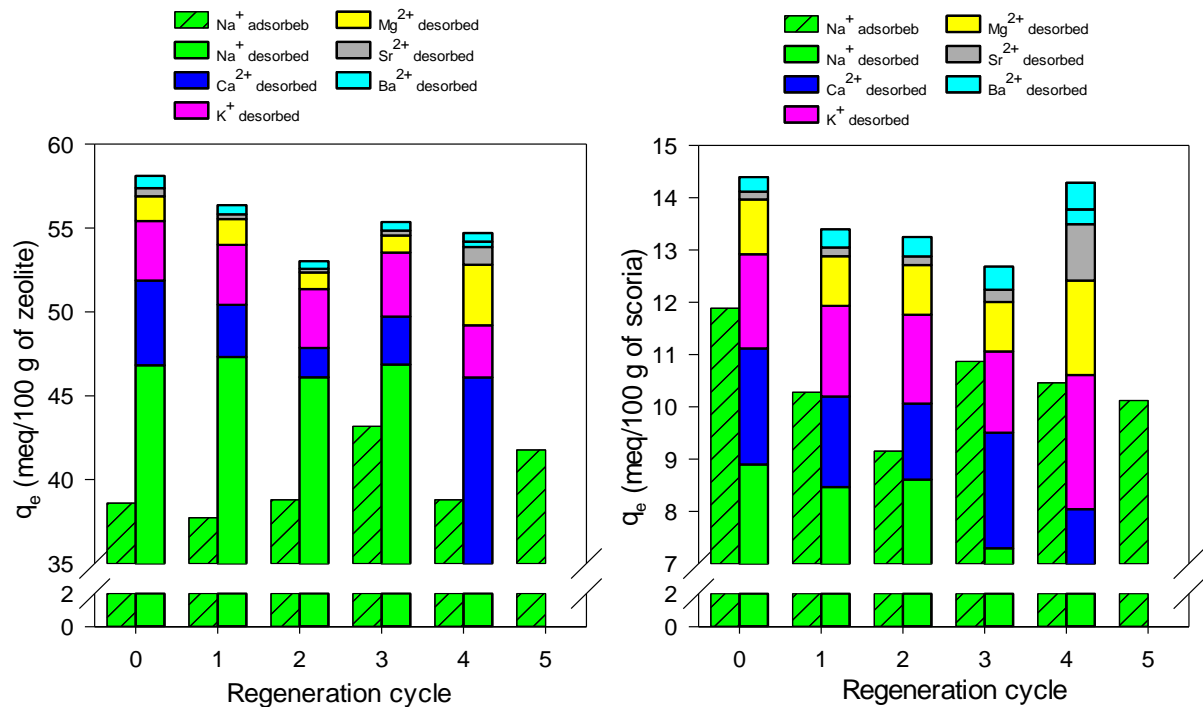


**Figure 7.15 Adsorption and desorption capacity of Na$^+$ for successive regeneration cycles for zeolite and scoria using synthetic CSG water and NH$_4$$^+$ regenerate solution. Each data point is a mean of two replicates, which did not vary by more than 5%.**

The Na$^+$ adsorption by scoria material using NH$_4$$^+$ regenerate solution resulted in a consistent adsorption pattern achieving on average 10 meq/100 g when synthetic CSG water was used (Figure 7.15). The mixture of cations in the synthetic solution, limited the Na$^+$ adsorption since cations in solution are more selective, diminishing ability of this material to adsorb Na$^+$ ions. Moreover, it was noticeable that the ability to adsorb Na$^+$ ions decreased with the number of regeneration cycles, reducing the capacity by 14% at the end of the fifth cycle.

Field CSG water was used to determine Na$^+$ adsorption, and desorption using NH$_4$$^+$ regenerate solution on zeolite and scoria materials (Figure 7.16). After each NH$_4$$^+$ regeneration cycle both materials showed consistent desorption and adsorption of Na$^+$.

The adsorption of Na$^+$ ions by zeolite regenerated with NH$_4$$^+$ presented consistent values above 40 meq/100 g for all regeneration cycles. The competing effect of cations

present in the field CSG water could limit the $Na^+$ adsorption. The adsorption of $Ca^{2+}$, $K^+$, $Sr^{2+}$ and $Ba^{2+}$ cations was evident since these cations were consistently desorbed through regeneration process. The recovery of the adsorption properties after 5 regeneration cycles was product of the effective desorption of $Na^+$ ions by $NH_4^+$ regenerate solution that allow the recovery of the material adsorptive properties. The adsorption decreases about 10% after each regeneration cycle, therefore the zeolite material will remove $Na^+$ from field CSG water for 30 regeneration cycles.



**Figure 7.16 Adsorption and desorption capacity of $Na^+$ for successive regeneration cycles for zeolite and scoria using field CSG water and $NH_4^+$ regenerate solution. Each data point is a mean of two replicates, which did not vary by more than 5%.**

The scoria material achieved an average $Na^+$ adsorption of 21 meq/100 g, with all the adsorption cycles above 15 meq/100 g (Figure 7.16). The results obtained for the $Na^+$ adsorption using field CSG water were higher than those adsorption values observed for synthetic solution. The larger $Na^+$ adsorption when using field CSG water was the product of a larger initial concentration of $Na^+$ ions that increased the concentration driving force of the system and augmented the adsorption capacity of the material. The $Na^+$ desorption capacity of scoria regenerated with $NH_4^+$ was comparable to the adsorption of $Na^+$, with a slight reduction after each regeneration cycle. It is then

expected that the adsorptive properties of the material would last for 20 regeneration cycles.

## Conclusions

Ion uptake rate and extent was influenced by particle size, initial ion concentration, solution pH, and presence of competing ions. Treatment and regeneration solutions were able to increase the adsorption behaviour of zeolite and scoria materials by replacement of cation on the CEC of the material with ions more exchangeable than those ions present in the material natural state. Adsorption of $Na^+$ ions was favoured by the use of small fraction sizes of zeolite and scoria particles, due to a larger surface area per volume of material that increased the accessibility of cation to those available exchange sites.

Scoria and zeolite were more selective for $Sr^{2+}$ and $Ba^{2+}$ than $Na^+$, which were removed > 90%. The ion selectivity can be explained by the properties of the cations in terms of their valence, electrostatic attraction, ion size, hydration energy and hydrated radii, which make $Sr^{2+}$ and $Ba^{2+}$ more selective than $Na^+$. Anions in solution also had a significant effect on the adsorption of $Na^+$ on the zeolite and scoria materials, associated with effect on solution pH. Solutions with pH greater than 8 presented higher adsorption of $Na^+$.

Treatment of zeolite and scoria with $NH_4^+$ gave the greatest increase in $Na^+$ adsorption, followed by treatment with $K^+$. These treatments increased the adsorption rates and total adsorption capacity. The adsorption process in zeolite was limited by pore diffusion, while scoria exhibited a film diffusion process, a description in agreement with the porous structure of both materials. These chemical treatments enhanced the adsorption because introduced cations have smaller hydrated radii and lower hydration energies that enabled higher cation interaction increasing the $Na^+$ capacity. Both natural exchangers behave similarly when removing $Na^+$ from synthetic $Na^+$ and field CSG water solutions. Moreover, treated natural exchangers showed significant improvement on the adsorption of $Na^+$ for CSG water solutions.

The adsorption and desorption of $Na^+$ ions were studied for five regeneration cycles. Both materials decreased their adsorptive properties as the number of regeneration cycles increased. Regeneration studies using field CSG water and $NH_4^+$ regenerate solution determined that zeolite and scoria will deplete their adsorptive with no reversible desorption properties after the 30 and 20 regeneration cycles respectively. It was also observed the $Sr^{2+}$, $Ca^{2+}$, $K^+$ and $Ba^{2+}$ present in field CSG water compete with $Na^+$ for adsorption sites, reducing $Na^+$ removal of the zeolite and scoria.

# Chapter 8:  Column studies

## Breakthrough curves and the modelling of fixed bed columns

When the concentration of the contaminant in the solution exiting a flow through column exchanger rises to a maximum concentration tolerated in the effluent stream, the is said to be at breakpoint (Inglezakis & Zorpas, 2012a; Millar *et al.*, 2015a). When breakpoint is reached, regeneration process of the adsorbent bed is necessary. A 'breakthrough curve' (plot of effluent concentration over bed volumes of solution passed through the material) allows determination of the service time or effective bed volume (BV) of a column. Effective BV describes the maximum adsorption capacity exhibited of the system (Motsi, 2010).

When the influent and effluent concentrations in the column are equal, the adsorbent is at complete exhaustion. Adsorption capacity can be calculated with Eq. 8.1, where $m$ is the mass of adsorbent in grams; $C_0$ and $C$ are the influent and effluent concentrations expressed in meq/L at any given volume, $V$ (Millar *et al.*, 2015a).

$$Bed\ capacity = \frac{1}{m} \int_0^{V_0} (C_0 - C)\ dV \qquad\qquad \textbf{Equation 8.1}$$

Experimentally determined breakthrough curves can be described by mathematical empirical models that describe the dynamic behaviour of the fixed bed columns (Medvidović *et al.*, 2006). In this study, the empirical models (Table 8.1) developed by Thomas, Bohart-Adams and Yoon-Nelson were used to describe the Na$^+$ removal from aqueous solutions on a fixed bed of scoria and zeolite. Where $C_0$ is the initial solute concentration (meq/L), $C$ is the concentration of solute from the effluent, $k_{Th}$ is the Thomas rate constant (L/meq h), $Q$ is the flow rate (L/h), $m$ is the mass of adsorbent in the bed (g), $V$ is the volume of effluent (L), $k_{BA}$ is the Bohart-Adams rate constant (L/meq h), $q_{BA}$ is the removal capacity (meq/g), $H$ is the bed height (m), $v$ is the linear flow velocity (m/h), $t$ is the bed service time (h), $k_{YN}$ is the Yoon-Nelson constant (h$^{-1}$) and $\tau$ is the time when $C/C_0 \approx 0.5$ (h).

**Table 8.1 Mathematical relations of empirical models for determination of breakthrough curves.**

| Model | Non-linear equation | Linear equation | Model parameters |
|---|---|---|---|
| Thomas | $\dfrac{C}{C_0} = \dfrac{1}{1 + exp\left[\dfrac{k_{Th}}{Q}(q \cdot m - C_0 \cdot V)\right]}$ | $\ln\left(\dfrac{C_0}{C} - 1\right) = \dfrac{k_{Th} \cdot q \cdot m}{Q} - \dfrac{k_{Th} \cdot C_0 \cdot V}{Q}$ | $k_{Th}$ , $q$ |
| Bohart-Adams | $\dfrac{C}{C_0} = exp\left[(k_{BA} \cdot C_0 \cdot t) - (k_{BA} \cdot q_{BA} \cdot \dfrac{H}{v})\right]$ | $\ln\left(\dfrac{C}{C_0}\right) = k_{BA} \cdot C_0 \cdot t - k_{BA} \cdot q_{BA} \cdot \dfrac{H}{v}$ | $k_{BA}$ , $q_{BA}$ |
| Yoon-Nelson | $\dfrac{C}{C_0} = \dfrac{\exp(k_{YN} \cdot t - k_{YN} \cdot \tau)}{1 + \exp(k_{YN} \cdot t - k_{YN} \cdot \tau)}$ | $\ln\left(\dfrac{C}{C_0 - C}\right) = k_{YN} \cdot (t - \tau)$ | $k_{YN}$ , $\tau$ |

The Thomas model has been the preferred model for the determination of breakthrough curves from column studies using adsorbents (Millar *et al.*, 2015a). This model assumes that there is a negligible axial and radial dispersion in the column; adsorption is described by a pseudo-second reaction rate and Langmuir isotherm at equilibrium; constant properties of solid and solutions; isothermal and isobaric process; and diffusion resistance is negligible.

The Bohart-Adams model assumes that equilibrium is not constant, therefore the adsorption rate is proportional to the remaining adsorption capacity of the adsorbent. This model is mathematically equivalent to the Thomas model but they differ in the assumption of the isotherm type being rectangular for Bohart-Adams. Chu (2010) determined that Bohart-Adams model is a limiting form of the Thomas model, therefore they are not independent.

The Yoon-Nelson model assumes that the decrease in the probability of adsorbate to be adsorbed is proportional to the ability of its adsorption and breakthrough on the adsorbent (Xu *et al.*, 2013). This model is often used for single solute present in the influent solution (Millar *et al.*, 2015a).

The breakthrough experimental data was fitted with the models of Table 8.1 using a non-linear error function implemented in Microsoft Excel and using the Solver function.

## Results and Discussion

### Effect of flow rate in the removal of Na$^+$ from single ion solution using natural scoria and zeolite

The adsorption behaviour of Na$^+$ was studied for three volumetric flow rates (1, 5 and 10 BV/h) with an influent solution containing 100 meq/L of Na$^+$ in an up-flow mode that passed through fixed bed columns packed with natural forms of scoria and zeolite materials (Figure 8.1).
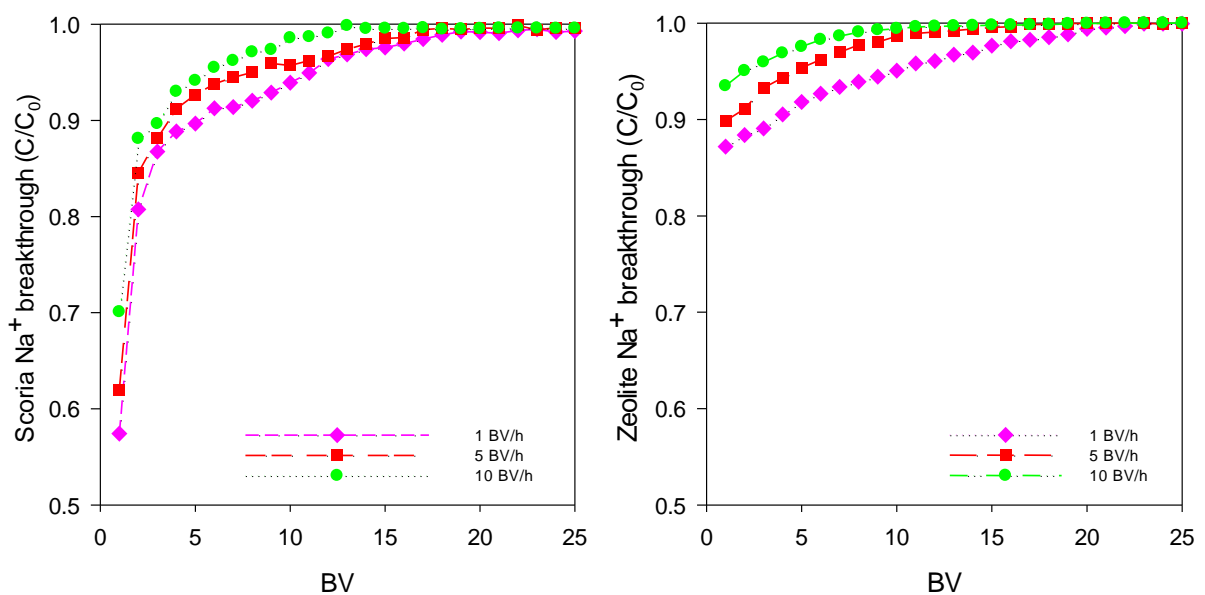


**Figure 8.1 Breakthrough curves for the effect of the flow rate (1, 5 and 10 BV/h) on the adsorption of Na$^+$ by natural scoria and zeolite. Scoria presented an initial rapid adsorption for all the flow rates. Each datum represents the average of two replicate measurements, which did vary by less than 5%.**

Na$^+$ removal (C/C$_0$) for natural scoria was greater than the removal achieved for zeolite material for the corresponding flow rate. The scoria material demonstrated steeper breakthrough curves than those observed for the zeolite, which indicates that a faster adsorption and equilibrium occurred along the column (Figure 8.1).

Increase in the volumetric flow rate caused a small reduction in the ability of the material to adsorb Na$^+$, directly affecting the total number of BVs achieved before complete exhaustion (Figure 8.1). Small flow rates (1 BV/h) achieved a larger number of BVs before exhaustion, while high flow rates (10 BV/h) exhibited a reduced BVs before reaching exhaustion, with this effect less marked for scoria, compared to

zeolite. A flow rate of 10 BV/h reduced by 4% and 6% the adsorption capacity exhibited at 1 BV/h when using scoria and zeolite, respectively. Although the adsorption of $Na^+$ was favoured when low flow rates were used, it was also determined that with an increment of the volumetric flow rate by 10x or 5x times, the $Na^+$ adsorption capacity was affected by a reduced fraction of the low flow rate. A flow rate of 5 BV/h reduced the adsorption of $Na^+$ by 2% and 4.5% of the adsorption observed at 1 BV/h when scoria and zeolite were used.

A low volumetric flow rate of 1 BV/h (Figure 8.1), results in higher contact time and increased capacity given the slow kinetics of the used sorbents (Stylianou *et al.*, 2007). Usually, increased contact time between the adsorbent and the solute is associated with higher adsorption of the solute, but often high flow rate increases the maximum adsorption capacity of the adsorbent, since there is a larger availability of solute along the packed bed to be adsorbed or exchanged (Can, 2004). In practice, the contact time between the adsorbent and solute is short, limiting the time for complete equilibrium which lowers the maximum adsorption capacity of the material when fixed bed columns are used (Helfferich, 1962).

The flow rate of 1 BV/h resulted in a beneficial adsorption capacity with an impractical retention time. The breakthrough curve for 10 BV/h showed a rapid exhaustion and with lower adsorption, when compared with the 1 BV/h curve. In contrast, the flow rate of 5 BV/h had a favourable adsorption capacity and a practical contact time for the removal of $Na^+$ ions for both of the materials. Inglezakis and Grigoropoulou (2004) used zeolite for the adsorption of $Cu^{2+}$, $Cr^{3+}$ and $Fe^{3+}$ and the practical and favourable flow rate was 5 BV/h. Therefore, a practical flow rate for the adsorption of $Na^+$ using scoria and zeolite in fixed bed columns is 5 BV/h.

Scoria and zeolite both reached complete exhaustion before 20 BVs for the range of flow rates tested. Similar studies were carried out by Inglezakis *et al.* (2001a) and Stylianou *et al.* (2007) who used columns packed with clinoptilolite for a range of flow rates from 1 to 45 BV/h, and determined that zeolite showed favourable adsorption for heavy metals at low flow rates (5 – 10 BV/h) due to slow adsorption rate of the material.

For natural scoria the maximum reduction after the first bed volume was approximately 30% of the initial influent concentration. The removal efficiency rapidly decreased with the number of bed volumes. For zeolite, the concentration of the inflow solution was lowered by 12% after the first bed volume, followed by a steady adsorption until exhaustion was reached after 20 BVs.

In other studies, $Pb^{2+}$, $Zn^{2+}$ and $Cu^{2+}$ solutions were passed through a clinoptilolite packed bed and breakpoint ($C/C_0$) of 0.1 (10% of the influent concentration) determined. Effective bed capacity for adsorption of $Pb^{2+}$ was achieved after 14 BV, while $Zn^{2+}$ and $Cu^{2+}$ adsorption achieved a breakpoint at less than 3 BV (Inglezakis *et al.*, 2001a; Stylianou *et al.*, 2007).

For this study, breakpoint for $Na^+$ in effluent of the scoria and zeolite packed beds was defined in terms of reduction of the sodicity (SAR < 12). This goal requires on average a reduction of 70% of the initial $Na^+$ concentration. Thus breakpoint was defined as a $Na^+$ $C/C_0 = 0.3$, with $Ca^{2+}$ and $Mg^{2+}$ adjustment. If $Ca^{2+}$ and $Mg^{2+}$ concentrations are not adjusted, the influent concentration of $Na^+$ needs to be reduced by 90% (Breakpoint $C/C_0 = 0.1$). The breakthrough curves of $Na^+$ removal for scoria and zeolite (Figure 8.1) exhibited a maximum removal after the first BV of 43% and 13% of the influent concentration respectively, which were lower than the removal required for the reduction of the sodicity.

### Removal of $Na^+$ from single ion solutions using scoria and zeolite in natural and treated form

Adsorbents or ion exchangers can be treated to increase the effective exchange capacity of the material (Chelishchev *et al.*, 1973). In practice, the treatment increases the presence of an introduced ion that is easily removed by the ion of interest (Semmens *et al.*, 1981; Semmens & Martin, 1988). The most common treatment for fixed bed columns is the washing of the packed bed with single ion solutions under specific operation conditions (Inglezakis *et al.*, 2001a). In this study, treatment of packed material in the column was performed with 4 BV (570 mL) of $NH_4CH_3CO_2$ or KCl solutions made at 1.0 M at constant 25 ˚C over 24 h in up-flow mode. The experimental breakthrough curves were determined using NaCl solutions at 0.1 M at a volumetric flow rate of 5 BV/h.

The treatment increased the number of BVs before the scoria material reached exhaustion and markedly improved the adsorption of $Na^+$ within the first 6 BV in comparison with material in the natural form (Figure 8.2). Scoria in $K^+$ and $NH_4^+$ forms reduced concentration observed for the same material in natural form by an additional 30% and 56% after the first BV. After 6 BV, the scoria breakthrough curve was similar for natural, $K^+$ and $NH_4^+$ treatments.
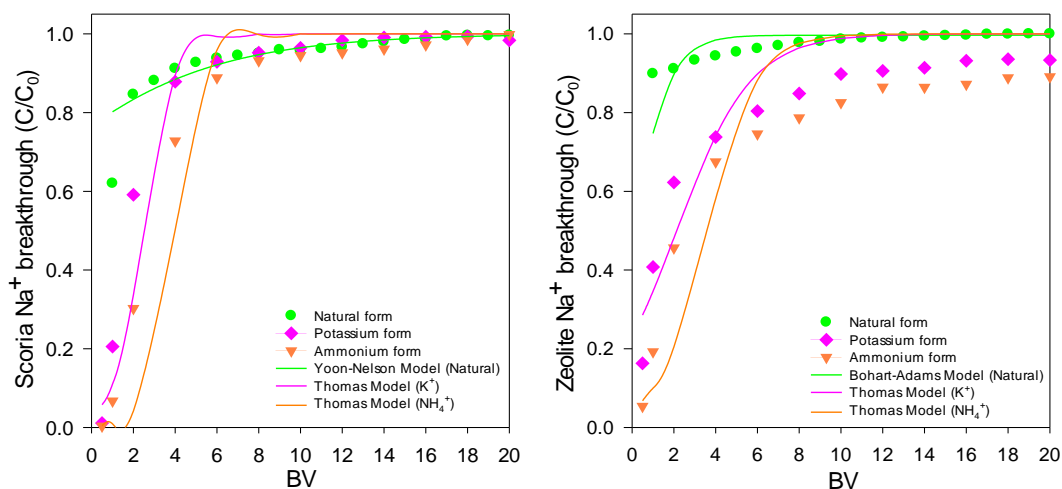


**Figure 8.2 Experimental and modelled breakthrough curves for the adsorption of $Na^+$ using scoria and zeolite in natural and enhanced forms. The continuous line is modelled behaviour. The results of the model with lowest SSE are displayed. Improved performance for $NH_4^+$ treated material relative to $K^+$ was also seen in the batch kinetic studies.**

**Table 8.2 Model parameters for the adsorption of $Na^+$ on scoria and zeolite for treated and enhanced materials**

| Model | Scoria | | | Zeolite | | |
|---|---|---|---|---|---|---|
| | Natural | $K^+$ | $NH_4^+$ | Natural | $K^+$ | $NH_4^+$ |
| $q_{c(exp)}$ (meq/100g) | 10 | 12 | 23 | 12 | 25 | 47 |
| **Thomas** | | | | | | |
| $k_{Th}$ (L/meq·h) | 0.052 | 0.014 | 0.016 | 0.038 | 0.006 | 0.009 |
| $q_c$ (meq/100g) | 8 | 10 | 21 | 10 | 19 | 40 |
| SSE | 0.07 | 0.08 | 0.13 | 0.05 | 0.1 | 0.24 |
| **Bohart-Adams** | | | | | | |
| $k_{AB}$ (L/meq·h) | $6.35 \times 10^{-4}$ | $9.17 \times 10^{-4}$ | $3.68 \times 10^{-4}$ | 0.002 | $9.8 \times 10^{-4}$ | $7.8 \times 10^{-4}$ |
| $q_{AB}$ (meq/L) | 1547.8 | 1548.4 | 1900.4 | 1853.1 | 1902.2 | 2479.2 |
| SSE | 0.06 | 0.94 | 1.77 | 0.08 | 0.4 | 0.71 |
| **Yoon-Nelson** | | | | | | |
| $k_{YN}$ (1/h) | 1.06 | 2.17 | 1.14 | 5.49 | 0.69 | 0.52 |
| $\tau$ (h) | 1.17 | $9.8 \times 10^{-5}$ | $3.48 \times 10^{-3}$ | $7.7 \times 10^{-4}$ | 0.83 | 0.96 |
| SSE | 0.03 | 0.47 | 0.62 | 0.3 | 0.33 | 0.6 |

Equilibrium and kinetic batch type experiments were in agreement with the dynamic adsorption in columns in terms of higher $Na^+$ adsorption was observed for treated materials, where treatment of scoria with single ion solutions effectively replaced naturally contained ions for those that were easily exchanged $K^+$ and $NH_4^+$ increasing the effective exchange capacity. With the Thomas model, the total adsorption observed for scoria was 8, 10, and 21 meq of $Na^+$/100 g in the natural, $K^+$ and $NH_4^+$ forms, respectively. The model that best fit the $Na^+$ breakthrough curve for the natural scoria was the Yoon-Nelson, while the treated material was better represented by the Thomas model (Table 8.2, Figure 8.2).

For zeolite, the breakthrough curves exhibited features analogous to those observed for the scoria material (Figure 8.2). Zeolite treated with $NH_4^+$ and $K^+$ demonstrated a larger reduction of the solute than the natural zeolite for the first 5 BVs. This was in agreement with the results obtained from batch type experiments where $NH_4^+$ enriched zeolite exhibited larger equilibrium and kinetic adsorption capacity for $Na^+$ than natural form of the same material from single ion or synthetic solutions. The model that better described the breakthrough curve for the natural zeolite was the Bohart-Adams model, which estimates an adsorption of 10 meq $Na^+$/100 g. For the treated zeolite, the Thomas model showed good fit, estimating a capacity of 40 and 19 meq $Na^+$/100 g for $NH_4^+$ and $K^+$ forms. However, treated material could exhibit greater capacity since exhaustion was not reached after 20 BV. The modelled breakthrough curves showed an early exhaustion across all the models used for both materials, scoria and zeolite, which may be related with the slow kinetics and the extended time that is required for the material to reached equilibrium. Similar observations were found by Han *et al.* (2009) who used treated zeolite for the adsorption of $Cu^{2+}$, and applied Thomas/Bohart-Adams models finding that calculated breakthrough curves presented early exhaustion.

Taulis and Milke (2009) tested the performance of natural and modified zeolite sourced from New Zealand for the adsorption of $Na^+$ from CSG water. Treated zeolite with $K^+$ exhibited a higher capacity (40.9 meq/100 g), while natural and $Ca^{2+}$ treated zeolite presented $Na^+$ adsorption capacities in the range of $11 - 20$ meq/100 g. The treatment methodology described by Taulis and Milke (2009) differed from the used in this study, since the treatment with KCl was performed with a large volume and the

influent solution was stopped once the material reached exhaustion, increasing the adsorption capacity of the material.

The total $Na^+$ adsorption estimate obtained from experimental and modelled breakthrough curves confirmed that treatment of scoria and zeolite increased the removal of $Na^+$, when compared with natural forms.

Increasing the concentration of the regenerate solution or extending the contact time could improve material conditioning prior to adsorption. However, the capacities achieved for $NH_4^+$ treated forms of scoria and zeolite correspond to a 62% and 30% of the measured REC. Thus improved material conditioning will not dramatically improve the column performance.

## The effect of co-existing ions in the removal of $Na^+$ from synthetic CSG solution using scoria and zeolite

A surrogate synthetic CSG water was created using a mixture of major and trace cations found in Bowen Basin site CSG water, containing $Na^+$, $K^+$, $Ca^{2+}$ $Mg^{2+}$, $Sr^{2+}$ and $Ba^{2+}$ (Table 4.1). Synthetic CSG solution was pumped through columns of natural and treated material at a flow rate of 5 BV/h for a total of 20 BV (Figure 8.3).
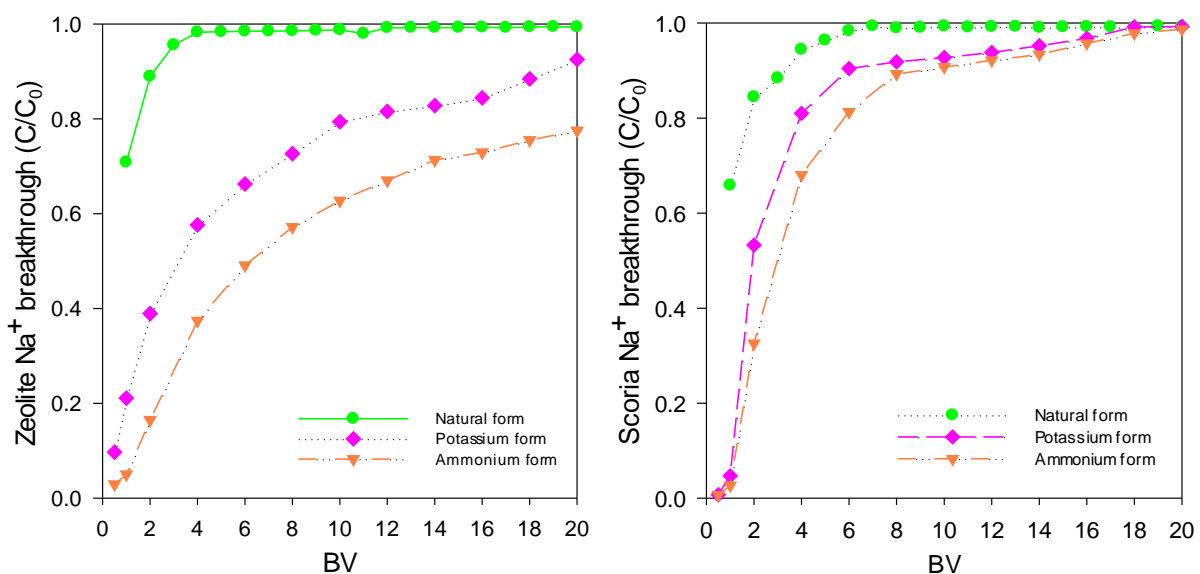


**Figure 8.3 Experimental and modelled breakthrough curves for the adsorption of $Na^+$ from synthetic CSG water using scoria and zeolite in natural and enhanced forms. Improved performance for $NH_4^+$ treated material.**

Zeolite in $NH_4^+$ form showed to have favourable adsorption towards $Na^+$, when competing cations were solution. Nonetheless, zeolite $Na^+$ adsorption capacity was reduced by the presence of other cations through competition for available exchange sites on the zeolite framework (Figure 8.3). The $Na^+$ adsorption capacity for natural material was reduced by 82% (1.8 meq/100 g) of the capacity observed when single $Na^+$ ion solutions were placed in contact with the same material. $NH_4^+$ and $K^+$ zeolite exhibited a $Na^+$ adsorption capacity of 47 and 28 meq/100 g, which were equivalent to the capacity observed when the material was placed in single $Na^+$ solutions. The capacity was calculated based on the adsorption occurred until 20 BV, but the treated materials did not reach complete exhaustion at that point, indicating that the total $Na^+$ adsorption may reach higher values (Figure 8.3).

The scoria breakthrough curves using synthetic CSG water (Figure 8.3) resembled the behaviour of the material when single $Na^+$ solutions were used, and material enhanced with $NH_4^+$ achieved a larger adsorption than material in natural state. Scoria enhanced with $K^+$ and $NH_4^+$ exhibited 9.8 and 13.3 meq/100 g, while natural material achieved 2.3 meq/100 g, reducing the $Na^+$ adsorption about 48%, when synthetic CSG water was used.
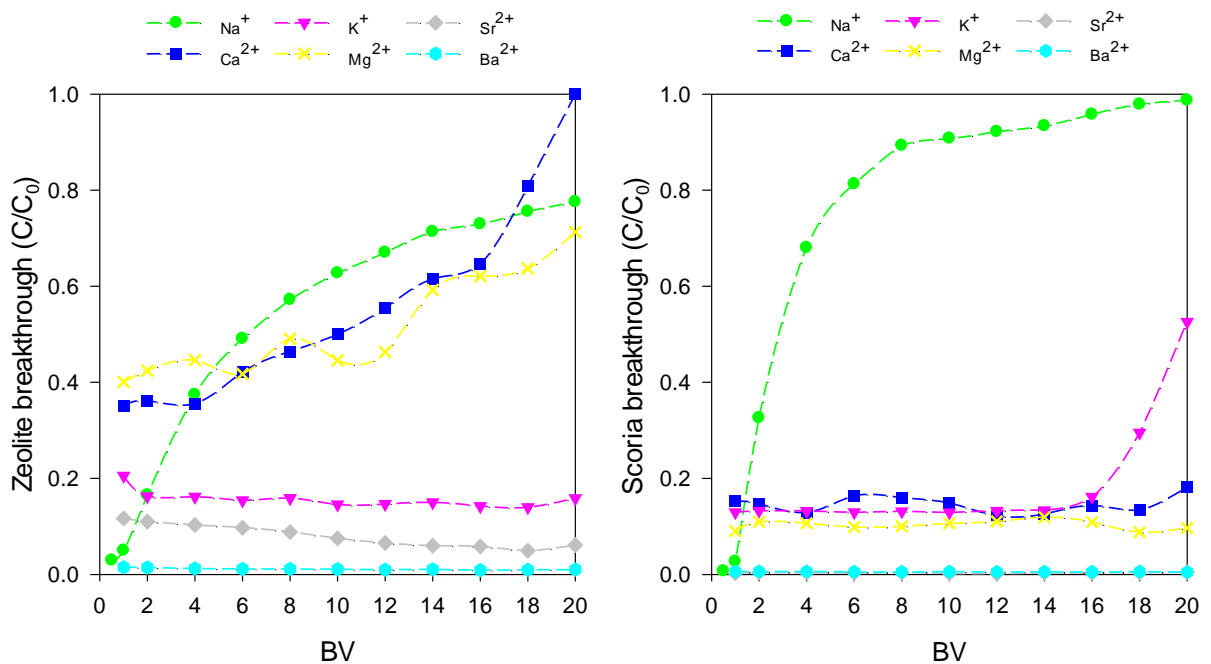


**Figure 8.4 Breakthrough curves of cations present in synthetic CSG water using zeolite and scoria enhanced with $NH_4^+$. Zeolite exhibited larger $Na^+$ adsorption than scoria but scoria reduced $Sr^{2+}$ and $Ba^{2+}$ concentrations more effectively than zeolite.**

The NH$_4^+$ zeolite exhibited preferences for the adsorption of some cations over other cations (Figure 8.4). Ba$^{2+}$, Sr$^{2+}$ and K$^+$ concentrations in the exit stream were reduced by more than 80% of the inlet concentration even after 20 BV, while Na$^+$ was reduced by only 23%. Treated zeolite showed a lower selectivity towards Mg$^{2+}$ and Ca$^{2+}$, with Ca$^{2+}$ the only cation that reached same concentration of the influent solution. This result is consistent with the batch type studies of Chapter 6, with higher selectivity of zeolite towards cations with low charge density, small hydrated radius, and low hydration energy, following the series K$^+$ >Ba$^{2+}$> Sr$^{2+}$ >> Ca$^{2+}$ > Na$^+$. Additionally, from batch type experiments it was determined that adsorption of Ca$^{2+}$ onto zeolite has a reversal behaviour, indicating that under certain conditions the cation could have no affinity and turn unselective as shown by releasing Ca$^{2+}$ after 17 BV (Figure 8.4). The findings from batch equilibrium experiments are in agreement with the selectivity and preference of cations observed for the packed zeolite column.

Scoria enhanced with NH$_4^+$ consistently removed all the Ba$^{2+}$ and Sr$^{2+}$ from the solution (Figure 8.4), and reduced Ca$^{2+}$ and Mg$^{2+}$ by 10% of influent concentration after 20 BV, and K$^+$ levels in the effluent increased only after 15 BV. The scoria showed a higher affinity for low density charge ions (divalent cations) over monovalent cations. The selectivity series determined for the scoria in batch type experiments follows Ba$^{2+}$ >Sr$^{2+}$ >> Ca$^{2+}$ > K$^+$ > Na$^+$, which is in agreement with the adsorption behaviour described by the breakthrough curves in Figure 8.4.

### Adsorption and desorption (regeneration) cycles for treated scoria and zeolite using single cation and synthetic CSG solutions

With repeated use and regeneration of scoria and in NH$_4^+$ form, adsorption curves for Na$^+$ in single solutions, and subsequent breakthrough curves for regenerated material started to shift towards the left of the Cycle 0 curve (pre-treated material) (Figure 8.5). This trend was not as pronounced for breakthrough curves for the adsorption of Na$^+$ from synthetic solutions (Figure 8.6). This indicates that there was a reduction of the effective adsorption of Na$^+$ as the number of regenerations increased while using single Na$^+$ solutions, causing the material to exhibit a reduced adsorption capacity after each regeneration cycle. The scoria in NH$_4^+$ form in contact with synthetic solutions showed constant Na$^+$ adsorption through the fourth cycles (Figure 8.6).
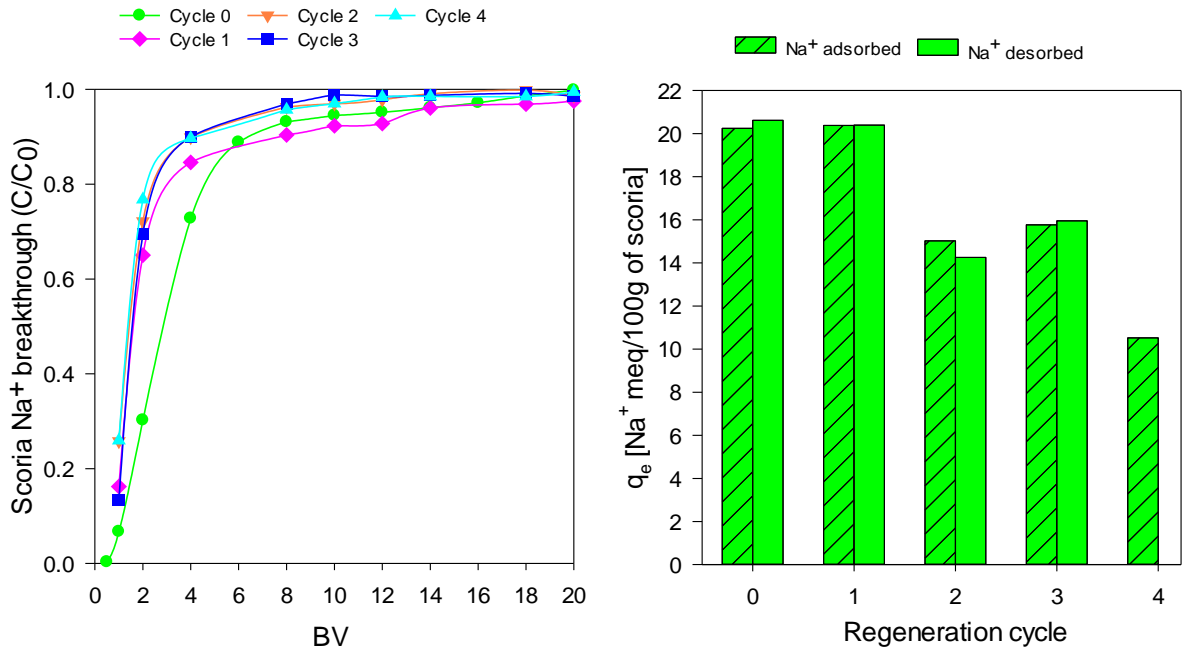
**Figure 8.5 Breakthrough curves for the adsorption of Na$^+$ from single cation solution by scoria. Total adsorption and desorption of Na$^+$ for multiple regeneration cycles with NH$_4^+$ solutions.**
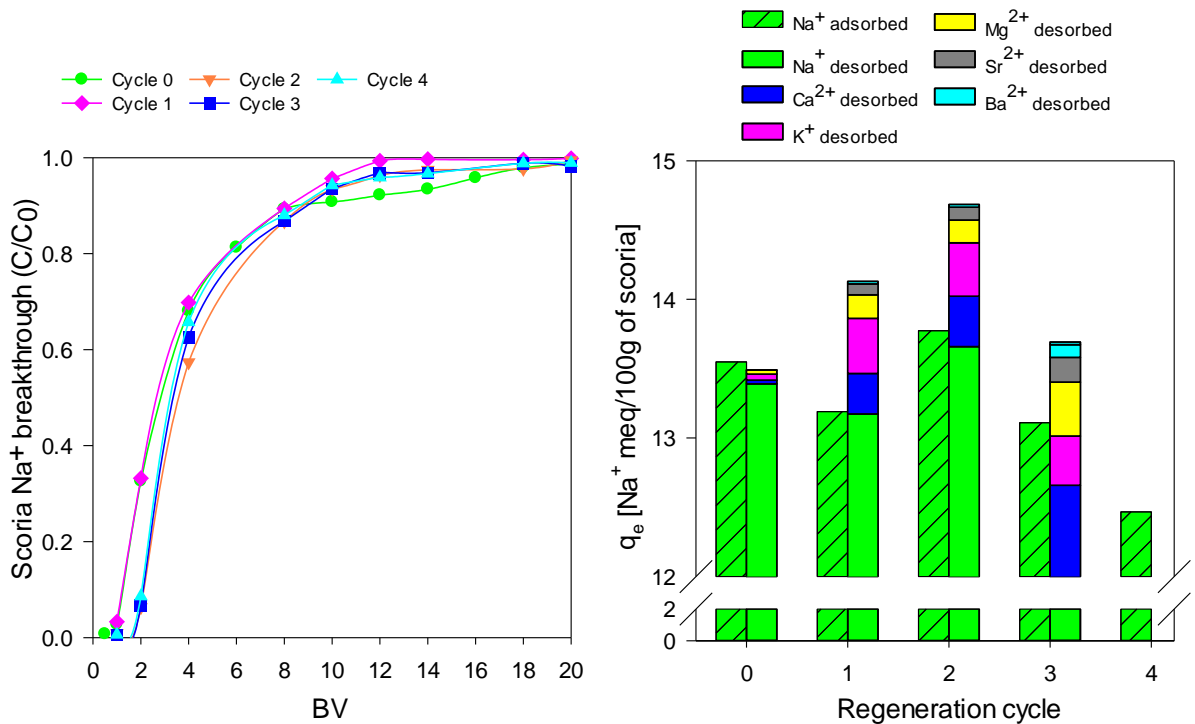


**Figure 8.6 Breakthrough curves for the adsorption of Na$^+$ from synthetic CSG water by scoria. Total adsorption and desorption of Na$^+$ for multiple regeneration cycles with NH$_4^+$ solutions.**

The initial Na$^+$ adsorption capacity (Cycle 0) for the scoria was 20 and 13.5 meq/100 g using single and synthetic solutions (Figures 8.5 and 8.6). Na$^+$ adsorption gradually

decreased after each regeneration cycle, achieving an adsorption of 11 meq/100 g after the fourth cycle, corresponding to a reduction of about 50% of the initial capacity (Figure 8.5). The amounts of $Na^+$ desorbed after each regeneration cycle was equivalent to the values achieved for the adsorption cycle. Adsorption and desorption decreased with the number of cycles.

The adsorption of $Na^+$ from the synthetic solution for scoria was consistent across regeneration cycles, with a reduction of 1.5 meq/100 g after the fourth cycle, which corresponds to a 11% decline of the initial capacity (Figure 8.6). When synthetic CSG solution was put through the scoria packed column, $Na^+$ adsorption was diminished by the presence of other cations that competed for the available adsorption sites. Scoria material showed a particular affinity towards divalent ions such as $Sr^{2+}$, $Ca^{2+}$ or $Mg^{2+}$ at the expense of adsorption of $Na^+$. Competing cations were adsorbed and consequently desorbed by regeneration (Figure 8.6). The desorption of competing ions was observed after each regeneration, except for Cycle 0 where small amounts were desorbed. These breakthrough curves and adsorption results are in agreement with the regeneration cycles performed in batch type using scoria and $Na^+$ solutions presented in Chapter 7, where adsorption decreased with the number of regeneration cycles.

Zeolite material treated with $NH_4^+$ (Cycle 0) exhibited a $Na^+$ adsorption reduction in the inflow concentration of 10% and 13% for single ion and synthetic solutions after 20 BV (Figures 8.7 and 8.8); which indicates that the zeolite material was not fully exhausted after 20 BVs.

Once zeolite was regenerated for the first time (Figures 8.7 and 8.8), the material exhibited a larger $Na^+$ adsorption than that observed in first instance for Cycle 0. For four regeneration cycles, the zeolite material recovered adsorptive capacity, and the additional adsorption can be observed on the shifting of the breakthrough curves towards the right of the previous curve. On the fourth cycle, the system started to exhibit equal adsorption as the curve determined immediately before (Cycle 3). In the fourth cycle, after 20 BV, the initial inflow concentration was reduced by 20 and 32% of the initial $Na^+$ inflow concentration from single cation and synthetic CSG solution.
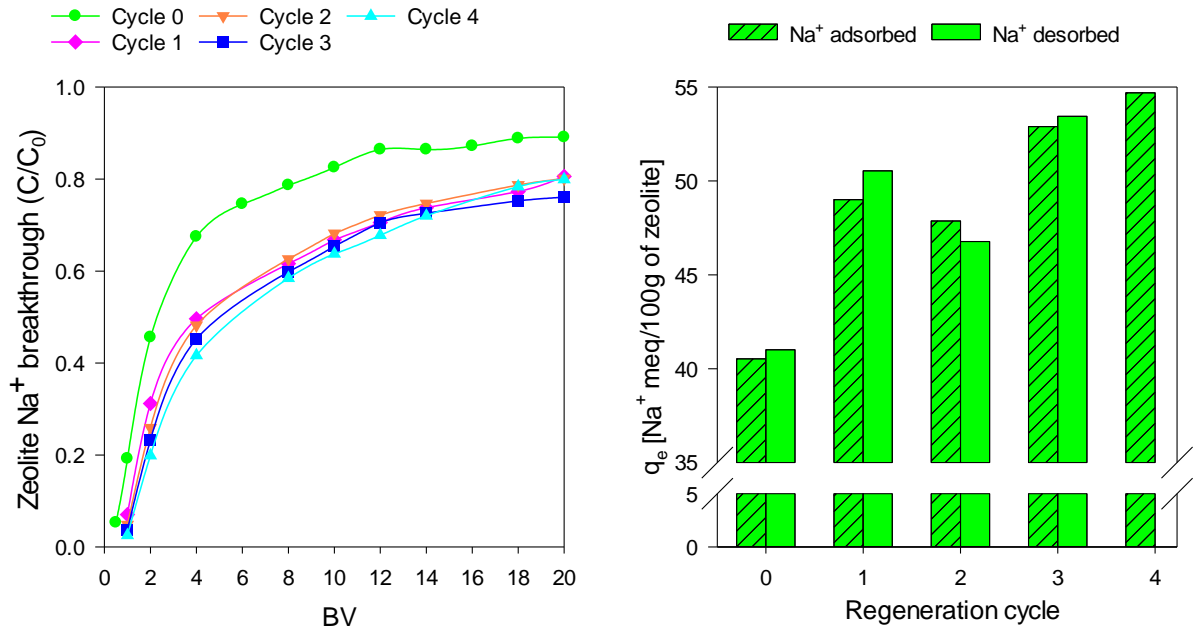
**Figure 8.7 Breakthrough curves for the adsorption of Na⁺ from single cation solution by zeolite. Total adsorption and desorption of Na⁺ for multiple regeneration cycles with NH₄⁺ solutions.**
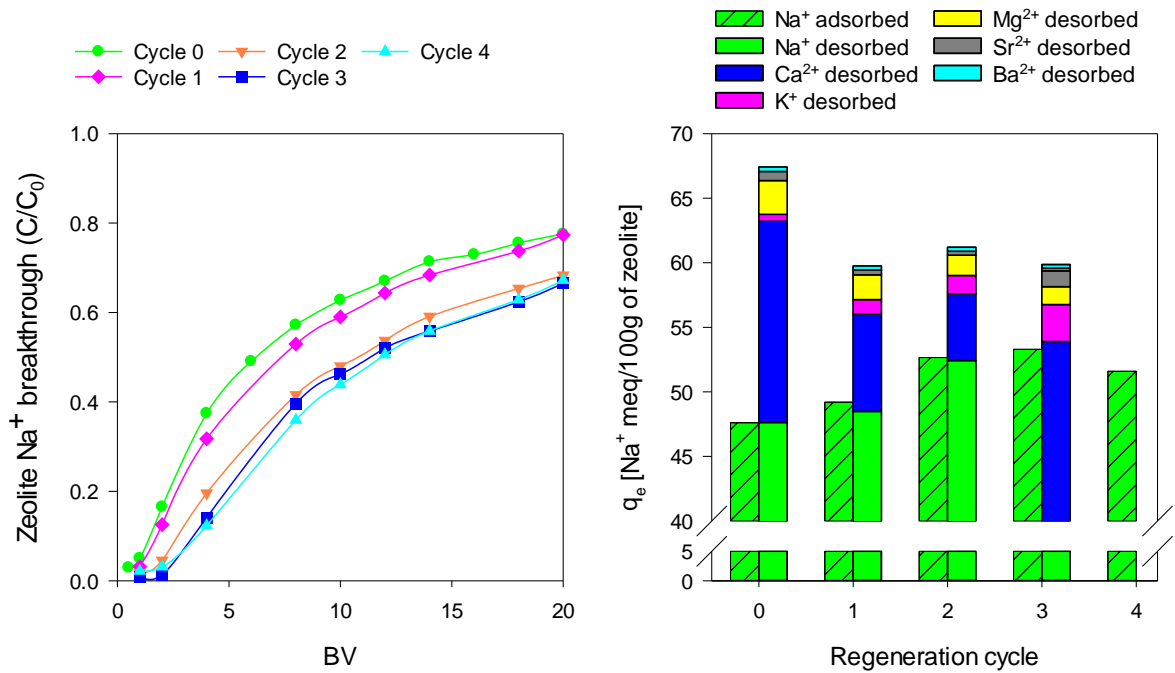


**Figure 8.8 Breakthrough curves for the adsorption of Na⁺ from synthetic CSG water by zeolite. Total adsorption and desorption of Na⁺ for multiple regeneration cycles with NH₄⁺ solutions.**

The Na⁺ adsorption for single cations solution increased after the first regeneration cycle by 9 meq/100 g (18% increment) (Figure 8.7). However, with further regeneration cycles, the adsorption on Cycle 4 reached 54.6 meq/100 g, which

corresponds to a 20% increment of the adsorption obtained in Cycle 0 for zeolite in contact with single $Na^+$ solutions. For zeolite in contact with synthetic CSG (Figure 8.8), it was observed that Cycle 0 showed an adsorption of 47.6 $Na^+$ meq/100 g, while subsequent cycles exhibited a larger adsorption, on average 10% higher than Cycle 0, reaching 52 $Na^+$ meq/100 g. The desorption values of $Na^+$ after regeneration (Figures 8.7 and 8.8), were in agreement with those values obtained for adsorption, so the regenerate solution effectively removes adsorbed ions and allowed successive adsorption cycles of $Na^+$ and co-existing cations contained in synthetic CSG water.

Regeneration cycles involved desorption of $Na^+$, $Ca^{2+}$, $Mg^{2+}$, $K^+$, $Ba^{2+,}$ $Sr^{2+}$ (in order of quantity), decreasing as the number of regeneration cycles increased (Figure 8.8). The additional desorption of $Ca^{2+}$ and $Mg^{2+}$ could be owing to incomplete transformation of the zeolite into a homoionic form during treatment, previous to the adsorption process in Cycle 0. Since, the complete homoionic form was not reached during treatment, $Ca^{2+}$ and $Mg^{2+}$ on the framework were removed after consecutive regenerations cycles by the introduced cation in the regenerate solution. The desorption of $Ca^{2+}$ and $Mg^{2+}$ from the zeolite allowed further adsorption of $Na^+$ or cations present in the synthetic solution for subsequent adsorption cycles as seen in Cycle 2 and 3, where 4 to 5 meq/100 g of $Na^+$ were additionally adsorbed (Figure 8.8).

### Scoria and zeolite packed fixed bed columns for the treatment of CSG from Bowen Basin site

The column studies undertaken with synthetic CSG water were repeated with field CSG water. The treated scoria exhibited a greater adsorption capacity towards $Na^+$ than the natural scoria form (Figure 8.9), with a larger number of BVs achieved for the same removal rate. $Na^+$ exhaustion was reached after the passage of 15 BV. The $NH_4^+$ treated scoria achieved the highest $Na^+$ adsorption with a capacity of 10.2 meq/100 g, while $K^+$ and natural form reached 96% and 39% of the adsorption exhibited by the scoria in $NH_4^+$ form. This indicates that interaction between incoming and outgoing cations during adsorption or ion exchange process was improved by the replacement of naturally contained ions for $NH_4^+$ cations by treatment on the scoria framework. Breakthrough curves determined for single $Na^+$ and synthetic CSG solutions using scoria material were found to be in agreement with the results obtained for actual CSG water.
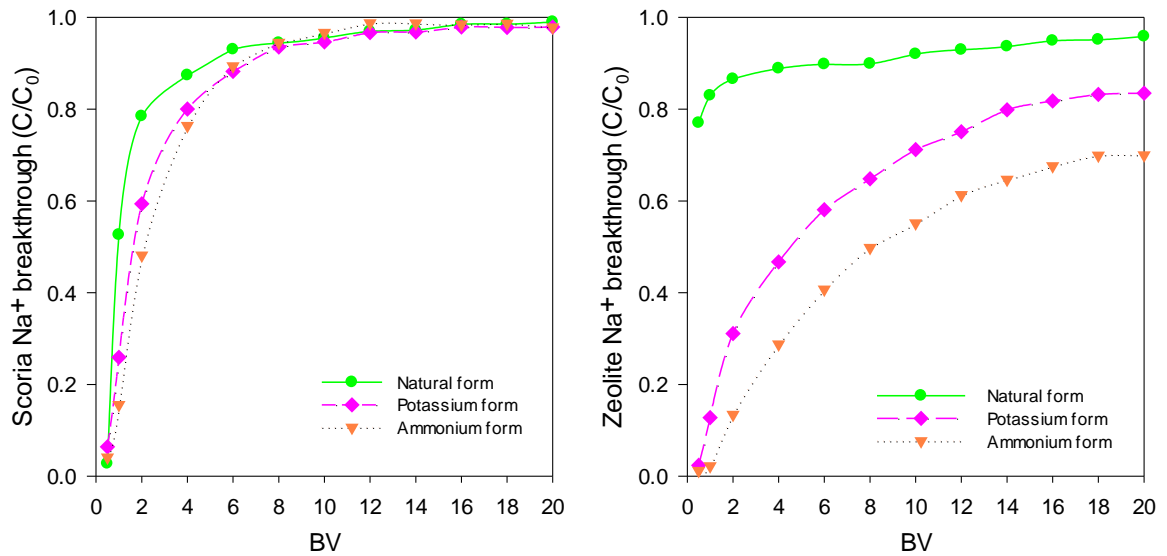
**Figure 8.9 Breakthrough curves for the adsorption of Na$^+$ from field CSG water using scoria and zeolite in natural and treated states.**

The zeolite material exhibited a larger adsorption of Na$^+$ from CSG water (Figure 8.9) when enhanced with NH$_4^+$, reducing the influent concentration after 20 BVs by 30% of the influent Na$^+$ concentration. NH$_4^+$ enriched zeolite achieved a Na$^+$ adsorption capacity of about 29.3 meq/100 g. After an equal number of BV, zeolite in natural and K$^+$ form effectively reduced Na$^+$ by 5% and 17% of the initial influent concentration, reaching a capacity of 10.1 and 19.7 Na$^+$ meq/100 g. However, in all cases more than 20 BVs were required to reach the exhaustion.
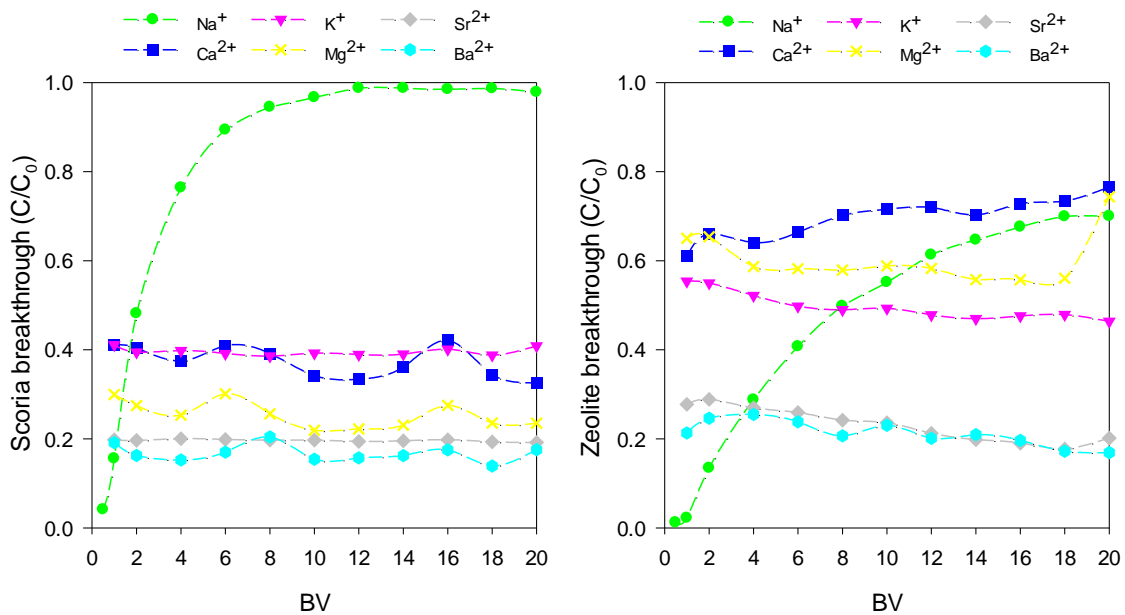


**Figure 8.10 Breakthrough curves of cations present in field CSG water using zeolite and scoria enhanced with NH$_4^+$.**

Scoria treated with $NH_4^+$ for the removal of $Na^+$ reached its maximum after the 15th BV (Figure 8.10). Competing ions such as $Ca^{2+}$ and $K^+$ reached an effective removal rate after 20 BV of about 60%, while cations such as $Ba^{2+}$ and $Sr^{2+}$ were removed by 80% of their initial influent concentration. This may be explained by the selectivity of the material towards divalent ions with lower energy of hydration, and the low initial concentration of those cations compared with other cations present in the solution such as $Ca^{2+}$ or $Na^+$.

Treatment of zeolite with $NH_4^+$ solutions enhanced the adsorption of $Na^+$ from CSG water by the replacement of naturally occurring ions for $NH_4^+$ that are more exchangeable due to the low hydration energy and hydrated radius. The breakthrough curves of co-existing ions in CSG water using zeolite material in $NH_4^+$ form, exhibited a particular behaviour during the adsorption cycle (Figure 8.10). The behaviour in reduction of the concentration for each cation in solution may be explained by the affinity and selectivity that the zeolite material exhibited over specific cations that exists in the CSG. The material exhibited high affinity for $Ba^{2+}$, $Sr^{2+}$ and $K^+$, reducing the initial concentration of these ions by more than 50% after 20 BV. Initial concentrations of $Ca^{2+}$ and $Mg^{2+}$ were reduced by 24%, which was comparable with the reduction observed for $Na^+$ after the 20th BV. The selectivity observed (Figure 8.10) was in accordance with affinity of the zeolite material towards those ions with low charge density, small hydrated radius and low energy of hydration, such as $K^+$ or $Ba^{2+}$.

The adsorption breakthrough curves and capacity of the scoria treated with $NH_4^+$ form showed a favourable adsorption and desorption of cations for several cycles (Figure 8.11). The breakthrough curves indicate that treatment and regeneration process removed adsorbed ions allowing the material to restore the adsorption properties for following adsorption cycles. On average, the $Na^+$ adsorption capacity of the scoria in $NH_4^+$ was about 10 meq/100 g. The regeneration process allowed the desorption of $Na^+$ which was about the same amount of $Na^+$ adsorbed per mass of material (Figure 8.11). Additionally, the regeneration process also desorbed cations that were removed during the adsorption cycle with CSG waters by a total of 3 meq/100 g. The desorption of cations from the scoria material by regeneration provided the favourable adsorption effect for consecutive adsorption for cations (Figure 8.11). Although scoria treated

with $NH_4^+$ increased the $Na^+$ adsorption capacity, the material exhibited only 53% of its REC, calculated in Chapter 5 for scoria as 28.4 meq/100 g. The reduced capacity can be related with the low selectivity of this material towards $Na^+$ ions.
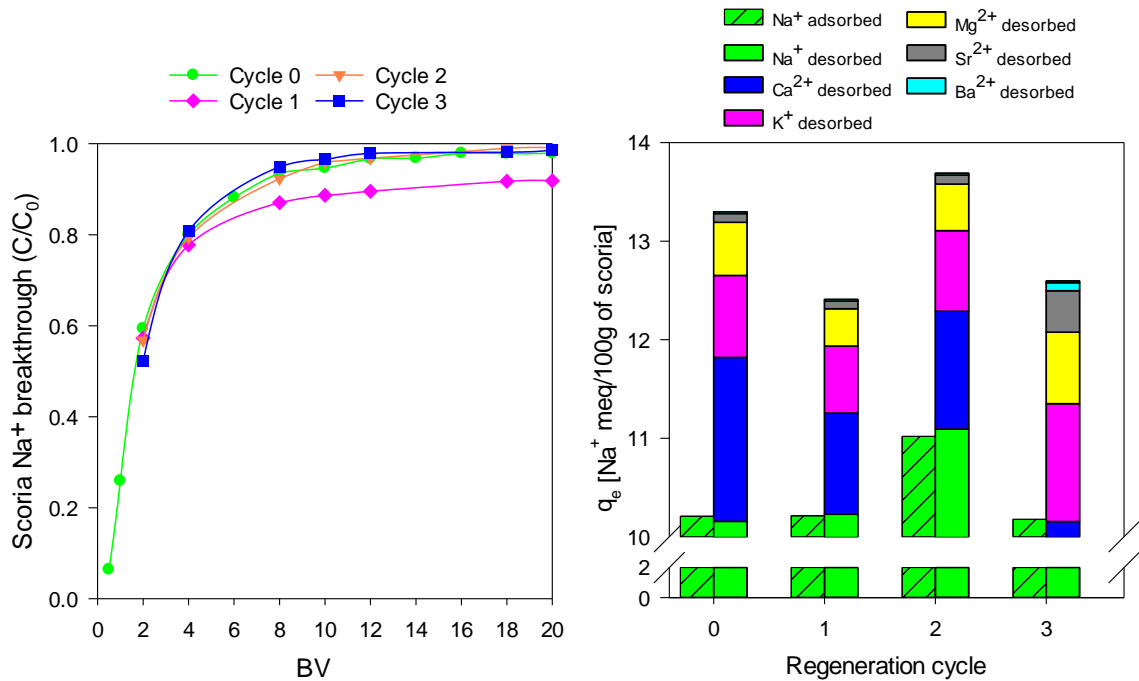


**Figure 8.11 Breakthrough curves for the adsorption of $Na^+$ from field CSG water by scoria. Total adsorption and desorption of $Na^+$ for multiple regeneration cycles with $NH_4^+$ solutions.**
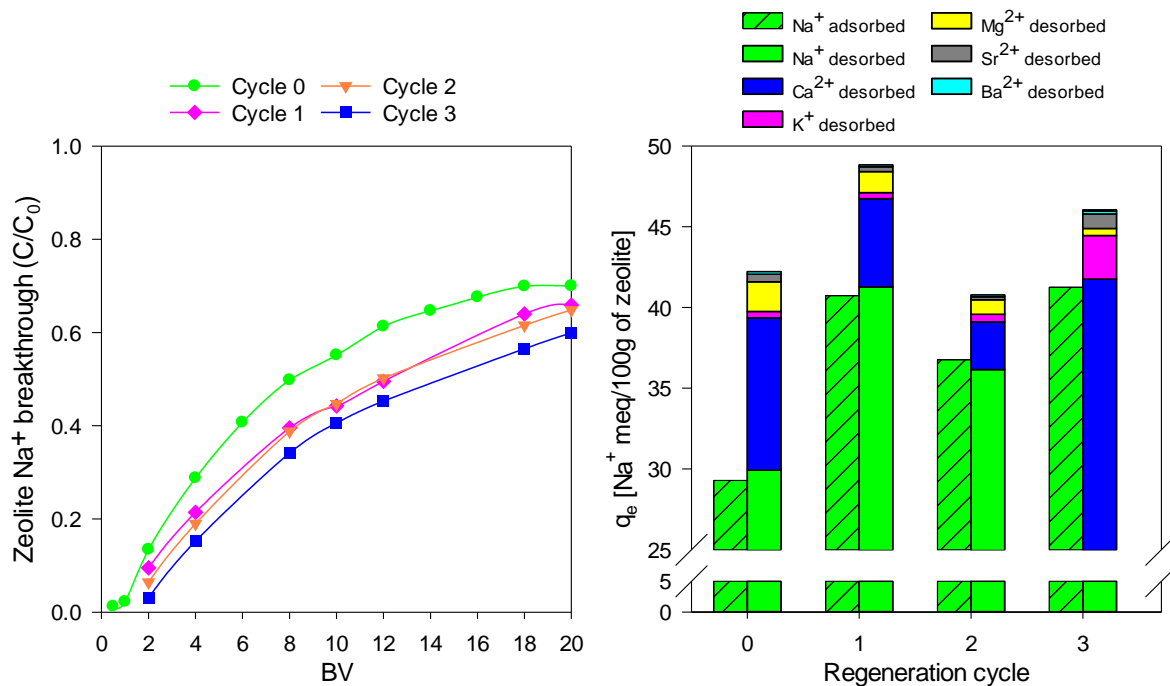


**Figure 8.12 Breakthrough curves for the adsorption of $Na^+$ from field CSG water by zeolite. Total adsorption and desorption of $Na^+$ for multiple regeneration cycles with $NH_4^+$ solutions.**

The repetitive adsorption of cations from CSG water, and regeneration using $NH_4^+$ solutions showed to have a favourable effect in overall performance of the material, since $Na^+$ was able to be adsorbed by the zeolite for several cycles (Figure 8.12). In fact, it was noticed that after the regeneration performed in Cycle 0, breakthrough curves slightly shifted to the right side of the Cycle 0 curve. This indicated that further reduction of the $Na^+$ concentration was achieved by the regenerated material achieving an additional 10% of the reduction observed for Cycle 0 after 20 BV. Since breakthrough curves showed additional reduction of $Na^+$, the adsorption of this ion also increased from 30 meq/100 g for Cycle 0 to an average of 40 meq/100 g for following cycles (Figure 8.12). The desorption values for $Na^+$ were equivalent to the adsorption values, removal of co-existing ions after regeneration was also achieved. From Cycle 0, it was evident that desorbed $Ca^{2+}$ and $Mg^{2+}$ correspond to cations that were not removed initially by the treatment and were desorbed by subsequent regeneration, providing additional adsorption of $Na^+$ in following cycles. The $Na^+$ adsorption capacity exhibited by $NH_4^+$ zeolite corresponds to 53% of the real exchange capacity. This may be explained by low selectivity for $Na^+$.

The recovery of the adsorption properties for both materials, scoria and zeolite, after several regenerations indicates the suitability of this material for the reduction of cations contained in CSG water, where cations such as $Ba^{2+}$ and $Sr^{2+}$ were removed effectively, while $Na^+$ ions were removed for few bed volumes only. The desorption of cations from scoria and zeolite material using $NH_4^+$ solutions was effective, allowing the removal of adsorbed cations and re-establishing the adsorption sites for subsequent cation removal from CSG water.

## Conclusions

The effect of flow rate on the removal of $Na^+$ by scoria and zeolite material was relatively small with the flow rates used in this study. The adsorption capacity of both materials at a flow rate of 5 BV/h was reduced by 3% of the adsorption obtained for 1 BV/h. This result showed that the adsorption of $Na^+$ was not directly affected by the increment of the flow rate, and was related to the slow adsorption kinetics. Other studies have recommended that flow rates for adsorption of metals using natural adsorbents are between 5 to 15 BV/h (Inglezakis *et al.*, 2001a).

Regeneration of scoria and zeolite columns with solutions containing $NH_4^+$ ions improved performance in terms of removal of $Na^+$ from CSG water. The adsorption of cations in CSG water exhibited a particular pattern that was related to selectivity and affinity that both materials, scoria and zeolite, have towards particular cations. Desorption of cations and multiple regeneration cycles proved that adsorption properties of both materials were recovered allowing multiple adsorption cycles for the removal of cations in CSG water.

The scoria and zeolite materials showed a high affinity towards $Sr^{2+}$ and $Ba^{2+}$, which were effectively removed from the solution for at least 20 BV. Other cations that presented moderate removal were $K^+$ and $Mg^{2+}$. Nonetheless, the adsorption capacity of both materials for the removal of $Na^+$ was limited due to the low selectivity of this cation, and on average $Na^+$ adsorbed was only 50% of the REC of the material.

# Chapter 9: Conclusions and Recommendations

In this thesis, a novel approach using natural ion exchange materials for the treatment of Coal Seam Gas (CSG) co-produced water has been studied. The CSG industry in the Australian context and the co-produced water main features were described in Chapter 2. The chemical characterisation of the CSG water from the research site (Bowen Basin) and the possible environmental impacts arising from disposal of the CSG water were described (Chapter 3). The use of zeolite and scoria materials for the removal of major and trace cations present in this described site CSG water; adsorption equilibrium and kinetic reactions were all assessed (Chapters 6 and 7). Finally, laboratory scales fixed bed columns were used to establish the dynamic adsorption of cations evaluating the practicality of both materials for the treatment of CSG co-produced water (Chapter 8).

This work is of high relevance to Australia and especially to the Central Queensland region, where currently three liquefied natural gas plants (LNG) at Curtis Island are operating, producing and exporting LNG sourced from the coal seam of the Surat and Bowen Basins. As a result of CSG extraction, a valuable by-product is produced as co-produced water that in an unprocessed state cannot be effectively re-used. This co-produced water is of particular importance to the Central Queensland region where farming and agricultural land management could be impacted by the quality and quantity of the extracted water when released to the surface. This project therefore has significant value to a number of stakeholders in Australia, demonstrating that this knowledge is unique, timely, novel and contributes to providing the stepping stones to a cheaper, cost effective strategy in managing CSG co-produced water for beneficial re-use. This research constitutes the foundations for the implementation of an on-site treatment methodology for CSG co-produced water, allowing the industry to engage in new treatment methods to their current water management strategies.

A number of experiments and analysis were conducted to study the CSG water composition, characterisation of the materials used, the adsorption capacity kinetics

and the dynamic adsorption of scoria and zeolite. The following conclusions and recommendations can be drawn from this research work:

## CSG co-produced water Bowen Basin site

This research examined the geochemical composition and variation of main ionic components of the CSG co-produced water from the research site located in the Bowen Basin. The CSG water can be described in ionic terms as a $Na^+$-$Cl^-$-$HCO_3^-$ type. Additionally, the co-produced water presented a high alkalinity with a pH averaging 8.3 and electrical conductivity of 6.0 dS/m with total dissolved solids (TDS) averaging 4,092 mg/L. The cationic composition of the CSG water exhibited an excess of $Na^+$ ions with an average concentration of 1,156 mg/L, and low average concentrations of $Ca^{2+}$ (28.3 mg/L), $Mg^{2+}$ (5.6 mg/L), and $K^+$ (67.46 mg/L). The calculated Sodium Adsorption Ratio (SAR) averaged 67. The main anions present were $Cl^-$ and $HCO_3^-$ with 1,993 mg/l and 618 mg/L respectively. Also, trace elements such as $Sr^{2+}$ and $Ba^{2+}$, were found to be in relatively high concentrations ($Sr^{2+}$ =3.7 mg/L and $Ba^{2+}$ =12.7 mg/L).

From this analysis of the CSG co-produced water from Bowen Basin it is recommended that the sodium ions; and hence the SAR; $Sr^{2+}$ and $Ba^{2+}$ ions (typically in high concentrations) require reduction. Furthermore, the overall reduction in salinity is required for the water to be re-used without impacting the environmental; soils, crops, and animal stocks. Adsorption studies were used to determine the effectiveness of the materials for the cations of interest considering the capacity, the rate of adsorption, the cation selective behaviour, and the reconditioning of adsorptive properties of both materials for cations of concern.

### Future work

The data presented corresponds to the CSG water samples taken from a balance tank that gathered water from the different CSG wells in the nearby area of the water treatment facility. Therefore, the variability on the concentration of major and trace elements could not be attributed to a particular well, natural variability of the underground water or even well operation procedures. Further research could be carried out to determine the singularity of the ionic characteristics of several wells across the CSG field in order to point out the causes of the variation and relate those

changes to the well operation/maintenance or natural underground water variability. Additionally, CSG water quantity and quality could be correlated to the gas production in order to predict the variability of the major and trace components present in co-produced water for the lifespan of the CSG well in the Bowen Basin. This will support the co-produced water management alternatives for future CSG projects in the region.

## Material characteristics and influence on the removal of cations

The comprehensive characterisation of the materials carried out, provided the range of unique minerals that are contained in each material zeolite and scoria. The study set out to characterise the natural occurring materials. The study of the materials aimed at gaining fundamental material properties to understand the material interaction with cations using the relevant equilibrium, kinetic and adsorption studies in batch and dynamic conditions.

The zeolite mineral composition contained clinoptilolite (41 wt%) and mordenite (29 wt%). The TEC calculated from XRF analysis was 154 meq/100 g, while REC was 75.1 and 142.2 meq/100 g on coarse and fine fraction sizes of the material. Meanwhile, the scoria material has a mineral composition of diopside (35 wt%), forsterite (33 wt%) and anorthite (29 wt%). The TEC of scoria was 46 meq/100 g, while REC measured for fine and coarse material was 28.4 and 34.2 meq/100 g respectively.

Equilibrium studies have shown that the scoria and zeolite treated with $NH_4^+$ exhibits greater adsorption capacities for $Na^+$, $Sr^{2+}$ and $Ba^{2+}$ than their natural, untreated forms. The maximum $Na^+$ adsorption observed for the scoria and zeolite materials enriched with $NH_4^+$ was 17.38 and 45.34 meq/100 g, which corresponds to 61.1% and 60.3% of the measured REC, respectively. The scoria and zeolite materials in their $NH_4^+$ form achieved an $Sr^{2+}$ adsorption of 4.5 and 8 meq/100 g that corresponds to a removal value of 44 and 80% of the initial $Sr^{2+}$ concentration. The maximum $Ba^{2+}$ adsorption achieved by the scoria and zeolite in their $NH_4^+$ form was 5.8 and 10.6 meq/100 g, which is a removal of 40 and 94% of the initial $Ba^{2+}$ concentration. Both materials have shown different removal behaviours, where $Sr^{2+}$ and $Ba^{2+}$ ions were removed more effectively than $Na^+$ ions. This adsorption behaviour is associated with the selective behaviour of the zeolite and scoria materials for cations.

The CSG water contained a mixture of cations that compete for adsorption sites and both materials have shown adsorption preference and different removal rates for certain cations, which led towards the study of the adsorption selectivity of cations of interest. Selectivity isotherms and coefficients showed that the scoria material was more selective towards high charged cations with low hydration energy, and also showed to have less affinity for monovalent cations with larger energy of hydration and hydrated radius, following the selective series $Ba^{2+} > Sr^{2+} >> Ca^{2+} > K^+ > Na^+$. The zeolite material exhibited higher selectivity towards cations with low charge density, small hydrated radius and low hydration energy, and exhibited the selectivity series $K^+ > Ba^{2+} > Sr^{2+} >> Ca^{2+} > Na^+$. Thus, the adsorption process can be limited by the efficiency of both materials on the removal of $Na^+$ ions, since it was shown that other cations present in solution are more selective.

The adsorption capacity and kinetic rates for $Na^+$ ions were favoured by smaller fractions of natural forms of zeolite and scoria and achieved 27.5 and 12 meq/100 g, increasing the accessibility to the available adsorption sites on the material. $NH_4^+$ and $K^+$ treated zeolite and scoria were best performing for $Na^+$ adsorption. Chemical treatment enhanced the adsorption because the introduced cations and the treatment solution had smaller hydrated ionic radii and lower hydration energies. CSG water typically had a mixture of anions that had a significant effect on the adsorption of $Na^+$ on the zeolite and scoria material, where $HCO_3^-$ and $F^-$ anions provided additional adsorption of $Na^+$ ions (30% increment) when compared with $Cl^-$ solution. This behaviour can be explained through the effect of pH on the adsorption of $Na^+$ ions, since alkaline solutions presented a higher adsorption of $Na^+$ ions.

The adsorption and desorption of $Na^+$ ions studied in batch type for five regeneration cycles showed that the ability of scoria and zeolite to adsorb cations decreased with the number of regeneration cycles. It was determined that materials regenerated with $NH_4^+$ will deplete their adsorptive properties after the $30^{th}$ and $20^{th}$ regeneration cycle for the zeolite and scoria. Additionally, it was observed that cations present in CSG water such as $Sr^{2+}$, $Ca^{2+}$, $K^+$ and $Ba^{2+}$, compete with $Na^+$ for adsorption sites reducing the capacity of the zeolite and scoria for $Na^+$, which corroborates the adsorption selective behaviour of these materials for cations of concern.

**Future work**

Equilibrium studies focused on the typical concentrations for $Na^+$, $Sr^{2+}$ and $Ba^{2+}$ in the CSG water from Bowen Basin and it was shown that initial concentration of cations had a large influence on the adsorptive capacity of both materials. For future studies a wider range of concentrations, especially for $Sr^{2+}$ and $Ba^{2+}$ ions, would be of interest for CSG water and industrial wastewater applications, since the modelled adsorption capacity predicted a significant removal of these cations. This future study will allow the determination of actual maximum adsorption capacities and removal of $Sr^{2+}$ and $Ba^{2+}$ cations using zeolite and scoria materials.

The selectivity studies showed that both materials have particular adsorptive behaviour for major and trace cations present in high concentrations in the CSG from Bowen Basin site. This work did not include other trace cations that are present in low concentrations but also are of concern such as $Fe^{2+}$, $Al^{3+}$, and $Br^+$. The adsorptive preference of these cations could be deducted from the theory and findings of this thesis, in order to describe the adsorption preferences of these cations using both materials. Nonetheless, further experimentation would be needed to determine the actual selective behaviour of $Fe^{2+}$, $Al^{3+}$ and $Br^+$ cations as well as their removal efficiency when using scoria and zeolite for CSG water that may contain a large concentration of these cations. Future studies may focus on the development of natural materials with enhanced selectivity towards certain cations, improving the overall capacity and selectivity by modifying surface or structure of the natural exchangers.

This research used chemical treatment for enhancement of the adsorption capacity exhibiting great results when compared with the natural materials. Additional work could be undertaken optimisation of the regeneration process for the recovery of the adsorptive properties of both materials, and the desorption of $Na^+$ in terms of concentration, reaction time, temperature, minimisation of regenerate solution, and possibly the combination of regenerate solutions to achieve higher desorption/adsorption rates, which in practice allow a greater utilisation of the materials. Other modifications worth exploring that could also provide additional adsorptive capacity but at the same time to some extent impractical for the removal of

ions in CSG water are heating the feed solution, chemical activation of the materials, and the use of cationic surfactants.

## Fixed bed columns for the treatment of CSG water

This study has shown the effect of the flow rate on the removal of $Na^+$ by scoria and zeolite material in fixed bed column was relatively small over the flow rates used. The adsorption capacity at a flow rate of 5 BV/h was reduced by 3% of the adsorption obtained for a flow rate of 1 BV/h, indicating that the adsorption of $Na^+$ was not directly affected by the increment of the flow rate. Columns packed with scoria and zeolite exhibited a larger $Na^+$ adsorption capacities when treated with $NH_4^+$ as well as larger desorption capacities than the same materials in natural and $K^+$ form. Nonetheless, the adsorption capacity exhibited for both materials was about 50% of the REC.

To meet regulatory requirement for re-use of CSG water, the removal of $Na^+$, $Sr^{2+}$ and $Ba^{2+}$ cations is required. In order to reduce sodium and the SAR below 12 (regulatory limit for irrigation with CSG water), it is required to remove $Na^+$ by 90% of the initial concentration, while maintaining the concentration of $Ca^{2+}$ and $Mg^{2+}$. However, decreasing the initial concentration of $Na^+$ by 70% (approximately 70 meq/L) while adding in the post-treatment $Ca^{2+}$ and $Mg^{2+}$ reduces the SAR to 12 also. Therefore, a suggested breakpoint for the treatment of CSG water for the optimal removal of $Na^+$ should be set at 0.3 ($C/C_0$) with the respective effluent adjustment of $Ca^{2+}$ and $Mg^{2+}$ to meet the regulatory requirement of SAR. The selected breakpoint ($C/C_0 = 0.3$) also guarantees that both materials remove up to 80% of the initial concentration of $Sr^{2+}$ and $Ba^{2+}$ ions in CSG water, adding consistency to the treated solution.

This research showed that the maximum bed volume obtained for experimental columns before the breakpoint ($C/C_0 = 0.3$) at a flow rate of 5 BV/h for scoria enriched with $NH_4^+$ was 1.5 BV, while zeolite enriched with $NH_4^+$ exhibited 4.5 BV when using field CSG water. For a column in real scale that contains 3,000 L (1 BV) of packed material operated at a flow rate of 15,000 L/h (5 BV/h), breakpoint ($C/C_0 = 0.3$) is reached after treating 4,500 L (1.5 BV) for scoria and 13,500 L (4.5 BV) for zeolite. At a lower flow rate of 3,000 L/h (1 BV/h), the breakpoint may occur at 1.6 and 4.7

BV that corresponds to a 3% increment of using a lower flow rate. The regeneration process to meet the regulatory limit is required after 20 min and 54 min when a flow rate of 5 BV/h is used for scoria and zeolite respectively. Therefore, it is recommended to use an arrangement with several columns of the same material in order to allow continuous treatment, since the regeneration process will be required often. It is also important to further investigate the regeneration process, including optimisation of the process and reduction of the use of chemical reagents in columns.

In summary, this research project has characterised CSG water for the southern Bowen Basin and the potential to transform the CSG co-produced water into a valuable resource for agricultural activities in the region. The zeolite and scoria materials are readily available in Australia and the cost of treating CSG water per cubic meter is in the range of AUD $ 1 - 1.7, which is a competitive price to the current alternatives. Nonetheless, additional elements need to be considered for the final costs associated with the treatment of CSG water, and further financial analysis is required. The scoria and zeolite can be regenerated and re-used for the removal of cations from CSG water, allowing their use in water treatment application. The main advantage of using these materials is the reduction of sodium, SAR, and trace elements to levels that make the water suitable for farming and irrigation; even if the treated CSG water is not used directly for those purposes, risks associated with disposal are reduced. The use of scoria and zeolite removes cations of concerns only; in order to reduce the salinity of the treated water; it is necessary to blend water with low TDS to meet the regulatory requirements. This thesis has dealt with co-produced CSG water exclusively, but it is possible to apply the same methodology to other industrial wastewaters such as mine-affected water from coal, uranium and iron mining activities.

# References

Abousnina, R. M., Nghiem, L. D., & Bundschuh, J. (2015). Comparison between oily and coal seam gas produced water with respect to quantity, characteristics and treatment technologies: a review. *Desalination and Water Treatment, 54*(7), 1793-1808.

Akdeniz, Y. (1999). *Cation exchange in zeolites structure modification by using a microwave.* (Master of Science), Izmir Institute of Technology, Izmir, Turkey.

Alberti, A., Armbruster, T., Artioli, G., Colella, C., Galli, E., Grice, J. D., Liebau, F., Minato, H., Nickel, E. H., & Passaglia, E. (1997). Recommended nomenclature for zeolite minerals: Report of the subcommittee on zeolites of the International Mineralogical Association, Commission on New Minerals and Mineral Names. *The Canadian Mineralogist, 35*, 1571-1606.

Alchin, D. (2013). Ion Exchange Resins. Drew New Zealand: XIII-Water-D-Ion Exchange Resins.

Alemayehu, E., & Lennartz, B. (2009). Virgin volcanic rocks: Kinetics and equilibrium studies for the adsorption of cadmium from water. *Journal of Hazardous Materials, 169*(1), 395-401. doi: 10.1016/j.jhazmat.2009.03.109

Alemayehu, E., Thiele-Bruhn, S., & Lennartz, B. (2011). Adsorption behaviour of Cr (VI) onto macro and micro-vesicular volcanic rocks from water. *Separation and Purification Technology, 78*(1), 55-61.

Alghoul, M., Poovanaesvaran, P., Sopian, K., & Sulaiman, M. (2009). Review of brackish water reverse osmosis (BWRO) system designs. *Renewable and Sustainable Energy Reviews, 13*(9), 2661-2667.

All-Consulting. (2003). Handbook on Coal Bed Methane Produced Water: Management and Beneficial Use Alternative Tulsa, Oklahoma: Ground Water Protection Research Foundation.

All-Consulting. (2012). The Modern Practices of Hydraulic Fracturing: A focus on Canadian Resources. Tulsa, Oklahoma: Petroleum Technology Alliance Canada and Science and Community Environmental Knowledge Fund.

All-Consulting, & Montana Board of Oil & Gas Conservation. (2002). Handbook on Best Management Practices and Mitigation Strategies for Coal Bed Methane in the Montana Portion of the Powder River Basin. Tulsa, Oklahoma: U.S Department of Energy.

All-Consulting, & Montana Board of Oil & Gas Conservation. (2006). Siting, Design, Construction and Reclamation Guidebook for Coalbed Natural Gas Impoundments: Montana Board of Oil and Gas Conservation.

Anderson, D., Rahman, Pf, Davey, Ek, Miller Bm and Glamore Wc. (2013). Background Paper on Groundwater Resources in Relation to Coal Seam Gas Production. *Office of the NSW Chief Scientist and Engineer*.

Argun, M. E. (2008). Use of clinoptilolite for the removal of nickel ions from water: kinetics and thermodynamics. *Journal of Hazardous Materials, 150*(3), 587-595.

Arrow Energy Ltd. (2011). Coal Seam Gas Water Management Strategy - Summary plan (Stage 2).

Arthur, D., & Seekins, J. (2010). Water and Shale Gas Development. *National Association of Royalty Owners* [PPT]. Pittsburg, PA, U.S.A.

Ates, A., & Hardacre, C. (2012). The effect of various treatment conditions on natural zeolites: Ion exchange, acidic, thermal and steam treatments. *Journal of Colloid And Interface Science, 372*(1), 130-140. doi: 10.1016/j.jcis.2012.01.017

Auerbach, S. M., Carrado, K. A., & Dutta, P. K. (2003). *Handbook of zeolite science and technology*. United States of America: Marcel Dekker, Inc.

Australia Pacific Lng Pty. (2011). Coal Seam Gas Water Qualty Monitoring Program: Talinga Water Treatment Facility (Vol. Q-4120-15-QA-0001): DERM.

Australian and New Zealand Environment Conservation Council. (2000). *Australian and New Zealand guidelines for fresh and marine water quality* (Vol. 1): A.C.T. : Environment Australia.

Averina, A., Rasul, M., & Begum, S. (2008). *Management of Coal Seam Gas (CSG) By-Product Water: A Case Study on Spring Gully Mine Site in Queensland, Australia.* Paper presented at the Proceedings of the 2nd International Conference on Waste Management: Waste Management, Water Pollution, Air Pollution, Indoor Climate (WWAI'08), Corfu, Greece, 26th-28th October.

Ayoub, J., Colson, L., Hinkel, J., Johnston, D., & Levine, J. (1991). Learning to produce coalbed methane. *Oilfield Review, 3*(1), 27-40.

Babak, K., Rahim, A. A., Wahid, S. A., Balasundram, S. K., & Afyuni, M. (2013). Sorption and desorption of zinc by clinoptilolite and clinoptilolite-tridymite. *Malaysian Journal of Soil Science, 17*, 69-83.

Babcock, K., & Schulz, R. (1963). Effect of anions on the sodium-calcium exchange in soils. *Soil Science Society of America Journal, 27*(6), 630-632.

Baker, G., & Slater, S. (2008). *The increasing significance of coal seam gas in eastern Australia*. Paper presented at the PESA Eastern Australasian Basins Symposium III, Sydney.

Baker, H., Massadeh, A., & Younes, H. (2009). Natural Jordanian zeolite: removal of heavy metal ions from water samples using column and batch methods. *Environmental Monitoring and Assessment, 157*(1), 319-330. doi: 10.1007/s10661-008-0537-6

Barthelmy, D. (2014). Mineralogy Database. Retrieved 10/11/2015, 2015, from http://www.webmineral.com/

Batley, G. E., & Kookana, R. S. (2012). Environmental issues associated with coal seam gas recovery: managing the fracking boom. *Environmental Chemistry, 9*(5), 425-428.

Bechtel, A., Reischenbacher, D., Sachsenhofer, R. F., Gratzer, R., Lücke, A., & Püttmann, W. (2007). Relations of petrographical and geochemical parameters in the middle Miocene Lavanttal lignite (Austria). *International Journal of Coal Geology, 70*(4), 325-349. doi: 10.1016/j.coal.2006.07.002

Bektaş, N., & Kara, S. (2004). Removal of lead from aqueous solutions by natural clinoptilolite: equilibrium and kinetic studies. *Separation and Purification Technology, 39*(3), 189-200.

Belbase, S., Urynowicz, M. A., Vance, G. F., & Dangi, M. B. (2013). Passive remediation of coalbed natural gas co-produced water using zeolite. *Journal of Environmental Management, 131*, 318-324.

Benjamin, E. R., Plank, T., Wade, J. A., Kelley, K. A., Hauri, E. H., & Alvarado, G. E. (2007). High water contents in basaltic magmas from Irazú Volcano, Costa Rica. *Journal of Volcanology and Geothermal Research, 168*(1), 68-92. doi: 10.1016/j.jvolgeores.2007.08.008

Benson, M., Bergman, H., Boelter, A., Coupal, R., Hoffer, N., Hulme, D., Korfanta, N., Lieske, S., Lovato, J., & Miller, S. (2005). Water Production from Coalbed Methane Development in Wyoming: A Summary of Quantity, Quality and Management Options—Final Report. Wyoming.

Berger, K. C. (2012). Forecasting Coal Seam Gas Water Production in Queensland's Surat and Southern Bowen Basins. Queensland, Australia: Klohn Crippen Berger.

Bern, C. R., Breit, G. N., Healy, R. W., Zupancic, J. W., & Hammack, R. (2013). Deep subsurface drip irrigation using coal-bed sodic water: Part I. Water and solute movement. *Agricultural Water Management, 118*, 122-134.

Biggs, A., Witheyman, S., Williams, K., Cupples, N., De Voil, C., Power, R., & Stone, B. (2012). Assessing the Salinity Impacts of Coal Seam Gas Water on Landscapes and Surface Streams. August 2012 *Final Report of Activity* (Vol. 3). Toowoomba, Australia.

Bishop, C. (2006). *Resource Recovery of Coal Bed Methane Formation Water.* (Master of Science), East Central University, Louisiana.

Can, Ö. (2004). *Ion exchange in natural zeolite packed column.* (Master of Science), İzmir Institute of Technology.

Caputo, D., & Pepe, F. (2007). Experiments and data processing of ion exchange equilibria involving Italian natural zeolites: a review. *Microporous and Mesoporous Materials, 105*(3), 222-231. doi: 10.1016/j.micromeso.2007.04.024

Castaldi, P., Santona, L., Enzo, S., & Melis, P. (2008). Sorption processes and XRD analysis of a natural zeolite exchanged with Pb 2+, Cd 2+ and Zn 2+ cations. *Journal of Hazardous Materials, 156*(1), 428-434. doi: 10.1016/j.jhazmat.2007.12.040

Cerri, G., Langella, A., Pansini, M., & Cappelletti, P. (2002). Methods of determining cation exchange capacities for clinoptilolite-rich rocks of the Logudoro region in northern Sardinia, Italy. *Clays and Clay Minerals, 50*(1), 127-135.

Chapman, H. (1965). Cation-exchange capacity. *Methods of soil analysis. Part 2. Chemical and microbiological properties*(methodsofsoilanb), 891-901.

Chelishchev, N., Berenshtein, B., Berenshtein, T., Gribanova, N., & Martynova, N. (1973). Ion-exchange properties of clinoptilolite. *Doklady Akademii Nauk, 210*, 1110-1112.

Chu, K. H. (2010). Fixed bed sorption: setting the record straight on the Bohart–Adams and Thomas models. *Journal of Hazardous Materials, 177*(1), 1006-1012.

Cincotti, A., Lai, N., Orrù, R., & Cao, G. (2001). Sardinian natural clinoptilolites for heavy metals and ammonium removal: experimental and modeling. *Chemical Engineering Journal, 84*(3), 275-282.

Clifford, D. A. (1999). Ion exchange and inorganic adsorption. *Water quality and treatment, 4*, 561-564.

Colella, C. (1996). Ion exchange equilibria in zeolite minerals. *Mineralium Deposita, 31*(6), 554-562. doi: 10.1007/BF00196136

Cook, P. (2013). Life cycle of Coal Seam Gas Projects: Technologies and Potential Impacts *Report commissioned for the independent review of coal seam gas activities in NSW by the NSW Chief Scientist & Engineer*. New South Wales: Office of the Chief Scientist and Engineer.

Crittenden, J. C., Trussell, R. R., Hand, D. W., Howe, K. J., & Tchobanoglous, G. (2012). Ion Exchange *MWH's Water Treatment: Principles and Design, Third Edition* (3rd Edition ed., pp. 1263-1334): John Wiley & Sons, Inc.

Darton, T., Annunziata, U., Del Vigo Pisano, F., & Gallego, S. (2004). Membrane autopsy helps to provide solutions to operational problems. *Desalination, 167*, 239-245. doi: 10.1016/j.desal.2004.06.133

Davies, P. (2013). Background paper on produced water and solids in relation to coal seam gas production. Macquarie University: Office of the NSW Chief Scientist and Engineer.

Department of Energy and Water Supply Queensland. (2012). CSG Water Quality Requirements. Queensland: State of Queensland.

Department of Energy and Water Supply Queensland. (2013). *Coal Seam Gas Recycled Water Management Plan Guideline Including Exclusion Desicion Application Guideline*. Queensland: State of Queensland.

Department of Environment and Heritage Protection, & Queensland, S. O. (2013). Guideline: Approval of coal seam gas water for beneficial use. *EM1176 Version 2*.

Department of Environment and Heritage Protection Queensland. (2012a). *Coal Seam Gas Water Management Policy*. Queensland: State of Queensland.

Department of Environment and Heritage Protection Queensland. (2012b). *CSC water management: Measurable criteria*. Queensland: State of Queensland.

Department of Environment and Heritage Protection Queensland. (2013). *General Beneficial Use Approval - Irrigation of Associated Water (Including coal seam gas water)*. Queensland: State of Queensland.

Department of Environment and Resource Management Queensland. (2009). Irrigation water quality—salinity and soil structure stability *Department of Environment and Resource Management (QLD)*. Queensland: Department of Environment and Resource Management Queensland.

Department of Environment and Resource Management Queensland. (2010a). *Guideline: Approval of coal seam gas water for beneficial use*. Queensland: Department of Environment and Resource Management Queensland,.

Department of Environment and Resource Management Queensland. (2010b). *Healthy headwaters Coal Seam Gas Water Feasibility Study*. Queensland: State of Queensland.

Department of Environment and Resource Management Queensland. (2011). *Salinity management handbook*. Queensland: State of Queensland.

Doula, M., & Ioannou, A. (2003). The effect of electrolyte anion on Cu adsorption–desorption by clinoptilolite. *Microporous and Mesoporous Materials, 58*(2), 115-130.

Du, Q., Liu, S., Cao, Z., & Wang, Y. (2005). Ammonia removal from aqueous solution using natural Chinese clinoptilolite. *Separation and Purification Technology, 44*(3), 229-234. doi: 10.1016/j.seppur.2004.04.011

El-Kamash, A., Zaki, A., & El Geleel, M. A. (2005). Modeling batch kinetics and thermodynamics of zinc and cadmium ions removal from waste solutions using synthetic zeolite A. *Journal of Hazardous Materials, 127*(1), 211-220.

El-Kamash, A. M. (2008). Evaluation of zeolite A for the sorptive removal of Cs+ and Sr2+ ions from aqueous solutions using batch and fixed bed column operations. *Journal of Hazardous Materials, 151*(2-3), 432.

El-Shafai, S. A., & Zahid, W. M. (2013). Performance of aerated submerged biofilm reactor packed with local scoria for carbon and nitrogen removal from municipal wastewater. *Bioresource Technology, 143*, 476-482.

Environmental Protection Agency. (2010). Coalbed Methane Extraction: Detailed Study Report. *Office of Water, EPA-820-R-10-022*.

Environmental Protection Agency. (2013). Technical Development Document for the Coalbed Methane (CBM) Extraction Industry. *EPA-820-R-13-009*.

Environmental Protection Agency Queensland. (2005). *Queensland Water Recycling Guidelines*. Brisbane: State of Queensland.

Environmental Protection Agency Queensland. (2008). *Decision to approve a resource for beneficial use - Associated water*. Brisbane: State of Queensland.

Erdem, E., Karapinar, N., & Donat, R. (2004). The removal of heavy metal cations by natural zeolites. *Journal of Colloid And Interface Science, 280*(2), 309-314. doi: 10.1016/j.jcis.2004.08.028

Ezlit, Y. D., Smith, R. J., & Raine Steven, R. (2010). A Review of Salinity and Sodicity in Irrigarion (U. o. S. Queensland, Trans.) *Irrigation Matters*: Cooperative Research Centre for Irrigation Futures.

Fakhru'l-Razi, A., Pendashteh, A., Abdullah, L. C., Biak, D. R. A., Madaeni, S. S., & Abidin, Z. Z. (2009). Review of technologies for oil and gas produced water treatment. *Journal of Hazardous Materials, 170*(2), 530-551. doi: 10.1016/j.jhazmat.2009.05.044

Fell Consulting Pty Ltd. (2014). Water Treatment and Coal Seam Gas *Office of the NSW Chief Scientist and Engineer*. Sydney.

Fernandez, A., Rendueles, M., Rodrigues, A., & Diaz, M. (1994). Co-ion behavior at high concentration cationic ion exchange. *Industrial & engineering chemistry research, 33*(11), 2789-2794.

Ganjegunte, G. K., Vance, G. F., Gregory, R. W., Urynowicz, M. A., & Surdam, R. C. (2011). Improving saline-sodic coalbed natural gas water quality using natural zeolites. *Journal of environmental quality, 40*(1), 57.

Gedik, K., & Imamoglu, I. (2008). Removal of cadmium from aqueous solutions using clinoptilolite: Influence of pretreatment and regeneration. *Journal of Hazardous Materials, 155*(1), 385-392. doi: 10.1016/j.jhazmat.2007.12.101

Geoscience-Australia (Cartographer). (2015). Mineral Maps Australia. Retrieved from http://www.ga.gov.au/cedda/maps/1085

Greenlee, L. F., Lawler, D. F., Freeman, B. D., Marrot, B., & Moulin, P. (2009). Reverse osmosis desalination: water sources, technology, and today's challenges. *Water Research, 43*(9), 2317-2348.

Günay, A., Arslankaya, E., & Tosun, İ. (2007). Lead removal from aqueous solution by natural and pretreated clinoptilolite: Adsorption equilibrium and kinetics. *Journal of Hazardous Materials, 146*(1), 362-371. doi: 10.1016/j.jhazmat.2006.12.034

Hamawand, I., Yusaf, T., & Hamawand, S. G. (2013). Coal seam gas and associated water: A review paper. *Renewable and Sustainable Energy Reviews, 22*, 550.

Han, R., Zou, L., Zhao, X., Xu, Y., Xu, F., Li, Y., & Wang, Y. (2009). Characterization and properties of iron oxide-coated zeolite as adsorbent for removal of copper(II) from solution in fixed bed column. *Chemical Engineering Journal, 149*(1), 123-131. doi: 10.1016/j.cej.2008.10.015

Harland, C. E. (1994). *Ion exchange: theory and practice* (Vol. 6). Cambridge, UK: Royal Society of Chemistry.

Hay, R. L. (1986). Geologic Occurrence of Zeolites and Some Associated Minerals. *Studies in Surface Science and Catalysis, 28*, 35-40. doi: 10.1016/S0167-2991(09)60853-3

Health, Q. (2013). *Coal Seam Gas in the Tara region: Summary risk assessment of health complaints and environment monitoring data*. Brisbane: State of Queensland.

Hedstrom, A. (2001). Ion exchange of ammonium in zeolites: Literature review. *Journal of Environmental Engineering, 127*(8), 673.

Helfferich, F. G. (1962). *Ion exchange*: Courier Corporation.

Hlavay, J., Vigh, G., Olaszi, V., & Inczedy, J. (1982). Investigations on natural Hungarian zeolite for ammonia removal. *Water Research, 16*(4), 417-420.

Ho, L., & Ho, G. (2012). Mitigating ammonia inhibition of thermophilic anaerobic treatment of digested piggery wastewater: Use of pH reduction, zeolite, biomass and humic acid. *Water Research, 46*(14), 4339-4350. doi: 10.1016/j.watres.2012.05.016

Holmes, G. G., Pecover, S. R., & Geological Survey of New South Wales. (1987). *Natural Zeolites: An Information Package for Exploration and Development in New South Wales*: Department of Mineral Resources.

Howe, K. J., Hand, D. W., Crittenden, J. C., Trussell, R. R., & Tchobanoglous, G. (2012). *Principles of water treatment*: John Wiley & Sons.

Huang, F. Y. C., & Natrajan, P. (2006). Feasibility of using natural zeolites to remove sodium from coal bed methane-produced water.(Author abstract). *Journal of Environmental Engineering, 132*(12), 1644.

Huang, H., Xiao, X., Yan, B., & Yang, L. (2010). Ammonium removal from aqueous solutions by using natural Chinese (Chende) zeolite as adsorbent. *Journal of Hazardous Materials, 175*(1), 247-252. doi: 10.1016/j.jhazmat.2009.09.156

Inglezakis, V. J. (2005). The concept of "capacity" in zeolite ion-exchange systems. *Journal of Colloid And Interface Science, 281*(1), 68-79. doi: 10.1016/j.jcis.2004.08.082

Inglezakis, V. J. (2010a). Ion Exchange And Adsorption Fixed Bed Operations For Wastewater Treatment-Part I: Modeling Fundamentals And Hydraulics Analysis. *Journal of Engineering Studies and Research, 16*(3), 29-41.

Inglezakis, V. J. (2010b). Ion Exchange And Adsorption Fixed Bed Operations For Wastewater Treatment-Part II: Scale-up and approximate design methods. *Journal of Engineering Studies and Research, 16*(3), 42-50.

Inglezakis, V. J., Diamandis, N. A., Loizidou, M. D., & Grigoropoulou, H. P. (1999). Effect of pore clogging on kinetics of lead uptake by clinoptilolite. *Journal of Colloid And Interface Science, 215*(1). doi: 10.1006/jcis.1999.6247

Inglezakis, V. J., & Grigoropoulou, H. P. (2004). Effects of operating conditions on the removal of heavy metals by zeolite in fixed bed reactors. *Journal of Hazardous Materials, 112*(1), 37-43. doi: 10.1016/j.jhazmat.2004.02.052

Inglezakis, V. J., Hadjiandreou, K. J., Loizidou, M. D., & Grigoropoulou, H. P. (2001a). Pretreatment of natural clinoptilolite in a laboratory-scale ion exchange packed bed. *Water Research, 35*(9), 2161-2166. doi: 10.1016/S0043-1354(00)00500-5

Inglezakis, V. J., Lemonidou, M., & Grigoropoulou, H. P. (2001b). Liquid holdup and flow dispersion in zeolite packed beds. *Chemical Engineering Science, 56*(17), 5049-5057. doi: 10.1016/S0009-2509(01)00189-0

Inglezakis, V. J., Loizidou, M. D., & Grigoropoulou, H. P. (2002). Equilibrium and kinetic ion exchange studies of Pb 2+, Cr 3+, Fe 3+ and Cu 2+ on natural clinoptilolite. *Water Research, 36*(11), 2784-2792. doi: 10.1016/S0043-1354(01)00504-8

Inglezakis, V. J., Loizidou, M. M., & Grigoropoulou, H. P. (2004). Ion exchange studies on natural and modified zeolites and the concept of exchange site accessibility. *Journal of Colloid And Interface Science, 275*(2), 570-576. doi: 10.1016/j.jcis.2004.02.070

Inglezakis, V. J., Papadeas, C. D., Loizidou, M. D., & Grigoropoulou, H. P. (2001c). Effects of pretreatment on physical and ion exchange properties of natural clinoptilolite. *Environmental technology, 22*(1), 75-82.

Inglezakis, V. J., & Poulopoulos, S. (2006). *Adsorption, ion exchange and catalysis: design of operations and environmental applications* (Vol. 3). Amsterdam, The Netherlands: Elsevier.

Inglezakis, V. J., Stylianou, M. A., Gkantzou, D., & Loizidou, M. D. (2007). Removal of Pb(II) from aqueous solutions by using clinoptilolite and bentonite as adsorbents. *Desalination, 210*(1), 248-256. doi: 10.1016/j.desal.2006.05.049

Inglezakis, V. J., & Zorpas, A. A. (2012a). Fundamentals of Ion Exchange Fixed-Bed Operations *Ion Exchange Technology I* (pp. 121-161): Springer.

Inglezakis, V. J., & Zorpas, A. A. (2012b). *Handbook of natural zeolites*: Bentham Science Publishers.

Inglezakis, V. J., Zorpas, A. A., Loizidou, M. D., & Grigoropoulou, H. P. (2003). Simultaneous removal of metals Cu 2+, Fe 3+ and Cr 3+ with anions SO 4 2− and HPO 4 2− using clinoptilolite. *Microporous and Mesoporous Materials, 61*(1), 167-171. doi: 10.1016/S1387-1811(03)00364-0

Inglezakis, V. J., Zorpas, A. A., Loizidou, M. D., & Grigoropoulou, H. P. (2005). The effect of competitive cations and anions on ion exchange of heavy metals. *Separation and Purification Technology, 46*(3), 202-207.

Internation Union of Pure and Applied Chemistry. (1971). Recommendations on Ion Exchange Nomenclature *Analytical Chemistry Division* (Vol. Commission on Analytical Nomenclature). London.

Islam, M. A., Khan, M. M., & Mozumder, M. S. (2004). Adsorption equilibrium and adsorption kinetics: a unified approach. *Chemical engineering & technology, 27*(10), 1095-1098.

Ismael, I., Melegy, A., & Kratochvíl, T. (2012). Lead Removal from Aqueous Solution by Natural and Pretreated Zeolites. *Geotechnical and Geological Engineering, 30*(1), 253-262. doi: 10.1007/s10706-011-9466-1

Jackson, R., & Reddy, K. (2007a). Geochemistry of Coalbed Natural Gas (CBNG) Produced Water in Powder River Basin, Wyoming: Salinity and Sodicity. *Water, Air, and Soil Pollution, 184*(1), 49-61. doi: 10.1007/s11270-007-9398-9

Jackson, R. E., & Reddy, K. (2007b). Trace element chemistry of coal bed natural gas produced water in the Powder River Basin, Wyoming. *Environmental science & technology, 41*(17), 5953-5959.

Jamshidi, M., & Jessen, K. (2012). Water production in enhanced coalbed methane operations. *Journal of Petroleum Science and Engineering, 92-93*, 56-64. doi: 10.1016/j.petrol.2012.06.009

Jha, V. K., & Hayashi, S. (2009). Modification on natural clinoptilolite zeolite for its NH4+ retention capacity. *Journal of Hazardous Materials, 169*(1-3), 29. doi: 10.1016/j.jhazmat.2009.03.052

Johnston, C. R., Vance, G. F., & Ganjegunte, G. K. (2008). Irrigation with coalbed natural gas co-produced water. *Agricultural Water Management, 95*(11), 1243-1252. doi: 10.1016/j.agwat.2008.04.015

Kammerer, J., Carle, R., & Kammerer, D. R. (2010). Adsorption and ion exchange: basic principles and their application in food processing. *Journal of agricultural and food chemistry, 59*(1), 22-42.

Kapanji, K. K. (2009). *The Removal of Heavy Metals from Wastewater Using South African Clinoptilolite.* (Masters of Science in Engineering), University of the Witwatersrand, Johannesburg.

Karthikeyan, S., Sivakumar, B., & Sivakumar, N. (2010). Film and Pore Diffusion Modeling for Adsorption of Reactive Red 2 from Aqueous Solution on to Activated Carbon Preparedfrom Bio-Diesel Industrial Waste. *Journal of Chemistry, 7*(S1), S175-S184.

Katsou, E., Malamis, S., Tzanoudaki, M., Haralambous, K. J., & Loizidou, M. (2011). Regeneration of natural zeolite polluted by lead and zinc in wastewater treatment systems. *Journal of Hazardous Materials, 189*(3), 773-786. doi: 10.1016/j.jhazmat.2010.12.061

Kele, B. (2005a). *Onsite Wastewater Treatment and Reuse Using Recirculatory Evapotranspiration Channels in Regional Queensland.* (Master degree), Central Queensland University, Queensland, Australia.

Kele, B. (2005b). *Onsite Wastewater Treatment and Reuse Using Recirculatory Evapotranspiration Channels In Regional Queensland.* (Master of Applied Science), Central Queensland University, Queensland, Australia.

Kele, B. (2007). Keynote: Round Tanks in Square Holes. *On-site 07, University of New England*(Armidale), Lanfax Laboratories.

Kele, B. (2008). Keynote: A New Dawn for Decentralised Sewerage. *Onsite and Decentralised Sewerage and Recycling Conference, S. West. Benalla Victoria Australia*(Australian Water Association).

Kele, B. (2016-Unpublished Doctoral Dissertation). *The Use of Selected Volcanic Rocks for the Sustainable Treatment of Wastewater* (Unpublished Doctoral Dissertation), Central Queensland University, Central Queensland University, Queensland.

Kele, B., Midmore, D., Harrower, K., & Hood, B. (2007). The Impact of Limiting Factors in a Recirculating Wastewater Treatment System. *Water and Environmental Management Series, London*(IWA).

Kele, B., Midmore, D., Harrower, K., Mckennariey, B., & Hood, B. (2005). An overview of the Central Queensland University self-contained evapotranspiration beds. *Water Science and Technology, 51*(10), 273-281.

Khan, S., & Kordek, G. (2014). Coal Seam Gas: Produced Water and Solids. *Report commissioned for the independent review of coal seam gas activities in NSW by the NSW Chief Scientist & Engineer: School of Civil Environmental Engineering, The University of New South Wales*.

Kinnon, E. C. P., Golding, S. D., Boreham, C. J., Baublys, K. A., & Esterle, J. S. (2010). Stable isotope and water quality analysis of coal bed methane production waters and gases from the Bowen Basin, Australia. *International Journal of Coal Geology, 82*(3), 219-231. doi: 10.1016/j.coal.2009.10.014

Kithome, M., Paul, J. W., Lavkulich, L. M., & Bomke, A. A. (1999). Effect of pH on ammonium adsorption by natural Zeolite clinoptilolite 1. *Communications in Soil Science and Plant Analysis, 30*(9-10), 1417-1430. doi: 10.1080/00103629909370296

Kitsopoulos, K. P. (1999). Cation-exchange capacity (CEC) of zeolitic volcaniclastic materials: applicability of the ammonium acetate saturation (AMAS) method. *Clays and Clay Minerals, 47*(6), 688-696.

Kocaoba, S., Orhan, Y., & Akyüz, T. (2007). Kinetics and equilibrium studies of heavy metal ions removalby use of natural zeolite. *Desalination, 214*(1), 1-10. doi: 10.1016/j.desal.2006.09.023

Korkuna, O., Leboda, R., Skubiszewska-Zie, J., Vrublevs'ka, T., Gun'ko, V., & Ryczkowski, J. (2006). Structural and physicochemical properties of natural zeolites: clinoptilolite and mordenite. *Microporous and Mesoporous Materials, 87*(3), 243-254.

Kowalczyk, P., Sprynskyy, M., Terzyk, A. P., Lebedynets, M., Namieśnik, J., & Buszewski, B. (2006). Porous structure of natural and modified clinoptilolites. *Journal of Colloid And Interface Science, 297*(1), 77-85. doi: 10.1016/j.jcis.2005.10.045

Kumar, S., & Jain, S. (2013). History, introduction, and kinetics of ion exchange materials. *Journal of Chemistry, 2013*(ID 957647), 13. doi: http://dx.doi.org/10.1155/2013/957647

Kwon, J.-S., Yun, S.-T., Kim, S.-O., Mayer, B., & Hutcheon, I. (2005). Sorption of Zn (II) in aqueous solutions by scoria. *Chemosphere, 60*(10), 1416-1426.

Kwon, J.-S., Yun, S.-T., Lee, J.-H., Kim, S.-O., & Jo, H. Y. (2010). Removal of divalent heavy metals (Cd, Cu, Pb, and Zn) and arsenic(III) from aqueous solutions using scoria: Kinetics and equilibria of sorption. *Journal of Hazardous Materials, 174*(1), 307-313. doi: 10.1016/j.jhazmat.2009.09.052

Langella, A., Pansini, M., Cappelletti, P., De Gennaro, B., De' Gennaro, M., & Colella, C. (2000). NH + 4, Cu 2+, Zn 2+, Cd 2+ and Pb 2+ exchange for Na + in a sedimentary clinoptilolite, North Sardinia, Italy. *Microporous and Mesoporous Materials, 37*(3), 337-343. doi: 10.1016/S1387-1811(99)00276-0

Lehto, J., & Harjula, R. (1995). Experimentation in ion exchange studies - the problem of getting reliable and comparable results. *Reactive and Functional Polymers, 27*(2), 121-146. doi: 10.1016/1381-5148(95)00038-H

Lemay, T. G., Konhauser, K.O. (2006). Water Chemistry of Coalbed Methane Reservoirs *Alberta Energy and Utilities Board, EUB/AGS Special Report 081*. Alberta, Canada: Alberta Energy and Utilities Board.

Leusch, F., & Bartkow, M. (2010). A short primer on benzene, toluene, ethylbenzene and xylenes (BTEX) in the environment and in hydraulic fracturing fluids. *Griffith University–Smart Water Research Centre Report, Brisbane*.

Li, M. (2012). Optimal plant operation of brackish water reverse osmosis (BWRO) desalination. *Desalination, 293*, 61-68.

Lima, A., Belkin, H. E., & Török, K. (1999). Understanding Vesuvius magmatic processes: evidence from primitive silicate-melt inclusions in medieval scoria clinopyroxenes (Terzigno Formation). *Mineralogy and Petrology, 65*(3-4), 185-206. doi: 10.1007/BF01161960

Malamis, S., & Katsou, E. (2013). A review on zinc and nickel adsorption on natural and modified zeolite, bentonite and vermiculite: Examination of process parameters, kinetics and isotherms. *Journal of Hazardous Materials, 252-253*, 428. doi: 10.1016/j.jhazmat.2013.03.024

Malliou, E., Loizidou, M., & Spyrellis, N. (1994). Uptake of lead and cadmium by clinoptilolite. *Science of the Total Environment, 149*(3), 139-144. doi: 10.1016/0048-9697(94)90174-0

Mannhardt, T., Cameron, I. (2009). Coal Seam Gas Water: Viability and Treatment. *Journal Australian Water Association, Desalination*, 87-91.

Manthey, B. (2014). *Pre–Treatment of Coal Seam Gas Produced Water.* (Bachelor of Engineering), University of Southern Queensland.

Margeta, K., Nataša Zabukovec, L., Šiljeg, M., & Farkaš, A. (2013). Natural Zeolites in Water Treatment – How Effective is Their Use. In W. Elshorbagy (Ed.), *Water Treatment*: InTech.

Mcbeth, I., Reddy, K. J., & Skinner, Q. D. (2003). Chemistry of trace elements in coalbed methane product water. *Water Research, 37*(4), 884-890. doi: 10.1016/S0043-1354(02)00382-2

Mccool, B. C., Rahardianto, A., Faria, J., Kovac, K., Lara, D., & Cohen, Y. (2010). Feasibility of reverse osmosis desalination of brackish agricultural drainage water in the San Joaquin Valley. *Desalination, 261*(3), 240-250.

Mcgovern, R. K., & Zubair, S. M. (2014). The cost effectiveness of electrodialysis for diverse salinity applications. *Desalination, 348*, 57-65.

Medvidović, N. V., Perić, J., & Trgo, M. (2006). Column performance in lead removal from aqueous solutions by fixed bed of natural zeolite–clinoptilolite. *Separation and Purification Technology, 49*(3), 237-244.

Millar, G. J., Couperthwaite, S. J., De Bruyn, M., & Leung, C. W. (2015a). Ion exchange treatment of saline solutions using Lanxess S108H strong acid cation resin. *Chemical Engineering Journal, 280*, 525-535.

Millar, G. J., Schot, A., Couperthwaite, S. J., Shilling, A., Nuttall, K., & De Bruyn, M. (2015b). Equilibrium and column studies of iron exchange with strong acid cation resin. *Journal of Environmental Chemical Engineering, 3*(1), 373-385.

Mineralogy, H. I. O. (2015). Mindat. 2015, from http://www.mindat.org/

Mondal, S., & Wickramasinghe, S. R. (2008). Produced water treatment by nanofiltration and reverse osmosis membranes. *Journal of Membrane Science, 322*(1), 162-170. doi: 10.1016/j.memsci.2008.05.039

Morgan-Sagastume, J. M., & Noyola, A. (2008). Evaluation of an aerobic submerged filter packed with volcanic scoria. *Bioresource Technology, 99*(7), 2528-2536. doi: 10.1016/j.biortech.2007.04.068

Motsi, T. (2010). *Remediation of Acid Mine Drainage Using Natural Zeolite.* (Doctor of Philosophy), The University of Birmingham, United Kingdom.

Mumpton, F. A. (1999). La roca magica: Uses of Natural Zeolites in Agriculture and Industry. *Proceedings of the National Academy of Sciences of the United States of America, 96*(7), 3463-3470.

National Research Council. (2010). *Management and Effects of Coalbed Methane Produced Water in the Western United States* (Vol. Committee on Management and Effects of Coalbed Methane Development and

Produced Water in the Western United States). Washington, D.C.: National Academies Press.

Negrea, A., Lupa, L., Ciopee, M., & Negrea, P. (2011). Experimental and Modelling Studies on As (III) Removal from Aqueous Medium on Fixed Bed Column. *Chemical Bulletin of "Politehnica" University of Timisoara, ROMANIA Series of Chemistry and Environmental Engineering, 56*(70), 2.

Nghiem, L. D., Elters, C., Simon, A., Tatsuya, T., & Price, W. (2015). Coal seam gas produced water treatment by ultrafiltration, reverse osmosis and multi-effect distillation: A pilot study. *Separation and Purification Technology, 146*, 94-100.

Nghiem, L. D., Ren, T., Aziz, N., Porter, I., & Regmi, G. (2011). Treatment of coal seam gas produced water for beneficial use in Australia: A review of best practices. *Desalination and Water Treatment, 32*(1-3), 316-323. doi: 10.5004/dwt.2011.2716

Nguyen, T. C., Loganathan, P., Nguyen, T. V., Vigneswaran, S., Kandasamy, J., & Naidu, R. (2015). Simultaneous adsorption of Cd, Cr, Cu, Pb, and Zn by an iron-coated Australian zeolite in batch and fixed-bed column studies. *Chemical Engineering Journal, 270*, 393-404.

Oldridge, S., & Whatman, L. (2009). Beneficial use of coal seam gas water. *Water,* 76-81.

Oren, A. H., & Kaya, A. (2006). Factors affecting adsorption characteristics of Zn2+ on two natural zeolites. *Journal of Hazardous Materials, 131*(1-3), 59.

Oster, J. (1994). Irrigation with poor quality water. *Agricultural Water Management, 25*(3), 271-297.

Oueslati, W., Mefath, M., Ben Rhaiem, H., & Ben Haj Amara, A. (2009). Cation Exchange Selectivity versus concentration of competing heavy metal cations (Pb2+,Zn2+) : case of Na-montmorillonite. *Physics Procedia, 2*(3), 1059-1063. doi: http://dx.doi.org/10.1016/j.phpro.2009.11.063

Pabalan, R. T., & Bertetti, F. P. (2001). Cation-Exchange Properties of Natural Zeolites. *Reviews in Mineralogy and Geochemistry, 45*(1), 453-518. doi: 10.2138/rmg.2001.45.14

Pacwest. (2012). Shale/Unconventional Resources. from http://pacwestcp.com/education/shaleunconventional-resources/

Perić, J., Trgo, M., & Medvidović, N. V. (2004). Removal of zinc, copper and lead by natural zeolite—a comparison of adsorption isotherms. *Water Research, 38*(7), 1893-1899.

Q.G.C. Pty Ltd. (2013). Preliminary Regional Hydrochemistry Characterisation *QCLNG-BE99-WAT-RPT-000002*(Rev 1).

Qi, N., & Levan, M. D. (2005). Adsorption equilibrium modeling for water on activated carbons. *Carbon, 43*(11), 2258-2263.

Railsback, L. B. (2006). Some fundamentals of mineralogy and geochemistry. *On-line book, quoted from: www. gly. uga. edu/railsback*.

Rajic, N., Stojakovic, D., Jovanovic, M., Logar, N. Z., Mazaj, M., & Kaucic, V. (2010). Removal of nickel(II) ions from aqueous solutions using the natural clinoptilolite and preparation of nano-NiO on the exhausted clinoptilolite. *Applied Surface Science, 257*(5), 1524-1532. doi: 10.1016/j.apsusc.2010.08.090

Reddy, K. J. (2010). *Coalbed Natural Gas: Energy and Environment*: Nova Science Publishers.

Rendueles, M., Fernández, A., & Diaz, M. (1997). Sorption of counter and co-ions at high concentration in ion exchangers. *Solvent extraction and ion exchange, 15*(4), 665-688.

Rengasamy, P., & Marchuk, A. (2011). Cation ratio of soil structural stability (CROSS).(Short Communication)(Report). *Soil Research, 49*(3), 280.

Rhoades, J. (1982). *Cation Exchange Capacity*. Wisconsin: ASA-SSA.

Rice, C. A., Ellis, M. S., & Bullock Jr, J. H. (2000). Water co-produced with coalbed methane in the Powder River basin, Wyoming; preliminary compositional data: US Department of the Interior, US Geological Survey.

Rice, C. A., & Nuccio, V. F. (2000). *Water produced with coal-bed methane*: US Geological Survey and US Department of the Interior.

Richard, U., Fabiana, R., Shevchenko, E., Spelta, A., & Sretenovic, N. (2011). Water Produced in Coal Bed Methane Recovery: Norwegian University of Science and Technology, Department of Petrolium and Applied Geophysics.

Richard, U., Rotelli, F, Shevchenko, E, Spelta, a, Sretenovic, N. (2011). Water Produced in Coal Bed Methane Revovery. *Norwegian University of Science and Technology, Department of Petrolium and Applied Geophysics, TPG 4140 - Natural Gas*.

Ross, C., Darby, P., Mudd, G. M., John, A. S., Lesman, B., & Macreadie, R. (2013). Unconventional gas: coal seam gas, shale gas and tight gas. Victoria, Australia.

Sajtar, E. T., & Bagley, D. M. (2009). Electrodialysis reversal: Process and cost approximations for treating coal-bed methane waters. *Desalination and Water Treatment, 2*(1-3), 284-294.

Schraufnagel, R. A. (1993). Coalbed methane production. *Hydrocarbons from coal: AAPG Studies in Geology, 38*, 341-359.

Semmens, M., Klieve, J., Schnobrich, D., & Tauxe, G. W. (1981). Modeling ammonium exchange and regeneration on clinoptilolite. *Water Research, 15*(6), 655-666. doi: 10.1016/0043-1354(81)90157-3

Semmens, M. J., & Martin, W. P. (1988). The influence of pretreatment on the capacity and selectivity of clinoptilolite for metal ions. *Water Research, 22*(5), 537-542. doi: 10.1016/0043-1354(88)90052-8

Shoumkova, A. (2011). Zeolites for water and wastewater treatment: An overview. *Research Bulletin of the Australian Institute of High Energetic Materials. Special Issue on Global Fresh Water Shortage, 2*(10).

Silva, F. F., Wallach, R., & Chen, Y. (1993). Hydraulic properties of sphagnum peat moss and tuff (scoria) and their potential effects on water availability. *Plant and Soil, 154*(1), 119-126. doi: 10.1007/BF00011080

Spiridonov, A., Sokolova, M., Okhlopkova, A., Koryakina, V., Shits, E. Y., Argunova, A., & Nikiforov, L. (2015). A study of the ion exchange effect on the sorption properties of heulandite-clinoptilolite zeolite. *Journal of Structural Chemistry, 56*(2), 297-303.

Sposito, G., Holtzclaw, K. M., Jouany, C., & Charlet, L. (1983). Cation selectivity in sodium-calcium, sodium-magnesium, and calcium-magnesium exchange on Wyoming bentonite at 298 K. *Soil Science Society of America Journal, 47*(5), 917-921.

Stearman, W., Taulis, M., Smith, J., & Corkeron, M. (2014). Assessment of geogenic contaminants in water co-produced with coal seam gas extraction in Queensland, Australia: implications for human health risk. *Geosciences, 4*(3), 219-239.

Stylianou, M. A., Hadjiconstantinou, M. P., Inglezakis, V. J., Moustakas, K. G., & Loizidou, M. D. (2007). Use of natural clinoptilolite for the removal of lead, copper and zinc in fixed bed column. *Journal of Hazardous Materials, 143*(1), 575-581. doi: 10.1016/j.jhazmat.2006.09.096

Tang, J. Y., Taulis, M., Edebeli, J., Leusch, F. D., Jagals, P., Jackson, G. P., & Escher, B. I. (2014). Chemical and bioanalytical assessment of coal seam gas associated water. *Environmental Chemistry, 12*(3), 267-285.

Taulis, M. (2007). *Groundwater Characterisation and Disposal Modelling for Coal Seam Gas Recovery.* (PhD), University of Canterbury, New Zealand.

Taulis, M. (2011). Ion Exchange Processes and CSG Water: Problems and Solutions. Queensland University of Technology: QUT isr.

Taulis, M., & Milke, M. (2007). Coal Seam Gas Water from Maramarua, New Zealand: Characterisation and Comparison to United States Analogues. *Journal of Hydrology (New Zealand), 46*(1), 1-17.

Taulis, M., & Milke, M. (2009). *Sodium removal from Maramarua CSG waters using Ngakuru zeolites.* Paper presented at the Water New Zealand's Annual Conference & Expo Rotorua, New Zealand.

Taulis, M., & Milke, M. (2012). Chemical variability of groundwater samples collected from a coal seam gas exploration well, Maramarua, New Zealand. *Water Research.* doi: 10.1016/j.watres.2012.11.003

Taylor, M., Sandy, N., & Raphael, B. (2013). Background paper on community concerns in relation to coal seam gas. *Report commissioned for the independent review of coal seam gas activities in NSW by the NSW Chief Scientist & Engineer: University of Western Sydney.*

Thomas, G. W. (1982). Exchangeable Cations *Methods of Soil Analysis Part 2*. Lexington, Kentucky: ASA-SSSA.

Thomas, W. J., & Crittenden, B. D. (1998). *Adsorption technology and design* (Vol. Elsevier Science & Technology Books): Butterworth-Heinemann.

Townsend, R. P. (1986). Ion Exchange in Zeolites: Some Recent Developments in Theory and Practice. *Studies in Surface Science and Catalysis, 28*, 273-282. doi: 10.1016/S0167-2991(09)60883-1

Townsend, R. P., & Coker, E. N. (2001). Ion Exchange in Zeolites. In H. van Bekkum, E. M. Flanigen, P. A. Jacobs & J. C. Jansen (Eds.), *Introduction to zeolite science and practice* (2 ed., Vol. 137, pp. 467-534): Amsterdam, New York : Elsevier.

Vacher, C., White, S., Eberhard, J., Schmidt, E., Huth, N., & Antille, D. (2014). *Quantifying the impacts of coal seam gas (CSG) activities on the soil resource of agricultural lands in Queensland, Australia.* Paper presented at the Proceedings of the American Society of Agricultural and Biological Engineers Annual International Meeting (ASABE 2014).

Valero, F., Barceló, A., & Arbós, R. (2011). *Electrodialysis technology-theory and applications*: INTECH Open Access Publisher.

Van De Graaff, R., & Patterson, R. A. (2001, 25-27 September). *Explaining the Mysteries of Salinity, Sodicity, SAR and ESP in On-site Practice.* Paper presented at the On-site '01 Conference: Advancing On-site Wastewater Systems, Armidale NSW Australia.

Van De Lisdonk, C. a. C., Van Paassen, J. a. M., & Schippers, J. C. (2000). Monitoring scaling in nanofiltration and reverse osmosis membrane systems. *Desalination, 132*(1), 101-108. doi: 10.1016/S0011-9164(00)00139-9

Van Voast, W. A. (2003). Geochemical signature of formation waters associated with coalbed methane. *AAPG bulletin, 87*(4), 667-676.

Vance, G. F., Ganjegunte, G. K., & Surdam, R. C. (2007). Innovative Technology Development to Maximize Beneficial Use of Produced Water from Coal Bed Natural Gas Operations in the Powder River Basin, Wyoming.

Venkatesan, A., & Wankat, P. C. (2011). Simulation of ion exchange water softening pretreatment for reverse osmosis desalination of brackish water. *Desalination, 271*(1), 122-131. doi: 10.1016/j.desal.2010.12.022

Wachinski, A. M. (2006). *Ion exchange treatment for water*. Denver, CO: American Water Works Association (AWWA).

Wang, S., & Peng, Y. (2010). Natural zeolites as effective adsorbents in water and wastewater treatment. *Chemical Engineering Journal, 156*(1), 11-24. doi: 10.1016/j.cej.2009.10.029

Wang, X., & Nguyen, A. V. (2016). Characterisation of electrokinetic properties of clinoptilolite before and after activation by sulphuric acid for treating CSG water. *Microporous and Mesoporous Materials, 220*, 175-182.

Wang, X., Ozdemir, O., Hampton, M. A., Nguyen, A. V., & Do, D. D. (2012). The effect of zeolite treatment by acids on sodium adsorption ratio of coal seam gas water. *Water Research, 46*(16), 5247-5254. doi: 10.1016/j.watres.2012.07.006

Watanabe, Y., Yamada, H., Kokusen, H., Tanaka, J., Moriyoshi, Y., & Komatsu, Y. (2003). Ion Exchange Behavior of Natural Zeolites in Distilled Water, Hydrochloric Acid, and Ammonium Chloride Solution. *Separation Science and Technology, 38*(7), 1519-1532. doi: 10.1081/SS-120019090

Wen, D., Ho, Y.-S., & Tang, X. (2006). Comparative sorption kinetic studies of ammonium onto zeolite. *Journal of Hazardous Materials, 133*(1), 252-256. doi: 10.1016/j.jhazmat.2005.10.020

Williams, J., Stubbs, T., & Milligan, A. (2012a). An analysis of coal seam gas production and natural resource management in Australia. Canberra, Australia: The Australian Council of Environmental Deans and Directors.

Williams, J., Stubbs, T., & Milligan, A. (2012b). An analysis of coal seam gas production and natural resource management in Australia: Issues and ways forward.

Wingenfelder, U., Hansen, C., Furrer, G., & Schulin, R. (2005). Removal of heavy metals from mine waters by natural zeolites. *Environmental science & technology, 39*(12), 4606.

Worch, E. (2008). Fixed-bed adsorption in drinking water treatment: a critical review on models and parameter estimation. *Journal of Water Supply: Research and Technology—AQUA, 57*(3), 171-183.

Worch, E. (2012). *Adsorption Technology in Water Treatment: Fundamentals, Processes, and Modeling* (Vol. Walter de Gruyter GmbH & Co. KG, Berlin/Boston). Germany: De Gruyter.

Wu, Z., An, Y., Wang, Z., Yang, S., Chen, H., Zhou, Z., & Mai, S. (2008). Study on zeolite enhanced contact–adsorption regeneration–stabilization process for nitrogen removal. *Journal of Hazardous Materials, 156*(1), 317-326. doi: 10.1016/j.jhazmat.2007.12.029

Xu, Z., Cai, J.-G., & Pan, B.-C. (2013). Mathematically modeling fixed-bed adsorption in aqueous systems. *Journal of Zhejiang University SCIENCE A, 14*(3), 155-176.

Yazdani, M., Mohammad Mahmoodi, N., Arami, M., & Bahrami, H. (2012). Isotherm, Kinetic, and Thermodynamic of Cationic Dye Removal from Binary System by Feldspar. *Separation Science and Technology, 47*(11), 1660-1672. doi: 10.1080/01496395.2011.654169

Yusaf, T., Hamawand, I., Schmidt, E., Binnie, J., Rees, S., & Chakrabarty, S. (2014). Coals seam gas (CSG) in agriculture–A review: Technical and market analysis for Australia. *Sustainable Energy Technologies and Assessments, 8*, 149-158.

Zaidi, S. (2012). Zeolites as inorganic ion exchangers for environmental applications: an overview *Ion Exchange Technology II* (pp. 183-215): Springer.

Zhao, H., Vance, G. F., Ganjegunte, G. K., & Urynowicz, M. A. (2008). Use of zeolites for treating natural gas co-produced waters in Wyoming, USA. *Desalination, 228*(1), 263-276. doi: 10.1016/j.desal.2007.08.014

Zhao, H., Vance, G. F., Urynowicz, M. A., & Gregory, R. W. (2009). Integrated treatment process using a natural Wyoming clinoptilolite for remediating produced waters from coalbed natural gas operations. *Applied Clay Science, 42*(3), 379-385. doi: 10.1016/j.clay.2008.03.007

# Appendices

## Appendix A. Composition of CSG water from Bowen Basin research site laboratory results

Proficiency tested by Aust. Soil & Plant Analysis Council

### Analysis of Water Sample

Client                                  Date

Source of water:

**RESULTS**

| Parameter | S1<br>Dam inlet | S2<br>side to middle | S3<br>right opp.corner | Units | Method |
|---|---|---|---|---|---|
| pH | 9.26 | 9.34 | 9.34 | units | APHA:4500 H$^+$ |
| Elect. cond. (EC) | 8.90 | 9.20 | 9.12 | dS m$^{-1}$ | APHA:2510 |
| Total dissolved solids TDS | 5960 | 6160 | 6110 | mg L$^{-1}$ | calculation |
| Total suspended solids TSS | 120 | 173 | 100 | mg L$^{-1}$ | APHA:2540 |
| Salinity hazard | very high | very high | very high | | |
| Sodium (Na$^+$) | 1656 | 1657 | 1620 | mg L$^{-1}$ | APHA:3120 |
| Potassium (K$^+$) | 96.4 | 96.6 | 98.7 | mg L$^{-1}$ | APHA:3120 |
| Magnesium (Mg$^{2+}$) | 7.3 | 7.1 | 7.2 | mg L$^{-1}$ | APHA:3120 |
| Calcium (Ca$^{2+}$) | 5.7 | 5.2 | 5.2 | mg L$^{-1}$ | APHA:3120 |
| Sodium adsorption ratio SAR | 109 | 111 | 108 | | calculation |
| Alkalinity (pH 4.5) as CaCO$_3$ | 1100 | 1150 | 1150 | mg L$^{-1}$ | APHA:2320 |
| Hardness as CaCO$_3$ | 44 | 42 | 43 | mg L$^{-1}$ | APHA:2340 |
| Saturation Index @ 25$^o$C | +1.41 | −1.47 | −1.47 | | APHA 2330-B |
| Manganese (Mn$^{4+}$) | 0.006 | <0.005 | <0.005 | mg L$^{-1}$ | APHA:3120 |
| Aluminium (Al$^{3+}$) | <0.005 | <0.005 | <0.005 | mg L$^{-1}$ | APHA:3120 |
| Zinc (Zn$^{2+}$) | <0.005 | <0.005 | <0.005 | mg L$^{-1}$ | APHA:3120 |
| Copper (Cu$^{2+}$) | <0.005 | <0.005 | <0.005 | mg L$^{-1}$ | APHA:3120 |
| Reactive phosphorus (PO$_4^{3-}$) | 0.37 | 0.38 | 0.37 | mg L$^{-1}$ | APHA 4110B |
| Total phosphorus (P) | 2.12 | 0.874 | 0.817 | mg L$^{-1}$ | APHA 4500 P E |
| Sulphur (SO$_4^=$-S) | 2.60 | 2.54 | 2.40 | mg L$^{-1}$ | APHA 4110B |
| Iron (Fe$^{2+}$) | <0.005 | <0.005 | <0.005 | mg L$^{-1}$ | APHA:3120 |
| Fluoride (F$^-$) | 2.89 | 2.76 | 2.90 | mg L$^{-1}$ | APHA 4110B |
| Bromide (Br$^-$) | <0.02 | <0.02 | <0.02 | mg L$^{-1}$ | APHA 4110B |

<0.x = measured but reading below detection level          mg L$^{-1}$ = part per million
**Reference:** APHA, 2005 Standard Methods for the Examination of Water and Wastewater. 21$^{st}$ Edition

CPSS   Soil survey and analytical assessments, landscape analysis and plant nutrient relationships
Qualified IS014000 environmental management systems consultants

**General comments.**
## RESULTS

| Parameter | S1<br>*Dam inlet* | S2<br>*side to middle* | S3<br>*right opp.corner* | | Units | Method |
|---|---|---|---|---|---|---|
| Chloride (Cl⁻) | 3615 | 3535 | 3765 | | mg L⁻¹ | APHA 4110B |
| Strontium (Sr) | 2.40 | 2.37 | 2.39 | | mg L⁻¹ | APHA:3120 |
| Barium ($Ba^{2+}$) | 0.562 | 0.545 | 0.560 | | mg L⁻¹ | APHA:3120 |
| Ammonia (NH3) | <0.02 | 0.19 | <0.02 | | mg L⁻¹ | APHA 4500-NH₃ C |
| Nitrate ($NO_3^- -N$) | 7.76 | 8.24 | 7.97 | | mg L⁻¹ | APHA 4110B |
| TKN | 1.96 | 2.24 | 2.24 | | mg L⁻¹ | APHA 4500-N₀ᵣₚ C |
| Total nitrogen (TN) | 9.73 | 10.5 | 10.2 | | mg L⁻¹ | calculation |
| Chemical oxygen demand | 32 | 40 | 24 | | mg L⁻¹ | APHA 5220 D |
| Total solids (TS) | 0.72 | 0.77 | 0.73 | | mg L⁻¹ | APHA 2540 D |
| Non-volatile (fixed) solids | 90.5 | 90.0 | 91.1 | | % | APHA 2540 E |
| Volatile solids | 9.5 | 10.0 | 8.9 | | % | APHA 2540 E |
| | | | | | | |
| | | | | | | |
| | | | | | | |
| Arsenic | 0.021 | 0.016 | 0.18 | | mg L⁻¹ | APHA:3120 |
| Cadmium | <0.005 | <0.005 | <0.005 | | mg L⁻¹ | APHA:3120 |
| Chromium | 0.014 | 0.032 | 0.029 | | mg L⁻¹ | APHA:3120 |
| Lead | <0.005 | 0.008 | 0.007 | | mg L⁻¹ | APHA:3120 |
| Silicon | 1.07 | 1.21 | 11.7 | | mg L⁻¹ | APHA:3120 |
| | | | | | | |
| | | | | | | |
| | | | | | | |
| | | | | | | |
| | | | | | | |
| | | | | | | |
| | | | | | | |
| | | | | | | |

<0.x = measured but reading below detection level          mg L⁻¹ = part per million
**Reference:** APHA, 2005 Standard Methods for the Examination of Water and Wastewater, 21ˢᵗ Edition

**General comments.**

Soil survey and analytical assessments, landscape analysis and plant nutrient relationships
Qualified IS014000 environmental management systems consultants

198                                                                                          Appendices

**Western Radiation Services**
analytical laboratory & consulting

ABN 64 135 436 092

Accredited Laboratory
No: 14174

Ref:
Order No:
Page 1 of 2

**ANALYTICAL REPORT**

The results (to 95%, 2σ confidence level) for Gross Alpha Beta, Radium-226, Radium-228 & Thorium-228 analyses of one (1) liquid sample

The Gross Beta results have been corrected for Potassium-40 concentrations. Potassium analysis was done by ARL (NATA Accreditation No:2377).

The results of other analyses are provided as an attachment to this report. For those MDL's and methods, please refer to the report of the originating laboratories.

| MDL: | Gross Alpha | 60 mBq/l | Gross Beta | 135 mBq/l |
|------|-------------|----------|------------|-----------|
|      | Radium-226  | 0.003 Bq/l | Radium-228 | 0.100 Bq/l |
|      | Thorium-228 | 0.100 Bq/l |            |           |

| Methods: | LTP No.16 | Gross Alpha/Beta Analysis-Liquid Scintillation Counting |
|----------|-----------|----------------------------------------------------------|
|          | LTP No. 3 | Radium 226 Analysis-Liquids |
|          | LTP No. 4(a) | Gamma Spectrometry Analysis |
|          | ICPMS     | Inductively Coupled Plasma Mass |

Signature redacted

Madassar A. Qureshi
Authorised Signatory

**Realtime**
Group Limited    solutions for today and tomorrow

Mackay Office: Lot J Mackay Marina
Mackay Qld 4740
**Tel:** 61 7 4955 5944
**Fax:** 61 7 4965 7099

Perth Office: 24 Brennan Way, Belmont W.A. 6104
**Tel:** 61 8 9475 0099
**Fax:** 61 8 9475 0165
**Email:** admin@westernradiation.com.au

**Gross Alpha and Beta -Liquid Scintillation Counting**

| WRS No. | Client Sample ID | Alpha (mBq/l) | Beta (mBq/l) | K (mg/l) |
|---|---|---|---|---|
| | Tank | <MDL | <MDL | 63 |

The reported expanded uncertainty of measurement is stated as the standard uncertainty of the measurement ± 7.5 %, multiplied by the coverage factor k=2, which corresponds to a coverage probability of approximately 95%.

**Radium 226 Analysis**

| WRS No | Client Sample ID | Ra-226 (Bq/l) |
|---|---|---|
| | Tank | 0.006 ± 0.004 |

The reported expanded uncertainty of measurement is stated as the standard uncertainty of the measurement ± 6 %, multiplied by the coverage factor k=2, which corresponds to a coverage probability of approximately 95%.

**Gamma Spectrometry Analysis**

| WRS No. | Client Sample ID | Ra-228 (Bq/l) | Th-228 (Bq/l) |
|---|---|---|---|
| | Tank | <MDL | <MDL |

The reported expanded uncertainty of measurement is stated as the standard uncertainty of the measurement ± 5.6 %, multiplied by the coverage factor k=2, which corresponds to a coverage probability of approximately 95%.

## Appendix B. SEM-EDS characterisation of zeolite and scoria material

### Natural zeolite
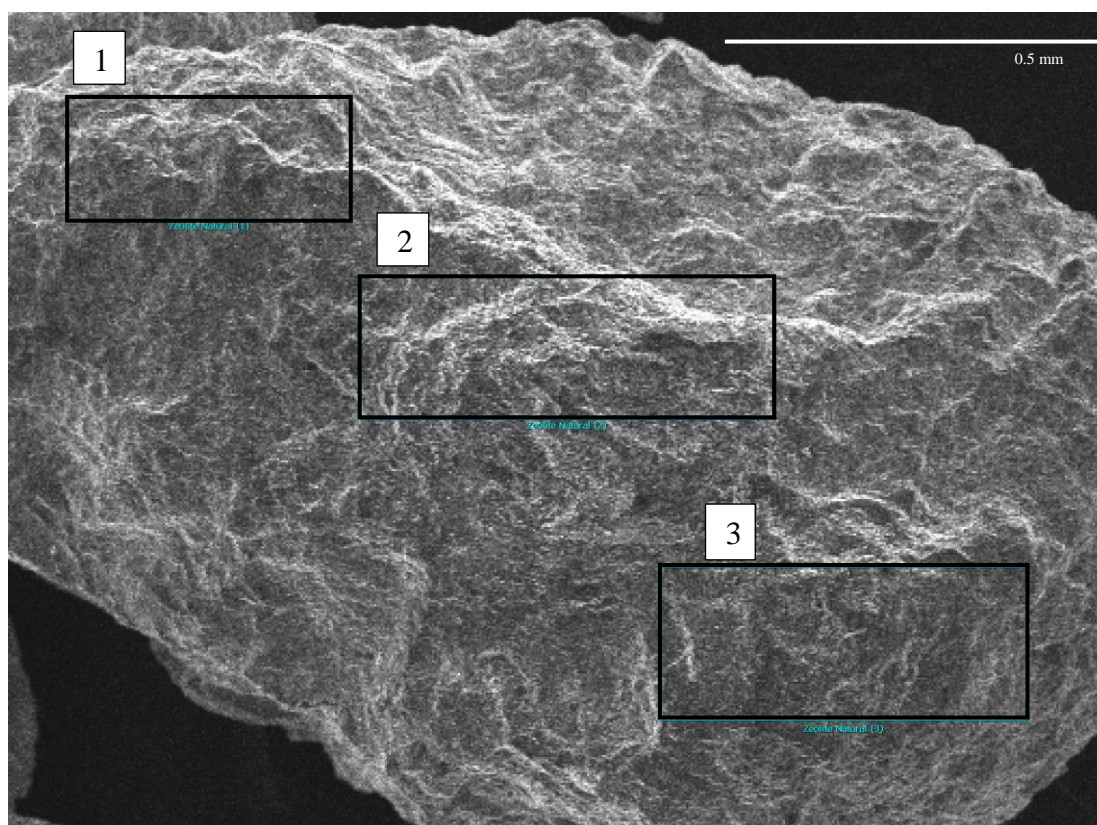


**Scanned areas for EDS elemental composition on natural zeolite.**

**EDS elemental composition (wt%) of natural zeolite for three locations.**

| Location | Na$_2$O | MgO | Al$_2$O$_3$ | SiO$_2$ | K$_2$O | CaO | FeO | Total |
|----------|---------|------|-------------|---------|--------|------|------|--------|
| 1 | 2.27 | 2.03 | 13.48 | 68.59 | 3.58 | 4.81 | 6.22 | 100.98 |
| 2 | 2.99 | 1.89 | 13.43 | 66.33 | 4.36 | 2.71 | 6.98 | 98.69 |
| 3 | 2.39 | 2.14 | 12.06 | 70.26 | 3.99 | 3.71 | 6.44 | 100.99 |
| Mean | 2.55 | 2.02 | 12.99 | 68.39 | 3.98 | 3.74 | 6.55 | 100.22 |
| Std. Dev. | 0.39 | 0.13 | 0.81 | 1.97 | 0.39 | 1.05 | 0.39 | |

**Potassium treated zeolite**
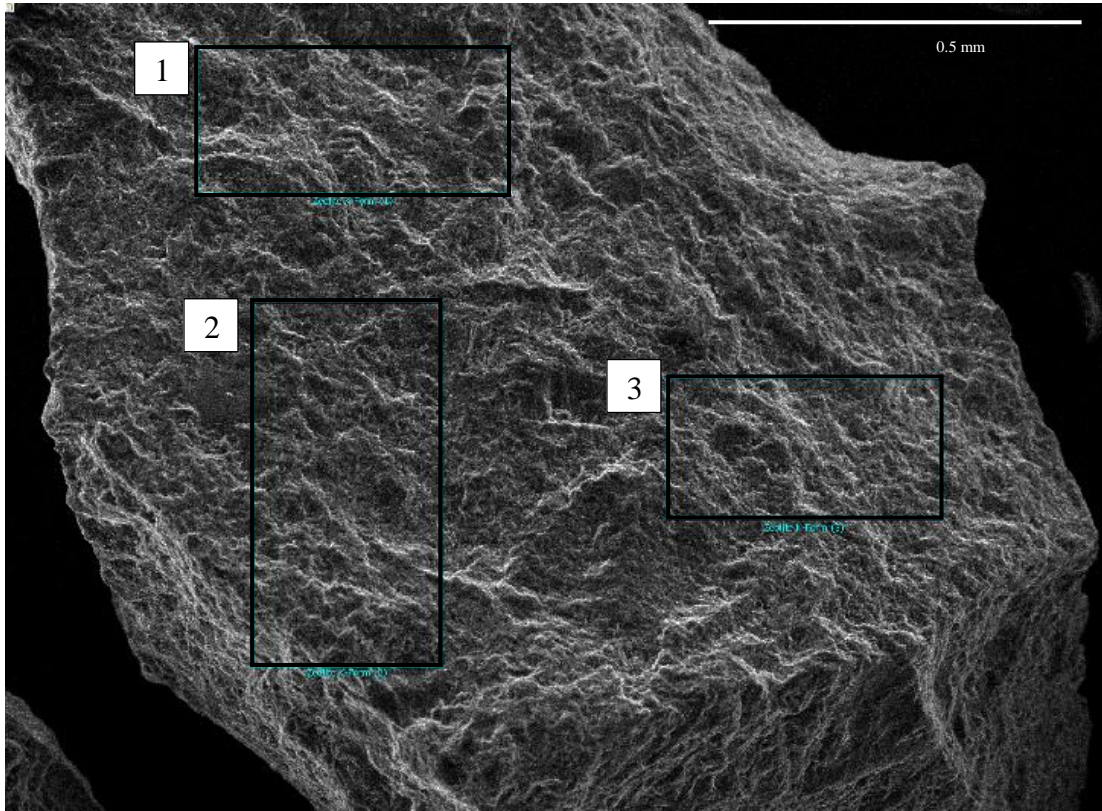


**Scanned areas for EDS elemental composition on potassium treated zeolite.**

**EDS elemental composition (wt%) of potassium treated zeolite for three locations.**

| Location | $Na_2O$ | $Al_2O_3$ | $SiO_2$ | $K_2O$ | CaO | FeO | Total |
|----------|---------|-----------|---------|--------|------|------|--------|
| 1 | 1.55 | 14.30 | 63.81 | 16.15 | 0.63 | 3.19 | 99.63 |
| 2 | 0.68 | 14.35 | 62.77 | 16.53 | 0.71 | 4.12 | 99.16 |
| 3 | 0.47 | 14.75 | 63.30 | 16.23 | 0.45 | 4.81 | 100.01 |
| Mean | 0.90 | 14.47 | 63.29 | 16.30 | 0.60 | 4.04 | 99.60 |
| Std. Dev. | 0.57 | 0.25 | 0.52 | 0.20 | 0.13 | 0.81 | |

### Acid treated zeolite
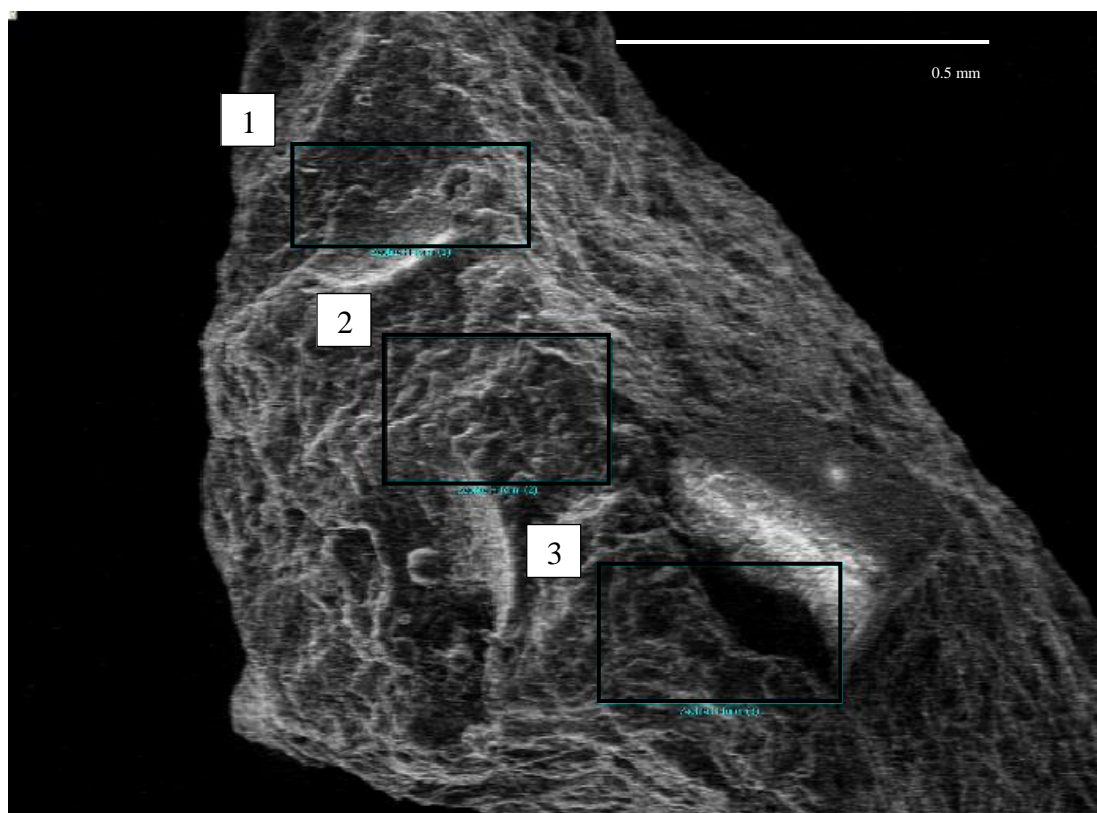


**Scanned areas for EDS elemental composition on potassium treated zeolite.**

**EDS elemental composition (wt%) of acid treated zeolite for three locations.**

| Location | $Na_2O$ | MgO | $Al_2O_3$ | $SiO_2$ | $K_2O$ | CaO | FeO | Total |
|----------|---------|------|-----------|---------|--------|------|------|--------|
| 1 | 2.66 | 3.38 | 13.12 | 70.93 | 1.75 | 4.78 | 3.78 | 100.40 |
| 2 | 2.94 | 3.21 | 17.06 | 69.47 | 1.34 | 4.19 | 2.56 | 100.77 |
| 3 | 2.17 | 4.63 | 13.02 | 71.55 | 1.56 | 4.27 | 2.83 | 100.03 |
| Mean | 2.59 | 3.74 | 14.40 | 70.65 | 1.55 | 4.41 | 3.06 | 100.40 |
| Std. Dev. | 0.39 | 0.78 | 2.30 | 1.07 | 0.21 | 0.32 | 0.64 | |

## Ammonium treated zeolite
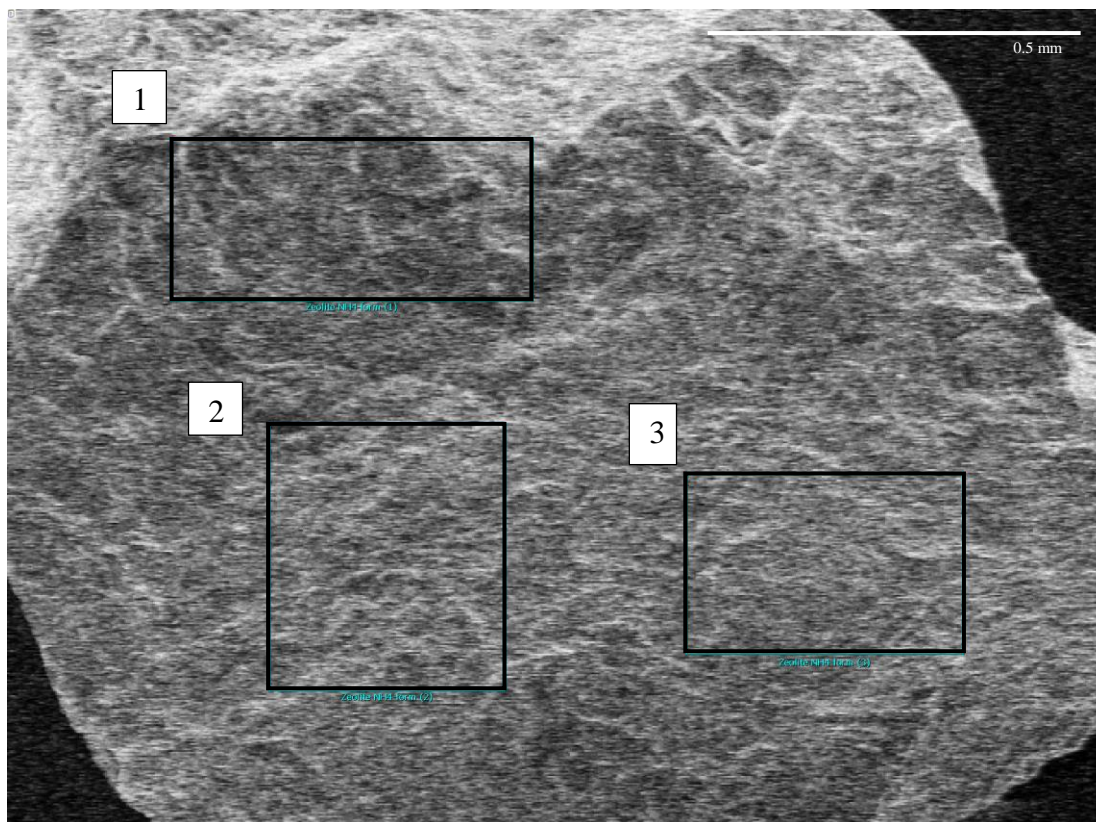


**Scanned areas for EDS elemental composition on ammonium treated zeolite.**

**EDS elemental composition (wt%) of ammonium treated zeolite for three locations.**

| Location | N | $Na_2O$ | $Al_2O_3$ | $SiO_2$ | $K_2O$ | CaO | FeO | Total |
|----------|-------|-------|-------|-------|-------|------|------|--------|
| 1 | 11.36 | 1.99 | 17.26 | 62.95 | 1.67 | 0.13 | 5.58 | 100.94 |
| 2 | 10.56 | 1.27 | 18.50 | 63.21 | 1.86 | 0.16 | 5.36 | 100.92 |
| 3 | 11.29 | 1.66 | 16.32 | 65.49 | 1.35 | 0.15 | 4.73 | 100.99 |
| Mean | 11.07 | 1.64 | 17.36 | 63.88 | 1.63 | 0.14 | 5.22 | 100.95 |
| Std. Dev. | 0.44 | 0.36 | 1.09 | 1.40 | 0.26 | 0.02 | 0.44 | |

**Scoria natural form**
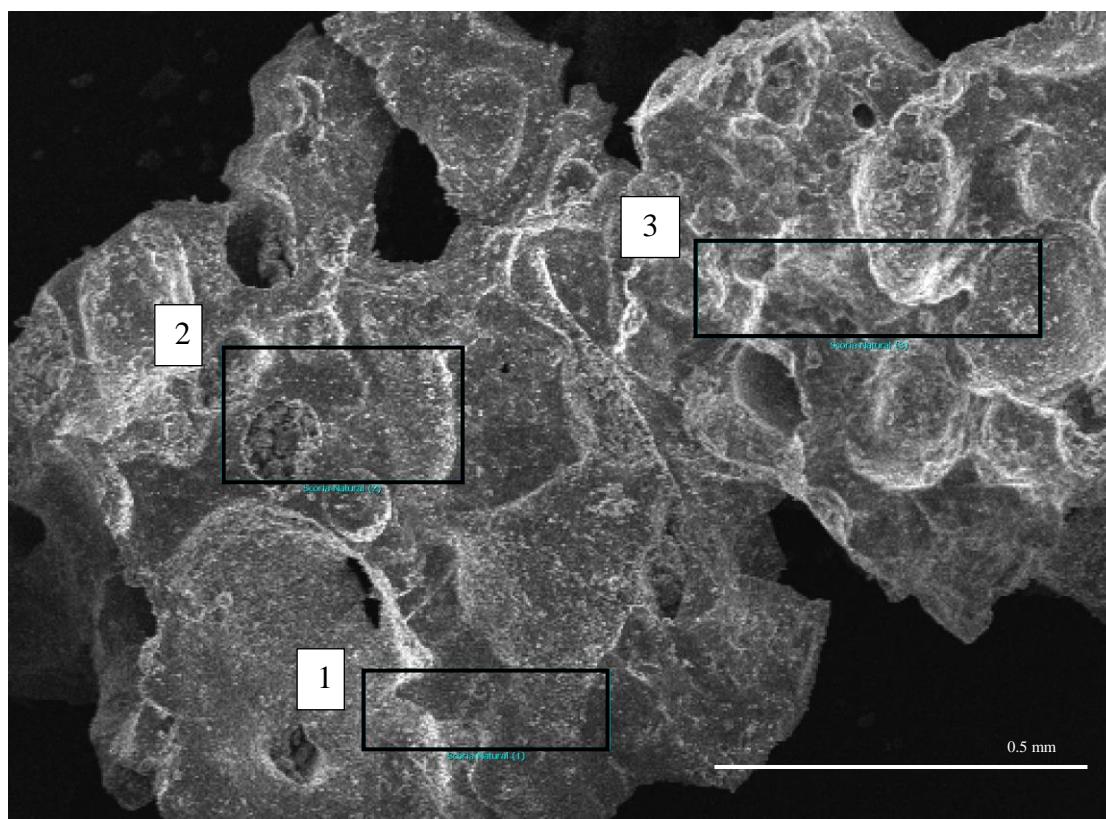


**Scanned areas for EDS elemental composition on natural scoria.**

**EDS elemental composition (wt%) of natural scoria material for three locations.**

| Location | Na$_2$O | MgO | Al$_2$O$_3$ | SiO$_2$ | K2O | CaO | FeO | Total |
|----------|---------|------|-------------|---------|------|------|-------|--------|
| 1 | 7.77 | 3.51 | 12.72 | 47.67 | 2.57 | 4.01 | 21.92 | 100.16 |
| 2 | 7.38 | 3.44 | 12.56 | 48.78 | 2.37 | 4.71 | 19.91 | 99.15 |
| 3 | 8.00 | 3.41 | 12.52 | 49.87 | 2.84 | 4.28 | 20.02 | 100.94 |
| Mean | 7.72 | 3.45 | 12.60 | 48.77 | 2.59 | 4.33 | 20.62 | 100.08 |
| Std. Dev. | 0.31 | 0.05 | 0.10 | 1.10 | 0.24 | 0.35 | 1.13 | |

## Potassium treated scoria
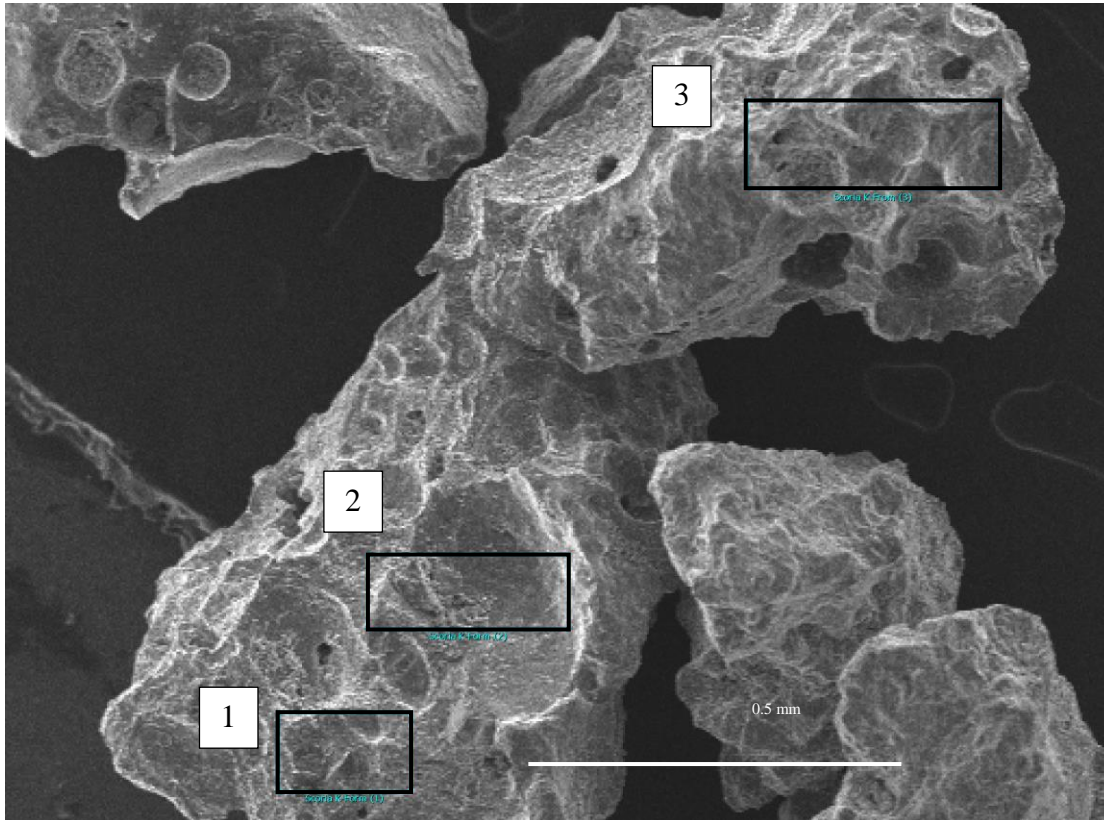


**Scanned areas for EDS elemental composition on potassium treated zeolite.**

**EDS elemental composition (wt%) of potassium treated scoria for three locations.**

| Location | $Na_2O$ | MgO | $Al_2O_3$ | $SiO_2$ | $K_2O$ | CaO | FeO | Total |
|----------|---------|------|-----------|---------|--------|------|-------|--------|
| 1 | 4.65 | 4.24 | 11.30 | 54.13 | 8.27 | 8.39 | 9.74 | 100.72 |
| 2 | 4.39 | 3.53 | 10.27 | 52.19 | 8.27 | 7.63 | 13.83 | 100.11 |
| 3 | 4.21 | 3.88 | 10.24 | 56.08 | 7.52 | 7.32 | 10.35 | 99.62 |
| Mean | 4.42 | 3.88 | 10.60 | 54.13 | 8.02 | 7.78 | 11.31 | 100.15 |
| Std. Dev. | 0.22 | 0.35 | 0.60 | 1.95 | 0.43 | 0.55 | 2.21 | |

**Acid treated scoria**
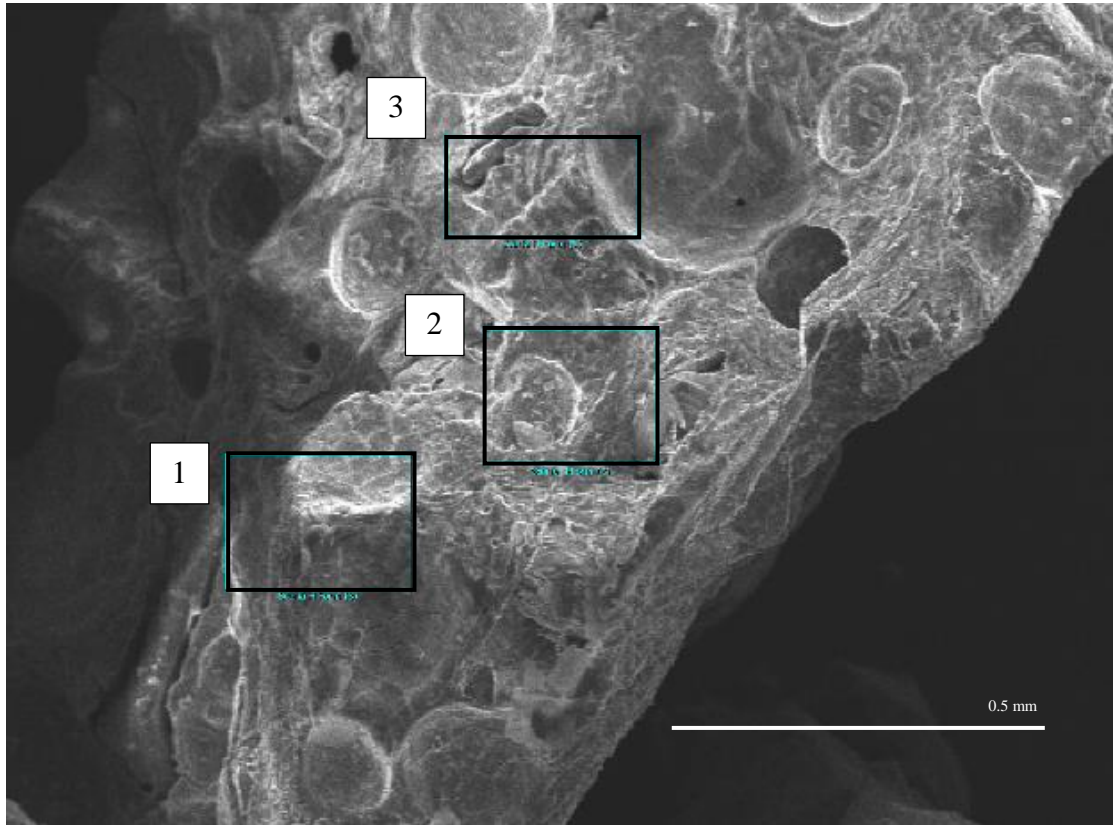


**Scanned areas for EDS elemental composition on acid treated zeolite.**

**EDS elemental composition (wt%) of acid treated scoria for three locations.**

| Location | Na$_2$O | MgO | Al$_2$O$_3$ | SiO$_2$ | K$_2$O | CaO | FeO | Total |
|----------|---------|------|-------------|---------|--------|------|------|--------|
| 1 | 9.59 | 5.10 | 11.49 | 57.32 | 1.67 | 7.24 | 8.11 | 100.52 |
| 2 | 9.28 | 4.85 | 11.56 | 57.97 | 2.66 | 6.44 | 7.47 | 100.23 |
| 3 | 9.72 | 4.59 | 11.59 | 57.90 | 2.91 | 6.44 | 6.51 | 99.66 |
| Mean | 9.53 | 4.85 | 11.55 | 57.73 | 2.41 | 6.71 | 7.36 | 100.14 |
| Std. Dev. | 0.22 | 0.26 | 0.05 | 0.36 | 0.66 | 0.46 | 0.81 | |

## Ammonium treated scoria
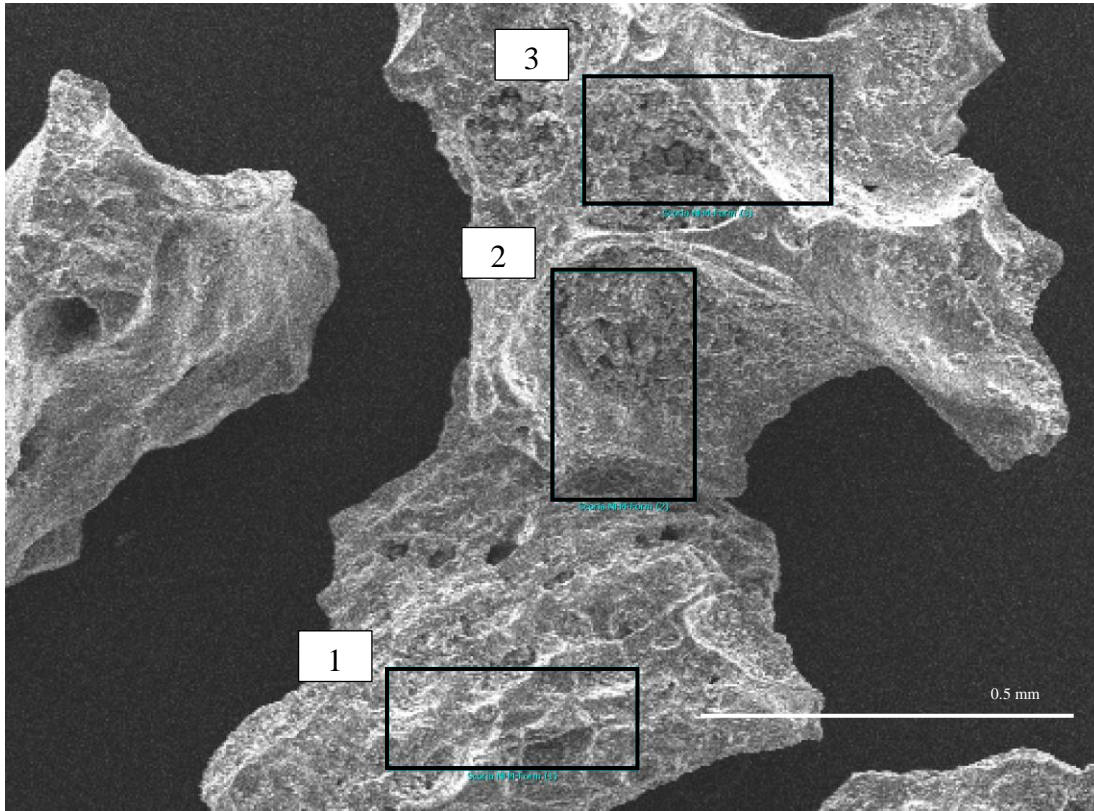


**Scanned areas for EDS elemental composition on ammonium treated zeolite.**

**EDS elemental composition (wt%) of ammonium treated scoria for three locations.**

| Location | N | $Na_2O$ | MgO | $Al_2O_3$ | $SiO_2$ | $K_2O$ | CaO | FeO | Total |
|---|---|---|---|---|---|---|---|---|---|
| 1 | 10.60 | 2.10 | 3.83 | 11.14 | 54.13 | 0.90 | 5.66 | 11.74 | 100.10 |
| 2 | 11.18 | 2.06 | 3.31 | 11.47 | 54.19 | 0.83 | 5.18 | 11.83 | 100.04 |
| 3 | 10.65 | 2.20 | 3.98 | 11.65 | 55.08 | 0.92 | 5.29 | 10.35 | 100.12 |
| Mean | 10.81 | 2.12 | 3.71 | 11.42 | 54.47 | 0.88 | 5.38 | 11.31 | 100.09 |
| Std. Dev. | 0.32 | 0.07 | 0.35 | 0.26 | 0.53 | 0.05 | 0.25 | 0.83 | |

**Appendix C. Na$^+$ adsorption and desorption of natural material with K$^+$ for batch experiments.**
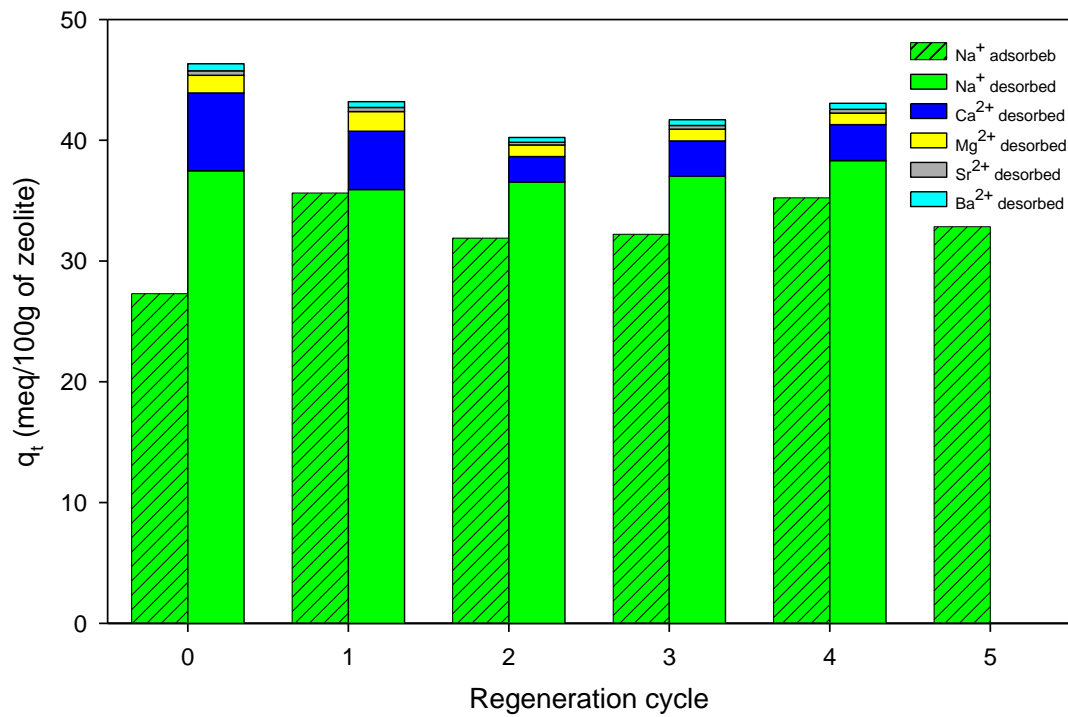


**Adsorption and desorption capacity of Na$^+$ onto zeolite with successive K$^+$ regeneration solutions using synthetic CSG water.**
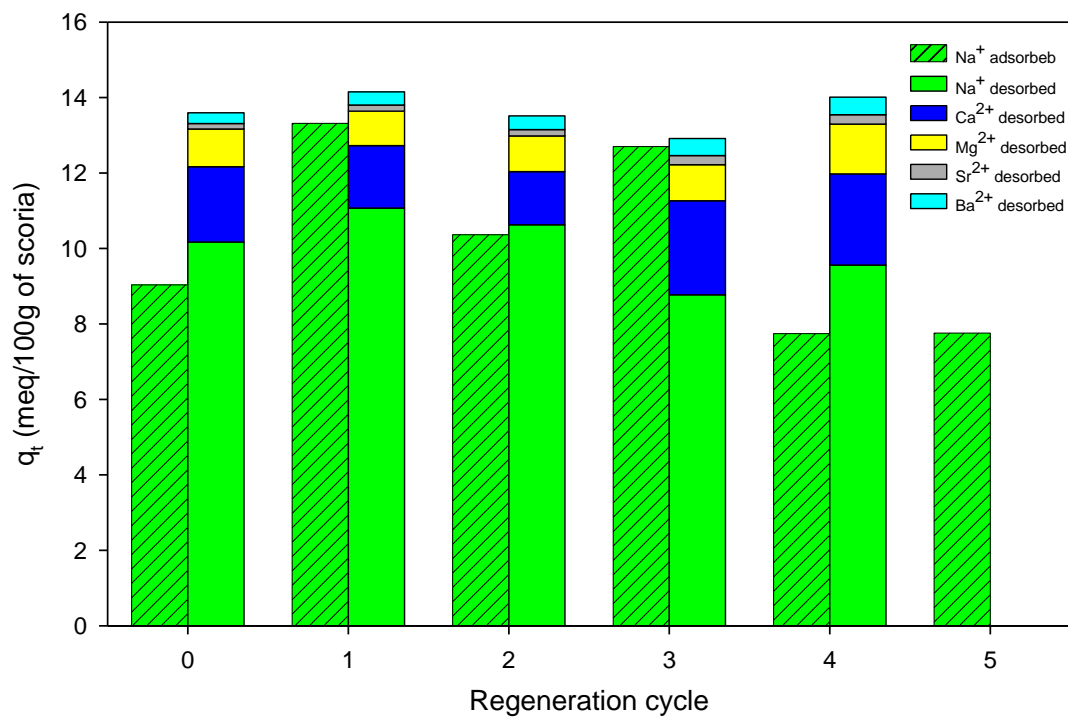


**Adsorption and desorption capacity of Na$^+$ onto scoria with successive K$^+$ regeneration solutions using synthetic CSG water.**
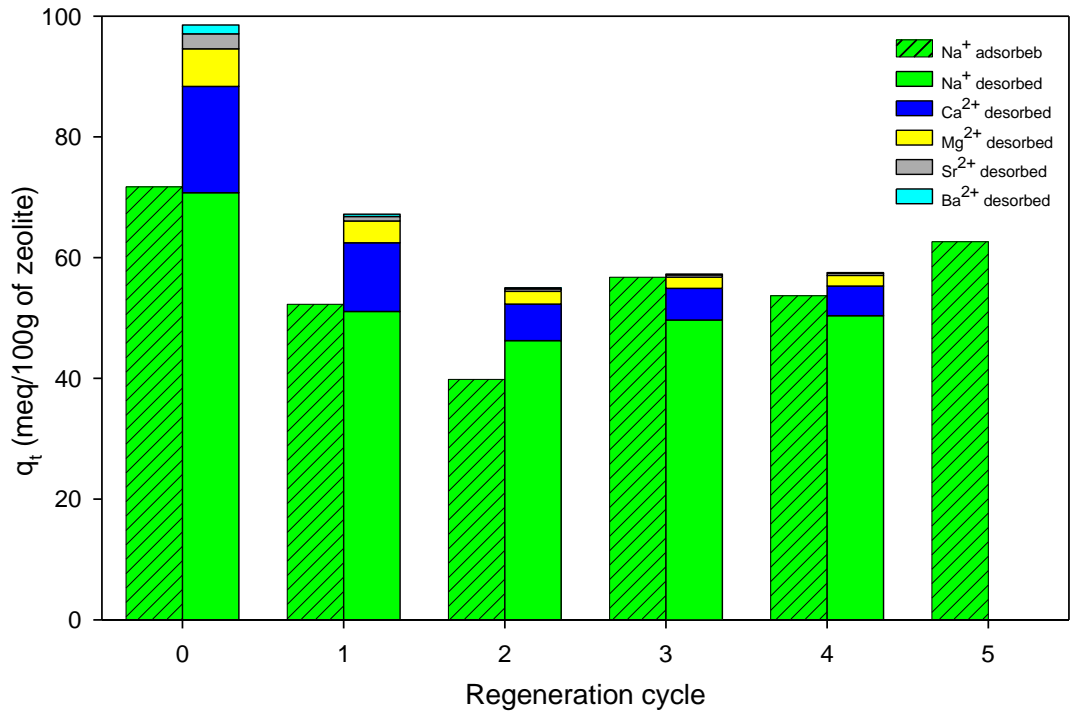
**Adsorption and desorption capacity of Na⁺ onto zeolite with successive K⁺ regeneration solutions using field CSG water.**
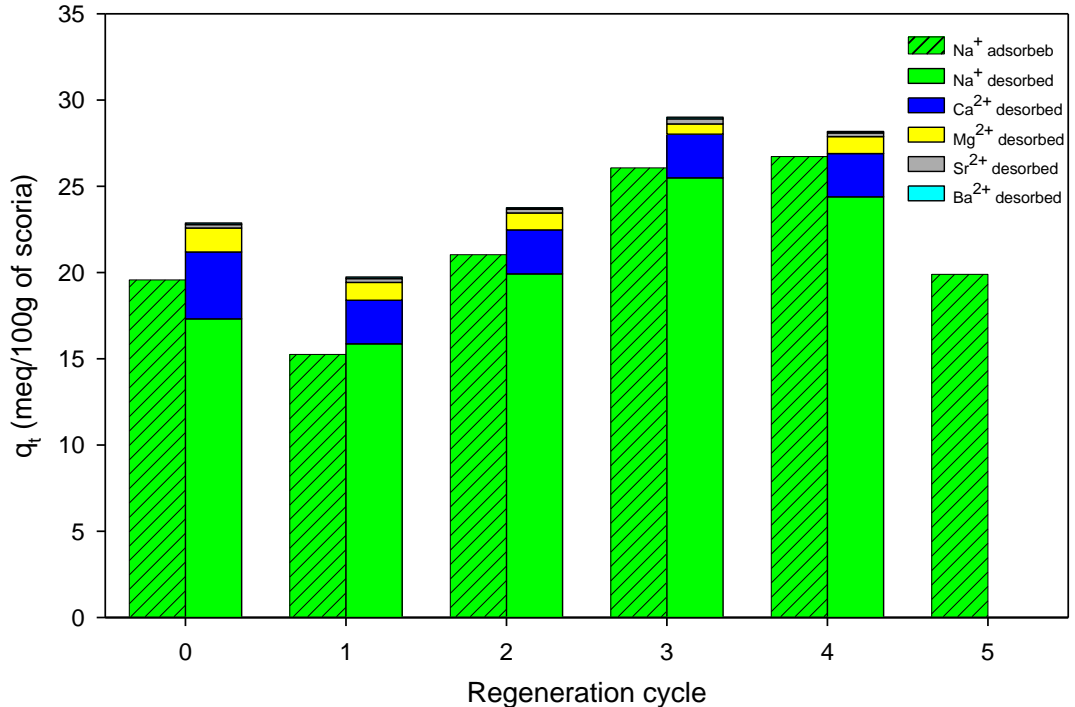


**Adsorption and desorption capacity of Na⁺ onto scoria with successive K⁺ regeneration solutions using field CSG water.**

# Appendix D. Na$^+$ breakthrough curves and adsorption/desorption of cations using fixed bed columns packed with scoria and zeolite materials.

Breakthrough curves of scoria and zeolite that demonstrate that flow misdistribution did not occur for three different volumetric flow rates, showing plug flow for all cases.
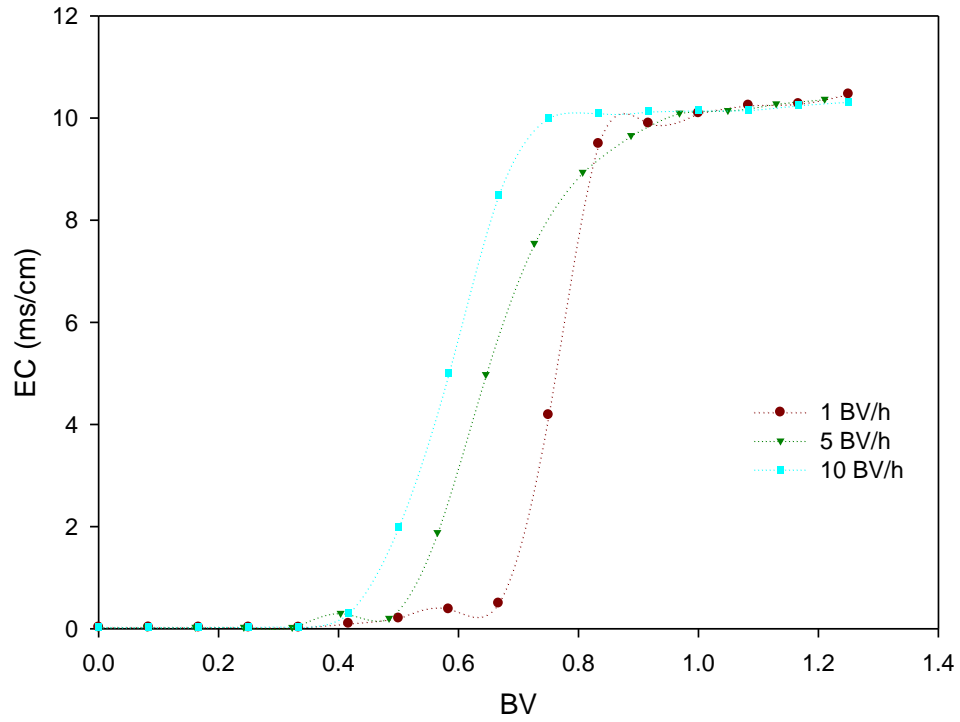


**Hydraulic performance for scoria at different flow rates showing and plug flow.**
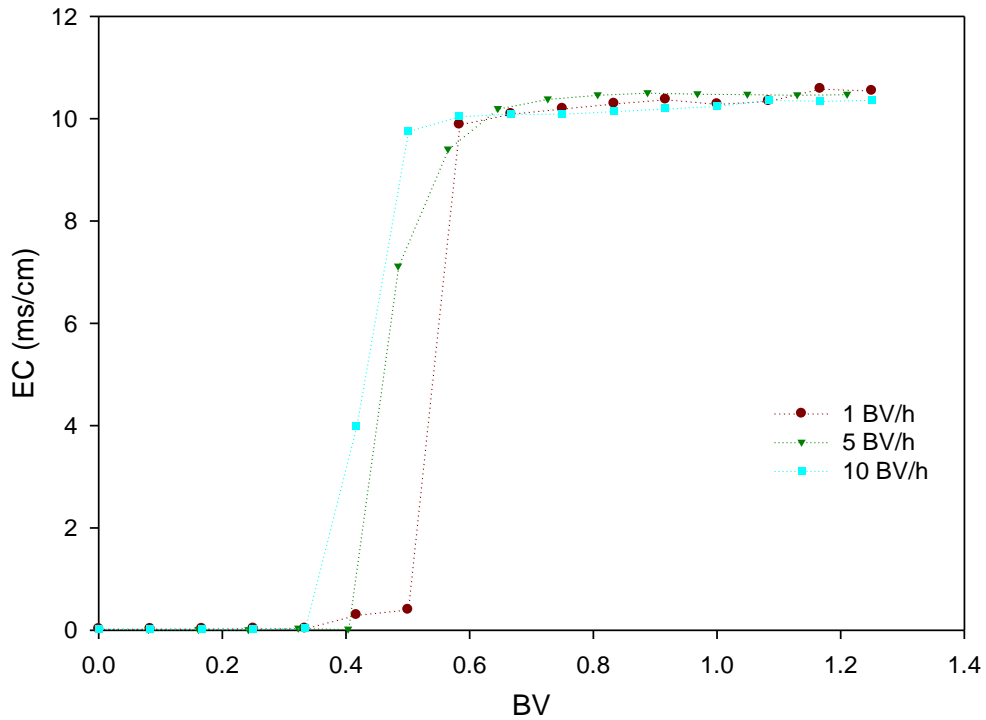


**Hydraulic performance for zeolite at different flow rates showing and plug flow.**

**Breakthrough curves for the adsorption of $Na^+$ from single cation solution by scoria treated and regenerated with $K^+$ solutions for four cycles.**
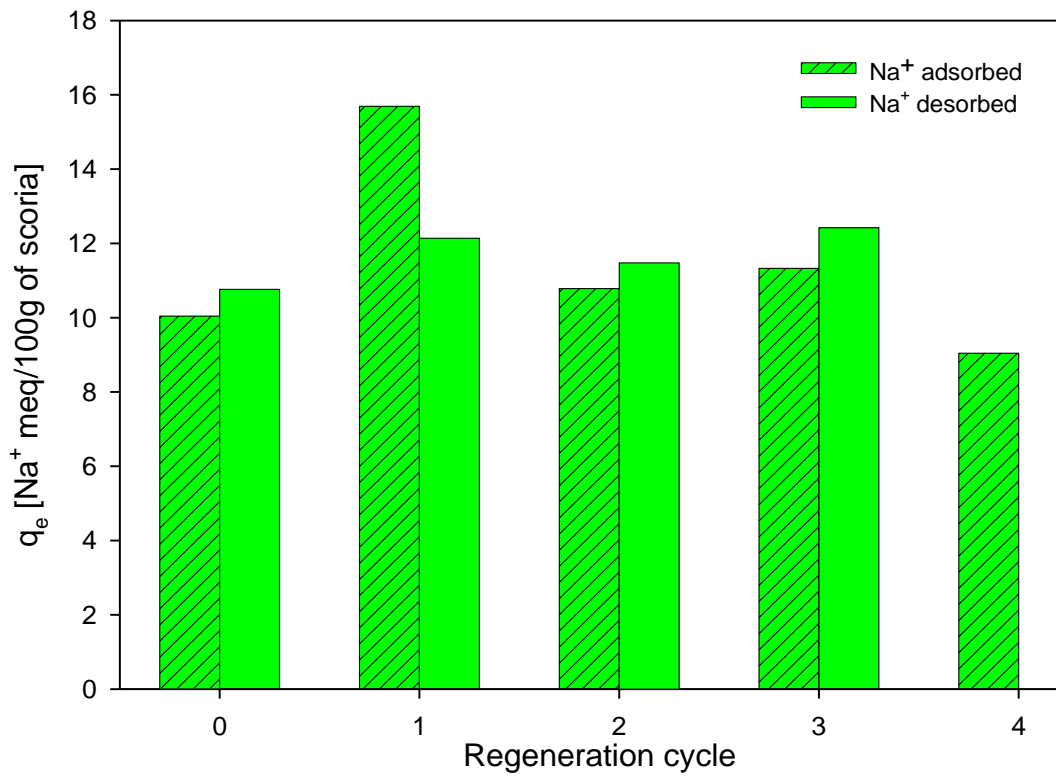


**Column adsorption and desorption of $Na^+$ from single ion solution by scoria at multiple regeneration cycles with $K^+$ solutions.**
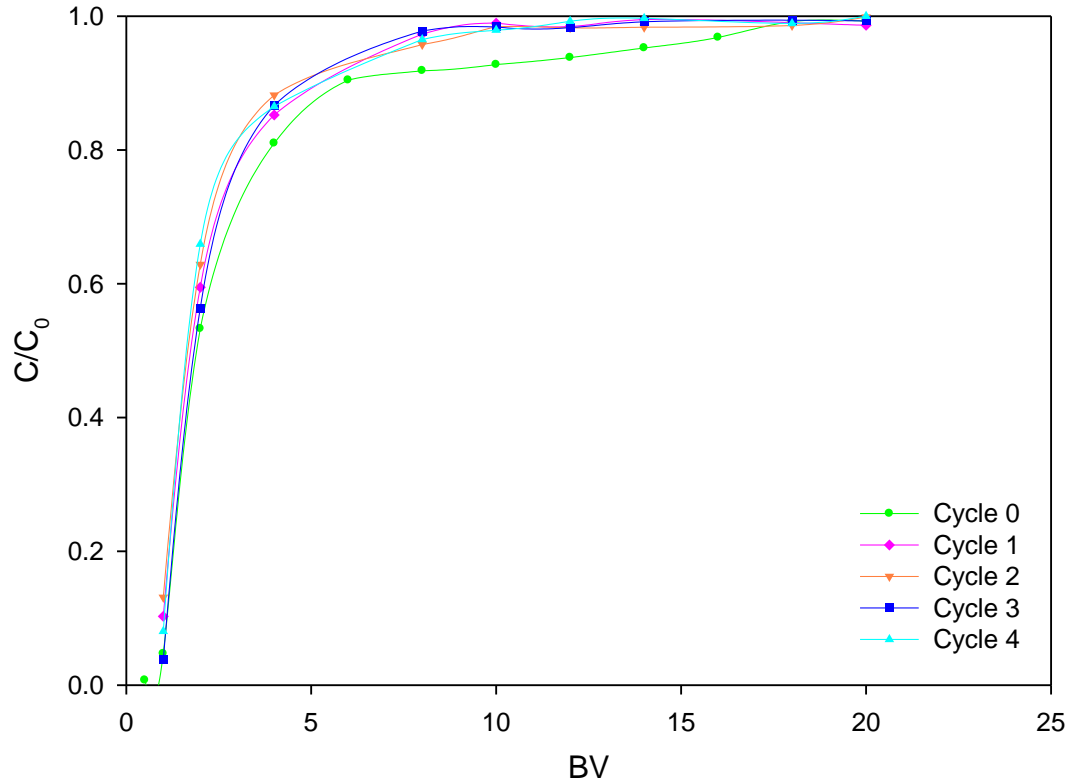
**Breakthrough curves for the adsorption of Na$^+$ from synthetic CSG solution by scoria treated and regenerated with K$^+$ solutions for four cycles.**
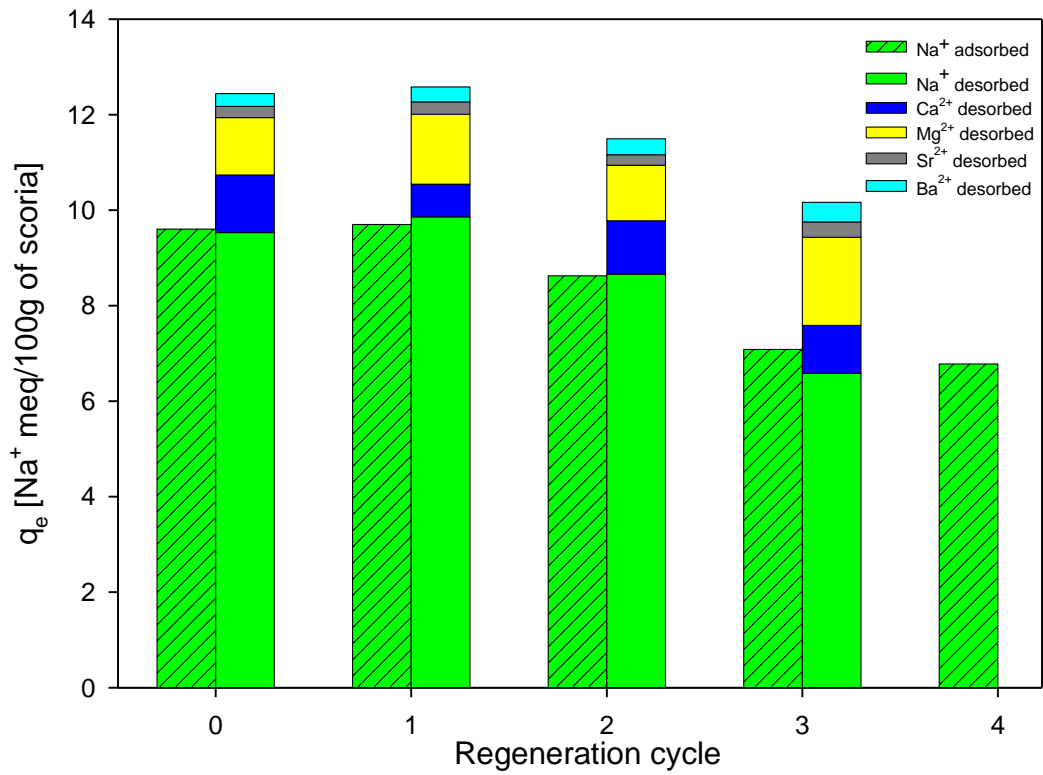


**Column adsorption and desorption of Na$^+$ from synthetic CSG solution by scoria at multiple regeneration cycles with K$^+$ solutions.**
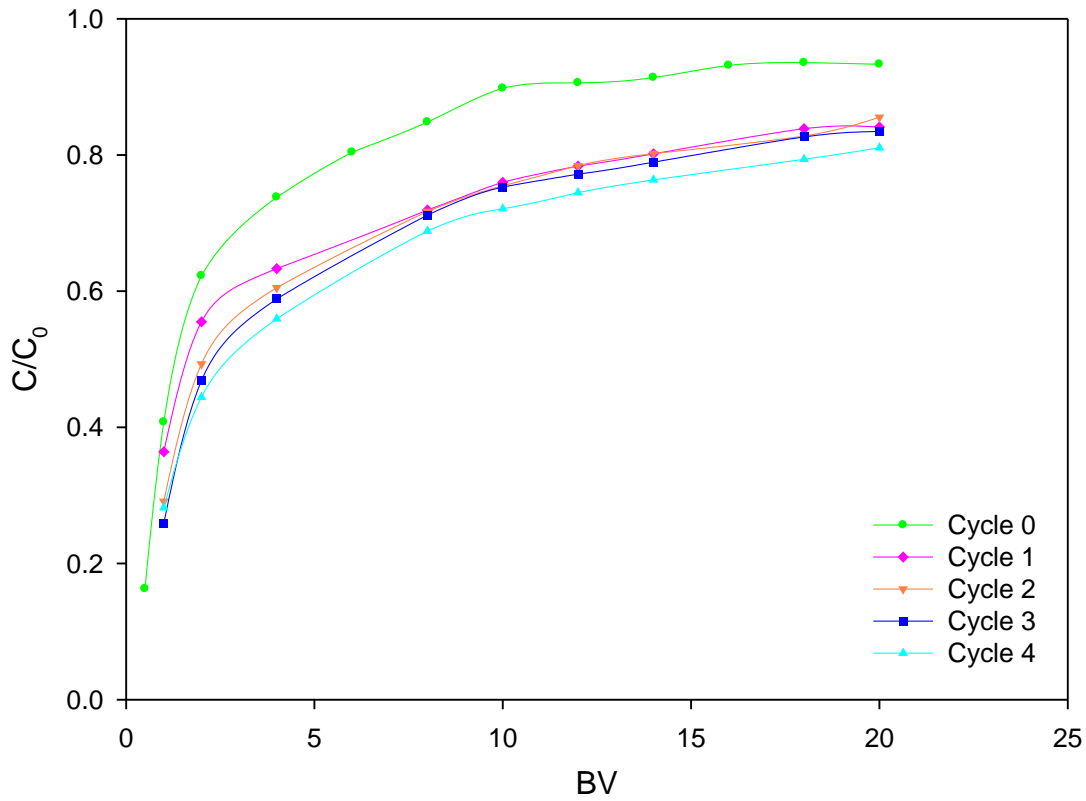
**Breakthrough curves for the adsorption of Na⁺ from single Na⁺ solution by zeolite treated and regenerated with K⁺ solutions for four cycles.**



**Column adsorption and desorption of Na⁺ from single ion solution by zeolite at multiple regeneration cycles with K⁺ solutions.**

**Breakthrough curves for the adsorption of Na$^+$ from synthetic CSG solution by zeolite treated and regenerated with K$^+$ solutions for four cycles.**



**Column adsorption and desorption of Na$^+$ from synthetic CSG solution by zeolite at multiple regeneration cycles with K$^+$ solutions.**
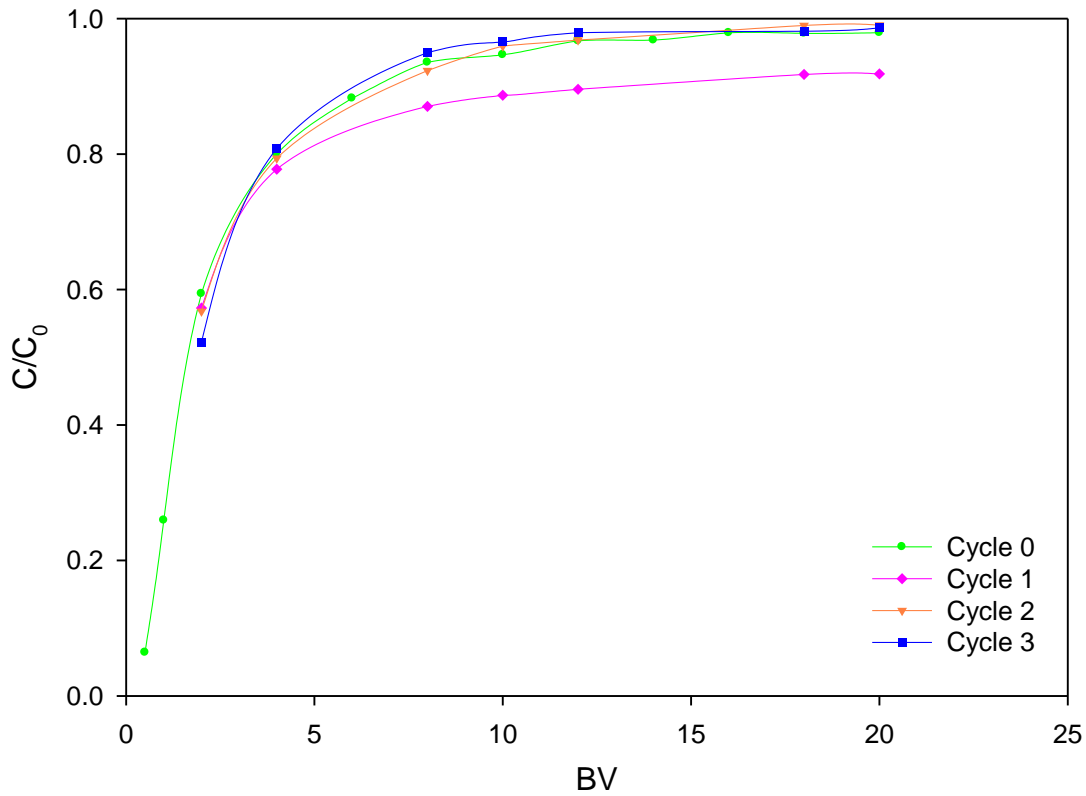
**Column adsorption and desorption of Na$^+$ from field CSG water by scoria at multiple regeneration cycles with K$^+$ solutions.**



**Column adsorption and desorption of Na$^+$ from field CSG water by scoria at multiple regeneration cycles with K$^+$ solutions.**

**Column adsorption and desorption of Na$^+$ from field CSG water by zeolite at multiple regeneration cycles with K$^+$ solutions.**
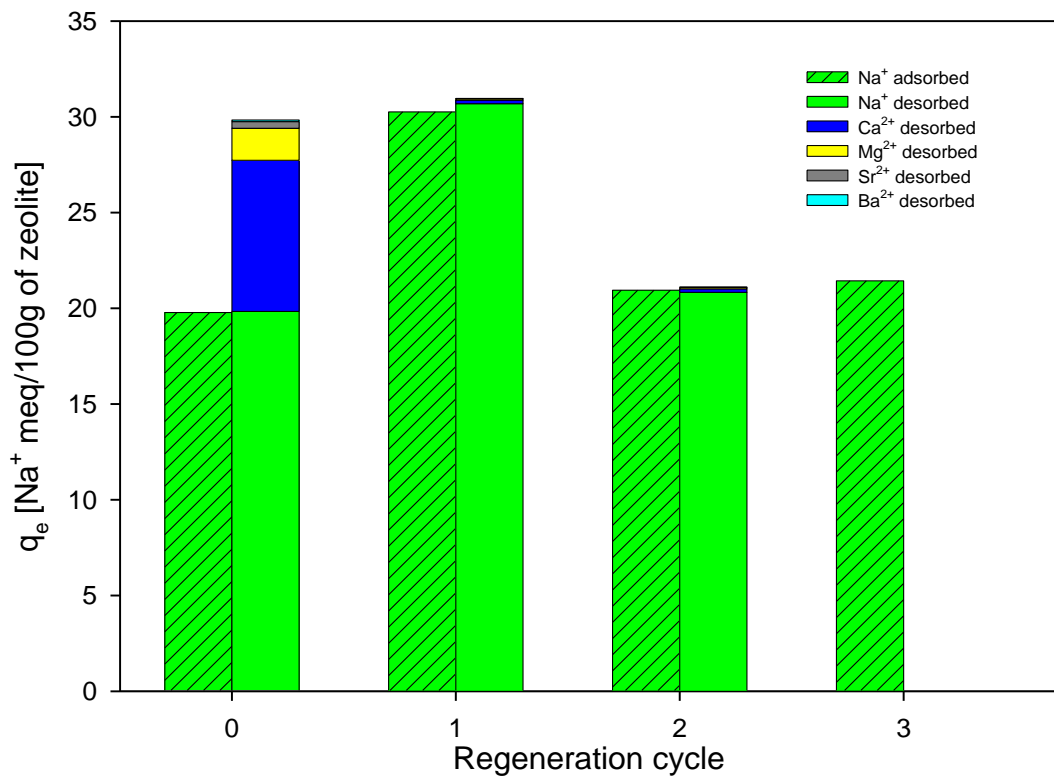


**Column adsorption and desorption of Na$^+$ from field CSG water by scoria at multiple regeneration cycles with K$^+$ solutions.**

# Appendix E. Cost associated with the treatment of CSG water using natural materials

The calculation of the costs of using natural materials for the treatment of co-produced coal seam gas water considers the capital costs of the material. Associated costs such as transportation, pre-treatment, regenerations and capital costs may increase the final costs.

| Scoria | | |
|---|---|---|
| **Item** | **Value** | **Unit** |
| Breakthrough point C/C0 (0.3) | 1.50 | BV |
| Total media volume | 1,000.00 | L |
| Treated water volume | 1,500.00 | L |
| Media cost per L | 0.05 | $/L |
| Cost total media | 50.00 | $ |
| Treatment cost per L | 0.03 | $/L |
| Treatment cost per ML | 33.33 | $/m3 |
| Regeneration cycles | 20.00 | - |
| Material cost over lifespan | 1.67 | $/m3 |

| Zeolite | | |
|---|---|---|
| **Item** | **Value** | **Unit** |
| Breakthrough Point C/C0 (0.3) | 4.50 | BV |
| Total media volume | 1,000.00 | L |
| Treated water volume | 4,500.00 | L |
| Media Cost per L | 0.15 | $/L |
| Cost total media | 150.00 | $ |
| Treatment cost per L | 0.03 | $/L |
| Treatment cost per ML | 33.33 | $/m3 |
| Regeneration cycles | 30.00 | - |
| Material cost over lifespan | 1.11 | $/m3 |